UNIVERSITÀ DEGLI STUDI DI BRESCIA

UNIVERSITÀ DEGLI STUDI DI BRESCIA

DOTTORATO DI RICERCA IN

GENETICA MOLECOLARE, BIOTECNOLOGIE, E MEDICINA SPERIMENTALE

Settore Scientifico Disciplinare:
Area 06 - Scienze mediche
MED/46 Scienze Tecniche di Medicina di Laboratorio

XXXIII Ciclo

Generation and Establishment of *In Vitro* Neuronal Models of Joubert Syndrome (JS) Derived from Patient-specific Induced Pluripotent Stem Cells (iPSCs)

DOTTORANDO
Eltahir Abdelrazig Mohamed Ali

RELATORE
Prof.ssa. Silvia Clara Giliani

JULY-2021

CERTIFICATE

UNIVERSITÀ DEGLI STUDI DI BRESCIA

UNIVERSITÀ DEGLI STUDI DI BRESCIA

CERTIFICATE

This is to certify that the dissertation entitled **"Generation and Establishment of *In Vitro* Neuronal Models of Joubert Syndrome (JS) Derived from Patient-specific Induced Pluripotent Stem Cells (iPSCs)"**, submitted to the University of Brescia in partial fulfillment of the requirements for the award of the degree of **Doctor of Philosophy** in **Molecular Genetics, Biotechnologies, and Experimental Medicine** is a record of original and independent research work done by **Dr. Eltahir Abdelrazig Mohamed Ali** during the period of study from **2017 - 2020** in the Department of Molecular and Translational Medicine, the University of Brescia, Brescia, under my guidance and supervision and the dissertation has not previously formed the basis for the award of any Degree, Diploma, Associateship, Fellowship or other similar title to any candidate of any University.

Signature of the Ph.D. Supervisor

ACKNOWLEDGEMENTS

ACKNOWLEDGEMENTS

All the praises and thanks be to **Allah Almighty**, the giver of bountiful blessings and gifts, for His blessings throughout my life and for giving me the ability to carry out this study successfully.

My sincere thanks and gratitude to my Ph.D. supervisor **Prof. Silvia Clara Giliani** for her great help and sustained guidance during the course of this study and for her valuable suggestions and evaluation of the contents of this thesis.

I am also most grateful to my colleagues **Dr. Gaetana Lanzi**, **Dr. Stefania Masneri**, **Dr. Rosalba Monica Ferraro**, **Adele Guglielmi**, **Dr. Elena Mazzoldi**, and all the staff members of Angelo Nocivelli Institute for Molecular Medicine, Civil Hospital of Brescia, for their support and encouragement.

I wish to express my special appreciation and gratitude to **Prof. Enza Maria Valente**, **Prof. Giovanna Piovani**, and **Dr. Lucio Giordano**, for their valuable support and contribution.

I would like to thank **Prof. Eugenio Monti**, the current Ph.D. Coordinator, **Prof. Giuseppina De Petro,** the former Ph.D. Coordinator in the Department of Molecular and Translational Medicine, University of Brescia, and **Dr. Fabiana Farro**, PhD Officer in Charge, University of Brescia, for their great support during this study.

A big thank to all **my friends** from my country and other countries, for their support and encouragement and for making my time in Italy so enjoyable and successful.

My hearty thanks to my beloved mother and my brother **Saif Eldin**, and my sisters, **Ensaf**, **Egbal**, **Fatima**, and **Sanaa** for their support and unwavering love. A very special thank and gratitude to my nephew **Eng. Osama Karar Eltahir** for his unstinted support and encouragement.

Last but not the least, my sincere thanks and deep appreciation to my wonderful wife **Reem**, for her love, care, support and patience throughout my educational journey in India and Italy.

Eltahir Ali

ABSTRACT

Generation and Establishment of *In Vitro* Neuronal Models of Joubert Syndrome (JS) Derived from Patient-specific Induced Pluripotent Stem Cells (iPSCs)

Eltahir Abdelrazig Mohamed Ali
Dipartimento di Medicina Molecolare e Traslazionale, Università Degli Studi di Brescia

ABSTRACT *(Italian)*

Le cellule staminali pluripotenti indotte (iPSCs) sono diventate negli ultimi anni uno strumento fondamentale per disease modelling grazie alla possibilità di essere differenziate in diversi stipiti cellulari e di superare i limiti correlati all'utilizzo di modelli animali. Nella presente dissertazione descriviamo la riprogrammazione *in vitro* di cellule di pazienti con Joubert syndrome (JS) come modello di malattia. JS è una rara malattia neurologica caratterizzata da ipotonia, ritardo psicomotorio e intellettivo e da una caratteristica peculiare dell'encefalo visibile mediante MRI, quale il molar tooth sign (MTS). Le linee iPSC JS-specifiche sono state generate mediante riprogrammazione di fibroblasti ottenuti da cinque pazienti JS con diverse mutazioni nei geni *C5orf42, CC2D2A* e *TMEM67* mediante il CytoTune-iPS 2.0 Sendai Reprogramming Kit. Tutte le linee generate sono state caratterizzate per staminalità, pluripotenza e stabilità genomica in colture a lungo termine. Inoltre due di queste linee con mutazioni in *C5orf42* e *CC2D2A* unitamente a iPSCs derivate dal controllo BJ sono state differenziate in neural stem cells (NSCs) e successivamente in neuroni. Il differenziamento da NSC a neuroni ha prodotto una popolazione eterogenea dove i neuroni dopaminergici risultano predominanti, particolarmente nel caso di BJ. Tutte le linee hanno mostrato alta espressione di *GFAP* dovuta a contaminazione gliale. Inoltre su fibroblasti, iPSCs, NSCs e neuroni sono state eseguite analisi funzionali del ciglio primario e della via di segnale Sonic-Hedgehog (SHH). Il ciglio primario è stato identificato in tutti i tipi di cellule analizzate. Come atteso, le cellule JS-derivate hanno un numero di cellule cigliate inferiore rispetto al controllo e ciò può essere dovuto al difetto nei geni cigliari *CC2D2A* and *C5orf42*. Nonostante la variazione nel numero di cellule cigliate fra pazienti JS e controllo, non è stata evidenziata alcuna differenza nella lunghezza del ciglio. Possiamo quindi concludere che variazioni in lunghezza del ciglio non possono essere utilizzate come biomarker per JS, almeno nei casi dovuti a difetti nei geni *C5orf42* e *CC2D2A*. Infine abbiamo testato l'espressione di molecole del segnale SHH quali *Gli1, Gli2, Smo*, e *Ptch1* in fibroblasti, iPSCs, NSCs, e neuroni JS. I risultati ottenuti mostrano espressione molto ridotta di almeno uno di questi geni (*Gli1*) in cellule JS quando confrontate con il controllo confermando la correlazione fra difetti di geni del ciglio e disregolazione della via di segnale SHH precedentemente evidenziata in modelli animali. Le cellule ottenute sono di fondamentale importanza per definire il ruolo del ciglio primario e dei geni correlati all'insorgenza di JS nell'eziogenesi della patologia e nel test di nuovi approcci terapeutici.

Generation and Establishment of *In Vitro* Neuronal Models of Joubert Syndrome (JS) Derived from Patient-specific Induced Pluripotent Stem Cells (iPSCs)

Eltahir Abdelrazig Mohamed Ali
Dipartimento di Medicina Molecolare e Traslazionale, Università Degli Studi di Brescia

ABSTRACT *(English)*

Disease-specific induced pluripotent stem cells (iPSCs) has become an essential tool for disease modelling due to their ability to differentiate into multiple cell lineages and to overcome the limitations of animal models. In this dissertation, we report successful establishment of human in vitro models of Joubert syndrome, a rare neurological disorder characterized by hypotonia, psychomotor impairment, intellectual disability, and a hallmark finding on brain MRI known as the molar tooth sign (MTS). JS-specific iPSC lines were generated by reprogramming of fibroblasts obtained from five JS patients with different mutations in *C5orf42, CC2D2A,* and *TMEM67* using the CytoTune-iPS 2.0 Sendai Reprogramming Kit. All the generated cell lines were characterized for stemness, pluripotency, and genomic stability during long-term maintenance in culture. Further, two JS-derived iPSC lines with mutations in *C5orf42* and *CC2D2A* and iPSCs derived from the healthy control BJ were differentiated into neural stem cells (NSCs) and subsequently into neurons. Differentiation of the NSCs into neurons has yielded heterogeneous neuronal populations, however, dopaminergic neurons were predominant in all the cell lines, particularly in the healthy control BJ. All the cell lines have shown high expression of *GFAP* indicative of a moderate contamination of glia cells. Furthermore, functional analyses of primary cilia and Sonic-Hedgehog (SHH) signaling pathway were performed in JS-derived fibroblasts, iPSCs, NSCs, and neuronal cell lines. Primary cilia have been identified in all the cell types studied. As expected, a significantly decreased number of ciliated cells in all JS-derived cell cultures has been observed as compared to the healthy control and that could be attributed to the defects in the ciliary genes *CC2D2A* and *C5orf42* in the patient-derived cells. Strikingly, despite the variation in the number of ciliated cells between the patients and control, no notable differences were found in the ciliary length between them. We suggest that variation in ciliary length cannot be utilized as a biomarker for JS or at least for *C5orf42*- and *CC2D2A*-related JS. Finally, the expression pattern of SHH signaling molecules *Gli1, Gli2, Smo*, and *Ptch1* was assessed in JS-derived fibroblasts, iPSCs, NSCs, and neurons. Our findings revealed markedly low expression levels of at least one of these molecules (*Gli1*) in JS-derived cells as compared to the control confirming the correlation between defects in the ciliary genes and dysregulation of SHH signaling pathway previously reported in animal model studies. The generated JS-derived cell lines are necessary for deciphering the role of primary cilia and JS-related genes in disease mechanisms and evaluating distinct therapeutic approaches.

LIST OF FIGURES

LIST OF FIGURES

LIST OF TABLES

LIST OF TABLES

TABLE OF CONTENTS

TABLE OF CONTENTS

LIST OF ABBREVIATIONS

LIST OF ABBREVIATIONS

2D	Two dimensional
3D	Three dimensional
5HTR6	Serotonin receptor 6
6- OHDA	6-hydroxydopamine,
AADs	Age-associated diseases
AC	Acrocallosal syndrome
AC3	Type 3 adenylyl cyclase
ACTA2	Actin alpha 2
ACTB	β-actin
aGSK-3β	Active glycogen synthase kinase-3β
AHI1	Abelson Helper Integration Site 1
AMD	Age-related macular degeneration
AN2	Aniridia type II protein
APC	Adenomatous polyposis coli
APP	Amyloid-β precursor protein
ARL13B	ADP-ribosylation factor-like protein 13B
ARPKD	Autosomal recessive polycystic kidney disease
ASD	Atrial septal defect
AURKA	Aurora-A kinase
BAV	Bicuspid aortic valve
BBS	Bardet-Biedl syndrome
bFGF	Basic fibroblast growth factor
C5orf42	Chromosome 5 open reading frame 42
cAMP	Cyclic adenosine monophosphate
CAR	Chimeric antigen receptor
CC2D2A	Coiled-coil and C2 domain containing 2A
CCCP	Carbonyl cyanide 3-chlorophenylhydrazone
CEP120	Centrosomal Protein 120
CGMP	Current good manufacturing practice
ChAT	Choline acetyltransferase
CHDs	Congenital heart defects
CK1	Casein kinase 1
CMD	Corticomedullary differentiation
CNK2	Connector enhancer of kinase suppressor of ras 2
CNS	Central nervous system
CNV	Copy number variation
COACH	Colobomas, oligophrenia, ataxia, cerebellar vermis hypoplasia and hepatic fibrosis syndrome
CPLANE1	Ciliogenesis and planar polarity effector 1
CRIPSR/Cas9	Clustered regularly interspaced short palindromic repeats and CRISPR-associated protein 9
CSF	Cerebrospinal fluid
CSPP1	Centrosome and spindle pole-associated protein 1
CT	Computed tomography
CXCR4	C-X-C chemokine receptor type 4
DG	Dentate gyrus
DHH	Desert Hh
DM I	Type I diabetes mellitus
DMD	Duchenne muscular dystrophy
DMEM/F-12	Dulbecco's Modified Eagle Medium/Nutrient Mixture F-12
DSBs	Double-strand breaks
dsDNA	Double-stranded DNA
Dvl	Dishevelled
ECCs	Embryonic carcinoma cells
EGCs	Embryonic germ cells
ERG	Electroretinography
ERK	Extracellular signal-regulated kinase
ESCs	Embryonic stem cells
ESRD	End-stage renal disease
FDA	Food and Drug Administration
FGF	Fibroblast growth factor
G_0	Gap phase
GATA4	GATA binding protein 4
GD	Gaucher disease
GFAP	Glial fibrillary acidic protein
GGT	Gamma-glutamyl transpeptidase
GHD	Growth hormone deficiency
Gli1, 2, and 3	Gli transcription factors type 1, 2, and 3
Glis1	Glis family zinc finger 1
GPCR	G-protein-coupled receptor
GSK3B	Glycogen synthase kinase 3 beta
GTT	Gamma-glutamyl transpeptidase
H1foo	H1 Histone Family, Member O, Oocyte-Specific
H1foo	H1 Histone Family, Member O, Oocyte-Specific
H_2O_2	Hydrogen peroxide
HD	Huntington disease
HDAC6	Histone deacetylase 6
HDR	Homology-directed repair
HEF1	Human enhancer of filamentation 1
hESCs	Human embryonic stem cells
Hh	Hedgehog gene
hiPSC	Human induced pluripotent stem cell
HLA	Human leukocyte antigen
HSCs	Hematopoietic stem cells
HTS	High throughput screening
ICFs	Informed consent forms
IFT	Intraflagellar transport
IFT-A	Intraflagellar transport protein complex-A
IFT-B	Intraflagellar transport protein complex-B
IHH	Indian Hh
iNPCs	Induced neural progenitor cells
INPP5E	Inositol Polyphosphate-5-Phosphatase E

iPSC-CMs	iPSC-derived cardiomyocytes
iPSCs	Induced pluripotent stem cells
IRCCS	Istituto di Ricovero e Cura a Carattere Scientifico
ISSCR	International Society for Stem Cell Research
JATD	Jeune asphyxiating thoracic dystrophy
JDM	Juvenile-onset type 1 diabetes mellitus
JS	Joubert syndrome
JSRDs	Joubert syndrome and related disorders
KIF7	Kinesin family member 7
KISS1R	Kisspeptin 1 receptor
Klf4	Kruppel-like factor 4
LCA	Leber congenital amaurosis
LFT	Liver function test
LRP	Lipoprotein receptor-related protein
Mbd3	Methyl-CpG-binding domain protein 3
MCHR1	Melanin-concentrating hormone receptor 1
MEFs	Mouse embryonic fibroblasts
min	Minutes
miRNA	MicroRNA
MKS	Meckel syndrome
MKS1 and 6	Meckel syndrome type 1 and 6
mPFC	Medial prefrontal cortex
MRI	Magnetic resonance imagimg
mRNA	Massenger RNA
mtDNA	Mitochondrial DNA
MTS	Molar tooth sign
NEI	National Eye Institute
NESTIN	Neuroepithelial stem cell protein
NGS	Next-generation sequencing
NIH	National Institutes of Health
NIMA	Never in mitosis gene A
No.	Number
NPHP	Nephronophthisis
NPHP1	Nephrocystin 1
NuRD	Nucleosome remodelling and histone deacetylation
OF	Oncogenic foci
OFD VI	Oral-facial-digital syndrome type VI
OFDs	Oral-facial-digital syndromes
OMA	Oculomotor apraxia
OSKM	Oct3/4, Sox2, Klf4 and c-Myc
PAX6	Paired box protein
PBMCs	Peripheral blood mononuclear cells
PCOS	Polycystic ovary syndrome
PCP	Planar cell polarity
PCR	Ploymerase chain reaction
PD	Parkinson disease
PIBF1	Progesterone immunomodulatory binding factor 1
PKA	Protein kinase A
PKD	Polycystic kidney disease
Pkd2	Polycystin 2
POU5F1	POU domain, class 5, transcription factor 1
PP2A	Protein phosphatase 2A
Ptch1	Patched1
RFT	Renal function test
RNA	Ribonucleic acid
ROS	Reactive oxygen species
RP	Retinitis pigmentosa
RPE	Retinal pigment epithelial
RPGRIP1	RPGR Interacting Protein 1
rpm	Revolutions per minute
RT	Reverse transcriptase
RT-qPCR	Quantitative real-time PCR
SAG	Smoothened agonist
SCNT	Somatic cell nuclear transfer
SCP	Superior cerebellar peduncles
SEM	Scanning electron microscopy
SeV	Sendai virus
SHH	Sonic Hedgehog
SLS	Senior-Løken syndrome
Smo	Smoothened
SOX1 and 2	SRY-box transcription factor 1 and 2
SSTR3	Somatostatin receptor 3
SuFu	Suppressor of fused
TAE	Tris Acetate-EDTA
TALENs	Transcription activator-like effector nucleases
TCF	T cell factor
TH	Tyrosine hydroxylase
THM1	Tetratricopeptide repeat-containing hedgehog modulator-1
TMEM237	Transmembrane protein 237
TMEM67	Transmembrane protein 67
TZ	Transition zone
VEP	Visual-evoked potential
Wnt	Wingless-related integration site
ZFNs	Zinc-finger nucleases
β-TrCP	β-transducin repeat-containing protein

INTRODUCTION

1. INTRODUCTION

1.1. Joubert syndrome - an overview

Joubert syndrome (JS) is a neurodevelopmental heterogeneous disorder characterized by hypotonia, psychomotor delay, intellectual disability, oculomotor apraxia (OMA), cerebellar motor syndrome, and a neuroradiographic finding known as the molar tooth sign (MTS) detected by brain magnetic resonance imaging (MRI) (Valente et al., 2008; Joubert et al., 1968). The neurological features of JS may be associated with or without neonatal breathing difficulties, nephronophthisis, ocular colobomas, facial dimorphism, and congenital hepatic fibrosis (Bachmann-Gagescu et al., 2015). The syndrome was first reported in 1968 by the paediatric neurologist Marie Joubert and colleagues who described four siblings in a French-Canadian family with ataxia, episodic tachypnea, agenesis of the cerebellar vermis, abnormal eye movements, and cognitive deficits (Joubert et al., 1968).

JS is caused by dysfunction of the primary cilium, a microtubule-based organelle, or its apparatus. Defects in primary cilium are associated with pathogenesis of a broader group of genetic disorders known as *ciliopathies* (Romani et al., 2013). Most cases of JS show an autosomal recessive pattern of inheritance, however, some rare cases with X-linked recessive pattern have also been reported (Coene et al., 2009). Mutations in more than 30 genes have been described in association with JS, such as *AHI1, C5orf42, CC2D2A, INPP5E,* and *TMEM237* (Table 1-1). These genes are involved in the formation of primary cilium or its functions (Romani et al., 2013). The extreme genetic heterogeneity and phenotypic variability of JS make understanding the pathogenesis and classification of JS a daunting task. Several disorders with the MTS are clinically and genetically overlapping with classic JS and they all known as *Joubert syndrome and related disorders (JSRDs)* (Brancati et al., 2010).

1.2. Epidemiology of Joubert syndrome

The prevalence of JS was previously estimated to be 1 in 80000 to 1 in 100000 newborns (Brancati et al., 2010; Parisi et al., 2007), however, it is thought to be underestimated due to its complex heterogeneity and the clinical overlap between JS and other ciliopathies, as well as lack of awareness of the MTS in early published reports on JS (Juric-Sekhar et al., 2012). Currently, the prevalence of JS is estimated to be 1 in 55000 to 1 in 200000 newborns (Bachmann-Gagescu et al., 2020), and is significantly higher in French Canadians (Srour et al., 2015), Ashkenazi Jews (1 in 34000 to 1 in 40000 population) (Edvardson et al., 2010) and Canadian Hutterites (1 in 1150 population) (Huang et al., 2011). The high prevalence in Ashkenazi Jews is due to the founder mutation p.R73L in the

TMEM216 gene (Edvardson et al., 2010), while in French-Canadians is due to multiple pathogenic variants in the *C5orf42* gene and other ciliary genes such as *CC2D2A, CEP104*, *TMEM231,* and *TMEM67* (Srour et al., 2015, 2012, 2012). In Canadian Hutterite population, the carrier frequency of the founder mutation p.R18X in the *TMEM237* gene is estimated to be 1 per 17 individuals (Huang et al., 2011). A recently published report by a research team from *the Italian Association for Joubert Syndrome and Congenital Ataxias* estimated the prevalence of JS in general Italian population to be 0.47 per 100000 individuals, while in child population it is thought to be 1.7 per 100000 children (Nuovo et al., 2020).

1.3. Clinical manifestations of Joubert syndrome

The clinical presentation of JS varies significantly among the patients. Some patients may suffer from severe symptoms, while others present with a milder condition (Parisi & Glass, 2003). The core signs and symptoms of this syndrome are associated with the central nervous system (CNS) (Joubert et al., 1968), but the majority of patients exhibit other clinical features involving different organs including eyes, kidneys, liver, and skeleton (Bachmann-Gagescu et al., 2015; Romani et al., 2013). The classic clinical features of JS are hypotonia, ataxia, abnormal ocular movements, neonatal breathing difficulties, developmental delay, and the MTS. Other clinical features associated with JS include:

- Hepatic disease such as hepatic fibrosis
- Renal diseases such as Nephronophthisis (NPHP) and polycystic kidney disease (PKD)
- Retinal dystrophy
- Skeletal deformities such as polydactyly of hands and feet
- Facial dysmorphism
- Congenital heart defects (CHDs)
- Occipital encephalocele
- Ocular colobomas
- Oral hamartomas
- Endocrine abnormalities

We briefly summarized the involvement of these clinical features in JS as follows:

1.3.1. Hypotonia

In infants with JS, hypotonia or low muscle tone is one of the most common clinical features and it evolves to motor delays and impaired coordination of voluntary movements (ataxia) seen in children with JS (Bachmann-Gagescu et al., 2019; Romani et al., 2013; Doherty et al., 2009).

1.3.2. Abnormal respiratory patterns

Abnormal respiratory control is one of the major clinical features described in the first report on JS by Marie Joubert and colleagues (Joubert et al.,1968). During infancy, most of JS patients show breathing difficulties characterized by episodes of apnea and/or tachypnea (Romani et al., 2013).

1.3.3. Cerebellar ataxia

Cerebellum is the midbrain part which is responsible for movement control. In patients with JS, structural defects in this part of the brain result in lack of muscle coordination (ataxia) that may affect voluntary control of gait, balance, limbs, eyes, and other voluntary movements (Maria et al.,1997).

1.3.4. Cognitive and developmental delay

Children with JS show persistent neuromotor developmental delay and moderate to severe intellectual disabilities with autistic-like behaviors, however, rare cases with normal cognitive ability have been reported (Poretti et al., 2009). Speech difficulties and other behavioral and psychiatric problems have also been reported in JS patients such as depression, auditory hallucinations, tantrums, and anxiety (Summers et al., 2017; Bachmann-Gagescu et al., 2015; Fennell et al., 1999). Although there are a strong genetic and clinical link between cerebellum dysfunction and autism, the co-occurrence of JS and autism is still unclear (Scott et al., 2009). Two studies showed conflicting results; the first study estimated that the incidence of autism in JS patients is 30% (Ozonoff et al., 1999). In contrast, although the children with JS in the other study showed autistic-like features, no one in the 31 families examined meets the clinical cut-off for autism (Takahashi et al., 2005). A mutation in *AHI1,* the first JS-related gene to be identified, was found to be also associated with autism (Alvarez Retuerto et al., 2008).

1.3.5. The Molar tooth sign (MTS)

Molar tooth sign (MTS) is a classic neuroimaging finding in JS. It is detected in JS patients by brain MRI or computed tomography (CT) scan. Axial brain MRI in patients with JS shows distinct defects in the cerebellum which form the MTS namely: deep interpeduncular fossa, hypoplasia of cerebellar vermis and thick and elongated superior cerebellar peduncles **(**SCP**).** Although the first report described JS and its association with brain structural defects was in 1968 (Joubert et al., 1968), the MTS as a key radiographic feature of JS was identified in 1997 by Maria and colleagues who described the cerebellar vermis and midbrain malformation in JS patients and called it the “molar tooth sign” due to the fact that its shape resembles the molar tooth (Fig.1-1) (Maria et al., 1997). The MTS is thought to be pathognomonic for JS, but this was contradicted by another report in which

authors described a 12-year-old girl with intellectual disability and dysmorphic features including tongue hamartomas, high arched palate, broad nasal tip, frontal bossing, low set ears, and bilateral preaxial polysyndactyly. Brain MRI revealed the MTS. Based on the clinical findings, the authors confirmed the diagnosis as oral-facial-digital syndrome type VI (OFD VI) and concluded that the MTS is not an exclusive neuroradiographic finding for JS and may be present in other medical conditions (Dirik et al., 2013). In response to this conclusion, the report by Poretti and colleagues demonstrated that OFD VI is not a distinct disorder but a subtype under the umbrella of JS because it shares the same causative gene *C5orf42* with JS (Poretti et al., 2014), in addition to their overlapping

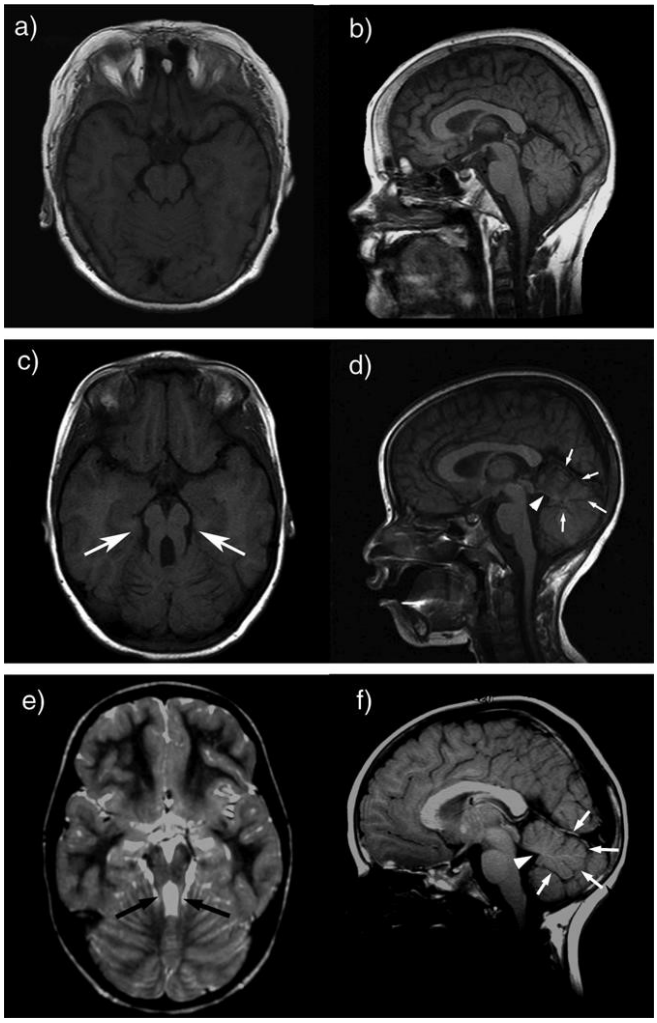

Figure 1-1. Brain MRI of a healthy individual and two patients with JS. (**a**) Axial and (**b**) mid-sagittal plane images show typical appearance of the cerebellar vermis in a normal brain. (**c**) The MTS (indicated by arrows) and (**d**) cerebellar vermis hypoplasia (indicated by surrounding four small arrows) and elevated fourth ventricle with abnormal position (indicated by arrowhead) in a patient with JS. (**e**) The "mild" MTS on sagittal imaging of the other JS patient and (**f**) mild elevation of the fourth ventricle (indicated by arrowhead) with mild cerebellar vermis hypoplasia (indicated by surrounding small arrows Adapted from 'Joubert syndrome (and related disorders)', by Parisi et al., 2007, *European Journal of Human Genetics*, *15*(5), 511-521.

clinical features (Lopez et al., 2014; Srour et al., 2012). Therefore, according to this report the MTS may still be considered as pathognomonic for JS. Several studies have demonstrated the link between a mild MTS and mutations in JS- related genes (Enokizono et al., 2017; Shaheen et al., 2016; Parisi et al., 2004). It is interesting to note that, although, the MTS is important for diagnosis of JS, it is not suitable for differential diagnosis of JS subtypes due to lack of neuroimaging-genotype correlations and variation in neuroradigraphic features in individuals of a same family (Poretti et al., 2011).

1.3.6. JS with Skeletal deformities

Patients with JS may exhibit skeletal anomalies particularly scoliosis and polydactyly of hands and feet (Fig.1-3C & 1-3D). Scoliosis and polydactyly are estimated to be in 5% and 15% of JS patients, respectively (Bachmann-Gagescu et al., 2015). Rarely, some cases show the cardinal features of JS with skeletal dysplasia (Bachmann-Gagescu et al., 2015; Malicdan et al., 2015; Tuz et al., 2014).

1.3.7. JS with renal disease

It is estimated that 25-30% of JS patients may develop kidney disease which manifests as NPHP or cystic kidney disease (Bachmann- Gagescu et al., 2015; Fleming et al., 2017; Doherty et al., 2009). NPHP may develop during childhood or before age of 20 years causing polyuria and polydipsia and eventually leads to end-stage renal disease (ESRD) (Parisi, 2019). Juvenile NPHP is the most common type seen in JS and the patients are more likely to develop ESRD at age of 13 years (Hildebrandt et al., 1997). The renal cyst disease in JS may develop prenatally and resembles autosomal recessive polycystic kidney disease (ARPKD). Affected individuals are at high risk for developing early-onset hypertension (Fleming et al., 2017; Gunay-Aygun et al., 2009). It is of note that kidney failure is a leading cause of death in JS patients (Dempsey et al., 2017) and Kidney disease in JS often associates with retinopathy (Brancati et al., 2010; Parisi et al., 2009).

1.3.8. JS with hepatic disease

The involvement of liver disease in JS is found in a small number of patients and most of the cases show high levels of the hepatic enzymes transaminases and gamma-glutamyl transpeptidase (GGT) but they may not be symptomatic at birth (Strongin et al., 2018; Vilboux et al., 2017). Portal hypertension is thought to be due to severe hepatic fibrosis, however, it occurs in a small portion of JS patients (Bachmann-Gagescu et al., 2019). In a cohort study of 100 patients with JS, 43 patients have shown a sign of hepatic disease such as elevated liver enzymes, liver hyperechogenicity and splenomegaly (Strongin et al., 2018). The authors revealed that portal hypertension in JS is strongly linked to elevated hepatic enzymes, coloboma, and renal disease.

1.3.9. Eye abnormalities in JS

Wang et al. (2018) reviewed the eye abnormalities in 325 patients with JS and found that the common ocular defects in JS are oculomotor apraxia (OMA) (an eye movement disorder), nystagmus (involuntary repetitive eye movements), strabismus (misaligned eyes), coloboma, retinopathy and ptosis (an abnormal drooping of the upper eyelid). OMA is the most frequent phenotype found in 80% of the patients, while approximately two-thirds of the patients exhibit strabismus and nystagmus. Unilateral or bilateral ptosis is seen in 43% of JS patients and occurs exclusively in affected children. The incidence of other ocular phenotypes was found to be low. Retinopathy and coloboma manifest in one-third of the patients (Fig.1-2), while optic nerve atrophy affects 22% of them. Although coloboma represents a small portion of eye defects in JS, it has been found in > 30% of JS with liver involvement (Doherty et al., 2010; Brancati et al., 2009). Retina dystrophy often occurs in JS patients with kidney involvement (Brancati et al., 2010; Parisi et al., 2009) and the pigmentary retinopathy in JS is often confused with retinitis pigmentosa (RP), an inherited disorder of the retina that causes progressive vision loss, but the retinal degeneration in JS is less progressive as compared to RP (Steinlin et al., 1997). The frequency of retinopathy in JS is estimated to be 24-32% (Brooks et al., 2018; Doherty et al., 2010), however, the co-occurrence of retinal dystrophy and ocular colobomas is rare (Brooks et al., 2018).

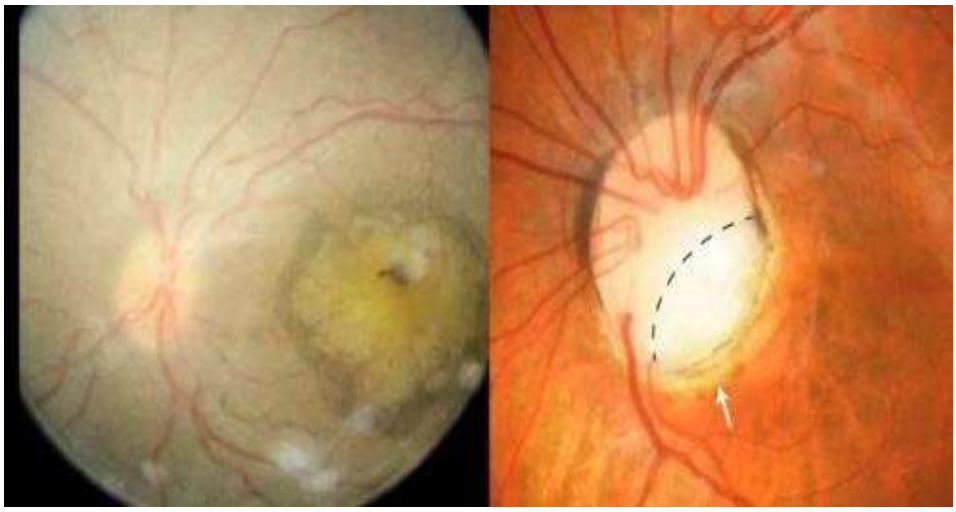

Figure 1-2. Eye abnormalities in JS. Coloboma of the optic disc (right, indicated by a dashed line) and retinal dystrophy with maculopathy (left) in two patients with JS. Adapted from 'Review of ocular manifestations of Joubert syndrome', by Wang et al.,2018, *Genes*, *9*(12), 605.

1.3.10. Abnormal facial and oral cavity features

There are no distinct facial or oral cavity features associated with JS, however, individuals with JS may have broad forehead, ptosis, strabismus, cleft lip and/or palate, prominent lower jaw, an open mouth posture due to hypotonia, midline groove of the tongue, oral hamartomas, and oral frenula (Fig.1-3A &1-3B) (Braddock et al., 2007; Maria et al., 1999). These features overlap significantly between JS and oral-facial-digital syndromes (OFDs) (Bonnard et al., 2018; Coene et al., 2009). However, OFDs are a group of distinct genetic ciliopathies, but the OFD type VI is thought to be a subtype of JS because mutations in the same gene *C5orf42* have been identified in JS and OFD VI and both exhibit overlapping phenotypic features (Bonnard et al., 2018; Lopez et al., 2014; Poretti et al., 2012; Srour et al., 2012).

1.3.11. Congenital heart defects

Congenital cardiac defects are extremely rare in JS (1-2% of cases) and manifest as atrial septal defects (ASD), aortic stenosis, bicuspid aortic valve (BAV) and coarctation of the aorta (Bachmann-Gagescu et al., 2015; Karp et al., 2012).

1.3.12. Endocrine abnormalities

It is estimated that 4% of JS patients exhibit one or more endocrine defects including hypothyroidism, premature puberty, neurogenic diabetes insipidus and growth hormone deficiency (GHD) (Bachmann-Gagescu et al., 2015). Type I diabetes mellitus (DM I), short stature, and polycystic ovary syndrome (PCOS) have also been reported in relatively few cases (Stephen et al., 2017; Vilboux et al., 2017; Bachmann-Gagescu et al., 2015).

1.3.13. Other brain structural anomalies in JS

In addition to the cerebellum defects that manifests radiographically as the MTS, JS patients may develop occipital encephalocele (Fig.1-3E), polymicrogyria, corpus callosum dysgenesis, ventriculomegaly, and hippocampal malrotation (Poretti et al., 2017; Bachmann-Gagescu et al., 2015).

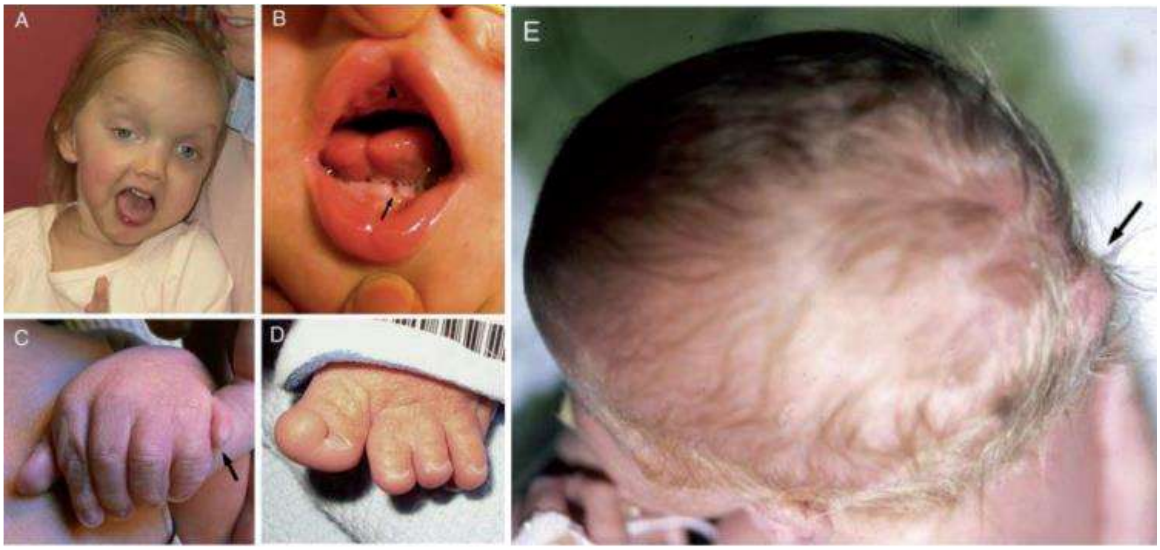

Figure 1-3. Clinical features of JS. (**a**) Facial dysmorphism in a girl with JS/COACH syndrome showing broad forehead, arched eyebrows, strabismus, eyelid ptosis (on the right eye), and open mouth configuration. (**b**) Midline upper lip cleft (indicated by an arrowhead), midline groove of tongue, and bumps of the lower alveolar ridge (indicated by an arrow) in a child with oral–facial–digital syndrome-like features of JS. (**c**) Postaxial polydactyly (indicated by an arrow) in a left hand of an infant with JS. (**d**) Preaxial polysyndactyly and fusion of the hallux in a left foot of an infant with JS. (**e**) A small occipital encephalocele with protrusion of the occiput of the skull (indicated by an arrow) in an infant with JS. Adapted from 'The molecular genetics of Joubert syndrome and related ciliopathies: The challenges of genetic and phenotypic heterogeneity', by Parisi, M.A., 2019, *Translational Science of Rare Diseases*, 4(1-2):25-49.

1.3.14. Other ciliopathies associated with JS

Several ciliopathy disorders overlap phenotypically and genetically with JS and may lead to misdiagnosis of JS. Some of these ciliopathies are mentioned below:

1.3.14.1. Oral-facial-digital syndrome (OFD) type VI is a rare condition that affect the development of the oral cavity, facial features and digits. It is caused by mutations in *C5orf42* gene (Field et al., 2012).

1.3.14.2. Acrocallosal syndrome (AC) is characterized by agenesis of the corpus callosum, polydactyly and distinctive facial features. It is caused by defects in *KIF7* gene (Bachmann-Gagescu et al., 2015; Putoux et al., 2011).

1.3.14.3. Jeune asphyxiating thoracic dystrophy (JATD) is an autosomal recessive skeletal dysplasia characterized by short stature and limbs, polydactyly, a long narrow chest with short ribs, and cystic kidney disease. It is associated with mutations in the *CEP120*, *CSPP1*, *KIAA0586,* and *PIBF1* (Parisi, 2019; Akizu et al., 2014; Lehman et al., 2010).

1.3.14.4. Bardet-Biedl syndrome (BBS) is an autosomal recessive disorder characterized by progressive retinal dystrophy and renal disease, intellectual disability, developmental delay of motor skills, obesity, postaxial polydactyly, hypogonadism, and impaired speech. To date, at least 24 genes have been identified to cause BBS and most of them are involved in ciliogenesis and cilia function (Haws et al., 2020; Forsythe & Beales, 2015).

1.3.14.5. Meckel syndrome (MKS) is characterized by enlarged polycystic kidney, congenital liver fibrosis, occipital encephalocele, and polydactyly. This condition is caused by defects in at least 21 genes and out of them 18 have been implicated in JS including *CC2D2A*, *C5orf42*, *CEP41, TMEM67,* and *TMEM237*. Mutations in these genes are associated with severe lethal phenotypes in MKS, while they cause non-lethal phenotypes in JS (Slaats et al., 2016; Romani et al., 2014).

1.3.14.6. COACH syndrome (COACH) is a rare ciliopathy with an autosomal recessive inheritance pattern. The acronym (COACH) stands for the major clinical features of this syndrome which are colobomas, oligophrenia, ataxia, cerebellar vermis hypoplasia and hepatic fibrosis (Verloes et al., 1989). The causative genes of COACH include *CC2D2A, RPGRIP1,* and *TMEM67* and it is thought to be a rare form of JS (Doherty et al., 2010; Doherty et al., 2009; Satran et al., 1999).

1.3.14.7. Leber congenital amaurosis (LCA) is a severe genetic eye disorder with both autosomal recessive and autosomal dominant mode of inheritance. The cardinal features of LCA are retinal dystrophy, photophobia, keratoconus, nystagmus, and extreme hyperopia. Cognitive impairment is also seen in 25% of affected children. LCA is caused by mutations in at least 19 genes comprising *CEP290* which accounts for 20% of the cases (Kumaran et al., 2018; Brancati et al., 2007).

1.3.14.8. Nephronophthisis (NPHP) is a renal disorder characterized by renal inflammation and fibrosis that eventually cause ESRD. About 15% of the affected individuals may exhibit additional features such as hepatic fibrosis, CHDs, situs inversus, and anemia. Several genes are involved in the pathogenesis of NPHP, but most of the cases are due to mutations in *NPHP1* gene (Srivastava et al., 2017). When NPHP is combined with retinopathy the condition is known as Senior-Løken syndrome (SLS) (Ronquillo et al., 2012).

1.4. Life expectancy of Joubert syndrome patients

Life expectancy of patients with JS varies due to the severity of symptoms. Patients with severe symptoms may not survive beyond the age of three years and the leading cause of death is multiorgan dysfunction or respiratory failure (Dempsey et al., 2017). However, those with mild symptoms who receive supportive treatments may have a normal life span.

1.5. Molecular genetics and current scenario of pathogenesis of Joubert syndrome

1.5.1. Genetic heterogeneity of Joubert syndrome

Many genes have been identified to be associated with JS (Table 1-1) and account for approximately 62-94% of JS patients (Phelps et al., 2018; Bachmann-Gagescu et al., 2015). The vast majority of these patients show an autosomal recessive pattern of inheritance (Bachmann-Gagescu et al., 2019), however, rare cases with X-linked recessive mechanism have also been reported (Coene et al., 2009). Although JS was first described in 1968, the genetic causes of JS remained unclear for more than three decades till the discovery of *AHI1* gene, the first gene reported to be associated with this neurodevelopmental disease (Ferland et al., 2004; Dixon-Salazar et al., 2004). Following that, several other causative genes of JS have been discovered and some of them previously identified are associated with other genetic disorders including ciliopathies (Shaheen et al., 2019; De Mori et al., 2017; Romani et al., 2014; Srour et al., 2012; Cantagrel et al., 2008; Gorden et al., 2008; Baala et al., 2007; Valente et al., 2006).

JS patients in our study exhibit mutations in the genes *C5orf42, CC2D2A,* or *TMEM67* which are briefly reviewed as follows:

1.5.1.1. *C5orf42* gene

The *C5orf42* gene, also known as *CPLANE1* (ciliogenesis and planar polarity effector 1), is a protein coding gene located in the 5p13.2 region. Srour and colleagues were the first to report that *C5orf42* is one of the causative genes of JS. They identified compound heterozygous mutations in *C5orf42* in nine individuals from seven French Canadian families. The C5orf42 protein is localized to the ciliary transition zone (TZ). Its function is still unclear, but it is thought to be involved in cilium biogenesis, regulation of cell polarity and directional cell migration during development (Srour et al., 2012). This gene was also found to cause two other ciliopathies namely: MKS (Shaheen et al., 2013) and OFD VI (Lopez et al., 2014).

1.5.1.2. *CC2D2A* gene

The *CC2D2A* gene encodes a coiled-coil and C2 domain containing 2A protein which is thought to involve in the primary cilium formation (Tallila et al., 2008). The genomic locus of *CC2D2A* is 4p15.32 and defects in this gene result in JS (Noor et al., 2008; Gorden et al., 2008) and Meckel syndrome type 6 (MKS6) (Tallila et al., 2008). The association between *CC2D2A* and JS was first identified in a consanguineous Pakistani family with RP and intellectual disabilities (Noor et al., 2008). It is estimated that mutations in *CC2D2A* account for almost 10% of cases with JS (Doherty et al., 2009; Gorden et al., 2008). It is noteworthy that patients with missense mutations in *CC2D2A* are more likely to have JS with less severe phenotypes, while patients with truncating mutations show

more severe or even lethal MKS6 (Brancati et al., 2010). Several studies have investigated the role of CC2D2A in ciliogenesis and its interactions with other ciliary proteins (Bachmann-Gagescu et al., 2015; Barker et al., 2014; Veleri et al., 2014; Garcia-Gonzalo et al., 2011).

1.5.1.3. *TMEM67* gene

The *TMEM67* (Transmembrane protein 67) gene encodes a protein known as meckelin. The genomic locus of this gene is 8q22.1 and it was the third JS causative gene to be identified (Baala et al., 2007) after *AHI1* (Ferland et al., 2004) and *CEP290* respectively (Sayer et al., 2006). Meckelin is a transmembrane receptor that is localized to the primary cilium and plasma membrane. It has been demonstrated that this protein plays a role in migration of the centrioles to the apical cell surface and in ciliogenesis (Adams et al., 2012). In addition to JS, mutations in this gene are associated with Meckel syndrome type 3 (MKS3) (Smith et al., 2006), and Rhyns syndrome (Brancati et al., 2018). Similar to defects in *CC2D2A*, missense mutations in *TMEM67* often result in JS, while nonsense and frameshift mutations are associated with severe MKS3 (Brancati et al., 2010).

1.5.2. Genotype-phenotype correlations in Joubert syndrome

Several studies have investigated genotype-phenotype correlations in JS and some relevant correlations have been identified. Mutations in *TMEM67* were found to be associated with JS phenotype with a liver disease in about 80% of patients (Iannicelli et al., 2010; Brancati et al., 2009). The remaining proportion of these patients have defects in other genes such as *CC2D2A*, *MKS3,* and *RPGRIP1L*. Moreover, the patients may show additional clinical phenotypes known as COACH syndrome (Doherty et al., 2010; Brancati et al., 2009). Although mutations in several JS-related genes have been identified in patients with ocular colobomas, mutations in *TMEM67* are the most frequent genetic defects in a significant number of patients (Wang et al., 2018; Vilboux et al., 2017; Bachmann-Gagescu et al., 2015). Defects in the primary cilium-associated genes *AHI1, ARL13B, CC2D2A,* and *INPP5E* are common in classic JS and in JS with retinopathy (Romani et al., 2013; Mougou-Zerelli et al.,2009; Bielas et al., 2009; Parisi et al., 2006; Dixon-Salazar et al., 2004). Other genes associated with retinal degeneration in JS are *ARL3, MKS1*, *NPHP1,* and *CEP290* (Alkanderi et al., 2018; Wang et al., 2018), however, mutations in *AHI1* and *CEP290* cause more severe retinopathy compared to other genes (Bachmann-Gagescu et al., 2019). *CEP290* loss-of-function is also strongly correlated with the clinical phenotype in a large number of JS patients with both retinal dystrophy and renal disease (Brancati et al., 2007). It is worth noting that retinopathy is absent or less likely to develop in JS patients with mutations in *C5orf52, KIAA0586,* or *TMEM67* (Vilboux et al., 2017). Several genes have been identified in JS patients with nystagmus including *AHI1, ARL13B, C5orf42, CCD2D2A, CEP120, CEP290, CSPP1, INPP5E, KIAA0556, KIAA0586, MKS1, NPHP1,*

POC1B, RPGRIP1L, TCTN2, TCTN3, TMEM67, and *TMEM237*. Interestingly, some of these genes were also found to be associated with strabismus namely *AHI1, C5orf42, CEOP120, CEP290, KIAA0586, MKS1, RPGRIP1l, TMEM67,* and *TMEM237*. It is also important to note that defects in *TMEM237* represent the most common mutations in JS patients who develop strabismus (Wang et al., 2018). JS patients with mutations in *AHI1, C5orf42, CC2D2A, CEP290, KIAA0586,* and *TMEM67* appear more likely to develop kidney disease. This renal involvement is strongly associated with defects in *AHI1, CEP290* and *TMEM67* (Fleming et al., 2017; Komatsu et al., 2016) and to a lesser extent with *NPHP1*, *RPGRIP1L,* and *TMEM237* (Huang et al., 2011; Brancati et al., 2008; Castori et al., 2005).

Table 1-1. Genes associated with Joubert syndrome. Adapted from 'Joubert syndrome: congenital cerebellar ataxia with the molar tooth', by Romani et al., 2013, *The Lancet Neurology*, *12*(9), 894-905.

Gene	Protein	Locus
AHI1	Jouberin	6q23.3
ARL13B	ADP-ribosylation factor-like 13B	3q11.1-11.2
ARL3	ADP-ribosylation factor-like GTPase 3	10q24.32
ARMC9	Armadillo repeat containing 9	2q37.1
B9D1	B9 domain-containing protein 1	17p11.2
B9D2	B9 domain-containing protein 2	19q13.2
C2CD3	C2 domain containing 3 centriole elongation regulator	11q13.4
C5Orf42 or *(CPLANE1)*	C5Orf42 or (Inositol polyphosphate-5- phosphatase)	5p13.2
C21Orf2	C21Orf2 or (Cilia and flagella associated protein 410)	21q22.3
CC2D2A	Coiled-coil and C2 domain-containing protein 2A	4p15.32
CEP41	Centrosomal protein 41kDa	7q32.2
CEP104	Centrosomal protein 104kDa	1p36.32
CEP120	Centrosomal protein 120kDa	5q23.2
CEP164	Centrosomal protein 164kDa	11q23.3
CEP290	Centrosomal protein 290kDa	12q21.32
CSPP1	Centrosome and spindle pole associated Protein 1	8q13.1-13.2
IFT172	Intraflagellar Transport 172	2p23.3
INPP5E	Inositol polyphosphate-5-phosphatase E	9q34.3
KIAA0556	KIAA0556	16p12.1
KIAA0586	KIAA0586	14q23.1
KIAA0753	KIAA0753	17p13.1
KIF7	Kinesin-like protein 7	15q26.1
MKS1	MKS1	17q22
MRE11	Double strand break repair nuclease	11q21
NPHP1	Nephrocystin 1	2q13
NPHP3	Nephrocystin 3	3q22.1
OFD1 or (CXOrf5)	Oralfaciodigital syndrome 1	Xp22.2
PDE6D	Phosphodiesterase 6D	2q37.1
RPGRIP1L	RPGRIP1L	16.q12.2
TCTN1	Tectonic-1	12q24.11
TCTN2	Tectonic-2	12q24.31
TCTN3	Tectonic-3	10q24.1
TMEM107	Transmembrane protein 107	17P13.1
TMEM138	Transmembrane protein 138	11q12.2
TMEM216	Transmembrane protein 216	11q12.2
TMEM231	Transmembrane protein 231	16q23.1
TMEM237	Transmembrane protein 237	2q33.1
TMEM67	Meckelin	8q22.1
TTC21B	Tetratricopeptide repeat protein 21B	2q24.3
ZNF423	Zinc finger protein 423	16q12

1.5.3. Clinical diagnosis of Joubert syndrome

Clinical diagnosis of JS is a difficult task since the clinical features of JS are overlapping with other neurological disorders. JS patients should undergo a neurological and neuro-ophthalmological examination to assess the motor system, cerebellar function and ocular motility as well as assessment of respiratory patterns (apnea and tachypnea). Family history and accurate health information about the patient should be collected and recorded (Bachmann-Gagescu et al., 2020). Presence of the MTS as a cardinal sign of cerebral malformations in JS is confirmed by brain MRI or CT scan (Enokizono et al., 2017; Maria et al., 1997). Abdominal ultrasound is used to detect hepatic fibrosis, polycystic kidney disease or other findings related to nephronophthisis (e.g., loss of corticomedullary differentiation). Hepatic fibrosis is suspected when there is an indication of hepatomegaly, elevated levels of hepatic enzymes or abnormal hepatic echogenicity. Liver function test (LFT) is recommended for JS patients even when they have no symptom of liver disease because they are at risk to develop a liver disease (Strongin et al., 2018), while renal function test (RFT) is recommended for JS patients who are asymptomatic or with a renal-related disease to monitor its progression (Fleming et al., 2017). The ophthalmological examination may include electroretinography (ERG), ocular motility test and visual-evoked potential (VEP) (Brooks et al., 2018). DNA sequencing by the Sanger sequencing or next-generation sequencing (NGS) methods are used to confirm or to rule out the diagnosis of JS. The number of genes in NGS panel for JS varies among different laboratories and it usually includes 25-36 genes (Table 1-1). Prenatal diagnosis and carrier testing are recommended for at risk-pregnancies and at-risk relatives, respectively, in families with history of JS. Genetic counseling is recommended prior to and after any genetic testing (Bachmann-Gagescu et al., 2020).

1.5.4. Treatment and management of Joubert syndrome

To date, there is no specific therapy for JS nor to alleviates its symptoms or improves its prognosis. A multidisciplinary approach is required for management of JS symptoms. Breathing difficulties in infants and children with JS may require use of mechanical ventilator, respiratory stimulants or rarely a tracheostomy. The patients may also benefit from speech therapy, physiotherapy, and rehabilitation program to cope with the developmental disabilities. Standard interventions are used to treat the hepatic and kidney disease associated with JS while surgery may be required for correcting polydactyly, ptosis and/or strabismus. Generally, annual follow up visits to a neurologist or a clinical geneticist is crucial to evaluate the prognosis of the disease and to treat the most frequent complications in patients with JS (Bachmann-Gagescu et al., 2020).

1.5.5. The role of primary cilia and signaling pathways in pathogenesis of JS

The extreme genetic heterogeneity and phenotypic variability seen in JS make understanding the pathogenesis of JS a daunting challenge. To date, 35 genes were identified to be associated with JS and all of them encode or interact with ciliary proteins. Intriguingly, JS genetically and clinically overlaps with other ciliopathies such as BBS, AC and MKS. This has led to intensive researches on the primary cilium and its roles in different cells and tissues, both under normal and abnormal conditions over the past two decades.

1.5.5.1. Primary Cilia

Cilia are microtubule-based projections from the cell surface of many cell types in both vertebral and non-vertebral organisms (Porter, 1955; Wheatley et al., 1996). The cilium structure consists of ciliary axoneme extending from a cylindrical-shaped microtubule-based structure known as the basal body and surrounded by a ciliary membrane (Satir, 2005). There are two types of cilia in human cells, the motile cilia and non-motile cilia which is commonly known as primary cilia. The ciliary axoneme is composed of microtubule bundles and is classified into 9 + 2 and 9 + 0 patterns based on the number of the microtubules (Fig.1-5). In the 9 + 2 axoneme, a central pair of singlet microtubules is surrounded by nine doublet microtubules, while in the 9 + 0 axoneme, the central pair is absent (Satir, 2005). Both motile and non-motile cilia can adopt the 9 + 2 or 9 + 0 configuration. There is a significant variation in the length of motile and primary cilia among different cell types ranging from 3-10 μm in epithelial cells to 200 μm in olfactory receptor neurons (Bernabé-Rubio & Alonso, 2017). Non-motile cilia lack cytoskeletal motor proteins known as dyneins, therefore, they are non-motile (King, 2016). In some types of cells such as epithelial cells, there are hundreds of motile cilia with the 9 + 2 pattern. In contrast, the fibroblasts and other types of mammalian cells exhibit a single copy of a primary cilium with the 9 + 0 pattern (Sorokin, 1962). In vertebrates, multiple motile cilia are present in the epithelial cells that line the inner surfaces of the respiratory tract, the Fallopian tubes and the brain ventricles (O'Callaghan et al., 1999). Continuous flow of secreted cerebrospinal fluid (CSF) through the brain ventricles and pulmonary mucous clearance are directed by a well-orchestrated beating of these *cilia.* The motile *cilia also function in left-right axis determination*, while the primary cilia are involved in the transduction of extracellular signals, regulation of cell division, development, and tissue regeneration (Goetz & Anderson, 2010).

1.5.5.2. Ciliogenesis

Ciliogenesis is a complex molecular assembly process by which the primary cilia and motile cilia are formed. The key event in ciliogenesis is docking of the basal body onto the plasma membrane through its distal appendages (Sorokin, 1962; Deane et al., 2001). The basal body emerges from the mother

centriole of the centrosome, and from which the axoneme arises. Each centrosome consists of two centrioles and each centriole comprises nine sets of microtubules doublets. In the S phase of cell cycle, the mother centriole assembles a daughter centriole, and they are arranged perpendicular to each other. The axoneme is the core microtubule structure of the primary cilium, and it extends from the basal body. It consists of nine doublet microtubules (9 + 0) surrounded by a membrane. The ciliary membrane continues with the plasma membrane, but it is distinct from the plasma membrane in its lipid and protein composition due to a diffusion barrier in the basal body known as the transition zone (TZ). The TZ regulates the traffic of specific molecules between the primary cilium and the cytoplasm (Endicott & Brueckner, 2018; Kozminski et al., 1993).

During cell cycle arrest in G_0 phase, the primary cilium extrudes from the surface of most mammalian cells. The axoneme invaginates the plasma membrane to be exposed to the extracellular environment. Cilia formation and maintenance relies on an efficient protein transport mechanism known as intraflagellar transport (IFT) (Pigino et al., 2009). During IFT, the IFT proteins associate to form protein complexes known as IFT particles or trains. The IFT machinery consists of two protein complexes: IFT-A complex and IFT-B complex with 6- and 12-subunits respectively. The IFT-A complex composed of IFT43, IFT121, IFT122, IFT139, IFT140, and IFT144, while the IFT-B complex includes, IFT20, IFT27, IFT46, IFT52,IFT55, IFT57, IFT72, IFT74 , IFT80, IFT81, IFT88, and IFT172 (Taschner et al., 2012; Behal et al., 2012; Cole & Snell, 2009). The outward and inward transports of the protein cargo in the ciliary axoneme are called anterograde and retrograde IFT respectively. The IFT system is mediated by two families of cytoskeletal motor proteins: kinesin and dynein for the anterograde and retrograde IFT, respectively (Rosenbaum & Witman, 2002). After docking onto the basal body, the IFT particles pass into the cilium and transport axonemal precursors from the basal body to the tip of the cilium where they reassemble and reverse direction back to the base carrying the cargo to be recycled (Rosenbaum & Witman, 2002; Scholey, 2008). Therefore, molecular defects in either the IFT system or cargo proteins may result in abnormal ciliogenesis (Wemmer & Marshall, 2007). In addition to the IFT system, primary ciliogenesis and ciliary function rely on formation of other protein complexes at the basal body and the TZ. Similar to the IFT machinery defects, malfunctions of many members of these complexes prevent normal ciliogenesis and transduction of extracellular signals and are associated with several ciliopathies (Valente et al., 2014). For example, defects in genes encode some of the TZ proteins mostly cause JS and MKS (Valente et al., 2010; Adams et al., 2012), whereas mutations in the basal body protein complex "BBSome" coding genes are associated with the pathogenesis of BB (Wei et al., 2012). Relative to other cellular compartments, the primary cilium processes a little volume but a higher plasma membrane to cytosol ratio that provides the ciliary membrane the capacity to occupy a large number

of receptors (Sterpka & Chen, 2018). This makes primary cilia extremely sensitive to extracellular signals and to serve as 'cellular antennae' to detect the extracellular signals (Lee & Gleeson, 2010; Goetz & Anderson, 2010; Singla & Reiter, 2006). ADP-ribosylation factor-like protein 13B (ARL13B) is a ciliary membrane protein and it was demonstrated to be essential for cilia structure and sonic hedgehog (SHH) signal transduction. A null mutation of *Arl13b* shortens the primary cilia and causes defects in Shh signaling cascade in mice (Larkins et al., 2011; Caspary et al., 2007).

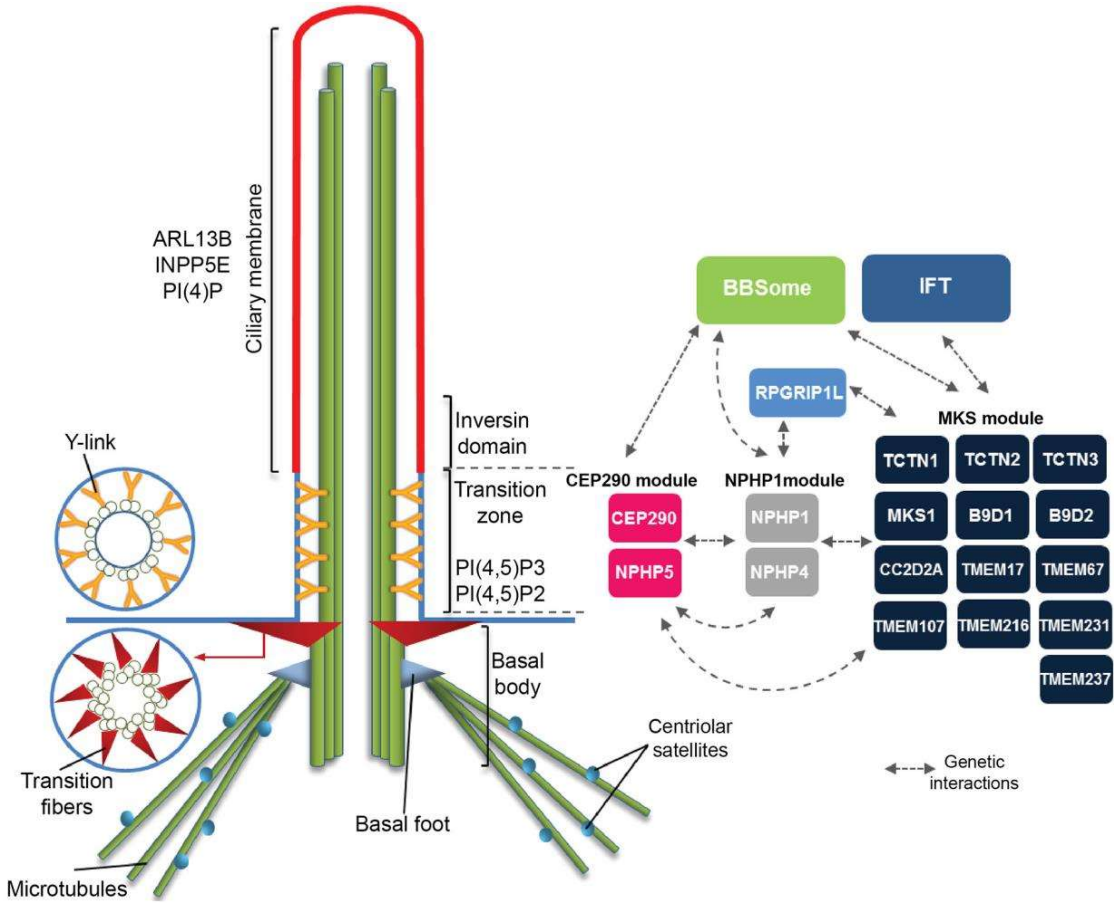

Figure 1-4. Schematic representation of the structure of primary cilium and the protein complexes associated with its assembly and functions. Adapted from 'The Ciliary Transition Zone: Finding the Pieces and Assembling the Gate', by Gonçalves & Pelletier, 2017, *Molecules and cells*, 40(4), 243–253.

1.5.5.3. Primary cilium disassembly

Primary cilium disassembly is associated with cell cycle progression, but little is known about the mechanisms governing this process as compared to its assembly. Several studies on mammalian primary cilia and *Chlamydomonas* motile cilia suggest that cilium assembly occurs during G_0 phase of cell cycle and it is disassembled independently of retrograde IFT and length (Engel et al., 2012; Marshall et al., 2005; Kozminski at al., 1995), shortly before mitosis (Avasthi & Marshall, 2013;

Archer & Wheatley, 1971). Hilton and colleagues demonstrated that CNK2, a member of NIMA-related protein kinases family in Chlamydomonas, plays a role in regulation of flagellar length and disassembly. In cnk2-1 mutant cells, delay in flagellar disassembly results in mild long flagella (Hilton et al., 2013). At the basal body, primary cilium loss is induced through activation of Aurora-A kinase (AURKA) by HEF1(a member of scaffold proteins family), Ca^{2+} and calmodulin. AURKA triggers the histone deacetylase 6 (HDAC6) by phosphorylation leading to de-acetylation of the axonemal tubulins (Plotnikova et al., 2012; Pugacheva et al., 2007). A recently published report on primary cilium disassembly in mammalian cells revealed that rapid deciliation and gradual resorption of cilium are the major modes of primary cilium loss. Gradual resorption at some point prior to rapid deciliation was also observed in cultured cells, however, rapid deciliation is thought to be the predominant mechanism of cilium disassembly due to ability to recover whole cilia from cultured medium that retain the same length (>1.5 μm) and axonemal and ciliary membrane proteins. It was demonstrated that elevated levels of katanin, a deciliation mediator, induces deciliation independently of intracellular Ca^{2+} (Mirvis et al., 2019).

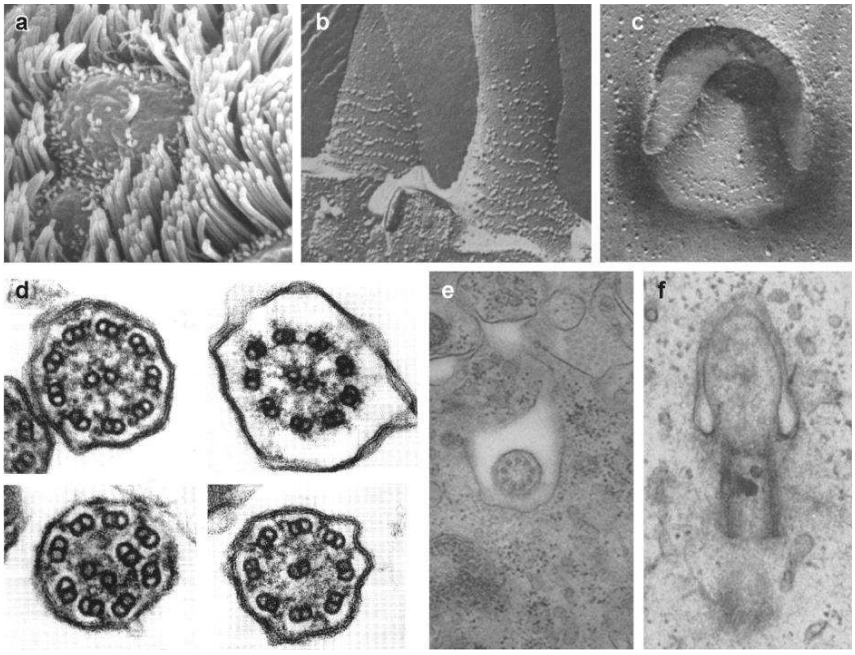

Figure 1-5. Scanning electron microscopy (SEM) images of primary cilia. (a) The SEM image shows a solitary primary cilium in the central cell and surrounding cells with multiple motile cilia of a mouse oviduct (a), multi-stranded ciliary necklace of motile tracheal cilia by the freeze-etching technique (b), ciliary necklace of a fibroblast primary cilium (c), cross sections of 9 + 2 axoneme of a normal human motile cilium (top left) and primary cilia axonemes from primary ciliary dyskinesia (PCD) (d). Cross section of a non-motile fibroblast primary cilium (e), and initial step of fibroblast primary cilium formation (f). (Ciliary diameter in (d) = 0.25 μm). Adapted from 'Overview of structure and function of mammalian cilia', by Satir & Christensen, 2007, *Annu. Rev. Physiol.,* 69, 377-400.

1.5.5.4. Stem cell primary cilia

Presence of primary cilia in human embryonic stem cells (hESCs) was first demonstrated by Kiprilov and colleagues who showed that the hESCs primary cilia possess the key components of the Shh signaling pathway such as patched 1 (Ptch1), smoothened (Smo) and glioma zinc finger transcription factors (Gli1, Gli2 and Gli3) (Kiprilov et al., 2008). When the pathway is stimulated by smoothened agonist (SAG), Smo and Ptch1 move into and out of the primary cilium, respectively, while Gli1 and Ptch1 are upregulated. These findings are consistent with results from a previous study on two hESC lines (Miz-hES1and SNU-hES3) which revealed high expression of Ptch1 and Smo, and upregulation of Gli1, Gli2 and Gli3 (Rho et al., 2006). Another study has demonstrated that in the absence of exogenous morphogens, neural progenitors differentiated from (hESCs) show ventral and dorsal telencephalic phenotypes due to coordinated Shh and Wnt signaling pathways (Li et al., 2009). Several reports have shown that the IFT proteins in the primary cilium are required for the Shh signaling pathway in mouse and zebrafish embryos. Huangfu and Anderson (2005) demonstrated that in mouse embryos, lack of *Ift172* induces loss of Shh signaling in the neural tube. It has also been demonstrated that SHH signaling pathway in mouse are negatively modulated by THM1 (tetratricopeptide repeat-containing hedgehog modulator-1) which affects retrograde IFT machinery in cilia (Tran et al., 2008).

Both motile and non-motile cilia were shown to be present in a variety of tissues of zebrafish and play essential role during embryonic development (Malicki et al., 2011; Liu et al., 2005). However, most of cells in the zebrafish embryo possess a solitary non-motile cilium with the 9 + 0 structural pattern (Song et al., 2016). Mutations in *Ift27* in zebrafish cause kidney cysts and abnormal retrograde transport (Aldahmesh et al., 2014; Huet et al., 2014). Interestingly, the presence of primary cilia and key proteins involved in the Shh signaling pathway in human induced pluripotent stem cells (hiPSCs) were also reported (Nathwani et al.,2014) and consistent with the previous reports on hESCs and mouse and zebrafish embryos (Malicki et al., 2011; Kiprilov et al., 2008; Huangfu & Anderson, 2005). The transmembrane receptors Smo, Ptch1, Gli1, and Gli2 were highly expressed in the hiPSCs as compared to the parental fibroblasts, while expression of Shh remained relatively constant after the reprogramming. The authors suggest that reprogramming of the fibroblasts alters the morphological features of primary cilia by demonstrating that the length of the primary cilia significantly decreased by 1 micron, while its curvature increased by approximately 4-fold (Nathwani et al., 2014).

1.5.5.5. Neuronal primary cilia

A solitary primary cilium exists in most brain cells including neural stem cells, neurons, and astrocytes (Fig. 1-6) (Del Cerro & Snider, 1969). It has been demonstrated that *de novo* ciliogenesis is absent in mature neurons due to their non-dividing nature (Sterpka & Chen, 2018). The fact that many ciliopathies are associated with neurological deficits drew attention to the critical role of primary cilia in neurodevelopmental processes. Although existence of neuronal primary cilia was first reported over 50 years ago (Dahl, 1963; Sjöstrand, 1953), but their function in the CNS remained unclear and unexplored until the discovery of some G protein-coupled receptors (GPCRs) selectively localized in neuronal primary cilia, namely somatostatin receptor 3 and serotonin receptor 6. These results suggest the role of neuronal primary cilia in activation of signaling pathways in response to sensory inputs to the brain (Brailov et al., 2000; Händel et al., 1999).

Type 3 adenylyl cyclase (AC3) is predominantly enriched in neuronal primary cilia in brain of adult mouse (Sterpka & Chen, 2018; Kasahara et al., 2015) and is important for the cyclic adenosine monophosphate (cAMP) signal transduction in olfactory sensory cilia (Qiu et al., 2016). Using double transgenic Arl mice to investigate the length of neuronal and astrocytic primary cilia in the CA1, CA3 and DG hippocampal regions revealed that the transgenic mice showed Arl13b-positive and AC3-positive neuronal cilia longer than in the FVB/N and C57BL/6 control mice. Similarly, the length of Arl13b-positive astrocytic primary cilia was nearly doubled when compared to the C57BL/6 control. It was also shown that the length of astrocytic and neuronal primary cilia in the hippocampus was shorter in Arl mice with a history of spontaneous seizures than in Arl mice without a history of seizures (Sterpka et al., 2020). In mouse embryos, neuronal ciliogenesis initiates with a pro-cilium after neuronal cells migration and docking of their mother centrioles to the cell membrane forming the cilium basal body. Maturation of the pro-cilium requires 8-12 weeks postnatal (Arellano et al., 2012). During this period the ciliary membrane is equipped with several receptors including somatostatin receptor 3 (SSTR3) serotonin receptor 6 (5HTR6), melanin-concentrating hormone receptor 1 (MCHR1), kisspeptin 1 receptor (KISS1R) and dopamine receptors 1, 2, and 5 (Wheway et al., 2018).

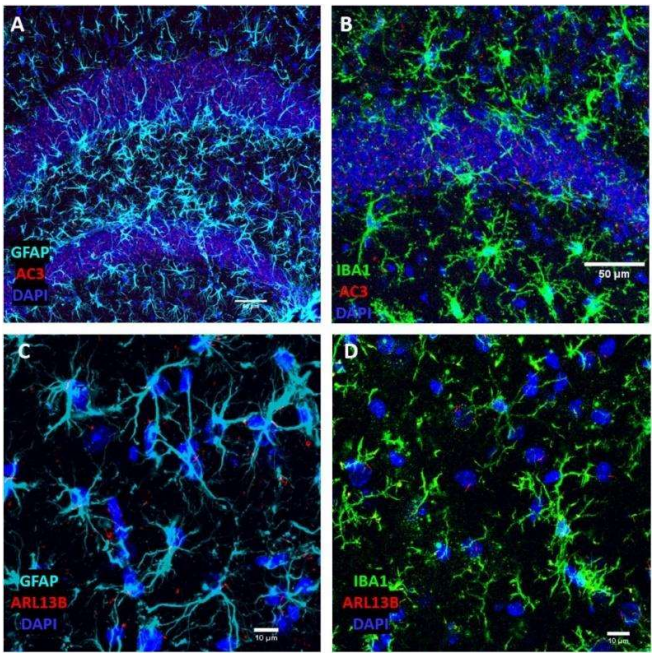

Figure 1**-6. Neuronal and astrocytic primary cilia derived from a mouse hippocampus.** Immunostaining images show neuronal primary cilia stained with AC3 (A), and astrocytic primary cilia stained with RL13B (C). AC3- and ARL13B-stained primary cilia are absent in IBA1-marked microglia **(B & D).** Adapted from 'Neuronal and astrocytic primary cilia in the mature brain', by Sterpka & Chen, 2018, *Pharmacological research, 137*, 114-121.

1.5.5.6. Sonic Hedgehog (Shh) Signaling Pathway in Joubert syndrome

Sonic hedgehog (Shh) signaling pathway is one of the major signaling pathways in human and many other living organisms. It was first identified in *Drosophila* when the hedgehog *(Hh)* gene found to be essential for development of *Drosophila* larva (Nüsslein-Volhard & Wieschaus, 1980). In mammals, there are three homologues of Hh namely: Sonic Hh (SHH), Indian Hh (IHH) and Desert Hh (DHH). Despite the variation in their structures and expression pattern, all the Hh homologues bind similar receptors to trigger downstream signaling cascades (Theunissen & de Sauvage, 2009). The Shh signaling pathway is essential for regulation of embryogenesis, cell differentiation, cell proliferation, tissue polarity and adult tissue homeostasis (Chen et al., 2018; Katoh & Katoh, 2006). Abnormal Shh signaling pathway was identified in several types of cancer such as gastric cancer (Yu et al., 2020), basal cell carcinoma, medulloblastoma (Jiang & Hui, 2008) and lukemia (Rubin & de Sauvage, 2006). The role of primary cilium machinery in Shh signaling pathway in mammals has been investigated extensively, and it has been revealed that the primary cilium is vital for Shh signaling pathway (Ocbina & Anderson, 2008; Rohatgi et al., 2007; Corbit et al., 2005; Haycraft et al., 2005; Huangfu et al., 2003). The major players in the Shh signaling pathway are the transmembrane receptors Ptch1, Smo, Gli1, Gli2, and Gli3 (Zeng et al., 2010). When the Shh ligand is absent, Smo activity is repressed and it is prevented to be localized to the cilium due to localization of the transmembrane receptor Ptch1 to the cilium basal body. The suppressor of fused (SuFu), a

negative regulator of the Shh signaling pathway, suppresses the Gli transcription factors by forming SuFu-Gli complexes which prevent translocation of Gli proteins into the nucleus (Zeng et al., 2010). Binding of Shh ligand to Ptch1 releases Smo to be activated and associated with kinesin family member 3A (Kif3A), a subunit of kinesin motor complex, to reach the tip of the primary cilium (Goetz et al., 2009). Before its association with Kif3A, Smo binds GRK2 to be phosphorylated and stabilized (Chen et al., 2010). It is delivered from the tip of the primary cilium into its membrane where it accumulates by Rab-dependent vesicle trafficking (Eggenschwiler et al.,2006). This represses SuFu and promotes dissociation of SuFu-Gli complexes. The dissociated Gli transcription factors are then transported from the tip of primary cilium to the nucleus where they involve in activation of transcription (Ryan & Chiang, 2012). The core components of Shh signaling are transported into and out of the cilium by the IFT transport system previously mentioned in (1.5.5.2). Dysfunction of the IFT proteins downregulates Ptch1 expression and with help of kinesin family member 7 (KIF7), an anterograde IFT motor protein, Gli2 and Gli3 accumulate at the tip of the cilium (Pedersen & Akhmanova, 2014; Qin et al., 2011). It is also important to mention that Gli proteins are not only deactivated by SuFu, but other proteins are involved in inhibition of Shh signaling pathway such as protein kinase A (PKA) and glycogen synthase kinase 3 beta (GSK3B). Activation of PKA and GSK3B prevents SuFu-Gli complexes to be localized in the primary cilium and blocks their dissociation by Shh signals (Zeng et al., 2010; Kise et al., 2009).

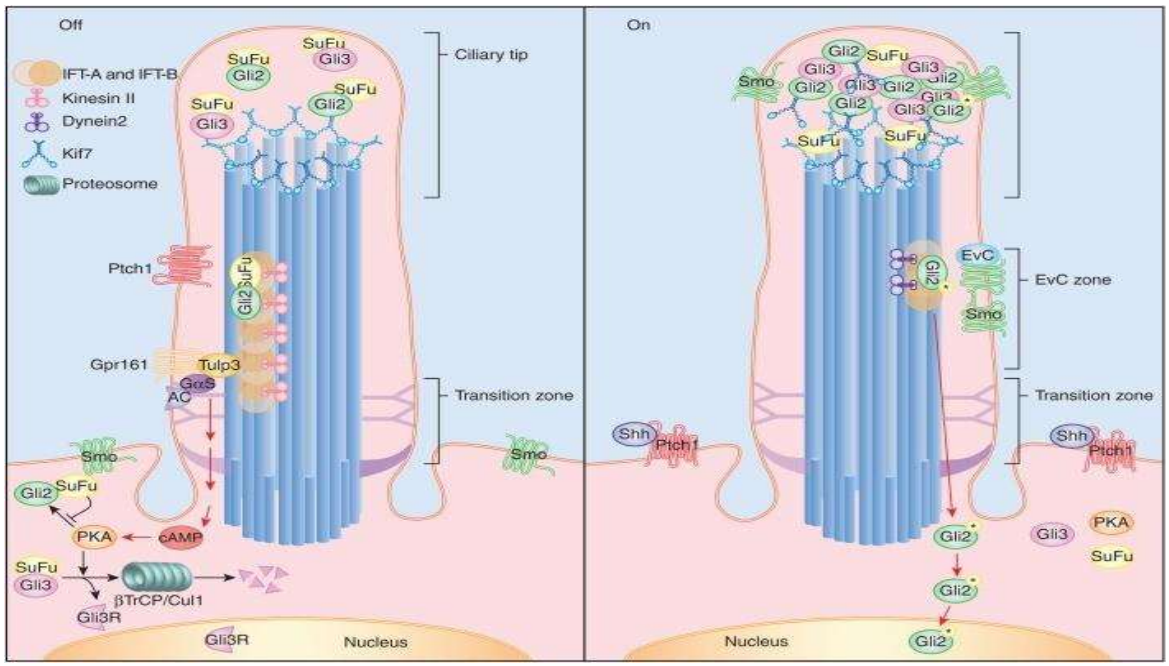

Figure 1.7. Sonic hedgehog (SHH) signaling pathway in the primary cilium. Schematic presentation shows SHH signaling pathway in the absence of SHH ligand (left) and in the presence of SHH ligand (right). Adapted from 'Primary Cilia and Mammalian Hedgehog Signaling', by Bangs et al., 2017, *Cold Spring Harbor Perspectives in Biology,* 1;9(5): a028175.

1.5.5.7. Wnt/β-catenin signaling pathway in Joubert Syndrome

Canonical Wnt/β-catenin signaling signal transduction pathway is a fundamental pathway in embryogenesis, tissue development and homeostasis (Logan & Nusse, 2004). It stabilizes and localizes β-catenin in the nucleus to activate the target genes (Fig. 1-8). In the absence of a Wnt signal, multiple proteins including the scaffold protein Axin, β-transducin repeat-containing protein (β-TrCP), the serine/threonine kinases CK1 and GSK-3, protein phosphatase 2A (PP2A) and adenomatous polyposis coli (APC) protein work together to degrade the β-catenin (Clevers et al., 2006). A defined β-TrCP recognition site on β-catenin is specified by this protein complex through phosphorylation of its N-terminal serine/threonine that is coordinated by Axin (Verheyen & Gottardi, 2010). The phosphorylated and ubiquitinated β-catenin is destructed by the proteasome. This degradation permits nuclear translocation and binding of the transcriptional corepressor Groucho to T cell factor (TCF) to eventually repress transcription of Wnt targets (Cavallo et al., 1998). Activation of Wnt/β-catenin pathway is initiated upon binding of Wnt to the transmembrane receptors Frizzled (FZD) and lipoprotein receptor-related protein (LRP). *Dishevelled* (Dvl) protein - a potential key player in activation of the pathway- is recruited to the plasma membrane when FZD is activated. This leads to dissociation of the destruction complex and stabilization of β-catenin to be translocated to the nucleus where it binds the TCF and upregulates the target genes (Lienkamp et al., 2012).

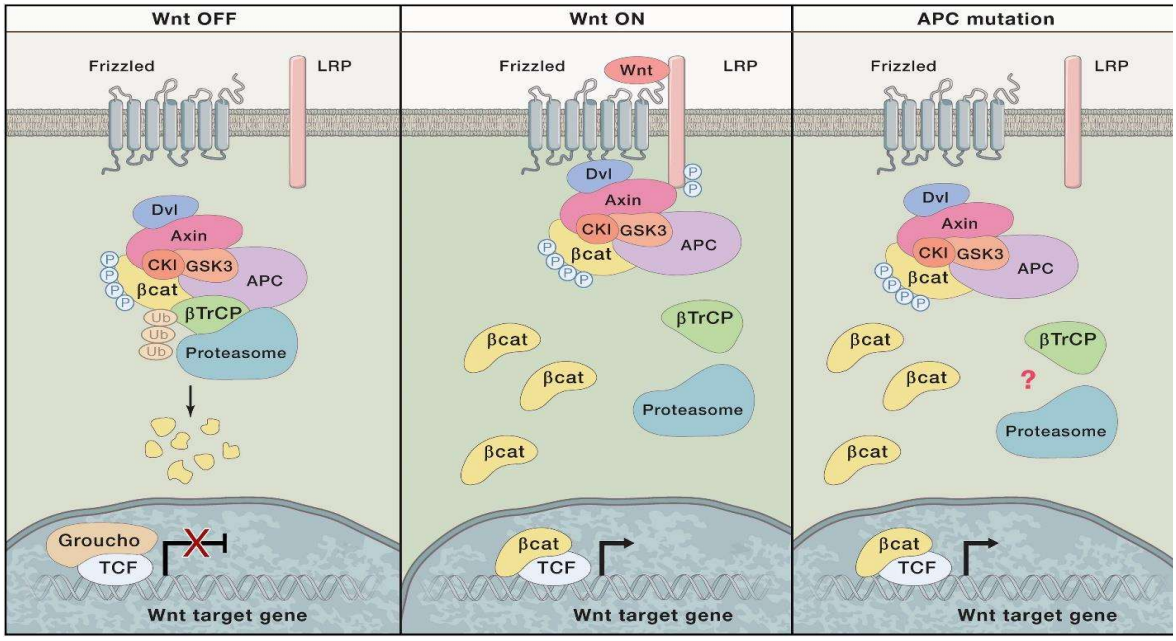

Figure 1-8. Wnt/β-catenin signaling pathway in mammalian cells. Schematic presentation shows Wnt binds to its transmembrane receptors and activates the signaling pathway (left), activation of the signaling pathway (Center), and defective APC activates the pathway by disrupting the destruction complex (right). Adapted from 'Wnt/β-catenin signaling, disease, and emerging therapeutic modalities', by Nusse & Clevers, 2017, *Cell, 169(6),* 985-999.

Dysregulation of this pathway leads to several pathogenic conditions including colon cancer, cardiovascular diseases, and some ciliopathies (Flores-Hernández et al., 2020; Kuckhahn et al., 2020; Nusse & Clevers, 2017; Valente et al., 2014). Generally, the role of primary cilia in activation of canonical Wnt/β-catenin signal transduction cascade remains - to some extent -controversial. Some reports support the hypothesis that primary cilia are associated with Wnt/β-catenin signaling, however, other studies contradict this hypothesis. Normal canonical and non-canonical Wnt signaling have been shown in IFT mutant zebrafish and mice indicating that primary cilia are not indispensable for Wnt signaling (Ocbina et al., 2009; Huang & Schier, 2009). On the contrary, other studies have reported that ciliary defects over-activate Wnt/β-catenin signaling in mouse and *in vitro* models (Abdelhamed et al., 2013; Wheway et al., 2013; Cano et al., 2004; Lin et al., 2003), while deactivation of Wnt/β-catenin signaling in *Ahi1* mutant mice causes cystic kidney disease (Lancaster et al., 2009). Furthermore, Lancaster and colleagues have demonstrated that jouberin, a protein encoded by the *AHI1* gene and involved in JS, plays a positive role in regulation of canonical Wnt/β-catenin signaling cascade by facilitating nuclear translocation of β-catenin. The role of primary cilium in this process is to sequester β-catenin and jouberin in the ciliary compartment, limiting their translocation into the nucleus (Lancaster et al., 2011). Involvement of this signaling pathway in neurodevelopment could partly explain the neurological defects in JS when this pathway is disrupted (Salinas., 2012).

Despite the contradictory results on the role of primary cilia in canonical Wnt/β-catenin signaling, normal ciliogenesis is thought to be essential for the planar cell polarity (PCP) non-canonical Wnt signal transduction (Gomez-Orte et al., 2013). Cell polarity in this process is achieved through the basal body migration to the apical cell surface (Jones et al., 2008). Therefore, abnormalities of proteins involved in initiation of cilia assembly results in defective PCP (Wheway et al., 2018). Several proteins have been identified to be essential for non-canonical Wnt signal transduction such as Dvl, Inversin, the basal body protein MKS1 and the TZ proteins TMEM67, TMEM237 and TMEM216 (Park et al., 2008; Simons et al., 2005). Defects in *MKS1*, *TMEM67,* and *TMEM216* are associated with JS and MKS (Valente et al., 2010; Adams et al., 2012).

1.5.5.8. B9/tectonic-like complex

As previously mentioned, the TZ is a diffusion barrier at the base of the primary cilium that selectively regulates the transport and localization of certain ciliary proteins between the cytosol and the primary cilium (Endicott & Brueckner, 2018). Many proteins are localized at this region including a protein network known as the B9 or tectonic-like complex. This protein network consists of at least 15 proteins including AHI1, B9D1, B9D2, CC2D2A, CEP290, TCTN1, TCTN2, TCTN3, TMEM17, TMEM67, TMEM216, TMEM231, TMEM237, and TMEM138 (Okazaki et al., 2020; Gonçalves &

Pelletier, 2017). All these proteins except TMEM17 are associated with JS and/or other ciliopathies. The B9/tectonic-like complex was demonstrated to prevent the passage of certain proteins through the TZ and simultaneously promotes the diffusion of specific proteins including Arl13b, AC3, Smo and Pkd2 into the ciliary compartment (Garcia-Gonzalo et al., 2011). Furthermore, the authors have shown that in *C. elegans*, Tctn1 controls the localization of Mks1 and Tmem67 to the TZ. The relationship between ciliogenesis and B9 complex has been studied both *in vitro* and *in vivo*, and revealed that defects in any component of the complex lead to reduction in ciliogenesis, loss of ciliary receptors and abnormal Shh signaling in the remaining cilia. As a consequence of disrupted B9 complex, the diffusion rate of proteins into the cilium increases (Chih et al., 2011). A recent study has revealed presence of other TZ protein modules in *Paramecium tetraurelia* namely the MKS, NPHP and CEP290 (Gogendeau et al., 2020). These results are consistent with those previously reported on TZ proteins in *C. elegans* and mouse models (Chih et al., 2011; Garcia-Gonzalo et al., 2011; Sang et al., 2011), suggesting that dysfunction of the TZ may cause JS and related ciliopathies. Interestingly, bioinformatic analyses of the TZ proteins in both ciliated and non-ciliated eukaryotic organisms revealed a core group of proteins conserved in >50% of all ciliated organisms examined in each subgroup. Out of 19 proteins analyzed, the conserved group of TZ proteins comprises CC2D2A, AHI1, B9D1, B9D2, TMEM67 and a single TCTN family member. The MKS1 protein is also thought to be a member of the core group of proteins, due to its presence in >50% of all supergroups except in Rhizaria (Barker et al., 2014).

1.5.5.9. BBSome complex

BBSome is a protein complex composed of BBIP10 protein and seven BBS proteins: BBS1, BBS2, BBS4, BBS5, BBS7, BBS8, and BBS9. It is localized at both the tip and basal body of the primary cilium and involved in ciliogenesis by regulating IF transport processes (Jin & Nachury, 2009; Nachury et al., 2007). It has been demonstrated that the BBSome regulates the assembly of IFT complexes at the basal body, before moving to the ciliary tip using the IFT-B machinery. At the ciliary tip, the BBSome complex rearranges the IFT complexes to form the IFT-A machinery for the retrograde transport (Wei et al., 2012). Proper trafficking of signaling molecules, structural proteins and receptors such as G-protein-coupled receptors (GPCRs) along the ciliary axoneme requires proper assembly of the IFT complexes. Thus, defects of BBS proteins lead to abnormal ciliogenesis and signal transduction, and eventually result in defective developmental pathways (Zhang et al., 2012; Nachury et al., 2007).

The current knowledge on the mechanisms underlying the pathogenesis of JS is gained mainly from studies on mouse, zebrafish and *in vitro* models (Zhang et al., 2012; Garcia-Gonzalo et al., 2011; Lancaster et al., 2009; Nachury et al., 2007; Park et al., 2008) These models have constructive contributions to the advancement of knowledge in the biomedical fields. Even though they are widely used for translational research, there are still some technical and ethical challenges to obtain relevant animal or cell line models. For example, the intrinsic complexity of these organisms varies from that of humans and may affect differently the genetic modification introduced. Moreover, the gene of interest may not be available in the animal model, certain human cell lines such as neurons and cardiomyocytes are difficult to be obtained from the human body and the use of hESCs poses ethical issues (King & Perrin, 2014; Houdebine, 2007; Hackam & Redelmeier, 2006). Some of these challenges lead to discrepancies between the data generated from animal models and humans and may not allow extrapolating the data generated from animals to humans and drawing clear conclusions (Perel et al., 2007). The emergence of the iPSCs technology and the advancement in genome editing approaches provide promising tools for translational research by establishing human isogenic cell lines with hESC-like characteristics.

1.6. Development of induced pluripotent stem cells (iPSCs) technology

Modeling human diseases using primary patient-derived cells is of great importance for investigating the etiology of human diseases and for developing tailored therapeutic strategies. However, one of the limitations of this disease modeling approach was the inability to find expandable sources of certain types of patient's primary cells, especially difficult-to-access cells such as cardiomyocytes and neurons (Shi et al., 2017). The development of iPSCs technology has solved this problem by providing different cell types and disease-specific cells that were inaccessible (Branco et al., 2020; Ban et al., 2013). Stem cells have a potential of self-renewal and differentiation into specific cell types. The concept of self-renewal is the ability of the cells to undergo infinite cell divisions without differentiation into other cell types, while pluripotency is the ability of the cells to produce specialized cells of the three embryonic layers: ectoderm, mesoderm, and endoderm (Niwa, 2007). Several types of pluripotent stem cells (PSCs) have been studied including ESCs, embryonic germ cells (EGCs), embryonic carcinoma cells (ECCs) and iPSCs (Takahashi &Yamanaka, 2006; Rohwedel et al., 1996; Andrews, 1984).

The establishment of iPSCs technology was based on numerous research findings in the last century starting from 1962 when John Gurdon and his associates had reprogrammed unfertilized eggs to generate tadpoles by transferring a nucleus obtained from intestinal cells of adult frogs (Gurdon et

al., 1962). In 1997, a furious debate had ignited by the cloning of Dolly the sheep by somatic cell nuclear transfer (SCNT) as the first mammal to be generated by this method (Wilmut et al., 1997). In the beginning of the second millennium, a research team led by the Japanese scientist Takashi Tada demonstrated that ESCs possess factors that can revert back somatic cells to ESC-like cells (Tada at al., 2001). These discoveries showed that the genetic information required for the development of an organism is present even in non-germinal cells and somatic cells nuclei can be reprogrammed by factors contained in oocytes. In 1987, a new concept known as master transcription factors was generated from the researches on antennapedia and *MyoD*, a *Drosophila* and mammalian transcription factors respectively. The ectopic expression of antennapedia induces development of legs instead of antenna in the *Drosophila* (Schneuwly et al., 1987), while *MyoD* differentiates fibroblasts into myocytes (Davis et al., 1987). The first *in vitro* generation of mouse ESCs (Evans & Kaufman, 1981) and human ESCs (hESCs) (Thomson et al., 1998) and improvements in cell culture conditions that maintain the pluripotency of these cells in addition to all the previous discoveries have paved the way for a breakthrough discovery by Shinya Yamanaka and Kenji Takahashi. They identified four transcription factors that can induce generation of PSCs from mouse fibroblasts when introduced by retroviral vectors (Fig. 1-9) (Takahashi & Yamanaka, 2006). These transcription factors are known as *Yamanaka factors* and abbreviated as OSKM namely: *OCT3/4, SOX2, KLF4,* and *c-MYC*. The homeodomain transcription factor OCT3/4 (octamer-binding transcription factor 4), also known as POU5F1, is involved in self-renewal and differentiation of PSCs (Jaenisch & Young, 2008; Takahashi & Yamanaka, 2006). SOX2 (SRY-box transcription factor 2) is important for maintenance of pluripotency in iPSCs, ESCs, and neural stem cells (NSCs) (Zhang & Cui, 2014; Takahashi & Yamanaka, 2006) and it also controls the expression of OCT3/4 (Masui et al., 2007). The combination of OCT3/4, SOX2 and Nanog represents the essential transcriptional players for pluripotency. The proto-oncogene c-MYC is also considered as being important for proliferation of stem cells, maintenance of pluripotency and inhibition of primitive endoderm formation (Smith et al., 2010; Takahashi & Yamanaka, 2006). Although generation of iPSCs without exogenous introduction of c-MYC has been reported suggesting that c-MYC is dispensable for reprogramming of somatic cells (Nakagawa et al., 2008; Wernig et al., 2008; Yu et al., 2007), other studies have shown that ectopic c-MYC plays a crucial role in maintaining pluripotency of iPSCs both *in vitro* and *in vivo* and its absence may reduce the efficiency of reprogramming (Smith et al., 2010; Varlakhanova et al., 2010). Klf4 (Kruppel-like factor 4) promotes somatic cell reprogramming through direct interaction with OCT3/4 and SOX2 (Wei et al., 2009; Takahashi & Yamanaka, 2006). Nevertheless, the precise mechanisms govern and coordinate these transcription factors to reprogram somatic cells into iPSCs remain largely unclear.

The generated iPSCs from mouse fibroblasts were morphologically similar to ESCs (Fig. 1-9) and they expressed some ESCs marker genes besides exhibiting some ESCs characteristics such as differentiation into all three germ layers and teratoma formation (Takahashi & Yamanaka, 2006). However, some variations between iPSCs and ESCs have been reported specifically in global gene expression, ability to produce adult chimaeras and DNA methylation (Chin et al., 2009; Deng et al., 2009; Doi et al., 2009). In contrast, overlapping variations in gene expression in both iPSC and ESC clones have been demonstrated making it difficult to distinguish iPSCs from ESCs by gene expression or DNA methylation. These variations were partly attributed to differences in induction and culture conditions used by different research laboratories (Guenther et al., 2010; Newman & Cooper et al., 2010). Furthermore, the number of clones compared in reports that showed variations in either gene expression or DNA methylations was relatively small (<10/group), while more clones analyzed from several laboratories showed that distinguishing iPSCs from ESCs was difficult. Somatic mutations, copy number variations (CNVs), and immunogenicity are other potential defects in iPSCs (Gore et al., 2011; Martins-Taylor et al., 2011; Hussein et al., 2011; Zhao et al., 2011), however, several studies have shown that these genetic variations in iPSCs seem to pre-exist in the parental somatic cells and are independent from the reprogramming process (Cheng et al., 2012; Young et al., 2012). One year after Yamanaka achievement, germline-competent iPSCs were successfully generated from mouse fibroblasts (Okita et al., 2007) and human somatic cells by two independent research teams (Takahashi et al., 2007; Yu et al., 2007). Yamanaka research group used the same four transcription factors *OCT3/4, SOX2, KLF4,* and *c-MYC* to generate human iPSCs from human fibroblasts while the other research group demonstrated that *NANOG* and *Lin28* can replace *KLF4* and *c-MYC* for reprogramming of somatic cells into iPSCs. Since then, extensive researches have been carried out to generate iPSCs from diverse populations of human somatic cells. To avoid vector integration into the genome of the host, several approaches have been developed (Table 1-2) including synthesized RNA (Warren et al., 2010), adenovirus (Stadtfled et al., 2008), plasmid (Okita et al., 2011), minicircles (Jia et al., 2010), removable PiggyBac transposons (Woltjen et al., 2009), proteins (Kim et al., 2009), Sendai virus (Fuskai et al., 2009) and small molecules (Hou et al., 2013). The quality of the iPSC clones may vary due to the combination of transcription factors, gene delivery approaches and culture conditions used. Additionally, stochastic events during reprogramming of somatic cells may contribute to some extent to the variation between the generated iPSC clones. Therefore, it is crucial to evaluate and select the iPSC clones that are suitable to be expanded and utilized for medical applications (Yamanaka, 2012).

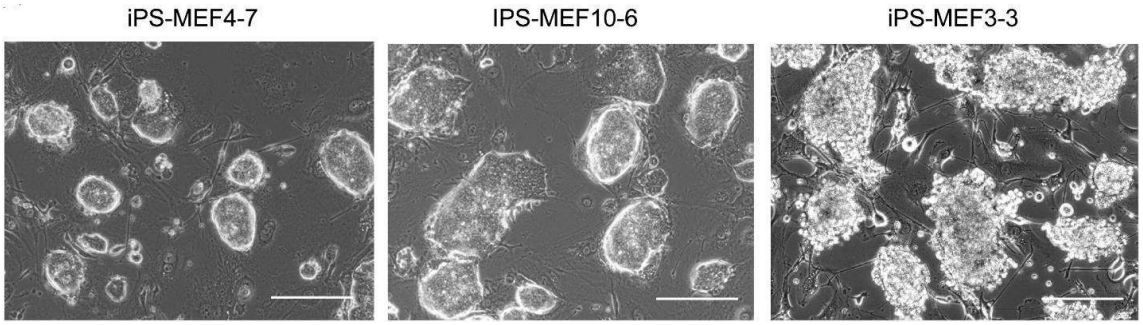

Figure 1-9. **Morphologies of three clones of the first induction of mouse PSCs from mouse embryonic and adult fibroblasts.** Scale bars correspond to 200 µm. Adapted from 'Induction of Pluripotent Stem Cells from Mouse Embryonic and Adult Fibroblast Cultures by Defined Factors', by Takahashi & Yamanak., 2006, *cell, 126(4),* 663-676.

Table 1-2. Reprogramming approaches used to generate iPSCs from human somatic cells

Method	Integrating*	Time(days)	Efficiency (%)#	Multiple cell types reprogrammed
Retroviral	Yes	25–35	0.02–0.08	Yes
Lentiviral	Yes	20–30	0.02–1	Yes
Lentiviral (miRNA)	No	18–26	10.4–11.6	No
miRNA (direct transfection)	No	20	0.002	Yes
Adenoviral	No	25–30	0.0002	No
Sendai virus	No	25	0.5–1.4	Yes
mRNA	No	20	0.6–4.4	No
Protein	No	56	0.001	No
Episomal	No	30	0.0006–0.02	Yes
Piggybac	Yes	14–28	0.02–0.05	No
Minicircles	No	14–16	0.005	No

*For all integrating methods there are strategies available to remove integrated sequences. #All efficiencies are for human cells only. Adapted from 'Assessing iPSC reprogramming methods for their suitability in translational medicine', by Rao & Malik., 2006, *Journal of cellular biochemistry, 113(10),* 3061-3068.

Simplicity and reproducibility are the attractive features of the iPSCs technology and have attracted the biomedical scientists to generate and differentiate iPSCs from numerous normal and disease-specific cell types for disease modeling and drug screening applications. The promising medical applications of this technology have led Shinya Yamanaka and John Gurdon to win the Nobel Prize in Physiology or Medicine in 2012 (The Noble Foundation, 2012). Initially the efficiency of the reprogramming process was low (0.01% - 0.02% of transfected cells converted into iPSCs) (Yoshida & Yamanaka., 2017; Yamanaka., 2012, Takahashi et al., 2007), however, addition of some chemical compounds such as histone deacetylase inhibitors, sodium butyrate and valproic acid (Mali et al., 2010; Huangfu et al., 2008) as well as modification of other culture conditions such as hypoxic cultivation was found to enhance the reprogramming efficiency (Yoshida et al., 2009). Other factors have been demonstrated to improve the generation of iPSCs and include Glis1 (Glis family zinc finger 1), H1foo (a gene encodes histone H1oo protein) (Kunitomi et al., 2016; Maekawa et al., 2011) and inhibitors of the p53 pathways or Mbd3 (methyl binding domain 3) a core component of the Mbd3/NuRD (nucleosome remodelling and histone deacetylation) repressor complex (Rais et al., 2013; Hong et al., 2009).

1.7. Potential clinical applications of iPSCs

1.7.1. iPSC-based disease modelling

The use of patient-derived iPSCs in disease modeling provides a potential source of disease-specific stem cells that allow researchers to recapitulate human diseases *in vitro* and to investigate their pathogenesis (Fig.1-10). The first disease-specific iPSC lines were developed by two independent research groups. Dimos et al. (2008) generated iPSCs from a female with amyotrophic lateral sclerosis (ALS), a progressive late-onset neurodegenerative disease that affects motor neurons in the CNS, while the other research group developed multiple disease-specific iPSC lines derived from patients with Mendelian and multifactorial disorders including Duchenne muscular dystrophy (DMD), Gaucher disease (GD) type III, Huntington disease (HD), juvenile-onset, type 1 diabetes mellitus (JDM) and Parkinson disease (PD) (Park et al., 2008). Since then, numerous laboratories have reported the generation of disease-specific iPSCs from patients' somatic cells and their differentiation into disease-relevant cell types to recapitulate disease phenotypes. iPSCs generated from somatic cells of healthy individuals are used as controls for patient-specific iPSCs. Although iPSCs have a potential to recapitulate disease phenotypes of the parental somatic cells, they exhibit line-to-line variations similarly to other cell types. These variations intricate interpretation of the data, thus, it is important to distinguish them from disease-related phenotypes. Patient-derived iPSCs provide other advantages for disease modeling by making available previously inaccessible cells specifically neurons and cardiac muscle cells and resolving the ethical dilemmas associated with hESCs (Djuric et al., 2015; Kim et al., 2013). Furthermore, personalized disease modelling could be possible because iPSCs can be derived from the affected individuals themselves.

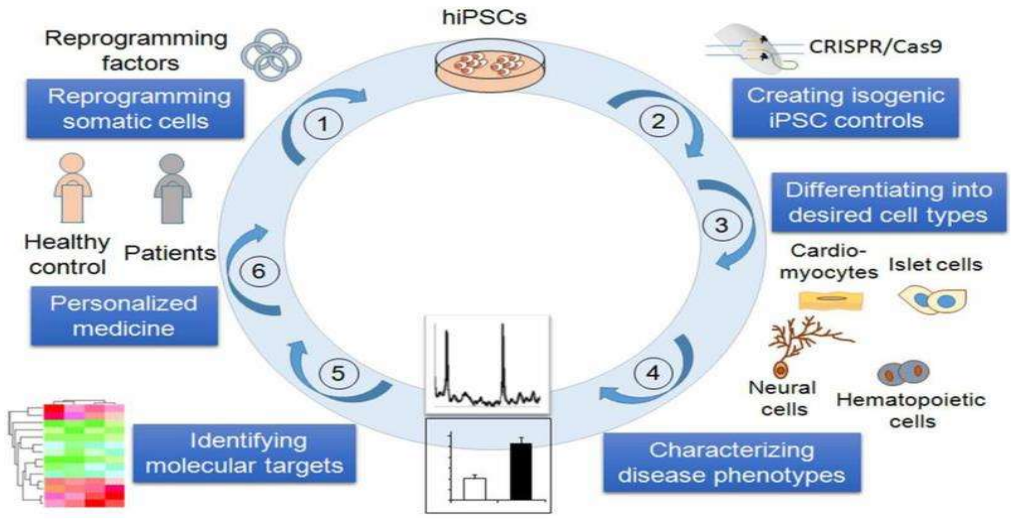

Figure 1-10. An illustration for disease modeling using patient- and healthy control-derived iPSCs. Adapted from 'Induced pluripotent stem cell technology: a decade of progress', by Shi et al., 2016, *Nature reviews. Drug discovery*, *16*(2), 115–130.

1.7.1.1. Genome editing in iPSC-based disease modelling

The rapid evolvement of genome editing technologies including transcription activator-like effector nucleases (TALENs) (Hockemeyer et al., 2011; Christian et al., 2010), zinc-finger nucleases (ZFNs) (Hockemeyer et al., 2009; Zou et al., 2009) and CRISPR/Cas9 (Perez-Pinera et al., 2013; Jinek et al., 2012) enable genetic modifications in iPSCs either by introducing disease-causing mutations into wild-type iPSCs or by eliminating genetic defects in patient-specific iPSCs to generate isogenic controls for disease modelling (Fig.1-11). Previously, it was challenging to edit the genome of hPSCs due to inefficiency of homology-directed repair (HDR) in these cells (Zwaka & Thomson, 2003), however, the use of precise custom-engineered endonucleases that target site-specific double-strand breaks (DSBs) in the DNA have increased the efficiency of genome-editing in hPSCs (Ding et al., 2013; Hockemeyer et al., 2011). The collaborative work of two research groups led by Jennifer Doudna from the University of California and Emmanuelle Charpentier from the Umeå University resulted in the development of CRIPSR/Cas9 genome-editing system which has become the approach of choice for genome-editing among custom-engineered endonucleases approaches (Jinek et al., 2012). This breakthrough achievement has led them to be jointly awarded the Nobel Prize in Chemistry 2020 (The Noble Foundation, 2020). The CRIPSR/Cas9 system has key advantages over the previously developed genome-editing systems such as TALENs and ZFNs including simplicity, high efficiency, low cost and less time to be achieved (Zhang et al., 2017; Ding et al., 2013).

The isogenic iPSCs controls are crucial to avoid any discrepancies associated with line-to-line variations and for modeling sporadic or polygenic pathological conditions in which phenotypic variations are likely to be low (Hockemeyer & Jaenisch, 2016). Currently, iPSC-based disease modelling is most commonly used to investigate the etiology of early-onset monogenic disorders (Luciani et al., 2020; Ebert et al., 2009; Lee et al., 2009), while it is challenging to model late-onset genetic disorders because of fetal-like properties of iPSC-derived differentiated cells (Studer et al., 2015).

Humans, like most multicellular organisms, are subject to biological aging or senescence because of gradual deterioration of functional characteristics over time which are often irreversible. Thus, there was a thought that iPSCs obtained from somatic cells of old individuals would be subject to early senescence which may impede their utility in disease modelling and clinical application. Some reports have shown that aging phenotypes were preserved by direct reprogramming of adult somatic cells (Mertens et al., 2015; Banito et al., 2009). In contrast, there are strong evidences that reprogramming reverses the cellular aging and rejuvenates adult somatic cells. Lapasset et al. (2011) have generated iPSCs -using an optimized protocol- from centenarian tissues demonstrating that the generated iPSCs

have the potential to re-differentiate into rejuvenated cells that are indistinguishable from hESCs. Moreover, another research group has successfully reprogrammed peripheral blood mononuclear cells (PBMCs) into iPSCs using optimized iPSC culture conditions. The PBMCs were obtained from 16 adult donors aged 21 to 100 years whose ages have shown no significant effect on the reprogramming efficiency or hESC-like state of the generated iPSCs (Sardo et al., 2017). Therefore, donor age does not hamper the use of iPSCs in disease modelling or regenerative medicine. However, the capability of reprogramming conditions to rejuvenate adult somatic cells poses a major challenge for modelling age-associated diseases (AADs) such as cancer, heart disease, diabetes, hypertension, Alzheimer's disease (AD). and other neurodegenerative disorders. To tackle this problem and to induce disease-associated phenotypes, introduction of specific stressors to normal culture conditions is required (Mertens et al., 2018). Several studies have utilized reactive oxygen species (ROS) or mitochondria-related stressors such as H_2O_2, 6-hydroxydopamine (6- OHDA), carbonyl cyanide 3-chlorophenylhydrazone (CCCP) or valinomycin to elicit abnormal neuronal phenotypes associated with familial PD (Pearson et al., 2016; Rakovic et al., 2013; Reinhardt et al., 2013; Nguyen et al., 2011). Similarly, other compounds have been used with iPSC-derived neurons from patients with HD (Nekrasov et al., 2016) and Machado-Joseph disease (Koch et al., 2011).

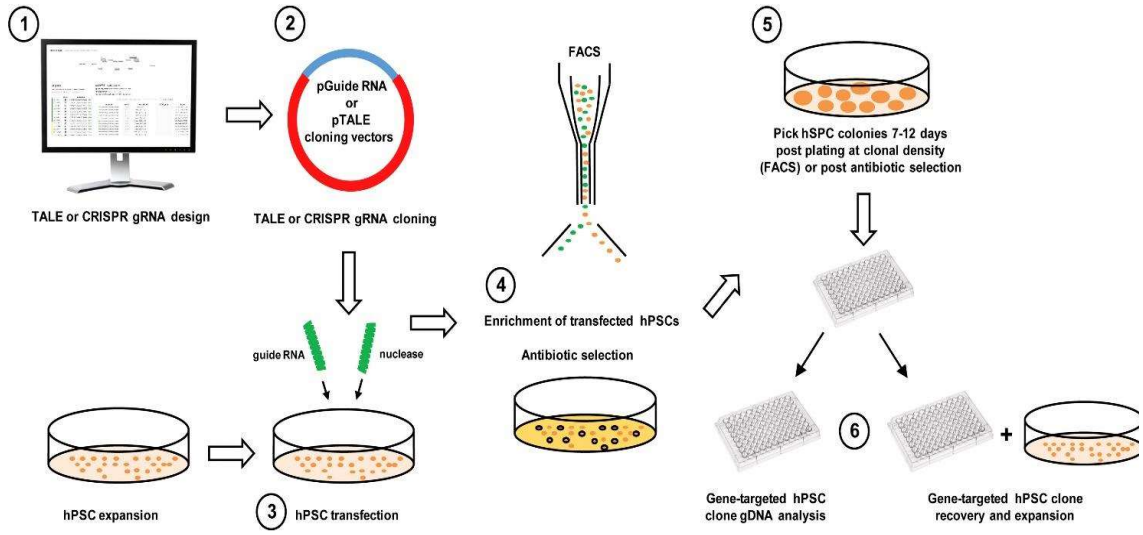

Figure 1-11. Schematic showing workflow of pluripotent stem cell gene-editing. Adapted from 'Genome editing in human pluripotent stem cells: approaches, pitfalls, and solutions', by Hendriks et al., 2016, *Cell Stem Cell, 18(1)*, 53-65.

1.7.1.2. Organoids in modelling neurological disorders

The 3D human organoid cultures derived from disease-specific iPSCs have become of great importance in *in vitro* disease modeling particularly for the neurological diseases and when it is difficult to study complex cellular interactions and organs development mechanisms using 2D monolayer cultures (Amin & Paşca, 2018). The 3D culture systems have several advantages over the conventional 2D cultures including better mimicking of *in vivo* cell-cell and cell-matrix interactions that enhance cell proliferation, mechano-responses, differentiation, functioning and cell survival (Skardal et al., 2016; Bonnier et al., 2015; Han et al., 2014; Baker & Chen, 2012). The use of 3D cultures minimizes the number of animal models used in clinical research and is more suitable for growth and treatment of malignant tumors as well (Schuster et al., 2020; Duval et al., 2017). It has been evident that expansion and differentiation of human iPSCs are highly efficient in 3D scalable culture systems (Ikeda et al., 2017; Lei & Schaffer, 2013). Furthermore, maturation of neuronal and glial cells is promoted better in 3D cultures than in 2D cultures. Modeling AD using 3D and 2D culture systems revealed more robust neural maturity in 3D cultures by expressing mature isoforms of tau protein which are associated with the pathogenesis of AD (Choi et al., 2014). Cerebral organoids have become the most common type of organoids developed and used to model neurological diseases in the last decade (Dong et al., 2020; Amin & Paşca, 2018; Bershteyn et al., 2017; Bagley et al., 2017; Lancaster et al., 2013). A recent study on cerebral organoids has shown interesting findings following the transplantation of small human cerebral organoids in the medial prefrontal cortex (mPFC) region of the mouse brain. The transplanted organoids survived and exhibited subcortical axonal projections that extended to basal regions of the mouse brain and integrated into its neural circuits. Furthermore, the glutamatergic neurons generated by the grafted organoids acquired maturation in the mouse cerebral cortex (Dong et al., 2020). The current application of iPSC-based organoids in neurological diseases modeling is challenged by the variations seen among individual organoids (Dang et al., 2016; Qian et al., 2016; Camp et al., 2015), however, patient-derived organoids have shown promising findings as a potential secondary screening tool for validation of screening results of 2D cultures and spheroids (Xu et al., 2016a). Improvement and optimization of human organoids media and growth conditions will enhance the uniformity of individual organoids and their reproducibility. This in turn will lead to better understanding of the pathological mechanisms of human diseases especially the neurological diseases and utilization of human organoids for screening of newly developed therapeutic agents. Additionally, advancements in 3D bio-printing technology to generate iPSC-derived organ systems are expected to revolutionize the area of clinical transplantation and regenerative medicine (Salaris et al., 2019; Neufurth et al., 2014; Guillotin et al., 2010).

1.7.2. iPSC-based drug screening

To investigate the predictive safety of new therapeutic agents during the process of drug development, scientists often use immortalized cell lines, and -to a lesser extent- primary cells and animal models. However, inherited chromosomal aberrations or genetic mutations in these cells due to their cancerous origin and long-term *in vitro* culture with countless passages make these cells non-representative of the actual behavior of normal cells *in vivo*. Another hurdle faces the toxicological screening tests is the heterogeneity of the primary cultures of somatic cells used owing to batch-to-batch variations. Moreover, the use of laboratory animals in toxicology studies raises ethical, technical and financial concerns, as well as the suitability issue associated with their use to mimic the human physiology. However, the possibility to generate iPSCs from non-malignant cells and healthy individuals and their availability in large numbers for high throughput screening (HTS) of new drugs make iPSCs the tool of choice for drug toxicology studies over the conventional approaches (Chaudhari et al., 2018; Shinde et al., 2016; Heng et al., 2009).

1.7.3. iPSC-based cell transplantation therapy

Development of cell transplantation therapies for human diseases using iPSC-derived specialized cells has been one of several promising applications of the iPSCs technology since the first successful generation of PSCs from mature mouse and human cells (Takahashi & Yamanaka, 2006). The first clinical trial to treat a degenerative disease using iPSCs was launched in 2014 by a group of Japanese researchers including Masayo Takahashi and Shinya Yamanaka. They successfully transplanted a sheet of retinal pigment epithelial (RPE) cells in a patient with advanced neovascular age-related macular degeneration (AMD), a major cause of blindness. The RPE cells were differentiated from iPSCs obtained from skin fibroblasts of two patients with AMD including the transplanted one. Interestingly, one-year post-surgery, the transplanted sheet of RPE cells remained undamaged and the repaired visual acuity had neither improved nor deteriorate (Mandai et al., 2017). In 2018, the Ministry of Health in Japan approved the second clinical trial on iPSC-based cell therapy to treat heart disease. This clinical study is carried out at Osaka University and is led by the Japanese cardiac surgeon Yoshiki Sawa (Cyranoski et al., 2018). It is of note that the regulatory approval for clinical translation of iPSC-based cell therapies varies among countries (Mendicino et al., 2019). In April 2020, the National Eye Institute (NEI) of the US National Institutes of Health (NIH) was granted permission from the Food and Drug Administration (FDA) to launch a US version of the AMD clinical trial (National Library of Medicine [NLM], NCT043397641). Interestingly, in July 2020, the FDA approved the first iPSC-derived chimeric antigen receptor (CAR) T-cell therapy to treat solid malignant neoplasms (Fate Therapeutics, 2020; Siegler et al., 2018). Based on the current

advancements in the iPSC-based cell therapy research, more new cell transplantation therapies are expected to be developed in the near future.

1.8. Principles of stem cell research and clinical translation

The clinical applications of stem cell research are governed by five principles in *the Guidelines for Stem Cell Research and Clinical Translation* set and updated in 2008 and 2016, respectively, by *the International Society for Stem Cell Research (ISSCR).* The five principles to be strictly adhered to are: integrity of the research enterprise, primacy of patient welfare, respect for research participants, transparency, and social justice (Kimmelman et al., 2016). The new guidelines address the novel scientific developments and ethical challenges that impede the clinical translation of stem cell research.

1.9. Current challenges in clinical translation of iPSCs technology

1.9.1. Immunogenicity of iPSCs

Although it is widely assumed that iPSC-derived autologous transplants cannot be rejected by the recipient, immunogenic effect of iPSC-derived cells was reported for the first time by Zhao and colleagues who transplanted allogeneic ESCs from 129/SvJ mice, inbred C57BL/6 (B6) mouse embryonic fibroblasts (MEFs)-derived iPSCs and autologous ESCs in B6 mice. The B6 recipient mice rejected the allogenic ESCs and prevented formation of teratomas, while they allowed formation of teratomas from the B6 ESCs without any immunogenic effect. Strikingly, the B6 iPSCs were largely rejected by the B6 recipient mice (Zhao et al., 2011). Another study has shown that *de novo* mitochondrial DNA (mtDNA) mutations elicit immunogenic response in humans and mice. The authors suggested that screening of iPSC derivatives for mtDNA defects is crucial to avoid graft rejection in the recipients (Deuse et al., 2019). Random genetic and epigenetic modifications occur during reprogramming of somatic cells, long-term cultivation of iPSCs, and immaturity of iPSC-derived cells *in vitro* are thought to be the causes of immunogenicity of iPSCs (Tang & Drukker, 2011; Polo et al., 2010; Kim et al., 2010). In contrast, other research groups have reported that syngeneic non-integrated iPSCs and their derivatives have no or minimal immunogenic effect supporting the notion that these cells could be used for cellular therapy without causing harmful immune responses (Lu et al., 2014; Guha et al., 2013; Morizane et al., 2013).

1.9.2. Production of clinical-grade patient-derived iPSCs therapies

One of the major advantages of autologous iPSC therapies is that it solves the problem of immunogenicity, but mass production of clinical-grade patient-derived iPSCs therapy is expensive

and time-consuming especially when it is required for treatment of urgent medical conditions such as spinal cord injuries and myocardial infraction (Ohnuki & Takahashi, 2015). Therefore, the use of allogeneic iPSCs is thought to be the preferred approach through biobanking of a restricted number of genetically stable, viral-free iPSCs lines from human leukocyte antigen (HLA)-homozygous donors. The production of allogeneic iPSCs must strictly follow the current good manufacturing practice (*CGMP)* regulations to substantially reduce the cost of iPSC-derived cell therapy besides waiving the need for regulatory approvals of individual patient-specific iPSCs (Doss & Sachinidis, 2019; Eschenhagen & Weinberger, 2019).

1.9.3. Heterogeneity and variability of iPSC lines

Another problem the researchers often face in creating iPSC-based disease models and therapies for regenerative medicine is the variability in iPSC lines (Kyttälä et al., 2016). Several studies have reported that exogenous-derived epigenetic modifications may cause mitochondrial mutations, chromosomal defects, genetic and epigenetic variations in iPSC lines and even in the same iPSC line at different passages. Thereby, they may modulate differentiation capacity of the iPSCs and demote their utility in translational medicine These variations may be retained from the parental somatic cells or produced during reprogramming and long-term growth and maintenance of iPSCs (Liu et al., 2020; Burrows et al., 2016; Liang & Zhang, 2013; Kim et al., 2010). Creating isogenic iPSC lines using gene editing tools is thought to largely tackle this issue (Menon et al., 2016).

1.9.4. Tumorgenicity of iPSCs

The remarkable similarities between induced pluripotency and tumorigenicity raise questions about the safety of the iPSC-based cell therapy. The gene expression profiles found in iPSCs and tumor cells are overlapping. The hypothesis that the induction of pluripotency and tumorigenicity are related processes was examined by generating iPSCs and oncogenic foci (OF) from common parental somatic cells. The researchers have found that iPSCs involve transcriptional patterns similar to those in OF (Riggs et al., 2013). Interestingly, it has been demonstrated that even PSCs derived from healthy donors may cause benign tumorigenesis after grafting into a recipient (Cooke et al., 2006). Potential tumorigenic factors such as chromosomal aberrations, duplication of oncogenes or deletion of tumor-suppressor genes may occur during generation and expansion of iPSCs or during their differentiation into specific cell types (Laurent et al., 2011; Mayshar et al., 2010). Therefore, transplanted iPSC-derived cells should be free of residual iPSCs through purification of targeted differentiated cells (Rojas et al., 2017; Lamba et al., 2010).

1.9.5. Incomplete differentiation of immature iPSCs into mature specialized cells

Most of iPSC-derived cells are developmentally immature due to their embryonic or fetal-like characteristics and heterogenous population of differentiated cells. This is obvious in iPSC-derived cardiomyocytes (iPSC-CMs) where the co-existence of atrial, ventricular and nodal subtypes may hamper the interpretation of experimental results and eventually the use of these cells in iPSC-based drug screening and cell therapy (Koivumäki et al., 2018; Goversen et al., 2018). The immature phenotype of iPSC-derived neurons may also hinder modeling of late-onset neurodegenerative diseases (Vera & Studer, 2015). This problem could be mostly solved by inducing maturity in the immature iPSC-derived neurons through several factors including introducing mitochondria-related stressors, ROS, a defined maturation medium for iPSCs and the use of 3D cell culture vessels (Feyen et al., 2020; Correia et al., 2018; Pearson et al., 2016; Bardy et al., 2015; Nguyen et al., 2011).

1.10. iPSC-based modelling of neurological diseases

The pluripotency characteristic of reprogrammed somatic cells is critical for disease modeling using patient-derived cells especially modeling of neurological disorders. It has been reported that hiPSCs possess neural differentiation capacity resembles that of hESCs with greater variability and minimal reduction in their efficiency that could be enhanced with modification of culture conditions (Hu et al., 2010). Several protocols for neural differentiation of PSCs have been reported and applied for modeling neurological disorders (Grigor'eva et al., 2020; de Leeuw et al., 2020; D'Aiuto et al., 2014; Sundberg et al., 2013). As previously mentioned, the first human iPSC-derived model for ALS was created from an 82-year-old female affected with the familial form of ALS. The generated iPSCs showed hESCs-like characteristics and were differentiated into motor neurons (Dimos et al., 2008). Another neurodegenerative disease model was developed for both familial and sporadic AD. The iPSCs were generated from fibroblasts obtained from two patients with familial AD caused by duplication of amyloid-β precursor protein gene (*APP*), two patients with sporadic AD and two healthy individuals as controls and subsequently differentiated into neurons. The patient iPSC-derived neurons showed significantly elevated levels of neuropathological markers associated with AD namely: amyloid-β (1-40), phospho-tau (Thr 231) and active glycogen synthase kinase-3β (aGSK-3β), compared to the controls (Israel et al., 2012). For several decades, animal and cellular models of PD have been used to investigate the etiology of this progressive neurodegenerative disorder, however, recently human iPSC-based PD models have been extensively developed (di Domenico et al., 2019; Ryan et al., 2013; Cooper et al., 2012; Byers et al., 2011; Soldner et al., 2009). The first models of PD using iPSCs have been established by reprogramming fibroblasts into iPSCs from five idiopathic PD patients using an integrating reprogramming method. The researchers

successfully excised the lentiviral vectors from the generated iPSCs and differentiated the iPSCs into dopaminergic neurons (Soldner et al., 2009). A recent study on rodent models of PD have shown an interesting finding. Following grafting of human autologous iPSC-derived dopaminergic progenitors into the rodent models, restoration of motor function and reinnervation of brain without tumorigenicity were evident (Song et al., 2020). The previous examples demonstrated that iPSC-based models are very powerful in modeling neurological disorders including late-onset neurodegenerative diseases. Therefore, establishment of iPSC-based JS models is expected to provide profound insights into the pathogenic mechanisms of JS and to greatly enable identification of potential molecular targets for therapeutic interventions.

AIM OF THE RESEARCH

2. AIM OF THE RESEARCH

Joubert syndrome is a rare genetic disorder characterized by neurological signs and symptoms that deteriorate the quality of life of affected individuals and its complications can lead to early death due to lack of an effective therapy. Previously, development of patient-specific models of neurological disorders to understand their development and progression was largely hampered by complexity and relative inaccessibility of the central nervous system (CNS) neurons. In recent years, this challenge has been overcome by development of induced pluripotent stem cells (iPSCs) technology which has led to generation of different types of human neural cells and thereby facilitate the establishment of human neuronal models to investigate developmental and pathological mechanisms of human CNS and allowing drugs testing.

The primary aim of this PhD thesis was to generate and establish *in vitro* neuronal models of JS derived from patient-specific iPSCs to decipher the disease mechanisms and evaluate novel therapeutic approaches. Therefore, to achieve this aim, the following four objectives have been set:

I. To develop iPSC-based models of JS by reprogramming fibroblasts obtained from skin biopsies of five patients with JS using the CytoTune™-iPS 2.0 Sendai Reprogramming Kit.

II. To differentiate and characterize the generated JS-derived iPSCs into NSCs and neurons.

III. To evaluate the effect of the genetic defects in JS-derived cells on the number and length of primary cilia in JS-derived fibroblasts, iPSCs, and NSCs.

IV. To assess the expression patterns of the key molecules in SHH signaling pathway in JS-derived fibroblasts, iPSCs, NSCs, and neurons.

MATERIALS & METHODS

3. MATERIALS AND METHODS

3.1. Joubert Syndrome patients involved in this study

To establish iPSC-based JS models, five JS patients of different ages have been enrolled in this study and they have been designated as JS1, JS2, JS3, JS4, and JS5. Ethical approval to conduct the study have been obtained from the Scientific Committee and the Board of the ASST Spedali Civili di Brescia, Brescia, Italy. The parents or guardians of the patients have signed the informed consent forms to be enrolled. All the patients exhibited different genetic defects in one of the causative genes of JS and variable clinical manifestations of the disease. The genetic characterization of JS1-JS5 has been performed by Prof. Enza Maria Valente, Department of Molecular Medicine, University of Pavia, Pavia. Table 3-1 shows the genetic mutations associated with each patient and their ages at the time of enrollment.

Table 3-1. JS patients enrolled in the study and the genetic mutations detected in their genomes

Patient	Sex	Gene	Exon(s)	Nucleotide alterations	Predicted effect on protein
JS1	Male	*CC2D2A*	31	c.3856T>C	p.C1286R
				c.3856T>C	p.C1286R
JS2	Female	*CC2D2A*	24	c.2999A>T	P.E1000V
			30	c.3638delG	p.G1213Afs*7
JS3	Male	*TMEM67*	13	c.G1319A	p.R440Q
			21	c.A2182G	p.S728G
JS4	Male	*TMEM67*	17	c.755T>C	p.M252T
			21	c.1769T>C	p.F590S
JS5	Female	*C5orf42*	22	c.T3868T>C	p.S1290P
			36	c.7477C>A	p.R2493X

3.2. Establishment of JS-derived fibroblast lines

3.2.1. Biopsy collection and establishment of JS fibroblast lines

For generation of induced pluripotent stem cells (iPSCs) for this study, the fibroblasts were obtained from skin biopsies of five Italian patients with JS (Table 3-1). The patients were referred by the Neurogenetics Unit, IRCCS Santa Lucia Foundation, Rome, and Unit of Child Neuropsychiatry, ASST Spedali Civili, Brescia. The skin biopsies collected by a dermatologist at Unit of Child Neuropsychiatry, ASST Spedali Civili, Brescia, were immediately delivered to the Angelo Nocivelli Institute for Molecular Medicine at the same hospital where setting up the fibroblast lines and generation of the iPSCs were carried out. Fibroblasts from the other patients have been sent frozen to the lab. Before the collection of biopsies, all the patients and/or their guardians underwent an informed consent session and signed the informed consent forms (ICFs). The specimen collection container and corresponding forms for each patient were properly labeled with the patient identification (ID) number. The ethical approval to conduct this research was obtained from the

Scientific Committee and the Board of the ASST Spedali Civili di Brescia (NP 3572- Studio iPSCREP). As a control for this research, we used the human fibroblast cell line BJ (ATCC® CRL-2522™) and its derived cell lines. It was reprogrammed into iPSCs in our laboratory and its pluripotency was characterized using the TaqMan® hPSC Scorecard™ Panel (Thermo Fisher Scientific). BJ iPSC lines were differentiated into the three germ layers, NSCs, and neurons.

Materials required for collection of skin biopsy specimens from JS patients

- Signed informed consent forms (ICFs)
- Specimen collection containers
- Disposable biopsy punch with plunger
- Antibiotic ointment (Mycitracin® Plus)
- Antiseptic solution (Chlorhexidine)
- Local anesthetic solution (Lidocaine HCL 1%)
- Disposable scalpels, 30-gauge needles, gauze, adhesive bandages, scissors, and gloves

Materials required for the establishment of the fibroblast cultures

- Dulbecco's Modified Eagle Medium (DMEM) (EuroClone®, Cat. No. ECB7501L)
- Fetal Bovine Serum (FBS) (EuroClone®, Cat. No. ECS0180L)
- L-Glutamine (EuroClone®, Cat. No. ECB3000D)
- Penicillin/Streptomycin (EuroClone®, Cat. No. ECB3001DCL)
- Trypsin/EDTA (1:250) (BioConcept, Cat. No. 5-52F00-H)

Protocol

1. The biopsy site was properly sterilized with an antiseptic solution (Chlorhexidine), then anesthetized by injecting a local anesthetic solution (Lidocaine HCL 1% 1: 100,000).
2. The biopsy site was examined to ensure that it is anesthetized and ready to be biopsied.
3. A sterile skin punch was used to collect the specimen and it was ensured that the epidermis of the skin was not damaged by the procedure. The biopsy was immediately placed in a container and submerged in the fibroblast growth medium (Dulbecco's Modified Eagle Medium (DMEM) with 10% Fetal Bovine Serum (FBS), 1% L-Glutamine and 1% Penicillin/Streptomycin).
4. A sterile gauze was used to wipe excess blood on the biopsy site and an antibiotic ointment (Mycitracin® Plus) was applied to the site and covered with an adhesive bandage. Under a laminar flow cabinet, the collected tissue was cut vertically into small pieces with all the skin layers using a sterile disposable scalpel. The tissue pieces were placed into all wells of a sterile 6-well culture plate and 5 ml of DMEM medium was added into each well.

5. Carefully and without shaking to avoid floating of the tissue pieces, the 6-well culture plate was placed in a 5% CO_2 humidified incubator at 37° C. The plate was incubated for 2 weeks without being moved during this period, then the growth of fibroblasts from the tissue pieces was visualized under an inverted phase contrast microscope.
6. After reaching approximately 100% confluence, the fibroblast growth medium was removed from the culture plate and 1 ml of trypsin-EDTA solution 1X was used to detach the fibroblasts from the surface of each well. The cells were counted using the Countess™ automated cell counter. Different concentrations of the detached cells were reseeded in new T-75 cell culture flasks containing 11 ml of DMEM medium. The DMEM medium was changed every 3 to 4 days and the cells were sub-cultured when they reached 100% confluence.
7. The fibroblast cultures established from the patients' biopsies were maintained by passaging the cells regularly when they reached nearly100% confluence. The cell cultures were tested for mycoplasma contamination at different passages.

3.3. PCR-based detection of *Mycoplasma* contamination in the fibroblast cultures

Mycoplasma, a member of the bacterial class *Mollicutes*, is the smallest free-living prokaryotic organism characterized by lack of cell wall, plasma-like form, basic genome and limited metabolic activity. In cell culture laboratories, *Mycoplasma* is known to be one of the common sources of contamination that can physiologically modify the infected cells in culture causing experimental artifacts and leading to spurious results. Therefore, for the induction of fibroblasts into iPSCs and their subsequent differentiation into NSCs and neurons, it is essential that the cell culture is free of *Mycoplasma* contamination. Due to its high sensitivity and specificity, the PCR-based method is the most common approach used for detection of *Mycoplasma* in cell cultures.

Materials required

- GoTaq® Flexi reaction buffer (Promega, Cat. No. M8901)
- GoTaq® G2 DNA polymerase (Promega, Cat. No. M7841)
- $MgCl_2$ solution, 25 mM (Promega, Cat. No. A3511)
- dNTP Mix, 10 mM (Thermo Scientific™, Cat. No. R0191)
- Betaine solution, 5M (Sigma-Aldrich, Cat. No. B0300)
- Forward and reverse primers
- 6X DNA loading dye (Thermo Scientific™, Cat. No. R0611)
- Milli-Q H_2O
- Agarose
- 1X TAE buffer

Protocol

1. From a highly confluent cell culture, 500 µl of the spent medium from each well was collected and transferred into a sterile 1.5-ml microcentrifuge tube to be incubated at 95° C for 5 min in an Eppendorf® Thermomixer Compact or a thermostatic water bath.
2. The collected medium was centrifuged at the 14000 rpm for 3 min to pellet any cellular debris.
3. For amplification of the *Mycoplasma* DNA, 2 µl of the supernatant was added to 23 µl of the PCR reaction mixture (Table 3-2) following the PCR conditions shown in Table 3-3.

Table 3-2. PCR reaction mixture for *Mycoplasma* detection	
Reagents	**Volume** (µl)
GoTaq® Flexi reaction buffer	5
$MgCl_2$ solution	1.5
dNTP Mix	0.5
Forward primer	0.25
Reverse primer	0.25
GoTaq® G2 DNA Polymerase	0.2
Betaine solution, 5M	2.5
Milli-Q H_2O	12.3
Cell culture supernatant	2.5
Total volume	**25**

Table 3-3. PCR reaction conditions for *Mycoplasma* detection					
Initial incubation step	**Cycle** (48 cycles)			**Final extension**	**Final hold**
	Denaturation	Annealing	Extension		
HOLD	Cycle			HOLD	HOLD
98º C 3 min	95º C 30 sec	60º C 30 sec	74º C 30 sec	72º C 10 min	4º C ∞

4. For result validation, two more samples were used as positive and negative controls.
5. The set of PCR primers used are shown in the following table:

Table 3-4. Reverse and forward PCR primers used for detection of *Mycoplasma* contamination		
Forward primer (5′-3′)	**Reverse primer (5′-3′)**	**Product size**
GGGAGCAAACAGGATTAGATACCCT	*TGCACCATCTGTCACTCTGTTAACCTC*	268 bp

6. To examine the amplification results, electrophoresis was performed using10 µl from each PCR product and 2 µl of a 6X DNA loading dye. The mixture was loaded in a well of 2% agarose gel and visualized using the iBright™ CL1500 Imaging System.

3.4. Reprogramming of JS-derived fibroblasts into iPSCs

The CytoTune™-iPS 2.0 Sendai Reprogramming Kit was used to reprogram the fibroblasts obtained from the five JS patients into iPSCs. This kit contains three CytoTune™ 2.0 reprogramming vectors based on a recombinant, non-transmissible form of Sendai virus (SeV) (Fusaki et al., 2009). The three SeV-based vectors CytoTune™ 2.0 KOS, CytoTune™ 2.0 hc-Myc, and CytoTune™ 2.0 hKlf4 are non-integrating and used to reprogram human somatic cells into iPSCs by delivering and expressing safely and effectively key transcription genes: *Oct4, Sox2, Klf4,* and *c-Myc*. These genes are known as Yamanaka factors; named after the Japanese scientist Shinya Yamanaka who discovered the role of these four transcription factors in reprogramming adult cells into iPSCs (Takahashi & Yamanaka, 2006). The viral vectors and the genetic factors were cleared from the generated iPSCs due to the non-integrating nature of SeV.

3.4.1. Reprogramming the fibroblasts in feeder-free condition

Materials required

- CytoTune™-iPS 2.0 Sendai Reprogramming Kit (Thermo Fisher Scientific, Cat. No. A34546). It contains CytoTune™ 2.0 KOS, CytoTune™ 2.0 hc-Myc and CytoTune™ 2.0 hKlf4.
- Fibroblast cell lines
- NutriStem® hPSC XF Medium (Biological Industries, Cat. No. 05-100-1A)
- Corning™ Matrigel™ hESC-Qualified Matrix (Corning, Cat.No.08-774-552)
- DMEM with GlutaMAX™-I (high glucose) (Thermo Fisher Scientific, Cat. No. 10569-010)
- DMEM/F-12, GlutaMAX™ supplement (Thermo Fisher Scientific, Cat. No. 12660-012)
- Fetal bovine serum (FBS), ES Cell-Qualified (Thermo Fisher Scientific, Cat. No. 16141-079)
- KnockOut™ Serum Replacement (KSR) (Thermo Fisher Scientific, Cat. No. 10565018)
- MEM Non-essential amino acids (NEAA) (Thermo Fisher Scientific, Cat. No. 11140-050)
- Basic FGF, recombinant human (Thermo Fisher Scientific, Cat. No. PHG0264)
- β-mercaptoethanol (Thermo Fisher Scientific, Cat. No. 21985-023)
- Attachment Factor (Thermo Fisher Scientific, Cat. No. S-006-100)
- TrypLE™ Select Cell Dissociation Reagent (Thermo Fisher Scientific, Cat. No. 12563)
- Dulbecco's PBS (DPBS) without $CaCl_2$ and $MgCl_2$ (Thermo Fisher Scientific, Cat. No. 14190)

Protocol

Day -2: **Cells preparation for transduction**

1. Two days before the transduction, the fibroblasts were seeded into at least two wells of a 6-well plate at the correct concentration to reach between 2×10^5–3×10^5 cells per well on the day of transduction (30-60% confluence).

Day 0: **Retroviral infection**

2. One well of the seeded fibroblasts was used for cell counting. The cells were counted using the Countess™ automated cell counter.
3. Transduction has been performed with KOS MOI=5, hc-Myc MOI=5 and hKlf4 MOI=3. The proper volume of each viral titer to be added was calculated in accordance with the number of live cells, following the titer information provided for the specific Cytotune Kit and the formula:

$$Volume\ of\ virus\ (\mu l) = \frac{MOI\ (CIU/cell) \times number\ of\ cells}{titer\ of\ virus\ (CIU/ml) \times 10^{-3}\ (ml/\mu l)}$$

4. The calculated volume of each viral titer was added to 1 ml of fibroblast medium and mixed very well.
5. Rapidly, the spent fibroblast medium was removed from the well and the reprogramming virus solution was added. Then the plate was incubated overnight in a 5% CO_2 humidified incubator at 37° C.

Day 1-6: Replacement of medium

6. 24 hr post-transduction, the medium was replaced with a fresh fibroblast medium. Cell death was elevated (>50%), but it was expected as an indication of high uptake of the virus.
7. The fibroblast medium was changed every other day, until day 6.

Day 7: Plating the transduced cells on Matrigel coated culture vessels

8. Several 6-well cell culture plates were coated with Matrigel.
9. The fibroblast medium was removed, and the cells were washed once with DPBS. Then the cells were detached using 0.5 ml of TrypLE™ Select reagent. After centrifugation at 1200 rpm for 4 min, the pellet was resuspended in 1 ml of the fibroblast medium. The cells were counted, then 2×10^4 –1×10^5 cells were seeded in each well of a Matrigel-coated plate and incubated in a 5% CO_2 humidified incubator at 37° C.
10. Depending on the total cell number, two to three different cell concentrations have been plated from each transduced fibroblast line. In addition, part of the cells has been collected for RNA extraction; to be used as a positive control in the RT-PCR detection of the Cytotune vectors.

Day 8-28

11. From day 8, the spent medium was replaced with complete NutriStem® hPSC XF medium every day, and the cells were visualized under an inverted phase contrast microscope for the emergence of cell clumps indicative of reprogrammed cells.
12. Three to four weeks post-transduction, colonies were ready to be transferred. Live Cell Staining was performed using Tra1-60 antibody for selecting proper reprogrammed colonies.

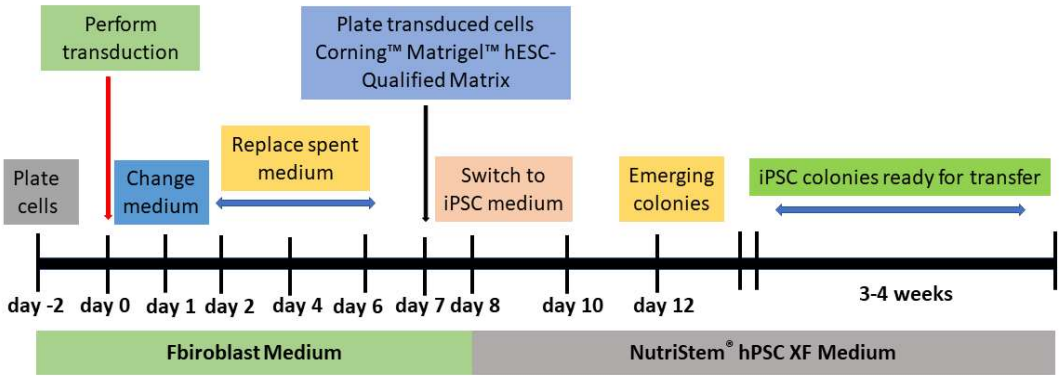

Figure 3-1. Workflow of reprogramming of fibroblasts into iPSCs using the CytoTune™-iPS 2.0 Sendai Reprogramming Kit. Adapted from CytoTune™-iPS 2.0 Sendai Reprogramming Kit User Guide, Thermo Fisher Scientific, (2016), Pub. No. MAN0009378, p.11.

.

3.4.2. Anti-TRA-1-60-Vio 488 live cell staining of the generated iPSCs

Anti-TRA-1-60-Vio 488 Live Cell Stain is used to visualize the expression of human TRA-1-60 protein under a fluorescence microscope. It has no effect on the proliferation or stemness of the cells which can normally continue their growth in culture after being stained. By days 26-28 post-induction, live staining with TRA-1-60 antibody was performed to recognize and to select the generated undifferentiated iPSCs to be picked for expansion of the cell lines.

Materials required

- Anti-TRA-1-60-Vio488 Live Cell Stain (Miltenyi Biotec, Cat. No. 130-106-872)
- DMEM/F12 Medium (Gibco™, Cat. No. 11320033)
- NutriStem® hPSC XF Medium (Biological Industries, Cat. No. 05-100-1A)

Protocol

1. Anti-TRA-1-60-Vio 488 was diluted in DMEM/F12 medium (1:100). Into each well of a 6-well plate, 1.2 ml of the medium was added.
2. The spent medium was removed, and the well was carefully washed with 1 ml of DMEM/ F-12 medium.
3. DMEM/F-12 medium was completely removed, and the antibody dilution prepared in step 1 was added.
4. The plate was gently rocked to ensure even distribution of the antibody solution to cover the entire surface of each well.
5. The plate was incubated for 30 min in a 5% CO_2 humidified incubator at 37° C.
6. The antibody solution was removed, and the cells were washed twice with DMEM/F12 medium.
7. 1.4 ml of a fresh complete NutriStem® hPSC XF Medium was added into each well, and the newly formed colonies were observed under Olympus IX70 fluorescence microscope.
8. Tra-1-60 positive colonies were selected and picked into a freshly coated 6-well plate for expansion.

3.4.3. Selection and expansion of the fibroblast-derived iPSC clones

1. The iPSC culture plate was transferred to a sterile laminar flow cabinet equipped with an inverted phase contrast microscope to be examined using 10X magnification.
2. The selected colonies to be manually picked were marked using a colored marker pen on the outer surface of the bottom of the culture plate. At least 15 distinct colonies were picked by the end of each reprogramming experiment and expanded in separate 6- or 12-well culture plates.
3. Using a 200-µl pipette, the selected colonies to be picked were dissected by the pipette tip into 5-6 pieces in a grid-like pattern and transferred to a Materigel-coated 6- or 12-well culture plate containing NutriStem® hPSC XF medium.
4. The culture plates containing the picked colonies were placed in a 5% CO_2 humidified incubator at 37° C. The colonies were incubated for 48 hr to be attached to the culture plates before replacing the spent medium with a fresh complete NutriStem® hPSC XF medium. Then, the medium was changed every day.
5. The generated colonies ware passaged, expanded, and maintained using standard culture procedures. The iPSCs were collected at different passages for cryopreservation and stored in a liquid nitrogen tank.

3.5. Detection of Sendai virus (SeV) genome and transgenes

For further characterization and differentiation into NSCs, neurons, or any other cell types, it is important to ensure that the generated iPSCs are free of CytoTune™ 2.0 Sendai reprogramming vectors. The time required to eliminate the viral vectors depends on the type of cell culture and passage conditions. Following the manufacturers' protocols to verify the elimination of SeV vectors, RNA was isolated from the iPSCs using NucleoSpin® RNA Mini Kit (Macherey-Nagel, Cat. No. 740955.250) (Section 3.7.5.1). The purified RNA was reverse-transcribed into cDNA using ImProm-II™ Reverse Transcription System (Promega, Cat. No. A3800) (Section 3.7.5.3). Using AmpliTaq Gold® DNA Polymerase Kit (Thermo Fisher Scientific, Cat. No. N8080241), PCR was performed using GeneAmp® PCR System 9700 (Applied Biosystems™) following the PCR reaction conditions shown in Tables 3-5 and 3-6.

Table 3-5. PCR reaction mixture for amplification of the targeted exons

Reagents	**Volume** (µl)
GeneAmp™ 10X Gold buffer	5
$MgCl_2$, 25 mM	4
dNTP Mix, 10 mM	2
Forward primer	2
Reverse primer	2
AmpliTaq Gold™ DNA polymerase	0.4
Milli-Q H_2O	32.6
dsDNA	2
Total volume	**50**

Table 3-6. PCR reaction conditions for detection of SeV genome and transgenes

Initial incubation step	**Cycle** (35 cycles)			**Final extension**	**Final hold**
	Denaturation	Annealing	Extension		
HOLD	Cycle			HOLD	HOLD
94º C 12 min	95º C 30 sec	55º C 30 sec	72º C 30 sec	72º C 7 min	4º C ∞

Table 3-7. RT-PCR primer sets used for detection of SeV genome and transgenes in the generated iPSCs

Target		**Primer sets (5′-3′)**	**PCR product size**
SeV	**F**	*GGATCACTAGGTGATATCGAGC**	181 bp
	R	*ACCAGACAAGAGTTTAAGAGATATGTATC**	
KOS	**F**	*ATGCACCGCTACGACGTGAGCGC*	528 bp
	R	*ACCTTGACAATCCTGATGTGG*	
Klf4	**F**	*TTCCTG CATGCCAGAGGAGCC C*	410 bp
	R	*AATGTATCGAAGGTGCTCAA**	
c-Myc	**F**	*TAACTGACTAGCAGGCTTGTCG**	532 bp
	R	*TCCACATACAGTCCTGGATGATGATG*	

* Primer contains SeV genome sequences. Pairing of these primers with transgene-specific primers allows specific detection of transgenes carried by the CytoTune™ 2.0 Sendai reprogramming vectors. F: forward primer, R: reverse primer. (Adapted from CytoTune™-iPS 2.0 Sendai Reprogramming Kit User Guide, Thermo Fisher Scientific, (2016), Publication No. MAN0009378, p.50).

3.6. PCR-based detection of *Mycoplasma* contamination in the iPSC cultures

Following the protocol in section (3.3), the supernatant of JS-derived iPSC cultures was collected and tested for the *Mycoplasma* detection at different passages before being characterized and differentiated into NSCs and neurons.

3.7. Characterization of the generated iPSC lines

3.7.1. Genetic analysis for confirmation of the pre-existing variants in parental cells

3.7.1.1. Isolation of DNA from the generated iPSC lines

Materials required

- QIAamp® DNA Mini Kit (QIAGEN, Cat. No. 51304). It contains QIAGEN Protease K, Buffer AL, Buffer AW1, Buffer AW2, Buffer AE and QIAamp Mini Spin Columns.
- Dulbecco's PBS (D-PBS) without $CaCl_2$ and $MgCl_2$ (Thermo Fisher Scientific, Cat. No. 14190)
- Ethanol (96-100%)

Protocol

DNA was extracted from the iPSCs using QIAamp® DNA Mini Kit.

1. The iPSCs were detached from the 12-well plate using a cell scraper, transferred to 1.5 ml microcentrifuge tube and centrifuged for 5 min at 1400 rpm. The supernatant was aspirated completely and discarded.
2. The cell pellet was resuspended in 200 µl of DPBS, then 20 µl of QIAGEN Protease K and 200 µl of Buffer AL were added to the sample. The sample was mixed by pulse-vortexing for 15 sec and incubated at 56° C for 10 min.
3. After incubation, the 1.5 ml microcentrifuge tube was briefly centrifuged to remove drops from the internal part of the lid. 200 µl of ethanol (96-100%) was added to the sample and mixed again by pulse-vortexing for 15 sec. After mixing, the 1.5 ml microcentrifuge tube was briefly centrifuged again to remove drops from the inside of the lid.
4. The mixture was applied to the QIAamp Mini Spin Column (in a 2 ml collection tube) without wetting the rim and centrifuged at 8000 rpm for 1 min. The collection tube containing the filtrate was discarded and the QIAamp Mini Spin Column was placed in a clean 2 ml collection tube.
5. Without wetting the rim, 500 µl of Buffer AW1 was added to the QIAamp Mini Spin Column and centrifuged at 8000 rpm for 1 min. The QIAamp Mini spin column was placed in a clean 2 ml collection tube and the collection tube containing the filtrate was discarded.
6. To the QIAamp Mini Spin Column, 500 µl of Buffer AW2 was added without wetting the rim and centrifuged at 14000 rpm for 3 min. The collection tube containing the filtrate was discarded.

Then, the QIAamp Mini Spin Column was placed in a clean 1.5 ml microcentrifuge tube and 200 µl of Buffer AE was added. After incubation at room temperature for 1 min, the QIAamp Mini Spin Column in 1.5 ml microcentrifuge tube was centrifuged at 8000 rpm for 1 min.

7. The QIAamp Mini Spin Column was discarded and the filtrate containing the DNA was retained and stored at 5º C. The DNA was quantified using the Tecan infinite® 200 microplate reader (GMI).

3.7.1.2. DNA sequencing by Sanger sequencing method

Materials required

- Exonuclease I (20 U/ul, 20000 U) (Thermo Scientific™, Cat. No. EN0581)
- FastAP (Thermo Scientific FastAP™ Thermosensitive Alkaline Phosphatase, 1 U/µl, 1000 U)
- BigDye™ Terminator v3.1 Ready Reaction Mix (Applied Biosystems™, Cat. No. 4337454)
- BigDye™ Terminator v1.1 & v3.1 5X Sequencing Buffer (Applied Biosystems™, Cat. No. 4336697)
- Hi-Di™ Formamide (Applied Biosystems™, Cat. No. 4311320)
- 5X GoTaq® Reaction Buffer (Promega, Cat. No. M7921)
- GoTaq® G2 DNA Polymerase (Promega, Cat. No. M7841)
- dNTP Mix, 10 mM (Thermo Scientific™, Cat. No. R0191)
- $MgCl_2$, 25 mM (Thermo Scientific™, Cat. No. R0971)
- dsDNA templates
- Forward and reverse PCR primers

Protocol

1. PCR amplification of the targeted sequences

The targeted sequences were amplified by PCR to detect the mutations in JS-related genes (Table 3-10) following the PCR reaction conditions shown in Table 3-9.

Table 3-8. PCR reaction mixture for amplification of the targeted sequences

Reagents	Volume (µl)
5X GoTaq® reaction buffer	5
$MgCl_2$, 25 mM	4
dNTP Mix, 10 mM	1
Forward primer	2
Reverse primer	2
GoTaq® G2 DNA polymerase	0.2
MQ H_2O	8.3
dsDNA	2.5
Total volume	**25**

Table 3-9. PCR reaction conditions for amplification of the targeted sequences					
Initial incubation step	**Cycle** (42 cycles)			**Final extension**	**Final hold**
	Denaturation	Annealing	Extension		
HOLD	Cycle			HOLD	HOLD
95º C 10 min	94 º C 30 sec	58º C/59º C/60º C* 30 sec	72º C 30 sec	72º C 7 min	4º C ∞

(*Annealing temperatures (T_a) for the forward and reverse primers of the genes *CC2D2A, TMEM67,* and *C5orf42* are 59º C, 60º C, and 58º C respectively)

Table 3-10. Primer sets used for amplification of the targeted sequences of the genes						
Patient	**Gene**	**Exon**	**Primer set**		**Tm (°C)**	**Length (bp)**
JS1	*CC2D2A*	31	**F**	*CTGCTACTTTATTTCAATCCTG*	60	723
			R	*TGTTGGCCAGGCTAGTGTC*		
JS2	*CC2D2A*	24	**F**	*CTAGTACAGAAAGCTAGAGGG*	54	410
			R	*CAGGTTTAACACATTATTCCTG*		
		30	**F**	*GATGGGATTGGCTTTGAATGC*	58	419
			R	*GTAAGGAAGGCTCTGTTTGTG*		
JS3	*TMEM67*	13	**F**	*AAGACATTCACATGAGTTAGAG*	59	365
			R	*AACTGTTCCAATTCAGTTGTCC*		
		21	**F**	*TTTACTGTAAAACTTCTCAGAGCC*	56	795
			R	*ACCTTCTTTCTGCTACAGAAG*		
JS4	*TMEM67*	17	**F**	*AGGTATCTCAGTTGGAAATGC*	56	682
			R	*ACTGAGTTTGTACCAACAACC*		
		21	**F**	*TGTGAAACAAGGCTTCAGGC*	58	358
			R	*ACTCAAGGAATGGGGAGTTG*		
JS5	*C5orf42*	22	**F**	*AAATGATCAGCAGAGTTGGAG*	61	313
			R	*AGATGGTAGACCAGAATGAGTTC*		
		36	**F**	TGTATTTGCAGAATATCTTGCC	54	374
			R	CAGCAATCAGACTAGATAAACC		

(F: Forward primer, R: Reverse primer, T_m: Melting Temperature)

II. DNA clean-up prior to sequencing

1. For each sample, a mixture of 8 µl of the PCR product, 1 µl of Exonuclease and 2 µl of FastAP was prepared in a microcentrifuge tube.
2. The tubes containing the mixture were incubated in the 96-well GeneAmp® PCR System 9700 under the following conditions:

37º C 15 min
85º C 15 min
4º C ∞

III. Preparation and processing of the sequencing reaction mixture

1. The sequencing reaction mixture was prepared as follows:

Table 3-11. Reagents for the sequencing reaction mixture	
Reagents	**Volume** (µl)
BigDye™ Terminator v3.1 Ready Reaction Mix	2
BigDye™ Terminator v1.1 & v3.1 5X Sequencing Buffer	3
Forward or reverse primer	1
Purified PCR product	5
Milli-Q H_2O	9
Total volume	**20**

2. The sequencing reaction mixture of each sample was placed in the GeneAmp® PCR System 9700 with the following reaction conditions:

Table 3-12. PCR reaction conditions for amplification of the targeted exons				
Initial incubation step	**Cycle** (25 cycles)		**Final extension**	**Final hold**
	Denaturation	Annealing/Extension		
HOLD	Cycle		HOLD	HOLD
95º C 5 min	94º C 10 sec	58º C/59º C/ 60º C * 5 sec	60º C 2.5 min	4º C ∞

(*Annealing temperatures (T_a) for the forward and reverse primers of the genes *CC2D2A, TMEM67,* and *C5orf42* are 59º C, 60º C, and 58º C respectively)

3. For each sample, a minicolumn tube was centrifuged at 3200 rpm for 2 min. The minicolumn was transferred into a new 1.5 ml centrifuge tube and the filtrate was discarded.
4. The prepared purified PCR product was transferred into the minicolumn assembly and centrifuged again at 3200 rpm for 2 min.
5. The minicolumn was discarded and the PCR product was kept to be used in the following step.
6. From each sample, 5 µl was transferred into a well in a 96-well plate, then 10 µl of formamide was added into each well under the cabinet.
7. The samples were denatured at 95º C for 2 min using GeneAmp® PCR System 9700.
8. The Genetic Analyzer was set for the samples, and the 96-well plate was placed in the instrument for the analysis.
9. The Applied Biosystems® SeqScape® Software v.3.0 was used to detect and analyze mutations in the sequenced samples.

3.7.2. Cytogenetic analysis

3.7.2.1. Karyotyping analysis

Cytogenetic analysis of the parental cell lines and the generated iPSCs as well as the iPSC-derived NSCs is essential to confirm that there are no numerical or structural chromosomal rearrangements in these cells. A high-resolution Q-banding technique (400–450 bands resolution) was used to make the structural features of the chromosomes visible by staining them with quinacrine dihydrochloride

stain. The process by which all the chromosomes of a single somatic cell are paired and ordered is known as *karyotyping*. All the karyotyping analyses were performed at the Biology and Genetics Division, Department of Molecular and Translational Medicine, University of Brescia.

Materials required

- Quinacrine dihydrochloride solution (Sigma-Aldrich, Cat. No. Q3251)
- KaryoMAX™ Colcemid™ solution in PBS (Gibco™, Cat. No. 15212012)
- Trypsin/EDTA (1:250) solution (BioConcept, Cat. No. 5-52F00-H)
- McIlvaine's buffer solution, pH 3.2, (Spectrum™, Cat. No. 18-611-512)
- KCl solution (0.075 M)
- Methanol/glacial acetic acid (3:1) solution
- Fibroblast cultures
- iPSC cultures

Protocol

1. To be arrested at metaphase stage, the cells were treated with 10 µg/ml of colcemid and incubated for 3 h in a 5% CO_2 humidified incubator at 37° C.
2. The cell culture medium with Colcemid was removed and 1 ml of trypsin/EDTA was added to the cells and incubated at 37° C for 5 min to detach the cells.
3. To the detach the cells, 2 ml of complete DMEM medium was added and the cell suspension was transferred into a 15-ml falcon tube to be centrifuged at 2000 rpm for 5 min.
4. The supernatant was discarded, and the tube was tapped gently to resuspend the cells in 2 ml of a hypotonic solution 0.075 M KCl for 7 min at 37° C.
5. A drop of a fixative (Methanol/glacial acetic acid (3:1)) solution was added to the cell suspension and centrifuged at 2000 rpm for 5 min.
6. The supernatant was discarded, and the tube was tapped gently to resuspend the cells in 2 ml of the fixative for 10 min at RT.
7. The cell suspension was centrifuged at 2000 rpm for 5 min and the supernatant was removed.
8. The tube was tapped gently to resuspend the cells in 2 ml of the fixative and kept at -20° C till slide preparation.
9. To prepare the slides, a drop from each metaphase preparation was added onto a clean and dry glass slide.
10. The slides were stained by emerging them in quinacrine dihydrochloride solution for 5 min, then in McIlvaine's buffer solution for 5 min at 400–450 bands resolution.

11. The slides were examined using a fluorescence microscope. At least, 20 metaphase spreads from each metaphase preparation were analyzed and karyotyped following the to the International System for Human Cytogenomic Nomenclature (ISCN 2016).

3.7.3. Short tandem repeat (STR) analysis

Short tandem repeat (STR) analyses were performed on three iPSC clones of each JS patient and the parental fibroblasts using the AmpFlSTR® Identifiler® Plus PCR Amplification Kit (Applied Biosystems™) to confirm that the generated iPSCs were derived from their parental cells. This STR-based kit amplifies 15 loci and Amelogenin in the genomic DNA of parental fibroblasts and the generated iPSCs. The amplified loci are consistent with STR reference databases.

Materials required

- AmpFLSTR™ Identifiler™ Plus PCR Amplification Kit (Applied Biosystems™, Cat. No. 4427368). It consists of AmpFlSTR® Identifiler® Plus Master Mix, AmpFlSTR® Identifiler® Plus Primer Set, AmpFlSTR® Control DNA 9947A and AmpFlSTR® Identifiler® Plus Allelic Ladder.
- GeneScan™ 600 LIZ™ dye Size Standard v2.0 (Applied Biosystems™, Cat. No. 4408399)
- Formamide (Applied Biosystems™, Cat. No. 17899)
- 1X TE Buffer (Invitrogen™, Cat. No. 12090015)
- dsDNA templates

Protocol

1. Using MQ H_2O, the DNA was diluted to the following concentrations 10 ng/µl, 1 ng/µl and 0.1 ng/µl.
2. The AmpFLSTR™ Identifiler™ Plus PCR amplification kit reaction mixture was prepared as follows:

Table 3-13. AmpFLSTR™ Identifiler™ Plus PCR Amplification reaction mixture	
	Volume (µl)
AmpFlSTR® Identifiler® Plus Master Mix	10
AmpFlSTR® Identifiler® Plus Primer Set	5
dsDNA	10 (0.1 ng/ µl)
Total volume	**25**

3. The positive and negative control for the amplification kit reaction mixture were prepared:

Table 3-14. Positive and negative control for the STR analysis			
Positive control	**Volume** (µl)	**Negative control**	**Volume** (µl)
AmpFlSTR® Identifiler® Plus Master Mix	10	AmpFlSTR® Identifiler® Plus Master Mix	10
AmpFlSTR® Identifiler® Plus Primer Set	5	AmpFlSTR® Identifiler® Plus Primer Set	5
AmpFlSTR® Control DNA 9947A	10	1X TE Buffer	10
Total volume	**25**		**25**

4. The reaction mixture was vortexed for 3 sec, and centrifuged at 3000 rpm for 20 sec.
5. The samples were amplified in a GenAmp PCR system 9700 with the silver 96-well block (Applied Biosystems™) and the reaction conditions were set as shown in the following table:

Table 3-15. PCR reaction conditions for amplification of the STRs

Initial incubation step	**Cycle** (28 cycles)		**Final extension**	**Final hold**
	Denaturation	Annealing/Extension		
HOLD	Cycle		HOLD	HOLD
95º C 11 min	94º C 20 sec	59º C 3 min	60º C 10 min	4º C ∞

6. In each well of a 96-well l reaction plate, 1 µl of each amplified DNA sample, AmpFlSTR™ Identifiler™ Plus allelic ladder, positive and negative control was loaded with 15 µl of formamide and 0.3 µl of GeneScan™ 500 LIZ™ Size Standard.
7. The loaded samples were heated at 95º C for 3 min using the GenAmp PCR system 9700, then the plate was immediately placed on ice for 3 min.
8. The plate assembly was prepared on the autosampler of the Applied Biosystems® 3130 Genetic Analyzer and the electrophoresis run was started.

3.7.4. Immunofluorescence assay for stemness assessment of the generated iPSC lines

All the selected clones of the iPSCs of JS1, JS2, JS3, JS4 and JS5 were sub-cultured in Matrigel-coated coverslips in 24-well plates were immunofluorescent-stained with the primary antibodies anti-OCT4 (Thermo Fisher Scientific) and anti-TRA-1-60 monoclonal antibodies to detect the endogenous OCT4 and the hESC surface antigen Tra-1-60 to confirm the stemness of these cells.

Materials required

- Fix & PERM® Cell Fixation and Permeabilization Kit (Nordic MUbio, Cat. No. Gas-002-1). It consists of Reagent A (Fixation Medium) and Reagent B (Permeabilization Medium).
- iBind™ Solution Kit (Invitrogen™, Cat. No. SLF1020)
- Rabbit monoclonal anti- OCT4 antibody (Thermo Fisher Scientific, Cat. No. A-13998)
- Mouse monoclonal anti- Tra-1-60 antibody (Thermo Fisher Scientific, Cat. No. 4110000)
- Goat anti-rabbit IgG (H+L) Alexa Fluor® 488 (Thermo Fisher Scientific, Cat. No. A-11008)
- Goat anti-mouse IgG (H+L) cross-adsorbed secondary antibody, Alexa Fluor® 568 (Thermo Fisher Scientific, Cat. No. A-11004)
- Hoechst 33342 solution (20 mM) (Thermo Fisher Scientific, Cat. No. H1399)
- Dulbecco's phosphate-buffered saline (DPBS) without $MgCl_2$ and $CaCl_2$ (Sigma-Aldrich, Cat. No. D8537)
- Glycerol Gelatin (Sigma Aldrich, Cat. No. GG1)

Protocol

1. The medium was removed from each well and the cells were washed with 1X DPBS solution. To fix the cells, 300 µl of a fixative (a mixture of Reagent A solution and DPBS (1:1)) was added to each well.
2. The plate was wrapped with an aluminum foil and incubated for 15 min on a shaker at RT.
3. The fixative was removed. (*Optional stopping point*: *After removing fixative, 1 ml of DPBS was added into each well. The plate was wrapped with an aluminium foil to prevent it from drying out and stored at 4° C for up to 2 weeks)*
4. The cells were permeabilized by adding 200 µl of a mixture of Reagent B solution and DPBS (1:1). The plate was wrapped with an aluminium foil and incubated at RT on a shaker for 15 min.
5. The permeabilization solution was removed and 500 µl of the blocking solution (IBind Solution) was added and incubated at RT for 45 min.
6. The blocking solution was removed.
7. 300 µl of the stemness markers anti- OCT4 and anti-TRA-1-60 monoclonal antibodies was added to each well, wrapped with an aluminium foil and incubated at RT on a shaker for 3 h.
8. The primary antibodies were removed, and the wells were washed once with 500 µl of DPBS.
9. 300 µl of anti-mouse IgG (H+L) Alexa Fluor® 568 and anti-rabbit IgG (H+L) Alexa Fluor® 488 diluted in DPBS was added to the cells. The plate was wrapped with an aluminium foil and incubated at RT for 1 h on a shaker.
10. The secondary antibodies were removed, and the wells were washed 3 times with 500 µl of DPBS.
11. For nuclear staining, 300 µl of Hoechst 33342 diluted in DPBS solution (1:100) was added to the cells. The plate was wrapped with an aluminium foil and incubated at RT for 5 min on a shaker.
12. The Hoechst 33342 solution was removed, and the wells were washed 3 times with 500 µl of DPBS.
13. The glass slides were prepared to visualize the cells. Each slide was labelled with the cells type, primary antibodies used and the date. A drop of Glycerol Gelatin (10 µl) was added onto the slide and the round glass coverslip containing the stained cells was picked using a tweezer. The coverslip was placed upside down on the drop on the slide. The cells were visualized under an inverted fluorescence microscope (Olympus IX70) and the images were analyzed using Image-Pro Plus software v7.0 (Media Cybernetics).

Table 3-16. Antibodies used for immunofluorescence staining of the neuronal markers					
Group	**Antibody**	**Manufacturer**	**Cat. No.**	**Dilution**	**Host**
Primary Ab.	Anti-OCT4 monoclonal antibody	Thermo Fisher Scientific	A-13998	1:400	Rabbit
Primary Ab.	Anti-TRA-1-60 monoclonal antibody	Thermo Fisher Scientific	4110000	1:100	Mouse
Secondary Ab.	Goat anti-mouse IgG (H+L) cross-adsorbed secondary antibody, Alexa Fluor® 568	Thermo Fisher Scientific	A-11004	1:250	Mouse
Secondary Ab.	Goat anti-rabbit IgG (H+L) Alexa Fluor® 488	Thermo Fisher Scientific	A-11008	1:250	Rabbit

3.7.5. SYBR Green-based real-time quantitative PCR (RT-qPCR) assay for stemness assessment

SYBR green-based real-time quantitative PCR assays were carried out to assess the stemness of the generated iPSCs using iTaq Universal SYBR Green Supermix (Bio-Rad).

3.7.5.1. RNA purification from the iPSCs using NucleoSpin® RNA Mini Kit

Materials required

- NucleoSpin® RNA Mini Kit (Macherey-Nagel, Cat. No. 740955.250). It contains: Buffer RA1, Buffer RA3, Buffer RAW2, Membrane desalting buffer (MDB), rDNase reaction buffer, NucleoSpin® Filter (violet ring), NucleoSpin® RNA column (light blue ring) and RNase-free H_2O.
- rDNase (Ambion, Cat. No. AM2235)
- β-mercaptoethanol (ß-ME) (Thermo Fisher Scientific, Cat. No. 21985-023)
- Ethanol (70%)
- DMEM/F12 Medium (Gibco™, Cat. No. 11320033)

Protocol

1. The iPSCs were washed using the spent medium in the wells, and the medium was discarded.
2. To each well, 1 ml of DMEM/F-12 medium was added, and the cells were detached using scrapers before being transferred into 1.5-ml Eppendorf tubes.
3. The Eppendorf tubes were centrifuged at 1400 rpm for 7 min and the supernatant was discarded.
4. For each sample, 350 µl of buffer RA1 and 3.5 µl of ß-mercaptoethanol (ß-ME) were added to the cell pellet and vortexed vigorously to lyse the cells.
5. To reduce viscosity and clear the lysate, the NucleoSpin® filter (violet ring) was placed in a 2-ml collection tube.
6. The mixture was applied into the tube and centrifuged for 2 min at 11000 x *g*.

7. The NucleoSpin® filter was discarded and 350 µl of ethanol (70%) was added to the homogenized lysate and mixed by pipetting up and down (5 times).
8. For each preparation one NucleoSpin® RNA column (light blue ring) was taken and placed in a 2-ml collection tube. The lysate was pipetted up and down 2-3 times and loaded into the column then centrifuged for 1 min at 11000 x *g*.
9. The column was placed in a new 2-ml collection tube and 350 µl of the membrane desalting buffer (MDB) was added and centrifuged at 11000 x *g* for 2 min to dry the membrane.
10. DNase reaction mixture was prepared in a sterile 1.5-ml microcentrifuge tube. For each sample, 10 µl of reconstituted rDNase was added to 90 µl of rDNase reaction buffer.
11. The rDNase reaction mixture was mixed by flicking the tube and 95 µl of it was applied directly onto the center of the silica membrane of the column. The tube was incubated at RT for 15 min.
12. To wash and dry the silica membrane, 200 µl of buffer RAW2 was added to the NucleoSpin® RNA column and centrifuged for 1 min at 11000 x *g*. The column was placed into a new 2 ml-collection tube and 600 µl of buffer RA3 was added to the column then centrifuged for 1 min at 11000 x *g*. The flow-through was discarded and the column was placed back into the collection cube. To dry the membrane completely, 250 µl of buffer RA3 was added to the NucleoSpin® RNA column and centrifuged for 2 min at 11000 x *g*. The column was placed into a 1.5-ml nuclease-free collection tube.
13. The RNA was eluted in 60 µl of RNase-free H_2O and centrifuged at 11000 x *g* for 1 min.
14. The RNA was quantified using the Tecan Infinite® 200 Microplate Reader (GMI).

3.7.5.2. TURBO™ DNase treatment and removal of contaminating DNA from RNA

Materials required

- RNA templates
- Invitrogen™ Ambion™ TURBO DNA-free Kit (Invitrogen™ Ambion™, Cat. No.10136824). It consists of TURBO DNase (2 Units/µl), 10X TURBO DNase buffer, DNase inactivation reagent and Nuclease-free H_2O.

Protocol

1. To 40 µl of each RNA sample in a microcentrifuge tube, 1 µl of TURBO DNase and 4 µl of 10X TURBO DNase buffer were added and mixed gently.
2. The samples were incubated at 37° C for 25 min using GeneAmp® PCR System 9700.
3. After incubation, the samples were placed on ice, then 5 µl of resuspended DNase inactivation reagent was added to each sample and mixed well.

4. The samples were incubated at room temperature for 5 min and flicked 2-3 times during the incubation period to re-disperse the DNase inactivation reagent.
5. The samples were centrifuged at 10000 × g for 2 min and each RNA sample was transferred into a fresh 1.5-ml tube. The white precipitate was discarded.
6. The RNA samples were quantified using TECAN Infinite® 200 Microplate Reader and kept at -80º C to be used for reverse transcription.

3.7.5.3. Reverse transcription PCR (RT-PCR)

Materials required

- ImProm-II™ Reverse Transcription System (Promega, Cat. No. A3800). It consists of ImProm-II™ reverse transcriptase, ImProm-II™ 5X reaction buffer, Recombinant RNasin® ribonuclease inhibitor, Random primers, $MgCl_2$, 25 mM solution, dNTP Mix and Nuclease-free H_2O.
- RNA templates

Protocol

1. The volume of the RNA required from each sample was calculated and transferred into an Eppendorf microcentrifuge tube.
2. To each RNA template, 1 µl of random primers was added, and the final volume was completed by nuclease-free H_2O to 10 µl.
3. An Eppendorf tube for -RT was prepared which contains 1 µl of random primers, the RNA templates of all the samples used per a 96-well reaction plate and the total volume was completed to 10 µl by adding nuclease-free H_2O.
4. For each 10 µl of RT and -RT sample, 10 µl of a PCR reaction mixture was prepared and mixed well. The samples were placed in the GeneAmp® PCR System 9700 at 70º C for 5 min, then on ice for 5 min. The PCR reaction mixture was prepared as follows:

Table 3-17. PCR reaction mixture for RT and -RT samples

PCR reaction mixture for RT sample	Volume (µl)	PCR reaction mixture for -RT sample	Volume (µl)
ImProm-II™ 5X reaction buffer	4	ImProm-II™ 5X reaction buffer	4
ImProm-II™ reverse transcriptase	1	ImProm-II™ reverse transcriptase	1
$MgCl_2$	2.4	$MgCl_2$	2.4
dNTP Mix	1	dNTP Mix	1
Recombinant RNasin® ribonuclease inhibitor	0.5	Recombinant RNasin® ribonuclease inhibitor	0
Nuclease-free H_2O	1.1	Nuclease-free H_2O	2.1
Total volume	**10**	**Total volume**	**10**

5. Each 10 µl of RT sample and -RT sample was mixed with 10 µl of the PCR reaction mixture to reach a final volume of 20 µl. The samples were run using the GeneAmp® PCR System 9700 under the following reaction conditions:

25º C	5 min
42º C	60 min
70º C	15 min
4º C	∞

6. The cDNA obtained was kept at -20º C to be used for RT-qPCR gene expression analysis.

3.7.5.4. RT-qPCR analysis of the stemness markers

Materials required

- cDNA
- iTaq Universal SYBR Green Supermix (Bio-Rad, Cat. No. 1725121)
- Forward and reverse primers
- Nuclease-free H_2O

Protocol

1.The RT-qPCR reaction mixture was prepared as follows:

Table 3-18. RT-qPCR reaction mixture for pluripotency gene expression analysis	
Reagents	**Volume** (µl)
iTaq Universal SYBR Green Supermix	12.5
Forward primer	1
Reverse primer	1
Nuclease-free H_2O	8.5
cDNA	2 (5ng/ µl)
Total volume/sample	**25**

2. In a 96-well plate, a triplicate of each sample was loaded for each of the five stemness markers *OCT4, SOX2, c-MYC, KLF4,* and *NANOG* and the house-keeping gene *ACTB* to be studied.

3. The samples in the 96-well plate were spun by centrifugation at 1900 rpm for 3 min.

4. The 96-well plate was placed in the BioRad CFX96 RT-PCR system and the system was run under the following reaction conditions:

Table 3-19. RT-qPCR reaction conditions for gene expression analysis of the pluripotency genes				
Initial incubation step	**Cycle** (39 cycles)		**Final extension**	**Final hold**
	Denaturation	Annealing		
HOLD	Cycle		HOLD	HOLD
98º C 30 min	95º C 5 sec	60º C 30 min	65º C 5 sec	95º C 5 min

5. The generated RT-qPCR data were analyzed using BioRad CFX Manager™ Software.

Table 3-20. Primer sets used for assessment of stemness of the generated cell lines by RT-qPCR

	Gene	Forward primer (5′-3′)	Reverse primer (5′-3′)
Stemness markers	*OCT4*	*CCTCACTTCACTGCACTGTA*	*CAGGTTTTCTTTCCCTAGCT*
	SOX2	*CCCAGCAGACTTCACATGT*	*CCTCCCATTTCCCTCGTTTT*
	c-MYC	*TGCCTCAAATTGGACTTTGG*	*GATTGAAATTCTGTGTAACTGC*
	KLF4	*GATGAACTGACCAGGCACTA*	*GTGGGTCATATCCACTGTCT*
	NANOG	*TGAACCTCAGCTACAAACAG*	*TGGTGGTAGGAAGAGTAAAG*
House-keeping gene	*ACTB*	*CGCCGCCAGCTCACCATG*	*CACGATGGAGGGGAAGACGG*

(*ACTB*: β-actin, *OCT4*: octamer-binding transcription factor 4, *SOX2*: SRY-box transcription factor 2, and *KLF4*: Kruppel-like factor 4)

3.7.6. Differentiation of the generated iPSCs into the three germ layers

The cardinal feature of PSCs is their potential to differentiate into the three embryonic layers: *ectoderm, mesoderm,* and *endoderm*, and this is known as pluripotency. Therefore, assessment of pluripotency is important for characterization of iPSCs besides morphology and surface marker analysis. Currently, the StemMACS Trilineage Differentiation Kit (Miltenyi Biotec) is the most used functional assay to validate the pluripotency of established hESCs and iPSCs. It requires only 7 days to be conducted and the embryonic cells can be analyzed by immunocytochemistry or flow cytometry.

Materials required

- StemMACS™ Trilineage Differentiation Kit (human) (Miltenyi Biotec, Cat. No. 130-115-660). It consists of StemMACS Trilineage MesoDiff Medium I, StemMACS Trilineage MesoDiff Medium II, StemMACS Trilineage EndoDiff Medium and StemMACS Trilineage EctoDiff Medium.
- Dulbecco's phosphate-buffered saline (DPBS) With $MgCl_2$ and $CaCl_2$ (Sigma-Aldrich, Cat. No. D8662)
- Dulbecco's phosphate-buffered saline (DPBS) without $MgCl_2$ and $CaCl_2$ (Sigma-Aldrich, Cat. No. D8537)
- NutriStem® hPSC XF Medium (Biological Industries, Cat. No. 05-100-1A)
- Corning™ Matrigel™ hESC-Qualified Matrix (Corning, Cat.No.08-774-552)
- Trypsin/EDTA (0.05%) (Sigma-Aldrich, Cat. No. SM-2002)
- Soybean Trypsin Inhibitor (0.5 mg/ml) (Gibco®, Cat. No. 17075029)
- DMEM/F12 with L-Glutamine, without HEPES (Sigma-Aldrich, Cat. No. DF-042-B)
- ROCK inhibitor (Y27632) (Sigma-Aldrich, Cat. No. Y0503)

Protocol

I. Harvesting of the iPSCs

For this assay, single-cell suspensions and 6-well plates coated with Matrigel were used. The media were thawed at 2-8° C overnight.

1. Cell culture medium was aspirated, and each well was washed with 3 ml of D-PBS without $CaCl_2$ and $MgCl_2$.
2. To each well, 1 ml of 0.05% Trypsin-EDTA was added. The plate was gently rocked to ensure even distribution of the enzyme solution, then incubated at 37° C in the dark for 5 min.
3. To stop enzymatic reaction, 2 ml of Soybean Trypsin Inhibitor (0.5 mg/ml) was added to each well.
4. The iPSC colonies in each well were dissociated to a single-cell suspension by carefully pipetting up and down using a 5-ml serological pipette.
5. The number of cells was counted using Countess™ automated cell counter.

II. Differentiation of the iPSCs into the three embryonic layers

Day 0

1. The cells were plated by transferring the desired number of cells into three 15-ml conical tubes. Table 3-21 shows recommended starting number of cells for differentiation of iPSCs into the three germ layers.

Table 3-21. Recommended starting number of cells for differentiation of iPSCs into the embryonic layers

Linage	12-well plate	24-well plate
Ectoderm	200000	100000
Mesoderm	150000	80000
Endoderm	250000	130000

2. The cells were centrifuged for 5 min at 200×g, and the supernatant was aspirated and discarded.
3. The cell pellets were resuspended into complete NutriStem® hPSC XF medium supplemented with ROCK inhibitor (10 μM StemMACS Y27632) and transferred into Matrigel-coated culture plates. The media and volumes required are shown in the following table:

Table 3-22. Media and volumes used for plating the iPSCs for differentiation into the embryonic layers

Linage	12-well plate	24-well plate	Medium
Ectoderm	1 ml	0.5 ml	StemMACS Trilineage EctoDiff Medium
Mesoderm	1 ml	0.5 ml	NutriStem® hPSC XF medium
Endoderm	1 ml	0.5 ml	NutriStem® hPSC XF medium

Media changes for ectoderm

Days 1-6. The medium was changed daily using 0.5 ml StemMACS Trilineage EctoDiff medium per well in a 24-well plate (or 1 ml per well in a 12-well plate).

Media changes for endoderm

Day 1. The PSC cultivation medium was not replaced on day 1.

Days 2-6. The cells were washed daily using 2 ml of D-PBS with $CaCl_2$ and $MgCl_2$ and 0.5 ml of StemMACS EndoDiff medium was added to each well in a 24-well plate (or 1 ml per well in a 12-well plate).

Media changes for mesoderm

Day 1. After 24 hr, the PSC cultivation medium was replaced with 1.5 ml of StemMACS MesoDiff medium I per well in a 24-well plate (or 3 ml per well in a 12-well plate).

Days 2-3. The differentiation medium was not replaced on days 2 and 3.

Days 4-6. The medium was replaced daily with 1 ml of StemMACS MesoDiff medium II per each well in a 24-well plate (or 2 ml per well in a 12-well plate).

3.7.7. TaqMan-based qRT-PCR assays for germ layer-specific markers

On day 7, TaqMan-based qRT-PCR assays were performed to study the expression of the ectodermal, mesodermal, and endodermal markers (Table 3-23) for JS1, JS2, JS3, JS4, and JS5 differentiated lines. RNA was extracted from the cell pellet in each tube using NucleoSpin® RNA Mini Kit (Macherey-Nagel, Cat. No. 740955.250) (Section 3.7.5.1). The purified RNA was reverse-transcribed into cDNA using ImProm-II™ Reverse Transcription System (Promega, Cat. No. A3800) (Section 3.7.5.3). TaqMan™ Gene Expression Master Mix (Applied Biosystems, Cat. No. 4369016) was used for this assay. For each reaction, 10 ng of the cDNA was added, and all the samples were analyzed and compared in triplicate. The qPCR cycling and running parameters were set as: 50º C for 2 min, 95º C for 10 min, and 40 cycles at 95º C and 60º C for 15 sec and 1 min respectively. Undifferentiated iPSCs of the same clone and passage of each JS-derived iPSC line were used as an internal control. *ACTB* was used as a house-keeping gene and the relative quantification of the target genes was calculated using the $2^{-\Delta\Delta CT}$ method (Livak & Schmittgen, 2001).

Table 3-23. Embryonic layers differentiation markers used for TaqMan-based qPCR

	Gene	Probe
Ectodermal markers	*PAX6*	Hs.PT.58.25914558
	SOX1	Hs.PT.58.28041414.g
Mesodermal markers	*ACTA2*	Hs.PT.56a.2542642
	CXCR4	Hs00607978_s1
Endodermal markers	*GATA4*	Hs.PT.58.259457
	SOX17	Hs.PT.58.24876513
House-keeping gene	*ACTB*	Hs.PT.39a.22214847

(*ACTA2*: actin alpha 2 gene, *ACTB*: β-actin gene, *CXCR4*: C-X-C chemokine receptor type 4 gene, *GATA4*: GATA binding protein 4 gene, *PAX6*: paired box protein gene, *SOX1*: SRY-box transcription factor 1 gene, *SOX17*: SRY-box transcription factor 17 gene).

3.8. Cryopreservation of the generated iPSCs

Cryopreservation of the generated iPSCs is extremely important to maintain a source of the cell lines for future research and to avoid loss of the cell lines due to contamination or incubator failure. The high quality iPSCs were cryopreserved when they reached 70-80% confluence in a well of a 6- or 12-well culture plate at different passages.

Materials required

- Bambanker™ Serum-Free Cell Freezing Medium (Nippon Genetics Europe GmbH, Cat. No. BB01)
- Dulbecco's PBS (D-PBS) without $CaCl_2$ and $MgCl_2$ (Thermo Fisher Scientific, Cat. No. 14190)
- Nalgene® Mr. Frosty® Freezing Container (Fisher Scientific, Cat. No. 15-350-50)

Protocol

1. The reagents, cryogenic vials and Nalgene® Mr. Frosty® Freezing Container (Fisher Scientific) were kept chilled (at 2° C - 8° C) during the cryopreservation procedure. The cryogenic vials were well-labelled before the procedure.
2. The spent medium was removed from the culture plates and each well was washed with 500-1000 µl of DPBS.
3. To cryopreserve high quality iPSCs, any differentiated part of the cell culture was removed using a pipette tip under the microscope.
4. 800 µl of Bambanker™ Serum-free cell freezing medium was added to each well of a 6- or 12-well culture plate, and the iPSCs colonies were detached using a cell scraper (EuroClone®).
5. The iPSC clumps were aspirated using a 2-ml serological pipette and transferred into the cryogenic vials which were immediately placed in a pre-chilled Mr. Frosty™ Freezing Container.
6. The freezing container was kept in a -80° C freezer overnight, then transferred into a liquid nitrogen storage or -150° C freezer.

3.9. Induction of NSCs from JS-derived iPSCs

Materials required

- PSC Neural Induction Medium. It consists of Neurobasal® Medium and Neural Induction Supplement, 50X (Thermo Fisher Scientific, Cat. No. A1647801).
- Advanced™ DMEM/F12 (Thermo Fisher Scientific, Cat. No. 12634)
- Corning™ Matrigel™ hESC-Qualified Matrix (Corning, Cat.No.08-774-552)
- ROCK Inhibitor Y27632 (Sigma-Aldrich, Cat. No. Y0503)
- Dulbecco's PBS (DPBS) without $CaCl_2$ and $MgCl_2$ (Thermo Fisher Scientific, Cat. No. 14190)

- StemPro® Accutase® Cell Dissociation Reagent (Cat. No. A11105)
- Dimethyl sulfoxide (DMSO), Sterile (Sigma-Aldrich, Cat. No. D2650)
- 100-µm strainer (Fisher Scientific, Cat. No. 08-771-19)
- Nalgene® Mr. Frosty® Freezing Container (Fisher Scientific, Cat. No. 15-350-50)

3.9.1. Preparation of PSC neural induction medium (for 500 ml)

Complete PSC neural induction medium was prepared by aseptically mixing 490 ml Neurobasal® Medium with 10 ml Neural Induction Supplement to have a final volume of 500 ml. Complete PSC Neural Induction Medium was stored at 2-8° C in the dark for up to 2 weeks. The Neural Induction Medium was warmed in a 37° C water bath for 5-10 min before use.

3.9.2. Preparation of neural expansion medium (for 100 ml**)**

Complete neural expansion medium was prepared by aseptically mixing 49 ml of Neurobasal® medium with 49 ml of Advanced™ DMEM/F12 and 2 ml of neural induction supplement. Complete neural expansion medium was stored at 2-8° C in the dark for up to 2 weeks. The neural expansion medium was warmed in a 37° C water bath for 5-10 min before being added to the cells.

3.9.3. Preparation of ROCK inhibitor Y27632 solution (5 mM)

ROCK inhibitor Y27632 solution (5 mM) was prepared by aseptically mixing 1 mg of ROCK inhibitor Y27632 with 0.625 ml of distilled water. The dissolved solution was filtered through a 0.22 µm filter, then 20-50 µl of the solution were aliquoted into sterile tubes and stored at -5° to -20° C in the dark.

3.9.4. Coating culture vessels with Corning™ Matrigel™ hESC-qualified matrix

1. For each culture vessels coating, Matrigel aliquot was thawed on ice, at 2-8° C overnight.
2. The thawed Matrigel aliquot was diluted in an appropriate volume of cold DMEM/F12 medium in a Falcon 50-ml conical centrifuge tube placed on ice.
3. To cover the whole surface of each culture vessel, 0.5 ml or 1 ml of the Matrigel solution was immediately added to each well of a 12- or 6-well plate, respectively, placed on ice.
4. The plates were incubated in a 5% CO_2 humidified incubator at 37° C for at least 60 min.
5. Just before use, the diluted Matrigel solution was aspirated from the culture vessels, and immediately replaced with 2.5 ml complete NutriStem® hPSC XF medium.

3.9.5. Preparation of JS-derived iPSCs for neural induction

1. For efficient neural induction, high quality JS iPSCs (with minimal or no differentiated colonies) were cultured in Matrigel-coated 6-well plates containing complete NutriStem® hPSC XF medium.
2. When the iPSCs reached 70–80% confluency, they were detached from the Matrigel-coated well.
3. The iPSC suspension was prepared up to 6 ml, and 1 ml of it was transferred to a 15-ml conical centrifuge tube to estimate the total number of the iPSCs. The cell suspension was centrifuged at 200 × *g* for 3 min and the supernatant was aspirated.
4. From the pre-warmed StemPro® Accutase® Cell Dissociation Reagent, 1 ml was added to the cells in the 15-ml conical tube, and incubated for 5 min at 37° C.
5. The cells were vigorously pipetted up and down 5 times with a 1-ml pipette to dissociate the cells into a single-cell suspension.
6. The total cell number was counted using Countess™ automated cell counter. The total number of cells in the remaining 5 ml of the iPSC suspension equals:

   Total cell number in 1 ml of StemPro® Accutase® reagent × 5
7. The diluted Matrigel solution was aspirated from the culture vessels, and immediately replaced with 2.5 ml of complete NutriStem® hPSC XF Medium into each well of the coated 6-well culture plates.
8. The conical tube containing the iPSC suspension was gently shaken and the iPSCs were seeded into each well at $2.5 \times 10^5 – 3 \times 10^5$ iPSCs per well.
9. The plates were moved in several quick back-and-forth and side-to-side motions to disperse the cells across the surface, then gently placed in a 5% CO_2 humidified incubator at 37° C.

   [The passaging ratio of confluent iPSCs to fresh iPSC medium depends on two factors: the variability and confluence of iPSC lines. 15–25% confluency is the starting density of the iPSCs for passaging and cells should be plated as small clumps and not as a single-cell suspension. The cells may be treated overnight with 10 μM of ROCK inhibitor Y27632 by adding it to the iPSC medium at the time of passaging].

3.9.6. Neural induction

The workflow of induction of NSCs from the iPSCs is shown in Fig.3-2.

1. On day 1 of iPSC passaging (15–25% confluency), the spent medium was aspirated to remove non-attached cells, and 2.5 ml of pre-warmed complete PSC Neural Induction Medium was added to each well of the 6-well plates. The plates were returned to the incubator.
2. On day 2 of neural induction, the uniform morphology of cell colonies was confirmed.

3. On day 2 (about 48 hr after switching to PSC Neural Induction Medium), the spent medium was aspirated from each well and 2.5 ml of pre-warmed complete Neural Induction Medium was added to each well.
4. On day 4 of neural induction, all colonies with non-neural differentiation if any were marked and removed with a Pasteur glass pipette, then the spent medium from each well was changed by adding 5 ml of pre-warmed complete PSC Neural Induction Medium per well.
5. On day 6 of neural induction (cells were close to maximal confluence), any non-neural differentiated cells were removed, and 5 ml of complete PSC Neural Induction Medium was added into each well.

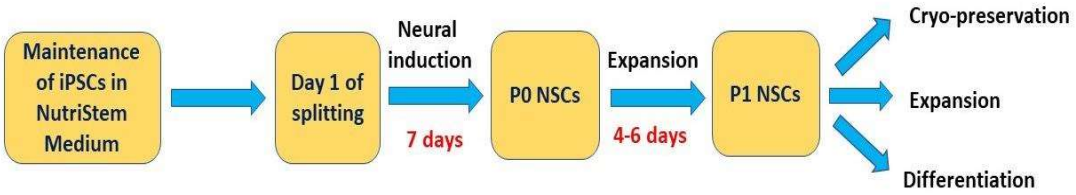

Figure 3-2. **Derivation of NSCs workflow.** Adapted from Induction of NSCs using Gibco Neural Induction Medium Protocol, Gibco, (2013), Pub. No. MAN0008031, p.6.

3.9.7. Harvesting and expansion of NSC passage 0 (P0)

On day 7 of neural induction, NSCs (P0) were ready to be harvested and expanded.

1. Matrigel-coated plates were prepared before performing the expansion process.
2. A Pasteur glass pipette was used to aspirate the spent PSC Neural Induction Medium from the 6-well plates to be split.
3. To each well of a 6-well plate and towards the wall of the well to avoid cell detachment, 2 ml of DPBS without Ca^{2+} and Mg^{2+} was added and the D-PBS was aspirated to rinse the cells.
4. 1 ml of pre-warmed StemPro® Accutase® Cell Dissociation Reagent was added to each well of the 6-well plates and incubated for 5–8 min at 37° C until most cells detached from the surface of the plates.
5. A cell scraper was used to detach the cells from the surface of the plates.
6. The cell clumps were transferred to a 15-ml conical tube using a 5-ml serological pipette.
7. 1 ml of D-PBS was added to each well of the 6-well plates to collect residual cells, then the cell suspension was transferred to the conical tube.
8. The cell suspension was gently pipetted up and down 3 times with a 5-ml pipette to break up the cell clumps and passed through a 100-µm strainer and the cells were centrifuged at 300 × *g* for 4 min.
9. The supernatant was aspirated, and the cells were re-suspended with DPBS (3–5 ml of DPBS for

all cells from 1 well of a 6-well plate), then the cells were centrifuged at 300 × *g* for 4 min.

10. The supernatant was aspirated, and the cells in each well of a 6-well plate were re-suspended in 1 ml of pre-warmed complete Neural Expansion Medium.
11. The cell concentration was determined using Countess™ automated cell counter.
12. The cell suspension was diluted with pre-warmed complete Neural Expansion Medium to 2×10^5 – 4×10^5 cells/ml.
13. ROCK inhibitor Y27632 was added to the cell suspension to a final concentration of 5 μM.
14. The Matrigel solution was aspirated from the Matrigel-coated plates and the diluted cell suspension was added to each culture vessel to seed the cells at a density of 0.5×10^5–1×10^5 cells/cm^2.
15. The culture vessels were moved in several quick back-and-forth and side-to-side motions to disperse the cells across the surface, then the vessels were gently placed in the incubator.
16. After overnight incubation, the spent medium was changed with complete Neural Expansion Medium to eliminate the ROCK inhibitor Y27632. The Neural Expansion Medium was continuously changed every other day thereafter.
17. When NSCs reached confluency, they were further expanded in complete Neural Expansion Medium. Part of the expanded NSCs were cryopreserved and differentiated into neurons.

(After dissociation of P0–P4 NSCs, addition of ROCK inhibitor Y27632 to the cell suspension to a final concentration of 5 μM for overnight treatment was required at the time of plating to prevent cell death for both expansion and differentiation into neuronal cells).

3.10. Characterization of JS-derived NSCs

3.10.1. Genetic analysis for confirmation of the pre-existing variants in parental cells

The genomic DNA was isolated from the generated NSCs using the QIAamp® DNA Mini Kit (Qiagen), according to the manufacturer's instructions (Section 3.7.1.1). The PCR was used to amplify the targeted sequences containing the mutations. The PCR products were sequenced, and the mutations were detected and analyzed using the Applied Biosystems® 3130 Genetic Analyzer and the Applied Biosystems® SeqScape® Software v.3.0, respectively. Detailed protocols were previously mentioned in section (3.7.1.2).

3.10.2. Cytogenetic analysis

The NSCs were analyzed to confirm that there is no structural or numerical rearrangement in their chromosomes following the protocol mentioned in section (3.7.2.1).

3.10.3.SYBR Green-based real-time quantitative PCR assay

Real-time qPCR assays were carried out to assess the expression of the neural markers *NESTIN*, *PAX6*, also known as aniridia type II protein (AN2), *SOX1,* and *SOX2* and the stemness marker *OCT4* in the iPSC-derived NSCs. The iTaq Universal SYBR Green Supermix (Bio-Rad) was used following the protocols shown in section (3.7.5.4). The forward and reverse primers of the marker genes used are shown in Table 3-24.

Table 3-24. Primer sets used for characterization of the iPSC-derived NSCs by SYBR Green-based RT-qPCR

	Gene	Forward primer (5′-3′)	Reverse primer (5′-3′)
Neural stemness genes	*SOX1*	*CCTCCGTCCATCCTCTG*	*AAAGCATCAAACAACCTCAAG*
	SOX2	*CCCAGCAGACTTCACATGT*	*CCTCCCATTTCCCTCGTTTT*
	NESTIN	*GCGTTGGAACAGAGGTTGGA*	*TGGGAGCAAAGATCCAAGAC*
	PAX6	*CTGAAGCGGAAGCTGCAAAG*	*TTGCTGGCCTGTCTTCTCTG*
Pluripotency gene	*OCT4*	*CCTCACTTCACTGCACTGTA*	*CAGGTTTTCTTTCCCTAGCT*
Endogenous control	*ACTB*	*CGCCGCCAGCTCACCATG*	*CACGATGGAGGGGAAGACGG*

3.10.4. Immunofluorescence assays for NSC markers

The NSCs (P0) of JS2, JS5 and BJ attached to Matrigel-coated coverslips in 24-well culture plates were stained with antibodies for specific NSC markers (SOX1, SOX2, and NESTIN) and the stemness marker (OCT4) to confirm the induction of the NSCs from the iPSCs. Four coverslips for each cell line were stained following the protocol previously mentioned in section (3.7.4).

Table 3-25. Antibodies used for immunofluorescence staining of the neural markers

Group	Antibody	Manufacturer	Cat. No.	Dilution	Host
Primary Ab.	Anti-NESTIN	Thermo Fisher Scientific	A24345	1:100	Mouse
Primary Ab.	Anti-SOX1	Thermo Fisher Scientific	A24347	1:100	Goat
Primary Ab.	Anti-SOX2	Thermo Fisher Scientific	A24339	1:100	Rabbit
Secondary Ab.	Goat anti-mouse IgG (H+L) cross-adsorbed secondary antibody, Alexa Fluor® 568	Thermo Fisher Scientific	A-11004	1:250	Mouse
Secondary Ab.	Goat anti-rabbit IgG (H+L) Alexa Fluor® 488	Thermo Fisher Scientific	A-11008	1:250	Rabbit

3.11. Differentiation of JS-derived NSCs into neurons

Differentiation of JS-derived NSCs into neurons was performed following a standard protocol in Gibco™ Neurobiology Protocol Handbook (Thermo Fisher Scientific). NSC lines of JS2, JS5, and BJ were selected and differentiated into neurons and the workflow is shown in Fig.3-3.

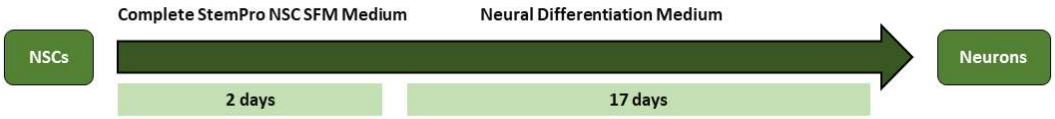

Figure 3-3. Workflow of differentiation of iPSC-derived NSCs into neurons.

Materials required

- NSCs
- Gibco™ Neurobasal™ Medium (Cat. No. 21103049)
- Gibco™ B-27™ Supplement (50X), serum free (Cat. No. 17504044)
- Gibco™ GlutaMAX™-I Supplement (Cat. No. 35050061)
- Gibco™ Antibiotic-Antimycotic (100X) solution (Cat. No. 15240096)
- Poly-L-Ornithine (Sigma-Aldrich, Cat. No. P3655)
- Gibco™ Laminin (Cat. No. 23017015)
- Gibco™ StemPro™ NSC SFM (Cat. No. A1050901). It consists of KnockOut™ DMEM/F-12 Basal Medium stored at 4° C, StemPro™ NSC SFM (Neural) Supplement stored at -20° C to -5°C in the dark and bFGF Recombinant Human and EGF Recombinant Human stored at 4° C.

Protocol

I. Preparation of neural differentiation medium

Neural differentiation medium is composed of Neurobasal Medium with B-27 Supplement (50X), serum free and GlutaMAX-I Supplement. For preparation of 100 ml of neural differentiation medium, the components shown in Table 3-26 were aseptically mix. For larger volumes, the component amounts were proportionally increased. When stored in the dark at 2° C to 8° C, this medium can be stable for 2 weeks.

Table 3-26. Preparation of neural differentiation medium

Component	Final concentration	Amount (ml)
Gibco™ Neurobasal™ Medium	1X	96
Gibco™ B-27™ Supplement	2%	2
Gibco™ GlutaMAX™-I Supplement	2mM	1
Antibiotic-Antimycotic solution	1%	1

II. Coating culture plates with poly-L-ornithine and laminin

1. Poly-L-ornithine was dissolved in cell culture–grade distilled water to prepare 10 mg/ml stock solution (500X). The solution was aliquoted into polypropylene tubes and stored at –20° C until use.

2. The laminin was slowly thawed at 2° C to 8° C and 10 µg/ml working solution was prepared using cell culture–grade distilled water. Aliquot the working solution was aliquoted into polypropylene tubes and stored at –20°C until use. Repeated freeze/thaw cycles were avoided.

3. The poly-L-ornithine stock solution was diluted 1:500 in cell culture–grade distilled water to prepare 20 µg/ml working solution.

4. For each JS cell line and the control, the surfaces of two wells of a 6-well culture plate, 6 wells of a 12-well culture plate and 4 wells (with cover slips) of a 24-well culture plate were coated with the poly-L-ornithine working solution (1.5 ml/well, 600 µl/well, 400 µl/well of 6-, 12-, 24-well culture plates respectively).

5. The culture vessels were incubated for 1 h at 37° C or overnight at 4° C.

6. The culture vessels were rinsed twice with sterile water.

7. The surfaces of the wells of the culture vessels were re-coated with the laminin working solution (1.5 ml/well, 600 µl/well, 400 µl/well of 6-, 12-, 24-well culture plates respectively).

8. The culture vessels were incubated for 2 h at 37° C or overnight at 4° C.

9. The culture vessels were rinsed with DPBS without Ca^{2+} and Mg^{2+} and stored covered with DPBS until use. Immediately before use, all DPBS were removed and replaced with complete StemPro NSC SFM medium.

III. Differentiation into neurons

The NSCs were seeded on poly-L-ornithine- and laminin-coated culture plates in complete StemPro NSC SFM medium at 500000, 200000, and 100000 cells/well in 6-, 12- and 24-well culture plates respectively. After 48 hr, the medium was replaced by the neural differentiation medium. The spent medium was changed every 3-4 days. The cells were kept unexposed to ambient air at any time after their differentiation into neurons.

3.12. Characterization of the neuronal cell lines

3.12.1.SYBR Green-based RT-qPCR) assay

Real-time qPCR analysis was performed to assess the expression of the neuronal markers *PAX6, DCX*, *MAP2, TUBB3, GFAP, GAD, CHAT,* and *TH*. The iTaq Universal SYBR Green Supermix (Bio-Rad) was used following the protocols shown in section (3.7.5.4). The forward and reverse primers of the marker genes used are shown in Table 3-27.

Table 3-27. Primer sets used for characterization of the neurons by SYBR-Green-based RT-qPCR			
	Gene	**Forward primer (5′-3′)**	**Reverse primer (5′-3′)**
	PAX6	*CTGAAGCGGAAGCTGCAAAG*	*TTGCTGGCCTGTCTTCTCTG*
Neuronal marker genes	*DCX*	*TATGCGCCGAAGCAAGTCTC*	*TACAGGTCCTTGTGCTTCCG*
	MAP2	*GACTGCAGCTCTGCCTTTAG*	*AAGTAAATCTTCCTCCACTGTGAC*
	TUBB3	*GGCCAAGTTCTGGGAAGTCAT*	*CTCGAGGCACGTACTTGTGA*
	GFAP	*GAGGTTGAGAGGGACAATCTGG*	*GTGGCTTCATCTGCTTCCTGTC*
	GAD	*GTCGAGGACTCTGGACAGTA*	*GGAAGCAGATCTCTAGCAAA*
	CHAT	*ACTGGGTGTCTGAGTACTGG*	*TTGGAAGCCATTTTGACTAT*
	TH	*TCATCACCTGGTCACCAAGTT*	*GGTCGCCGTGCCTGTACT*
Endogenous control	*ACTB*	*CGCCGCCAGCTCACCATG*	*CACGATGGAGGGGAAGACGG*

3.12.2. Immunofluorescence assays for the neuronal markers

The neurons of JS2, JS5 and BJ attached to the poly-L-ornithine and laminin-coated coverslips in the 24-well plates were stained for specific neuronal markers to confirm the differentiation of the NSCs into neurons. Following the protocol previously mentioned in section (3.7.4), cells on four coverslips for each patient and the control were immunofluorescent-stained with MAP2 monoclonal antibody (M13) and purified anti-tubulin β-3 (TUBB3) antibody (Table 3-28).

Table 3-28. Antibodies used for immunofluorescence staining of the neuronal markers					
Group	**Antibody**	**Manufacturer**	**Cat. No.**	**Dilution**	**Host**
Primary Ab.	MAP2 monoclonal antibody (M13)	Invitrogen™	13-1500	1:250	Mouse
Primary Ab.	Purified anti-tubulin β-3 (TUBB3) antibody	BioLegend	802001	1:400	Rabbit
Secondary Ab.	Goat anti-mouse IgG (H+L) cross-adsorbed secondary antibody, Alexa Fluor® 568	Thermo Fisher Scientific	A-11004	1:250	Mouse
Secondary Ab.	Goat anti-rabbit IgG (H+L) Alexa Fluor® 488	Thermo Fisher Scientific	A-11008	1:250	Rabbit

3.13. Functional analysis of primary cilia in JS-derived cell lines

3.13.1.Immunofluorescence staining of JS-derived fibroblast primary cilia

The fibroblasts of JS2 (P9), JS5(P7), and BJ (P22) were counted using Countess™ automated cell counter (Invitrogen™) and 100000 cells/well were seeded on 10 mm round glass coverslips placed in 2 wells of 24-well cell culture plates. In each well, 1 ml of complete DMEM medium containing (10% FBS) was added and after 24 hr the medium was replaced in the first well with 1 ml of a serum-starved DMEM medium containing (0.5% FBS) to induce ciliogenesis, and in the second well, 1 ml of complete DMEM medium was added. Immunofluorescence staining was performed to detect the expression of the primary cilium marker, acetylated α-tubulin, following the protocol in section (3.7.4). The primary and secondary antibodies used are shown in Table 3-29. The experiments were performed in triplicate for cells in serum-starved and serum-enriched medium. The cells were counted from 10 randomly selected fields on a microscope slide.

Table 3-29. Antibodies used for immunofluorescence staining to visualize the primary cilia of the cells					
Group	**Antibody**	**Manufacturer**	**Cat. No.**	**Dilution**	**Host**
Primary Ab.	Monoclonal mouse anti-acetylated alpha-tubulin	Sigma-Aldrich	T7451	1:10000	Mouse
Secondary Ab.	Goat anti-mouse IgG (H+L) cross-adsorbed secondary antibody, Alexa Fluor® 568	Thermo Fisher Scientific	A-11004	1.6:1000	Mouse
Conjugated Ab.	Alexa Fluor™ 488 Phalloidin	Molecular Probes	A12379	1:1000	-

3.13.2.Immunofluorescence staining of JS-derived iPSC primary cilia

The iPSCs of JS2 (C6), JS5 (C6), and BJ (C21) were picked and re-plated in 12-well culture vessels containing complete NutriStem® hPSC XF Medium for each iPSC line. The medium was changed every day for 4-5 days. On the day when the iPSC colonies seem to be ready for picking, the cells were fixed and stained to visualize and assess the number and length of the primary cilia in the iPSCs of the patients and BJ. The immunofluorescence staining was performed following the protocol previously mentioned in section (3.7.4). The experiments were performed in triplicate for the iPSCs of each clone and the cells were counted from 10 randomly selected fields on a microscope slide.

3.13.3. Functional analysis of primary cilia in JS-derived NSCs

3.13.3.1. Immunofluorescence staining of JS-derived NSC primary cilia

The NSCs of JS2 (P16), JS5 (P6), and BJ (P12) derived from iPSCs C6P26, C6P26, and C23P145 were picked and re-plated in 12-well culture plates containing the Neural Expansion Medium for each NSC line. The medium was continuously changed every other day for 4-6 days. On the day when the NSCs seem to be ready for passaging, the cells were fixed and stained to visualize and assess the number and length of the primary cilia in JS-derived NSCs and BJ-derived NSCs. The immunofluorescence staining was performed following the protocol previously mentioned in section (3.7.4). The experiments were performed in triplicate for each NSC line grown in Neural Expansion Medium and the cells were counted from 10 randomly selected fields on a microscope slide.

3.14. Functional analyses of SHH signaling pathway in JS-derived cell lines

Functional analyses of four key components of SHH signal transduction pathway (Gli1, Gli2, Smo, and Ptch1) were performed on fibroblast, iPSC, NSC, and neuronal lines derived from JS2, JS5, and BJ.

3.14.1. Functional analysis of SHH signaling pathway in JS-derived fibroblasts

3.14.1.1. SAG stimulation of JS-derived fibroblasts

Materials required

- Dulbecco's Modified Eagle Medium (DMEM) (EuroClone®, Cat. No. ECB7501L)
- Fetal bovine serum (FBS) (EuroClone®, Cat. No. ECS0180L)

- L-Glutamine (EuroClone®, Cat. No. ECB3000D)
- Penicillin/Streptomycin (EuroClone®, Cat. No. ECB3001DCL)
- Trypsin-EDTA (1:250) (BioConcept, Cat. No. 5-52F00-H)
- Smoothened agonist, SAG - CAS 364590-63-6 - Calbiochem (Sigma-Aldrich, Cat. No. 566660)
- Dimethyl sulfoxide (DMSO), Sterile (Sigma-Aldrich, Cat. No. D2650)

Protocol

1. Fibroblasts of JS2 (P20), JS5 (P12), and BJ (P26) were grown in T-75 cell culture flasks containing 11 ml of complete DMEM medium.
2. When the cells reached 80-90% confluency, the spent medium was removed, and cells were washed with 10 ml of DPBS.
3. To dissociate the adherent cells, 1 ml of Trypsin-EDTA solution was added to each flask to cover all the cells. The flask was placed for 5 min in a 5% CO_2 humidified incubator at 37° C.
4. After incubation, the flask was tapped gently to detach any adherent cells and 9 ml of complete DMEM medium was added to deactivate the effect of Trypsin-EDTA.
5. The cell suspension was transferred into a Falcon 50-ml conical centrifuge tube to be centrifuged at 1400 rpm for 10 min.
6. The supernatant was discarded, and the bottom of the tube was gently tapped to loosen the cell pellet. The cells were resuspended in 1 ml of complete DMEM medium containing (10% FBS) and counted using the Countess™ automated cell counter.
7. From the cell suspension, 100000 cells/well were seeded in a 12-well plate. Two wells were prepared for JS2, JS5, and BJ fibroblasts for each experiment.
8. After 24 hr, the spent medium in the first well was changed with 1 ml of complete DMEM medium and 1 µl of DMSO, while the in the second well, the spent medium was replaced with 1 ml of serum-starved DMEM medium (0.5% FBS) and 2 µM of smoothened agonist (SAG). The cells were incubated for another 24 hr.
9. RNA was extracted from the cell pellet in each tube using NucleoSpin® RNA Mini Kit (Macherey-Nagel, Cat. No. 740955.250) (Section 3.7.5.1). The purified RNA was reverse-transcribed into cDNA using ImProm-II™ Reverse Transcription System (Promega, Cat. No. A3800) (Section 3.7.5.3).
10. The expression levels of SHH signaling pathway molecules Gli1, Gli2, Smo, and Ptch1 were assessed following the SYBR Green-based RT-qPCR assay protocol mentioned in section (3.7.5.4). The primer sets used for this assay are shown in Table 3-30.

Table 3-30. Primer sets used for functional analysis of SHH signaling pathway by SYBR-Green-based RT-qPCR		
Gene	**Forward primer (5′-3′)**	**Reverse primer (5′-3′)**
Gli1	*GCCGTGTAAAGCTCCAGTGAACACA*	*TCCCACTTTGAGAGGCCCATAGCAAG*
Gli2	*TGGCCGCTTCAGATGACAGATGTT*	*CGTTAGCCGAATGTCAGCCGTGAAG*
Ptch1	*GCACTACTTCAGAGACTGGCTTC*	*AGAAAGGGAACTGGGCATACTC*
Smo	*ACCCCGGGCTGCTGAGTGAGAAG*	*TGGGCCCAGGCAGAGGAGACATC*
ACTB	*CGCCGCCAGCTCACCATG*	*CACGATGGAGGGGAAGACGG*

3.14.2. Functional analysis of SHH signaling pathway in JS-derived iPSCs

3.14.2.1. SAG stimulation of JS-derived iPSCs

Materials required

- NutriStem® hPSC XF Medium (Biological Industries, Cat. No. 05-100-1A)
- Basic FGF, recombinant human (Thermo Fisher Scientific, Cat. No. PHG0264)
- Corning™ Matrigel™ hESC-Qualified Matrix (Corning, Cat.No.08-774-552)
- DMEM/F12 with L-Glutamine, without HEPES Medium (Sigma-Aldrich, Cat. No. DF-042-B)
- Smoothened agonist, SAG - CAS 364590-63-6 - Calbiochem (Sigma-Aldrich, Cat. No. 566660)
- Dimethyl sulfoxide (DMSO), Sterile (Sigma-Aldrich, Cat. No. D2650)

Protocol

1. The iPSCs of JS2 (C6), JS5 (C6), and BJ (C21) were grown in 12-well cell culture plates containing 700 µl of NutriStem® hPSC XF Medium.
2. When the iPSC colonies reached high confluency and ready to be picked, the spent medium was removed and replaced with a fresh NutriStem® hPSC XF Medium.
3. For each iPSC line, the iPSC colonies were divided into small pieces and picked manually using a pipette tip under an inverted phase contrast microscope.
4. The iPSC pieces of each cell line were transferred into two Matrigel-coated wells of a 12-well plate. The plate was moved in several quick back-and-forth and side-to-side motions to disperse the cells across the surface, then gently placed in a 5% CO_2 humidified incubator at 37° C.
5. The medium was changed every day for 3-4 days after passaging.
6. 24 hr before the next passage, 1 ml of complete NutriStem® hPSC XF Medium was added into each well, then 1 µl of DMSO was added into the first well and 2 µM of SAG was added into the second well for each iPSC line.
7. After 24 hr, the spent medium was removed and 500 µl of DMEM/F12 medium was added into each well. Using a cell scraper, the iPSC colonies were detached, and cell clumps were transferred into 1.5-ml centrifuge tubes to be centrifuged at 1400 rpm for 7 min.

8. RNA was extracted from the cell pellet in each tube using NucleoSpin® RNA Mini Kit (Macherey-Nagel, Cat. No. 740955.250) (Section 3.7.5.1). The purified RNA was reverse-transcribed into cDNA using ImProm-II™ Reverse Transcription System (Promega, Cat. No. A3800) (Section 3.7.5.3).
9. The expression levels of SHH signaling pathway molecules Gli1, Gli2, Smo, and Ptch1 were assessed following the SYBR Green-based RT-qPCR assay protocol mentioned in section (3.7.5.4). The primer sets used for this assay are shown in Table.3-30.

3.14.3. Functional analysis of SHH signaling pathway in JS-derived NSCs

3.14.3.1. SAG stimulation of JS-derived NSCs

Materials required

- Neurobasal® Medium and Neural Induction Supplement, 50X (Thermo Fisher Scientific, Cat. No. A1647801).
- DMEM/F12 with L-Glutamine, without HEPES (Sigma-Aldrich, Cat. No. DF-042-B)
- Advanced™ DMEM/F12 (Thermo Fisher Scientific, Cat. No. 12634)
- Smoothened agonist, SAG - CAS 364590-63-6 - Calbiochem (Sigma-Aldrich, Cat. No. 566660)
- Dimethyl sulfoxide (DMSO), Sterile (Sigma-Aldrich, Cat. No. D2650)
- Complete neural expansion medium was prepared by aseptically mixing 49 ml of Neurobasal® medium with 49 ml of Advanced™ DMEM/F12 and 2 ml of neural induction supplement.

Protocol

1. The NSCs of JS2 (P11), JS5 (P9), and BJ (P3) derived from the iPSCs C6P26, C6P53, and C21P134 respectively were grown in 12-well cell culture plates containing 600 µl of complete Neural Expansion Medium. Two wells were prepared for each NSC line.
2. The Neural Expansion Medium was continuously changed every other day.
3. When the NSCs reached high confluency, 1 ml of complete Neural Expansion Medium was added to each well, then 1 µl of DMSO was added into the first well and 2 µM of SAG was added into the second well for each NSC line.
4. After 24 hr, the spent medium was removed and 500 µl of DMEM/F12 medium was added into each well. Using a cell scraper, the NSCs were detached, and transferred into 1.5-ml centrifuge tubes to be centrifuged at 1400 rpm for 7 min.
5. RNA was extracted from the cell pellet in each tube using NucleoSpin® RNA Mini Kit (Macherey-Nagel, Cat. No. 740955.250) (Section 3.7.5.1). The purified RNA was reverse-transcribed into

cDNA using ImProm-II™ Reverse Transcription System (Promega, Cat. No. A3800) (Section 3.7.5.3).

6. The expression levels of SHH signaling pathway molecules Gli1, Gli2, Smo, and Ptch1 were assessed following the SYBR Green-based RT-qPCR assay protocol mentioned in section (3.7.5.4). The primer sets used for this assay are shown in Table.3-30.

3.14.4. Functional analysis of SHH signaling pathway in JS-derived neurons

3.14.4.1. SAG stimulation of JS-derived neurons

Materials required

- NSC lines
- Gibco™ Neurobasal™ Medium (Cat. No. 21103049)
- Gibco™ B-27™ Supplement (50X), serum free (Cat. No. 17504044)
- Gibco™ GlutaMAX™-I Supplement (Cat. No. 35050061)
- Gibco™ Antibiotic-Antimycotic (100X) solution (Cat. No. 15240096)
- Poly-L-Ornithine (Sigma-Aldrich, Cat. No. P3655)
- Gibco™ Laminin (Cat. No. 23017015)
- Gibco™ StemPro™ NSC SFM (Cat. No. A1050901). It consists of KnockOut™ DMEM/F-12 Basal Medium stored at 4° C, StemPro™ NSC SFM (Neural) Supplement stored at -20° C to -5° C in the dark and bFGF Recombinant Human and EGF Recombinant Human stored at 4°C.
- Smoothened agonist, SAG - CAS 364590-63-6 - Calbiochem (Sigma-Aldrich, Cat. No. 566660)
- Dimethyl sulfoxide (DMSO), Sterile (Sigma-Aldrich, Cat. No. D2650)

Protocol

1. The NSC lines of JS2, JS5 and BJ were seeded on poly-L-ornithine- and laminin-coated 12-well culture plates in complete StemPro NSC SFM medium at 100000 cells/well. For each line, 6 wells were prepared.
2. After 48 hr, the medium was replaced by the neural differentiation medium. The spent medium was changed every 3 days. The cells were kept unexposed to ambient air at any time after their differentiation into neurons.
3. On day 17 after replacement of complete StemPro NSC SFM medium with the neural differentiation medium and when the all the NSCs were completely differentiated into neurons, 1 ml of the neural differentiation medium was added into all the 6 wells of each cell line, then 2 µM of SAG was added into 3 wells of them while the other 3 wells were kept unstimulated to be used as negative controls.

4. After 24 hr, the spent medium was removed, and the cells were collected and transferred into 1.5-ml centrifuge tubes to be centrifuged at 1400 rpm for 7 min.
5. RNA was extracted from the cell pellet in each tube using NucleoSpin® RNA Mini Kit (Macherey-Nagel, Cat. No. 740955.250) (Section 3.7.5.1). The purified RNA was reverse-transcribed into cDNA using ImProm-II™ Reverse Transcription System (Promega, Cat. No. A3800) (Section 3.7.5.3).
6. The expression levels of SHH signaling pathway components Gli1, Gli2, Smo, and Ptch1 were analyzed following the SYBR Green-based RT-qPCR assay protocol mentioned in section (3.7.5.4). The primer sets used for this assay are shown in Table.3-30.

RESULTS

4. RESULTS

4.1. JS patients enrolled in the study

To established iPSC-based JS models, five JS patients of different ages have been enrolled in this study and they have been designated as JS1, JS2, JS3, JS4, and JS5. Ethical approval to conduct the study have been obtained from the Scientific Committee and the Board of the ASST Spedali Civili, Brescia. The parents or guardians of the patients have signed the informed consent forms to be enrolled. All the patients exhibited different genetic defects in one of the causative genes of JS and variable clinical manifestations of the disease. The following table 4-1 shows the genetic mutations associated with each patient and their ages at the time of enrollment.

Table 4-1. JS patients enrolled in the study and the genetic mutations detected in their genomes

Patient	Sex	Gene	Exon(s)	Nucleotide alterations	Predicted effect on protein
JS1	Male	*CC2D2A*	31	c.3856T>C	p.C1286R
				c.3856T>C	p.C1286R
JS2	Female	*CC2D2A*	24	c.2999A>T	P.E1000V
			30	c.3638delG	p.G1213Afs*7
JS3	Male	*TMEM67*	13	c.G1319A	p.R440Q
			21	c.A2182G	p.S728G
JS4	Male	*TMEM67*	17	c.755T>C	p.M252T
			21	c.1769T>C	p.F590S
JS5	Female	*C5orf42*	22	c.T3868T>C	p.S1290P
			36	c.7477C>A	p.R2493X

4.2. Establishment of JS-derived fibroblast lines

As an initial step towards generation of JS-specific iPSCs for this research, we established fibroblast lines from skin biopsies obtained from five Italian patients with JS. The skin biopsies were collected at the Child Neuropsychiatry Unit of the ASST Spedali Civili, Brescia, or from the the Neurogenetics Unit, IRCCS Santa Lucia Foundation, Rome, and immediately transferred to the Angelo Nocivelli Institute for Molecular Medicine where setting up the fibroblast lines and generation of the iPSCs were carried out. We successfully established and maintained fibroblast lines of JS1, JS2, JS3, JS4, and JS5 patients (Fig.4-1).

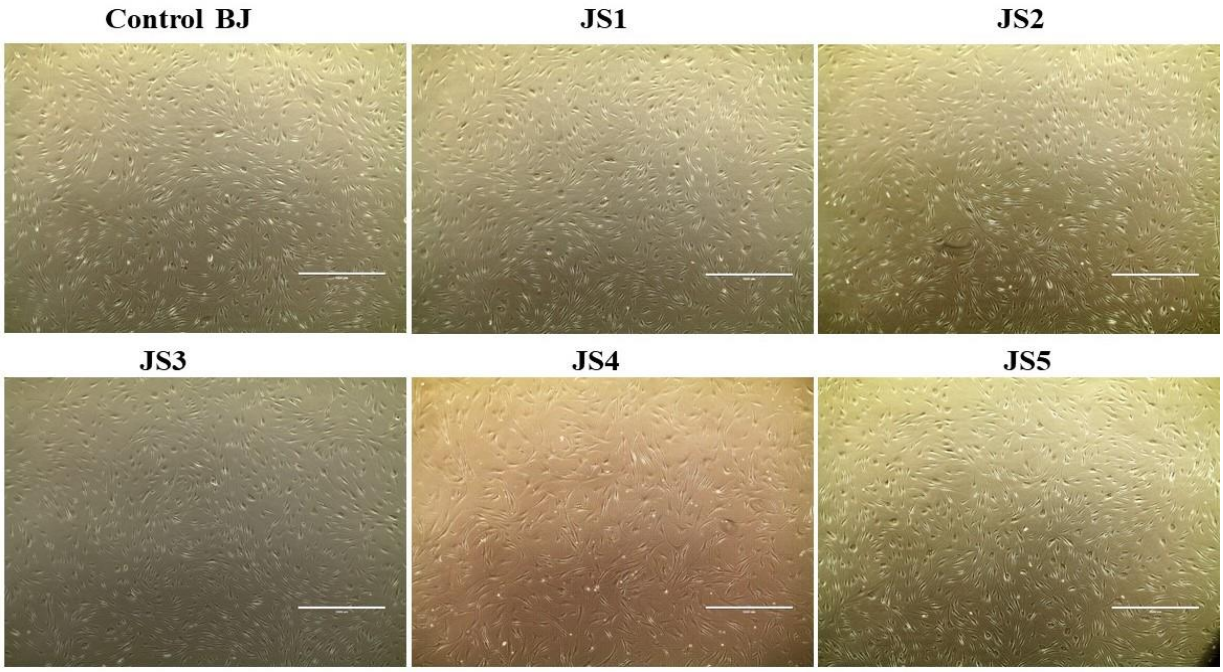

Figure 4-1. **Establishment of JS-derived fibroblast lines.** Representative images show the fibroblast lines of the control BJ and JS1-5 prepared for iPSC reprogramming. The images were obtained using a 4X microscope objective. Scale bars correspond to 1000 µm.

4.3. PCR-based detection of *Mycoplasma* contamination in the fibroblast cultures

Before being induced into iPSCs, all the fibroblast cell lines have been tested for detection of *Mycoplasma* to avoid the effect of this bacterium on the reprogramming efficiency, maintenance of the generated iPSC lines in culture, and their differentiation capacity. All the cell lines were not contaminated with *Mycoplasma* (Fig.4-2).

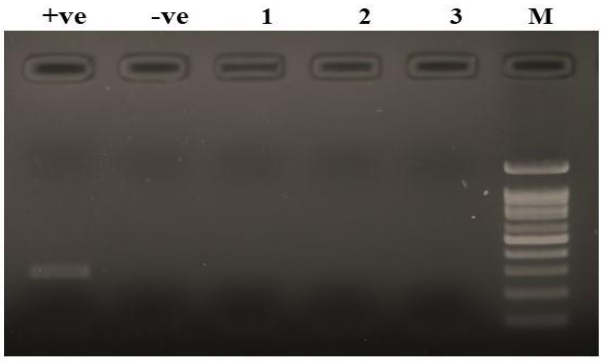

Figure 4-2. **PCR-based *Mycoplasma* detection in JS-derived fibroblast lines.** A representative image of *Mycoplasma* detection in a 2% gel electrophoresis shows negative testing result in all JS-derived fibroblast lines. Lanes 1, 2, and 3 correspond to fibroblast lines of JS1, JS2, and JS3. Lane M: 100bp marker. Lane +ve: positive control. Lane: -ve: negative control.

4.4. Establishment of JS-derived iPSC lines

4.4.1. Reprogramming of JS-derived fibroblasts in feeder-free conditions

To establish iPSC-based models for JS, we used the CytoTune™-iPS 2.0 Sendai Reprogramming Kit (Fusaki et al., 2009) to reprogram the JS-derived fibroblasts. We transduced the fibroblasts obtained from five JS patients (JS1, JS2, JS3, JS4, and JS5) with different mutations in one of three different JS causative genes *CC2D2A*, *C5orf42*, and *TMEM67*. To observe the morphological alterations during the reprogramming, the transduced cells were checked daily. Due to a high uptake of the virus, a significant number of dead cells (>50%) were detected 24 hr post-transduction. The fibroblast medium was changed every other day, until day 6. On day 7, the transduced cells were plated on Matrigel coated culture wells with two to three different concentrations from each fibroblast line. From day 8, the spent medium was replaced with complete NutriStem® hPSC XF medium every day, and the cells were visualized under an inverted phase contrast microscope for the emergence of cell clumps indicative of reprogrammed cells. The new colonies emerged on day 8 post-transduction of JS2-derived fibroblasts, however for the other JS-derived fibroblast lines, the emergence of colonies started on day 12 post-transduction. On day 26 post-transduction, some of the newly formed iPSC colonies were selected to be picked and expanded using TRA-1-60 antibody which detects the human antigen podocalyxin. This antigen is used as a surface marker for iPSCs, hESCs, hEGCs, and ECCs. On day 28, at least 15 clones from each reprogrammed fibroblast line were transferred into Matrigel-coated 12-well culture plates containing complete NutriStem® hPSC XF medium. After reprogramming and during the long-term maintenance in culture, our generated iPSC lines showed distinct ESC-like morphological features such as compact round colonies with distinct borders and well-defined edges, dense and flat cells with a high nucleus/cytoplasm ratio (Fig.4-3).

4.4.2. Selection and expansion of JS-derived iPSC clones

To establish JS-derived iPSC lines, the selected 15 clones from each reprogrammed fibroblast line have been picked manually and expanded based on morphology and live staining with human TRA-1-60 antibody (Fig.4-8). The colonies were continuously picked and passaged every 4-5 days and maintained in culture for at least 25 passages using standard culture procedures (Fig.4-4). The iPSCs were collected at different passages for cryopreservation and stored in a liquid nitrogen tank in the Bio-bank of Angelo Nocivelli Institute for Molecular Medicine. Further, we have selected three clones from each JS-derived iPSCs namely: JS1 (C1, C2, and C11), JS2 (C6, C7, and C17), JS3 (C1, C4, and C13), JS4 (C4, C5, and C10), and JS5 (C3, C5, and C10) for extensive characterization, expansion, and differentiation into NSCs and neurons.

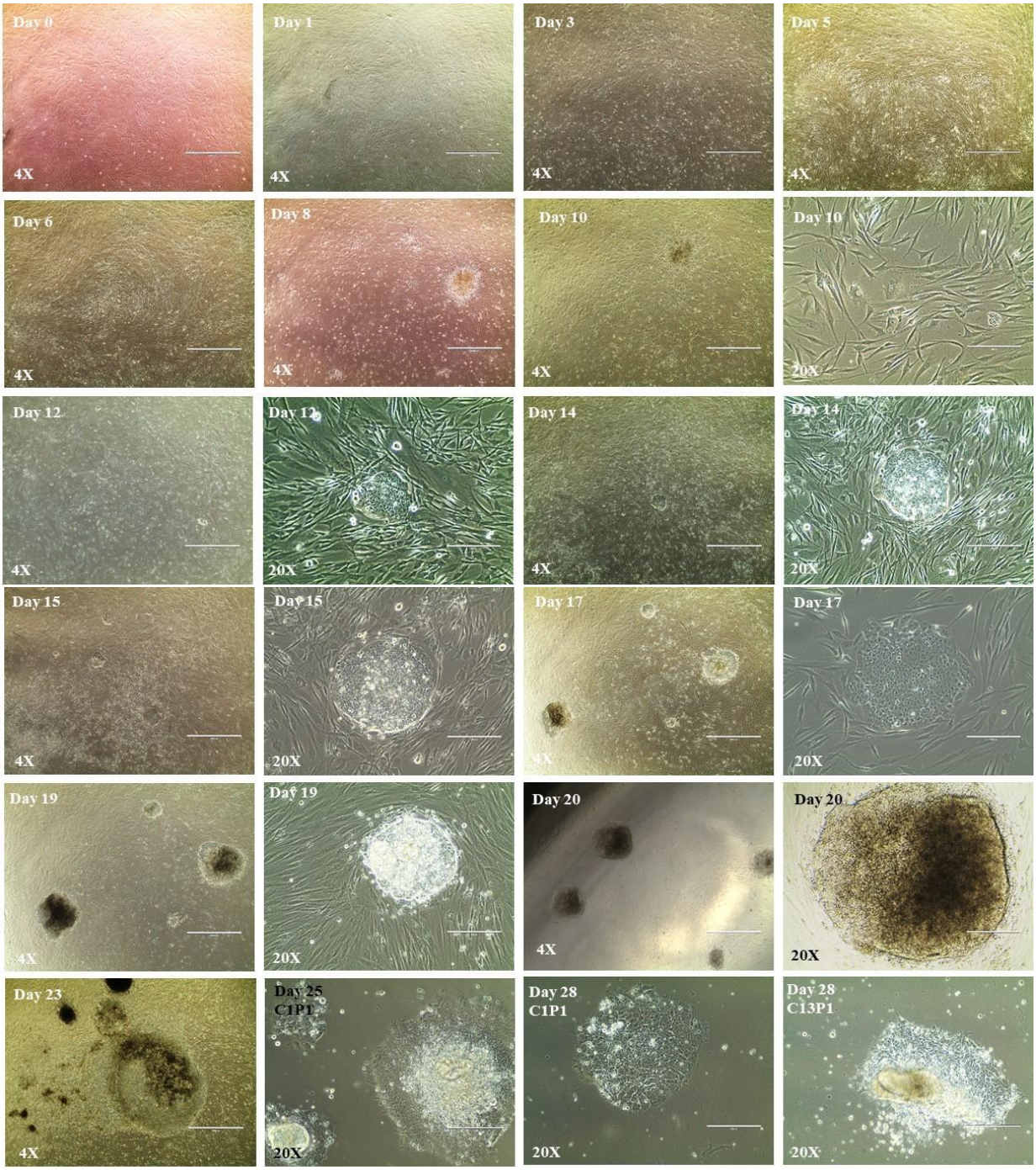

Figure 4-3. **Generation of iPSC lines from JS-derived fibroblasts.** Representative images show the morphological alterations occurred during the reprogramming process of JS2-derived fibroblasts into iPSCs**.** At day 0, the fibroblasts were counted and transduced using the CytoTune™ 2.0 Sendai viruses and the cells underwent progressive morphological changes for 23 days before selecting and passaging the generated iPSC colonies for further expansion. At day 8, cell clumps indicative of reprogrammed cells were observed. Images of clone 1 and 13 picked on day 24 show iPSC colonies on day 25 and 28 respectively. The images were obtained using 4X and 20X microscope objectives. Scale bars correspond to 1000 µm in 4X images and 200 µm in 20X images.

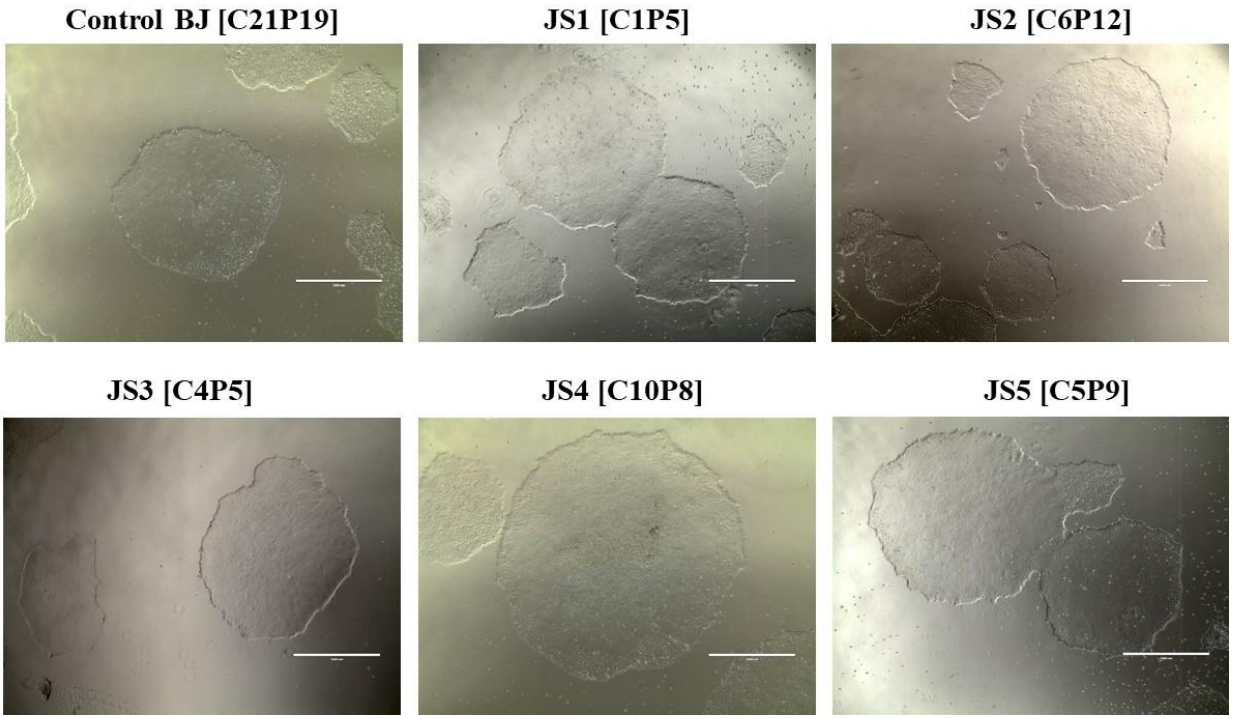

Figure 4-4. **iPSC colonies of JS- and BJ-derived cell lines.** Representative images show compact round iPSC colonies with well-defined edges of C21, C1, C6, C4, C10, and C5 of iPSCs derived from BJ, JS1, JS2, JS3, JS4, and JS5 respectively. The images were obtained using a 4X microscope objective. Scale bars correspond to 1000 µm.

4.5. Detection of Sendai virus (SeV) genome and transgenes

RNAs were collected and extracted from all JS iPSC lines at passage 5 to assess the gene expression profiles for Sendai virus and its transgenes. RT and PCR analysis were carried out with the 4 sets of specific primers to detect the SeV genome and transgenes *KOS, KLF4*, and *c-MYC*. The results confirmed that the generated iPSCs were free of CytoTune™ 2.0 Sendai reprogramming vectors (Fig.4-5)

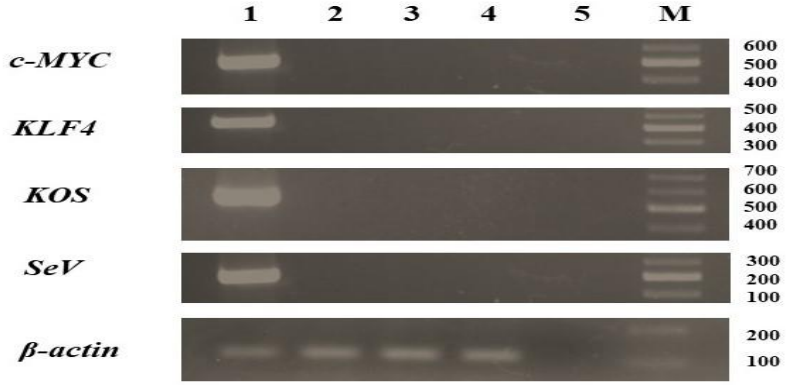

Figure 4-5. PCR-based detection of SeV genome and transgenes in the generated iPSCs using the CytoTune™ 2.0 Sendai reprogramming vectors. Representative images of detection of SeV genome and transgenes *c-MYC, KLF4*, and *KOS* in a 2% gel electrophoresis show negative testing result in all JS2-derived iPSC lines. A representative image of detection of endogenous *β-actin* shows positive result in all the samples except the negative control. Lanes 1: positive control extracted at day 7 post-transduction and used as an internal control. Lanes 2, 3 and 4 correspond to C6P5, C7P5, and C17P5 of JS2-derived iPSCs respectively. Lane 5: negative control. Lane M: 100bp marker.

4.6.Characterization of the generated iPSC lines

4.6.1. Sequencing analysis of the iPSC lines

The DNA extracted from the JS-derived iPSC lines have been sequenced using the Sanger sequencing method. This is to ensure that the generated iPSC lines retained the pre-existing mutations in the genes *CC2D2A*, *C5orf42*, and *TMEM67* in the parental cells, and the reprogramming process and long-term maintenance of the iPSCs did not cause any genetic variation in the mutation sites as compared to the parental fibroblasts. The sequencing analysis revealed that all JS-derived iPSC lines retained the same genetic mutations of their parental cells (Fig.4-6).

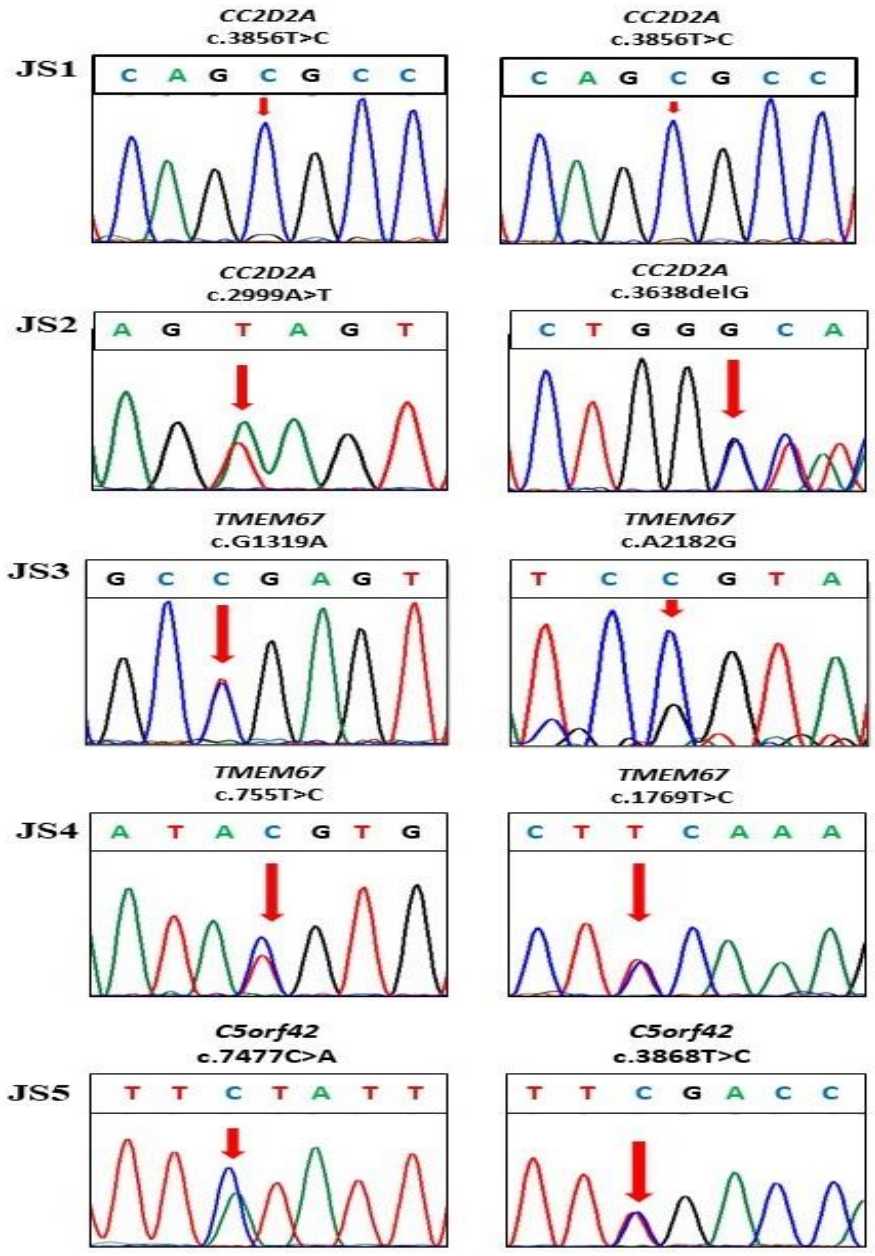

Figure 4-6. Sequencing analysis of genetic mutations in *CC2D2A*, *C5orf42*, and *TMEM67* in the generated iPSC lines.

4.6.2. Karyotyping analysis of the iPSC lines

To assess the long-term genomic stability of the generated iPSCs, cytogenetic analyses have been carried out on low and high passages of JS-derived fibroblasts and three selected clones of each generated iPSC line, namely: JS1 (C1, C2, and C11), JS2 (C6, C7, and C17), JS3 (C1, C4, and C13), JS4 (C4, C5, and C10), and JS5 (C3, C5, and C10) and the control BJ (C21 and C23). The karyotyping analyses were performed on these clones and their parental fibroblasts using the Q-banding technique at 400–450 bands resolution. For karyotype analysis of each clone preparation, at least 20 metaphase spreads were analysed and karyotyped following the International System for Human Cytogenomic Nomenclature (ISCN 2016). The analyses revealed that all the parental cells and their derived iPSC lines possess structurally and numerically normal karyotype (46, XX) or (46, XY) (Fig.4-7). These results suggest that the generated JS-derived iPSC lines were genetically stable during reprogramming and prolonged maintenance in culture.

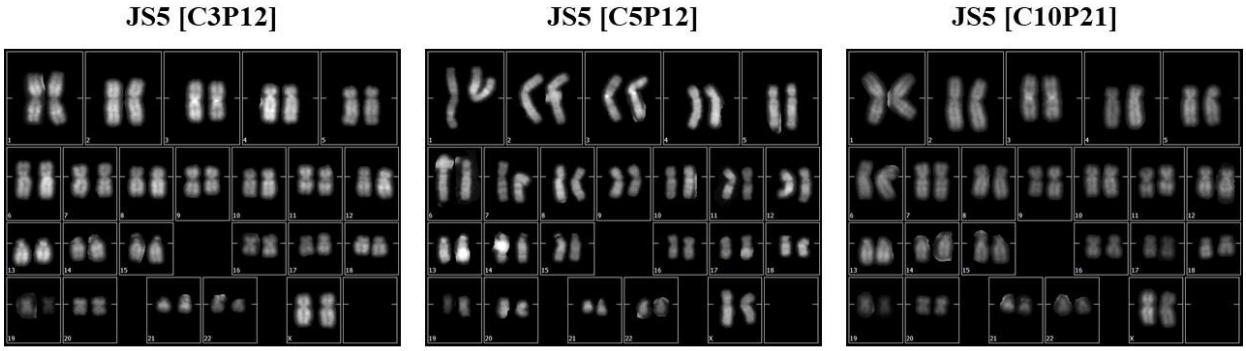

Figure 4-7. Q-banding chromosome analysis of JS-derived iPSCs. Representative images of karyotype analysis of three iPSC lines derived from JS5 fibroblasts show a normal female karyotype (46, XX). Bands resolution: 400-450.

4.6.3. Short tandem repeat (STR) analysis

For further assessment of the genomic stability and real identity of the generated iPSC lines, short tandem repeat (STR) analyses were performed on three iPSC clones of each JS patient and the parental fibroblasts using the AmpFlSTR® Identifiler® Plus PCR Amplification Kit (Applied Biosystems™). Analysis of the amplified loci confirmed that the generated iPSCs were derived from the parental fibroblasts. (Table 4-2 & 4-3).

Table 4-2. Analysis of 16 STR loci in JS2-derived iPSCs and the parental fibroblasts					
Locus designation	**Chr location**	**Parental line (fibroblasts)**	**Clone**		
			C6	**C7**	**C17**
D8S1179	8	13-15	13-15	13-15	13-15
D21S11	21q11.2-q21	30-32.2	30-32.2	30-32.2	30-32.2
D7S820	7q11.21-22	11	11	11	11
CSF1PO	5q33.3-34	11-12	11-12	11-12	11-12
D3S1358	3p	15-16	15-16	15-16	15-16
TH01	11p15.5	8-9	8-9	8-9	8-9
D13S317	13q22-31	11	11	11	11
D16S539	16q24-qter	11-13	11-13	11-13	11-13
D2S1338	2q35-37.1	16-17	16-17	16-17	16-17
D19S433	19q12-13.1	13	13	13	13
vWA	12p12-pter	18-19	18-19	18-19	18-19
TPOX	2p23-2per	8-11	8-11	8-11	8-11
D18S51	18q21.3	16-17	16-17	16-17	16-17
Amelogenin	X:p22.1-22.3 Y:p11.2	XX	XX	XX	XX
D5S818	5q21-31	12	12	12	12
FGA	4q28	19-21	19-21	19-21	19-21

Table 4-3. Analysis of 16 STR loci in JS5-derived iPSCs and the parental fibroblasts					
Locus designation	**Chr location**	**Parental line (fibroblasts)**	**Clone**		
			C3	**C5**	**C10**
D8S1179	8	12-16	12-16	12-16	12-16
D21S11	21q11.2-q21	29-31	29-31	29-31	29-31
D7S820	7q11.21-22	10-14	10-14	10-14	10-14
CSF1PO	5q33.3-34	10-11	10-11	10-11	10-11
D3S1358	3p	16	16	16	16
TH01	11p15.5	8-9,3	8-9,3	8-9,3	8-9,3
D13S317	13q22-31	12	12	12	12
D16S539	16q24-qter	10-12	10-12	10-12	10-12
D2S1338	2q35-37.1	16-23	16-23	16-23	16-23
D19S433	19q12-13.1	13-15	13-15	13-15	13-15
vWA	12p12-pter	16	16	16	16
TPOX	2p23-2per	8	8	8	8
D18S51	18q21.3	15-18	15-18	15-18	15-18
Amelogenin	X:p22.1-22.3 Y:p11.2	XX	XX	XX	XX
D5S818	5q21-31	12-13	12-13	12-13	12-13
FGA	4q28	23	23	23	23

4.6.4. Immunofluorescence assay for stemness assessment of the generated iPSC lines

Immunostaining was performed as described in section (3.7.4) for evaluation of the stemness of all the selected iPSC clones derived from JS fibroblasts. The immunocytochemistry assays showed positive expression of stemness markers OCT4, and TRA-1-60 in that the generated iPSC lines (Fig.4-8). These results confirmed the stemness state of JS-derived iPSC lines.

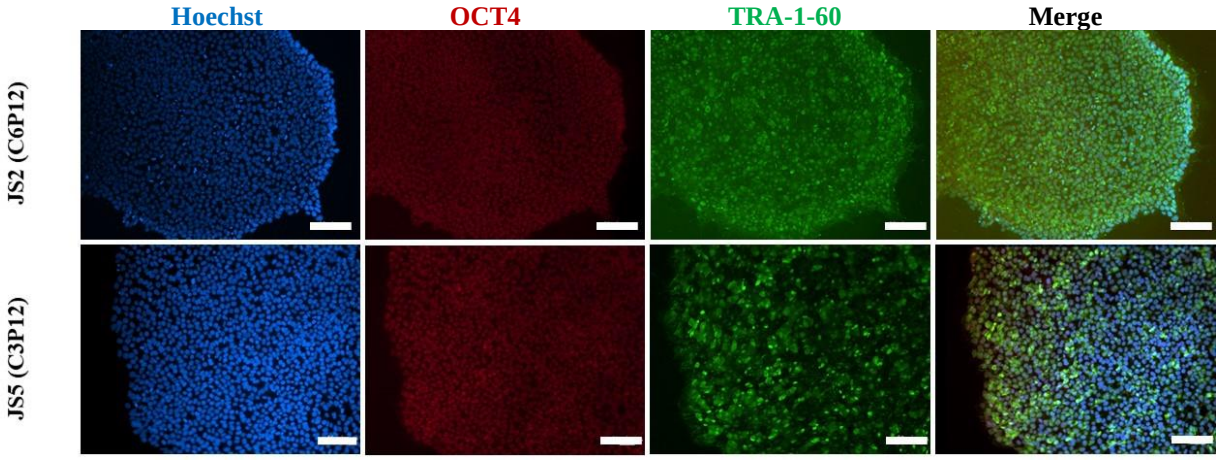

Figure 4-8. Immunofluorescence assay for detection of stemness markers in the generated iPSC lines derived from JS2 and JS5 fibroblasts. Representative immunofluorescence images of the iPSC lines show typical iPSC colonies double immuno-stained with anti-OCT4 (red) and anti-TRA-1-60 (green) antibodies to detect the expression of the stemness marker proteins OCT4 and TRA-1-60 in JS2- and JS5-derived iPSC lines. The nuclei are stained with Hoechst (blue). The images were obtained using a 10X microscope objective. Scale bars correspond to 100 µm.

4.6.5. SYBR Green-based RT-qPCR analysis of the stemness markers

SYBR Green-based RT-qPCR assay was used to assess stemness markers *OCT4*, *SOX2*, *KLF4*, *C-MYC*, and *NANOG* gene expression in three iPSC clones of each JS patient enrolled. For the relative quantification we used as calibrator gene expression of three control iPSC lines derived from BJ commercial line (ATCC® CRL-2522™) that we reprogrammed in our laboratory and checked with a deeper pluripotency characterization by TaqMan® Human Pluripotent Stem Cell Scorecard™ analysis. In the generated iPSC lines derived from JS1, JS3, and JS5, RT-qPCR assays for the stemness markers exhibited a relatively similar gene expression patterns to BJ-derived iPSCs (Fig.4-9, 4-10, & 4-11). Unexpectedly, iPSCs derived from JS2 and JS4 showed a relatively lower level of expression as compared to iPSCs of the control (Fig.4-12 & 4-14). To confirm that JS2- and JS4-derived iPSC lines have been transformed into pluripotent stem cells, we re-assessed the expression levels of the same stemness markers in these cell lines relative to their parental fibroblasts by RT-qPCR gene expression assay. As expected, all the iPSC lines of JS2 and JS4 showed high expression levels of *NANOG*, *OCT4*, and *SOX2*, while the expression of *c-MYC* and *KLF4* was significantly low

in the iPSCs as these markers are also expressed in fibroblasts (Fig.4.13 and 4-15). These results confirmed the stemness of the generated cell lines.

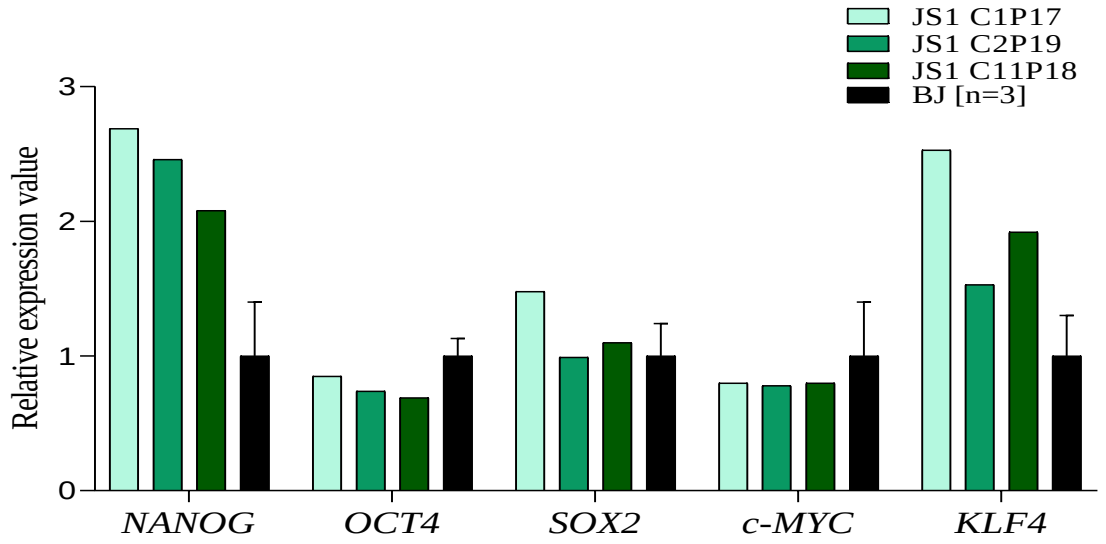

Figure 4-9. Relative expression levels of stemness markers in JS1-derived iPSC clones. RT-qPCR analysis of relative gene expression of the stemness markers *OCT4*, *SOX2*, *c-MYC*, *KLF4*, and *NANOG* in JS1-derived iPSC clones 1, 2, and 11 relative to BJ iPSCs. BJ-derived iPSCs were analyzed in triplicate and the relative quantification (RQ) value was calculated from the mean Ct values of the triplicates.

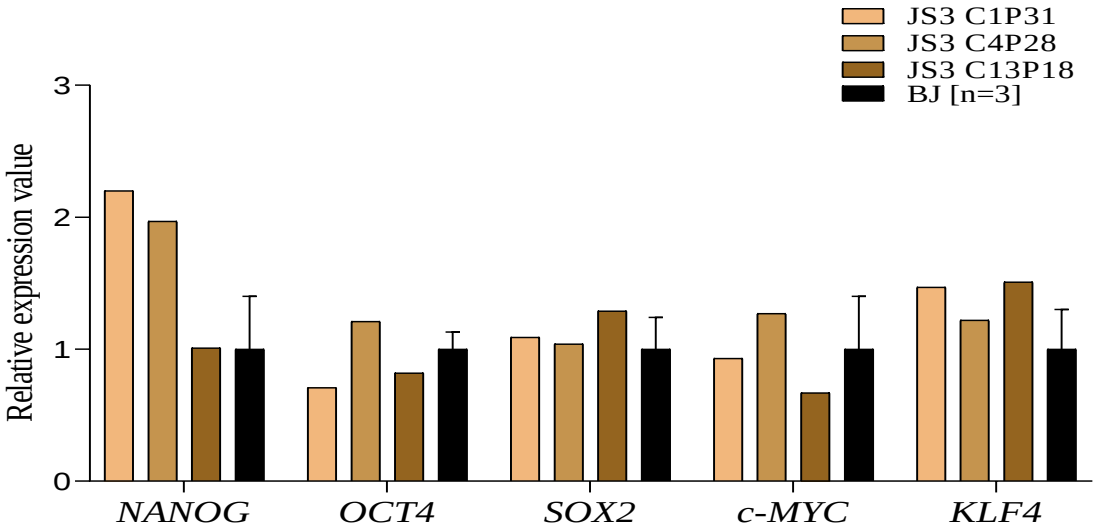

Figure 4-10. **Relative expression levels of stemness markers in JS3-derived iPSC clones.** RT-qPCR analysis of relative gene expression of the stemness markers *OCT4*, *SOX2*, *c-MYC*, *KLF4*, and *NANOG* in JS3-derived iPSC clones 1, 4, and 13 relative to BJ iPSCs BJ-derived iPSCs were analyzed in triplicate and the relative quantification (RQ) value was calculated from the mean Ct values of the triplicates.

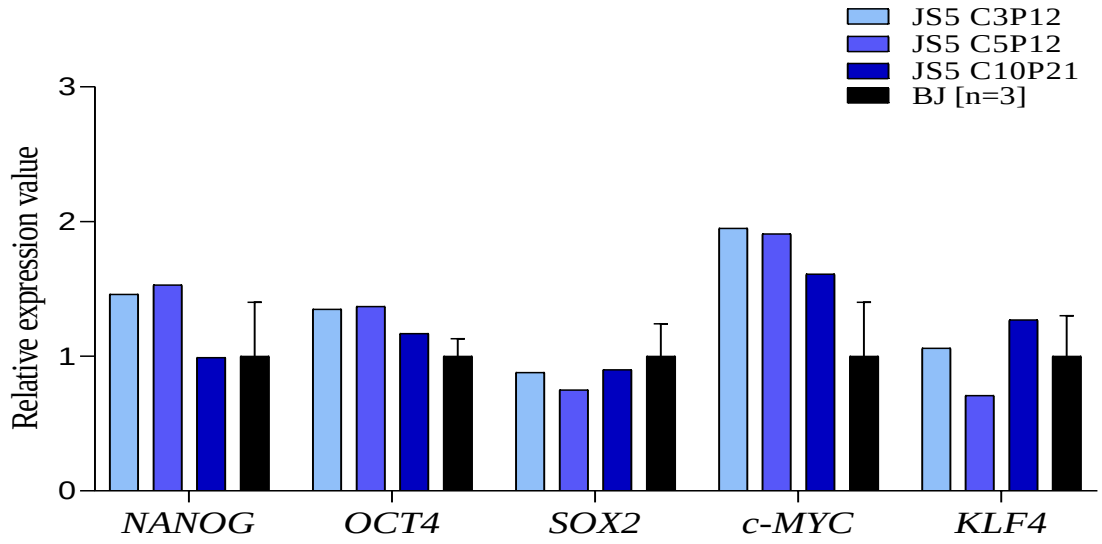

Figure 4-11. Relative expression levels of stemness markers in JS5-derived iPSC clones. RT-qPCR analysis of relative gene expression of the stemness markers *OCT4*, *SOX2*, *c-MYC*, *KLF4*, and *NANOG* in JS5-derived iPSC clones 3, 5, and 10 relative to BJ iPSCs. BJ-derived iPSCs were analyzed in triplicate and the relative quantification (RQ) value was calculated from the mean Ct values of the triplicates.

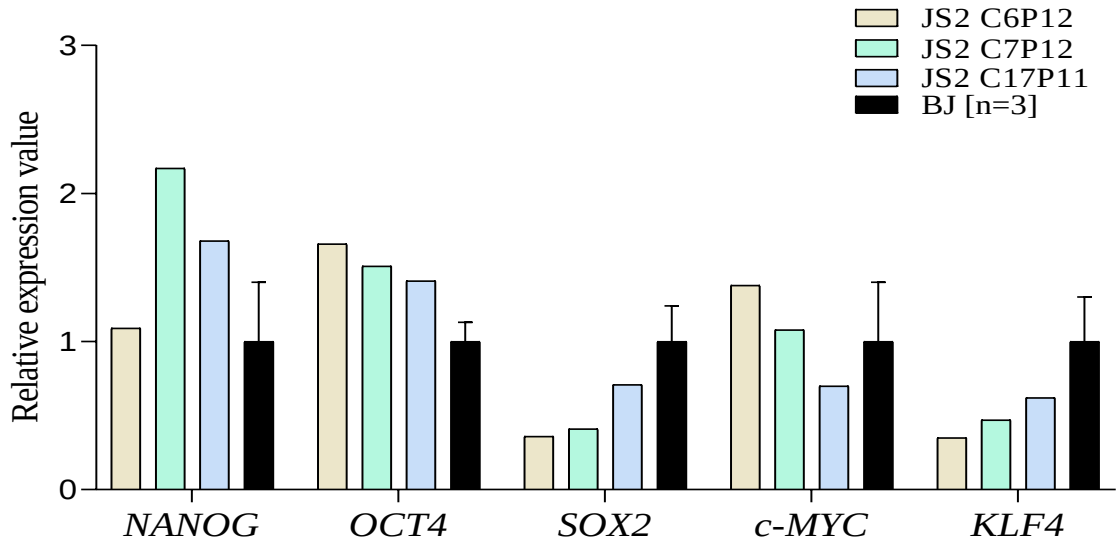

Figure 4-12. Relative expression levels of stemness markers in JS2-derived iPSC clones. RT-qPCR analysis of relative gene expression of the stemness markers *OCT4*, *SOX2*, *c-MYC*, *KLF4*, and *NANOG* in JS2-derived iPSC clones 6, 7, and 17 relative to BJ iPSCs. BJ-derived iPSCs were analyzed in triplicate and the relative quantification (RQ) value was calculated from the mean Ct values of the triplicates.

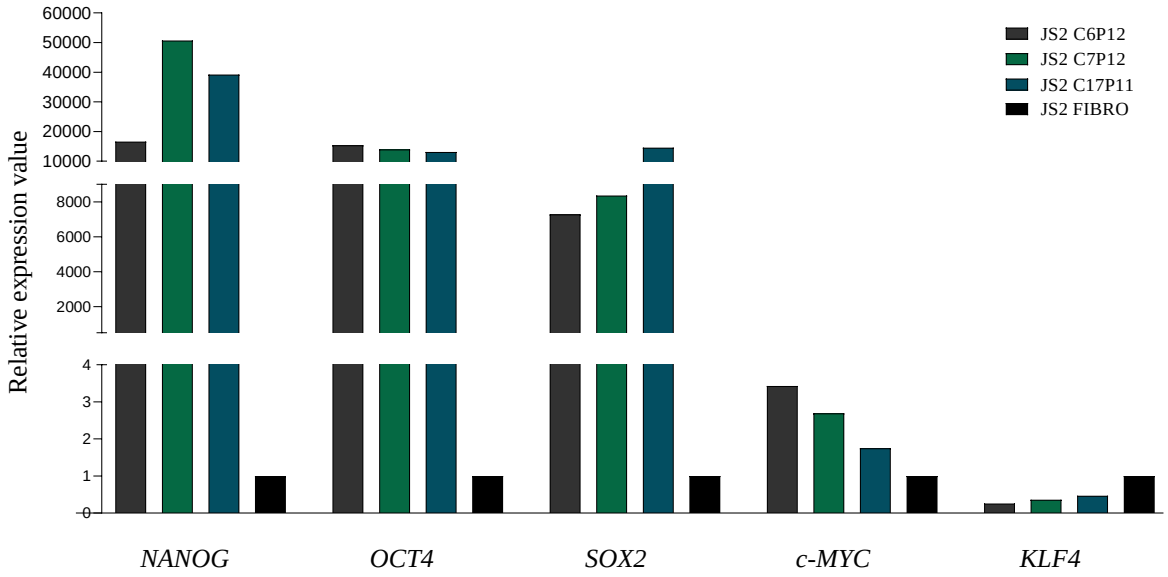

Figure 4-13. **Expression levels of stemness markers in JS2-derived iPSC clones relative to the parental fibroblasts.** RT-qPCR analysis of relative gene expression of the stemness markers *OCT4*, *SOX2*, *c-MYC*, *KLF4*, and *NANOG* in JS2-derived iPSC clones 6, 7, and 17 relative to JS2-derived fibroblasts.

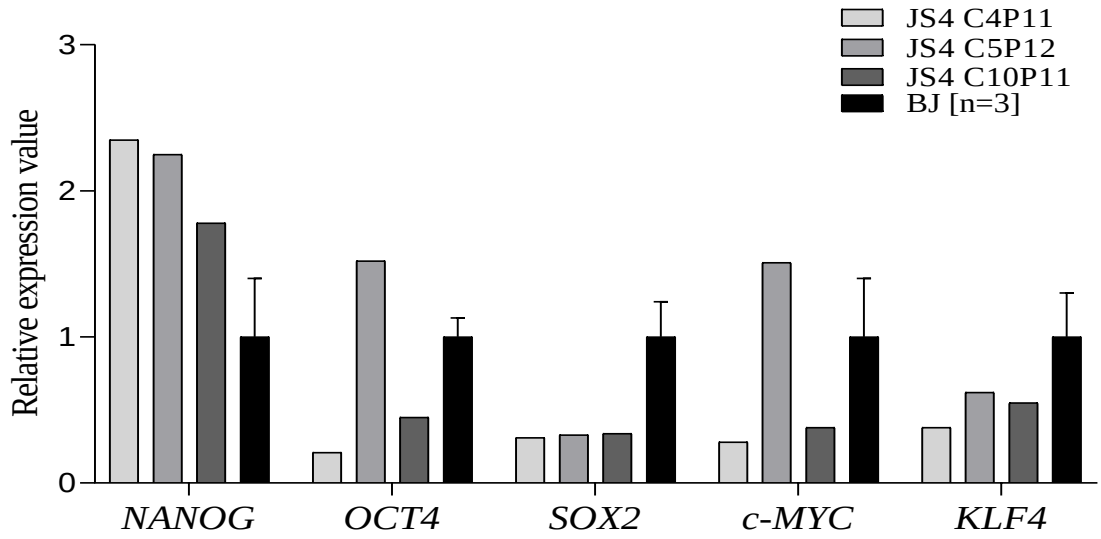

Figure 4-14. **Relative expression levels of stemness markers in JS4-derived iPSC clones.** RT-qPCR analysis of relative gene expression of the stemness markers *OCT4*, *SOX2*, *c-MYC*, *KLF4*, and *NANOG* in JS4-derived iPSC clones 4, 5, and 10 relative to BJ iPSCs. BJ-derived iPSCs were analyzed in triplicate and the relative quantification (RQ) value was calculated from the mean Ct values of the triplicates.

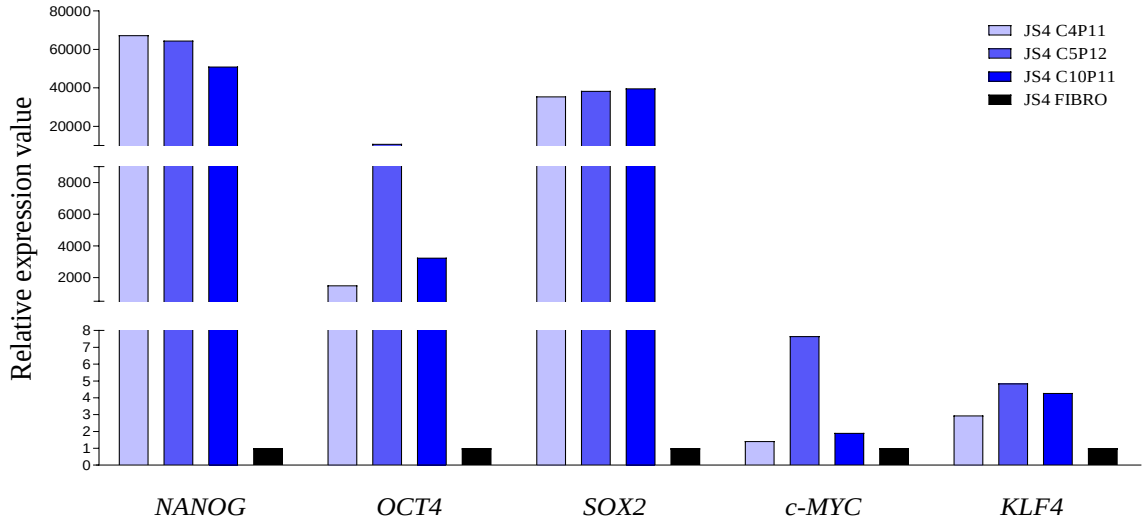

Figure 4-15. **Expression levels of stemness markers in JS4-derived iPSC clones relative to the parental fibroblasts.** RT-qPCR analysis of relative gene expression of the stemness markers *OCT4, SOX2, c-MYC, KLF4,* and *NANOG* in JS4-derived iPSC clones 4, 5, and 10 relative to JS4-derived fibroblasts.

4.6.6. Differentiation of the generated iPSCs into the cells of all three germ layers

To further demonstrate the pluripotency of JS-derived iPSCs, the iPSC lines were differentiated into ectodermal, mesodermal, and endodermal cells using the StemMACS Trilineage Differentiation Kit (Miltenyi Biotec). On day 7, TaqMan-based qPCR assays were performed to assess the expression levels of two specific markers (*PAX6, SOX1*), (*ACTA2, CXCR4*), and (*GATA4, SOX17*) for ectoderm, mesoderm, and endoderm respectively.

4.6.6.1.TaqMan-based RT-qPCR assays for expression of germ layer-specific markers

TaqMan-based qPCR assays were performed to examine the expression of the ectodermal, mesodermal and endodermal markers in all the differentiated iPSCs derived from JS2, JS4, and JS5 patient. Expression of these markers was assessed in differentiated and undifferentiated iPSCs of three clones of each JS patient. *β-actin* was used as a house-keeping gene and the relative quantification of the target genes was calculated using the $2^{-\Delta\Delta CT}$ method (Livak & Schmittgen, 2001). All the differentiated cells exhibited significantly high expression levels of lineage-specific molecular markers as compared to their corresponding undifferentiated iPSCs. The three clones of each JS-derived iPSCs showed a relatively similar gene expression pattern (Fig.4-16, 4-17 & 4-18). These results confirmed the ability of the generated JS-derived iPSCs to differentiate into three germ layer lineages and therefore their potential to transform into almost all cell types including neurons.

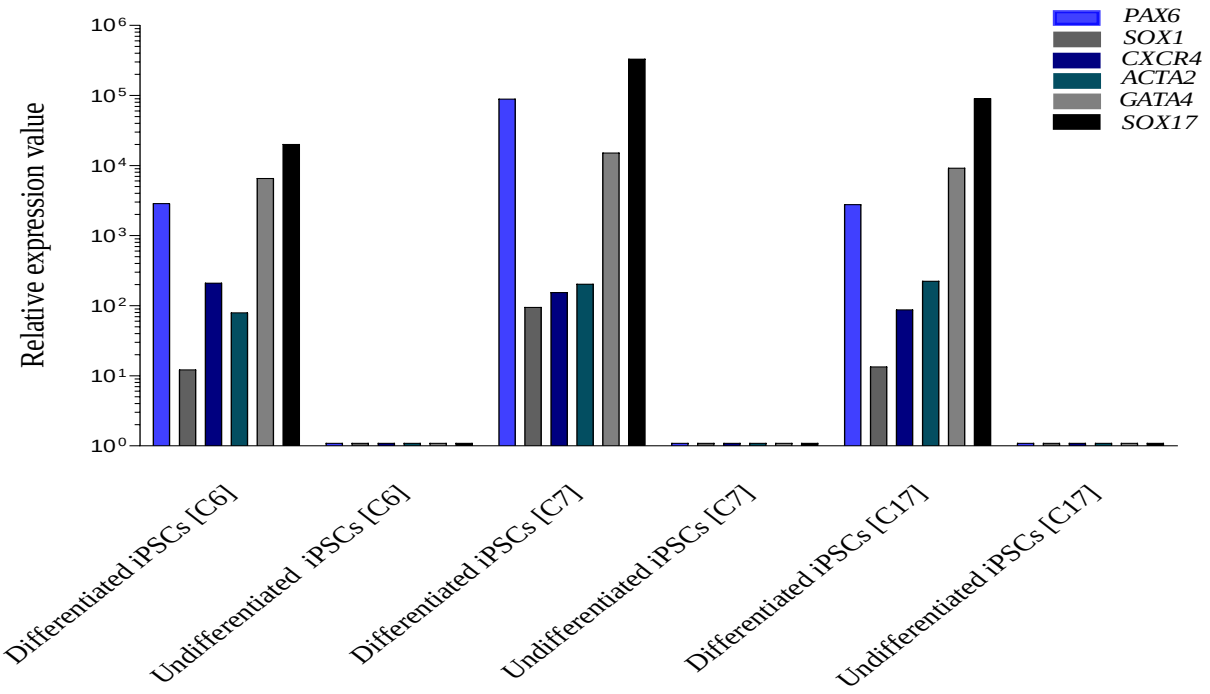

Figure 4-16. Relative gene expression levels of germ layer-specific markers in differentiated JS2-derived iPSC clones. A representative image of RT-qPCR analysis of relative gene expression of ectodermal, mesodermal, and endodermal markers (*PAX6 and SOX1*), (*ACTA2 and CXCR4*), and (*GATA4 and SOX17*) respectively, in differentiated JS5-derived iPSC clones 6, 7, and 17 relative to their corresponding undifferentiated iPSCs.

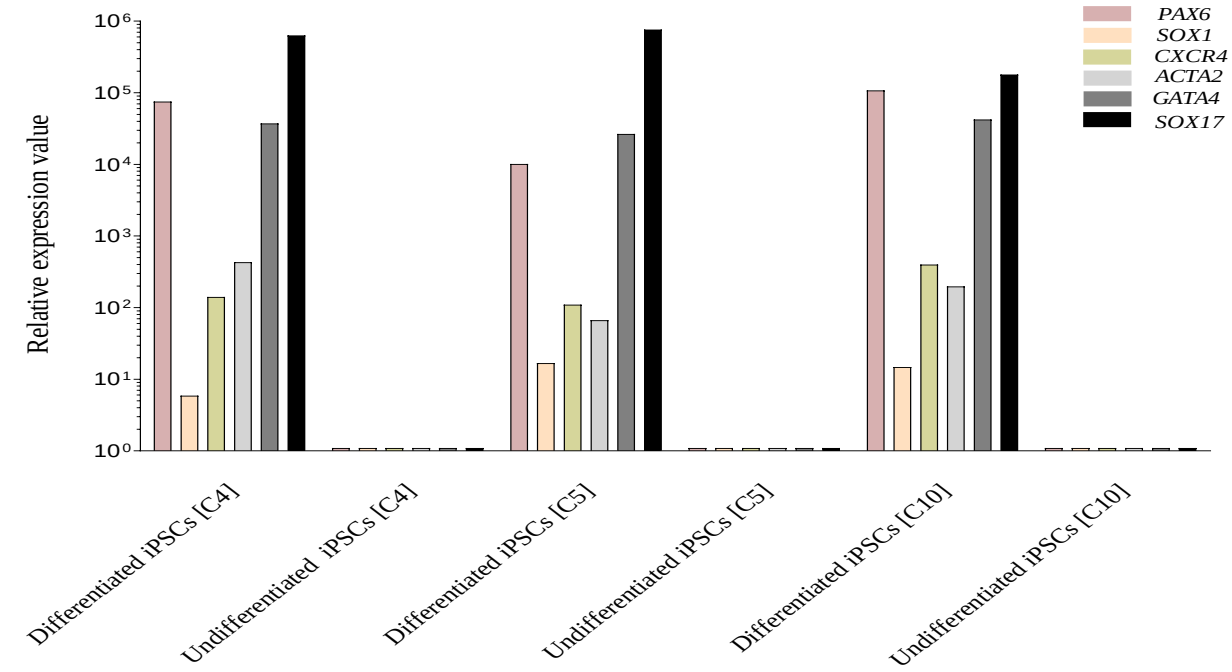

Figure 4-17. Relative gene expression levels of germ layer-specific markers in differentiated JS4-derived iPSC clones. A representative image of RT-qPCR analysis of relative gene expression of ectodermal, mesodermal, and endodermal markers (*PAX6 and SOX1*), (*ACTA2 and CXCR4*), and (*GATA4 and SOX17*) respectively, in differentiated JS5-derived iPSC clones 4, 5, and 10 relative to their corresponding undifferentiated iPSCs.

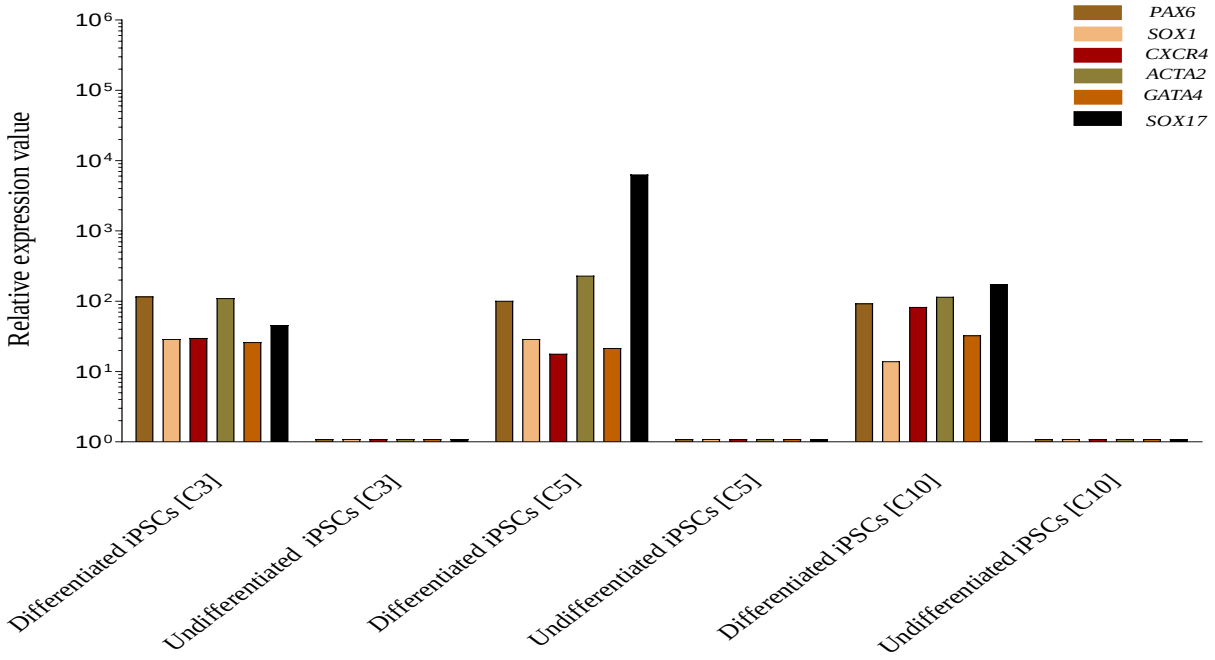

Figure 4-18. Relative gene expression levels of germ layer-specific markers in differentiated JS5-derived iPSC clones. A representative image of RT-qPCR analysis of relative gene expression of ectodermal, mesodermal, and endodermal markers (*PAX6 and SOX1*), (*ACTA2 and CXCR4*), and (*GATA4 and SOX17*) respectively, in differentiated JS5-derived iPSC clones 3, 5, and 10 relative to their corresponding undifferentiated iPSCs.

4.7. PCR-based detection of *Mycoplasma* contamination in the iPSCs

All the generated iPSC lines have been tested for detection of *Mycoplasma* at different passages during their long-term maintenance in culture to ensure that they are free of *mycoplasma* contamination before being cryopreserved and before differentiation of JS3 and JS5 and BJ into NSCs and neurons. All the iPSC lines have been confirmed by specific PCR to be free of *Mycoplasma* contamination (data not shown).

4.8. Cryopreservation of the generated iPSCs

From all the generated iPSC lines, high quality iPSCs were cryopreserved at different passages when they reached 70-80% confluence and stored in a liquid nitrogen tank at the Bio-bank of Angelo Nocivelli Institute for Molecular Medicine, the ASST Spedali Civili, Brescia.

4.9. Induction of NSCs from JS-derived iPSC lines

JS is associated with defects in the CNS particularly in the cerebellum at the posterior part of the brain. The inaccessibility of neurons from the cerebellum makes establishment of human neuronal *in*

vitro models of JS not possible without differentiation of iPSCs derived from somatic cells of JS patients. Therefore, the fibroblast-derived iPSCs of JS2 (C6), JS5 (C6) and BJ (C21) were induced to NSCs as an intermediate state between the iPSCs and the iPSC-derived neurons. The NSCs are multipotent and have the capacity to differentiate into all types of the nervous system cells. The iPSCs were induced into NSCs using Matrigel-coated 6-well plates and complete PSC Neural Induction Medium for 7 days (Fig.4-19). The medium was continuously changed every other day and any non-neural differentiated cells were removed. At day 7 post-induction, P0 NSCs were enzymatically detached and replated in Matrigel-coated 6-well plates containing Neural Expansion Medium for further passaging, cryopreservation, and differentiation into neurons. Morphologically heterogenous population consists of compact NSCs and flat non-neural cells were observed at day 4 post-expansion of P0 NSCs (Fig.4-19C). At day 2 of re-plating of P1 NSCs, a relative homogenous morphology of NSCs (Fig.4-19D & 4-19H) were observed and further expanded (Fig.4-20). The generated NSC lines were analyzed for NSC markers by immunofluorescence and qPCR assays.

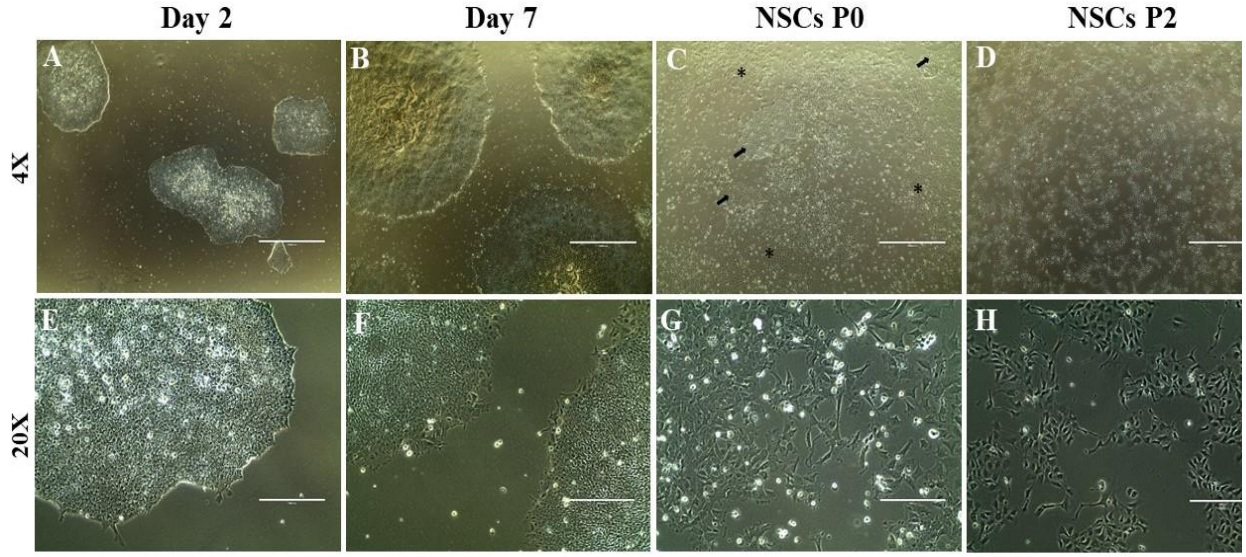

Figure 4-19. **Induction of NSCs from a JS2-derived iPSC line.** Representative phase contrast images of day 2 and day 7 of neural induction and P0 and P2 of JS2-derived NSCs show morphological changes in the iPSC colonies (A, B, E, and F), a heterogenous morphology with compact NSCs (indicated by arrows) and flat non-neural cells (indicated by asterisks) (C) and a relative homogenous morphology of P2 NSCs (D and H). The images were obtained using 4X and 20X microscope objectives. Scale bars correspond to 1000 µm in 4X images and 200 µm in 20X images.

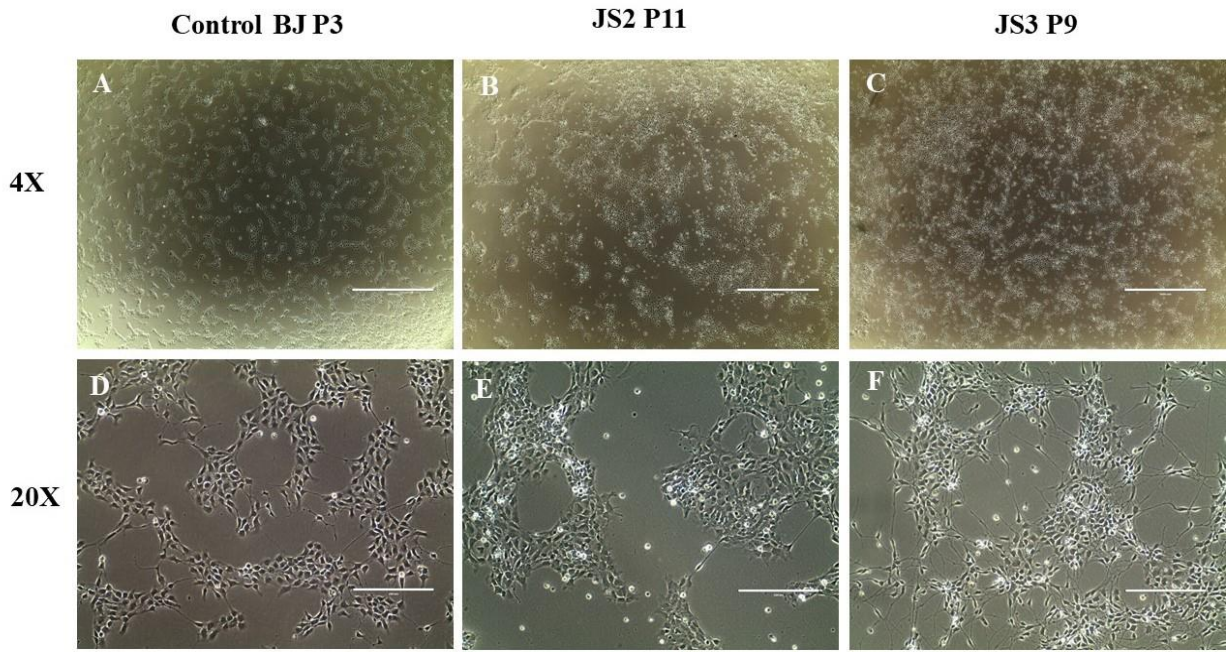

Figure 4-20. **NSCs differentiated from JS- and BJ-derived iPSC lines.** Representative phase contrast images show a relative homogenous morphology of P3, P11, and P9 of NSCs derived from iPSCs of BJ, JS2, and JS5 respectively. The images were obtained using 4X and 20X microscope objectives. Scale bars correspond to 1000 µm in 4X images and 200 µm in 20X images.

4.10. Characterization of JS-derived NSC lines

4.10.1.Genetic analysis for confirmation of the pre-existing variants in parental cells

The Sanger sequencing of the genomic DNA isolated from JS-derived NSCs revealed that the NSC lines retained the genetic mutations of the corresponding parental cell lines (data not shown).

4.10.2. Immunofluorescence analysis for detection of NSC markers

The NSCs (P0) of JS2, JS5 and BJ attached to Matrigel-coated coverslips in 24-well culture plates were stained with antibodies for NSC markers SOX1, SOX2, and NESTIN to confirm the differentiation of the iPSC lines into NSCs. All the cell lines stained positive for SOX1, SOX2, and NESTIN antibodies confirming the complete differentiation of the iPSC lines into NSC lines (Fig.4-21).

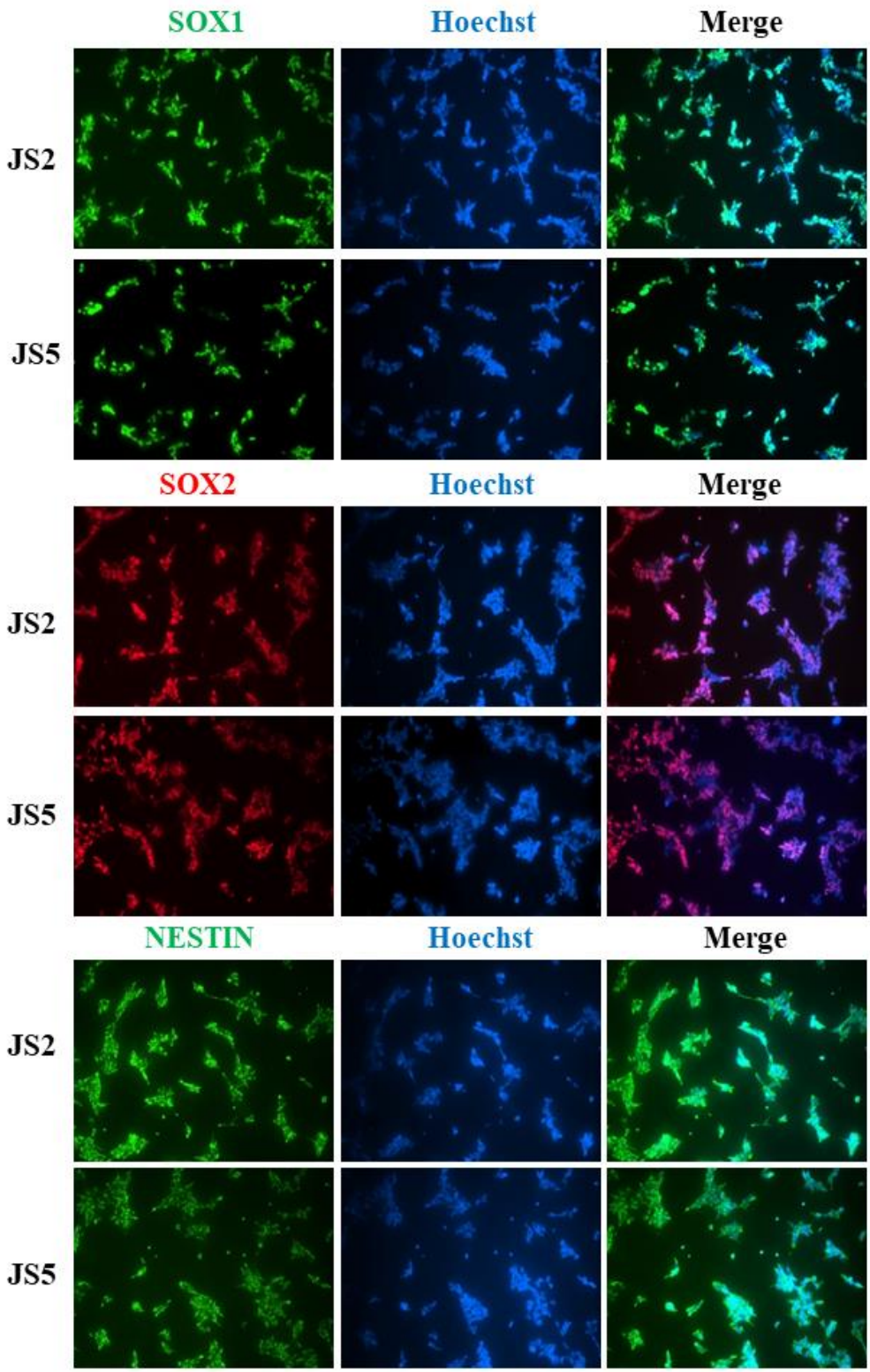

Figure 4-21. Immunofluorescence analysis for detection of NSC markers in JS-derived NSC lines. Representative immunofluorescence images of the NSCs show positive expression of the NSC marker proteins SOX1 (green), SOX2 (red), and NESTIN (red). The nuclei are stained with Hoechst (blue). The images were obtained using a 10X microscope objective.

4.10.3. SYBR Green-based RT-qPCR gene expression analysis of NSC markers

Neural induction of JS-derived iPSCs was assessed also by key NSC-related genes *NESTIN*, *SOX1*, *SOX2*, and *PAX6* and iPSCs marker *OCT4* gene expression analysis. RNAs were purified at the end of induction treatment (day 7- NSCs P0) and cDNAs were prepared to perform RT-qPCR assessment. The relative expression of the marker genes was calculated using the $2^{-\Delta\Delta C_T}$ method with *β-actin* (*ACTB)* as the internal reference. The quantitative results of each NSC line were calculated relative to the corresponding undifferentiated iPSC line. RT-qPCR analysis on JS2- and JS5-derived NSC lines revealed a significant increase in the gene expression level of *SOX1* and *PAX6* and an expected moderate expression of *SOX2* and *NESTIN* as these markers are also expressed in iPSCs. Both the NSC lines showed a markedly low expression level of the pluripotency marker *OCT4* indicating that the generated NSC lines are free of residual iPSCs (Fig.4-22 & 4-23). These findings confirmed that JS-derived iPSC lines were successfully differentiated into a relatively pure NSC lines.

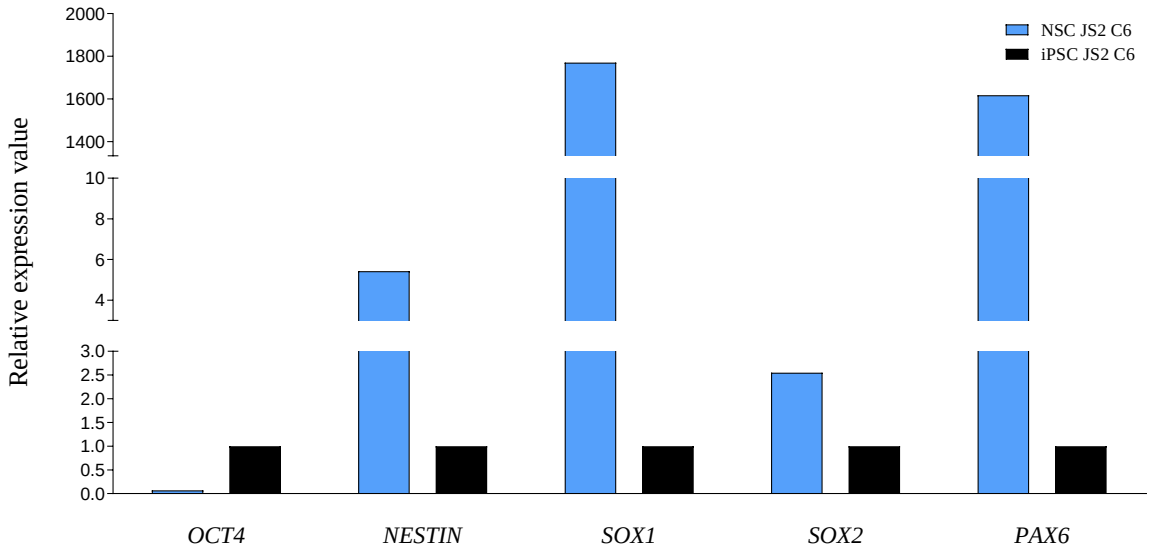

Figure 4-22. **Relative expression levels of NSC markers in JS2-derived NSC line.** RT-qPCR analysis of relative gene expression of *OCT4*, *NESTIN*, *SOX1*, *SOX2*, and *PAX6* in a JS2-derived NSC line (C6) relative to the undifferentiated JS2-derived iPSCs.

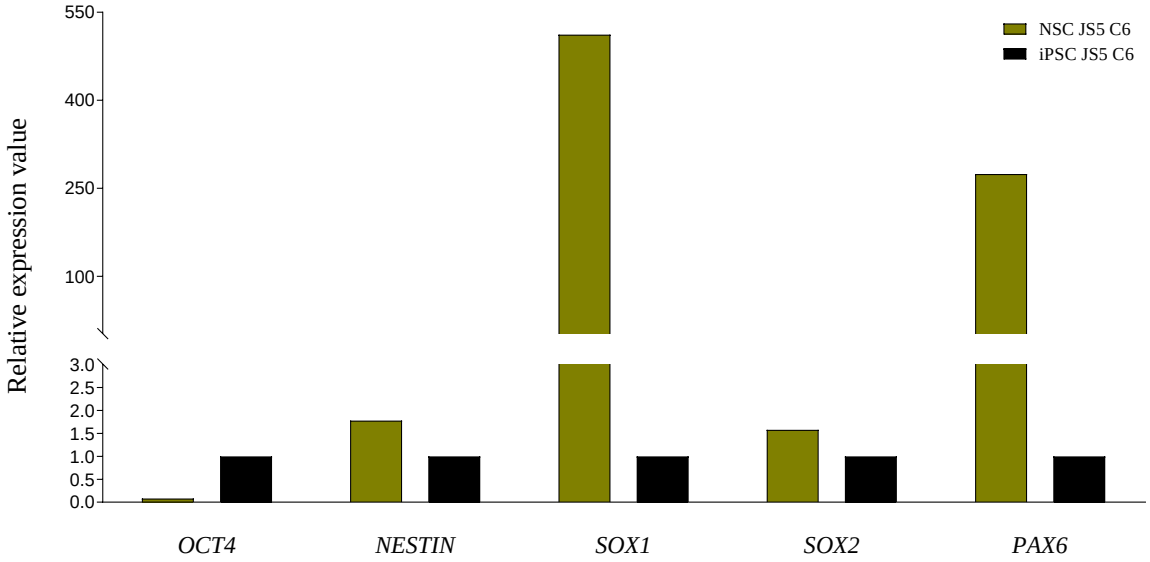

Figure 4-23. **Relative expression levels of NSC markers in JS5-derived NSC line.** RT-qPCR analysis of relative gene expression of *OCT4*, *NESTIN*, *SOX1*, *SOX2*, and *PAX6* in a JS5-derived NSC line (C6) relative to the undifferentiated JS5-derived iPSCs.

4.10.4. Cytogenetic analysis of JS-derived NSC lines

All the iPSC-derived NSC lines were karyotyped, and no structural or numerical alteration was found (Fig.4-24). The analysis results were consistent with the previous karyotype analyses of the parental cells and their derived iPSCs.

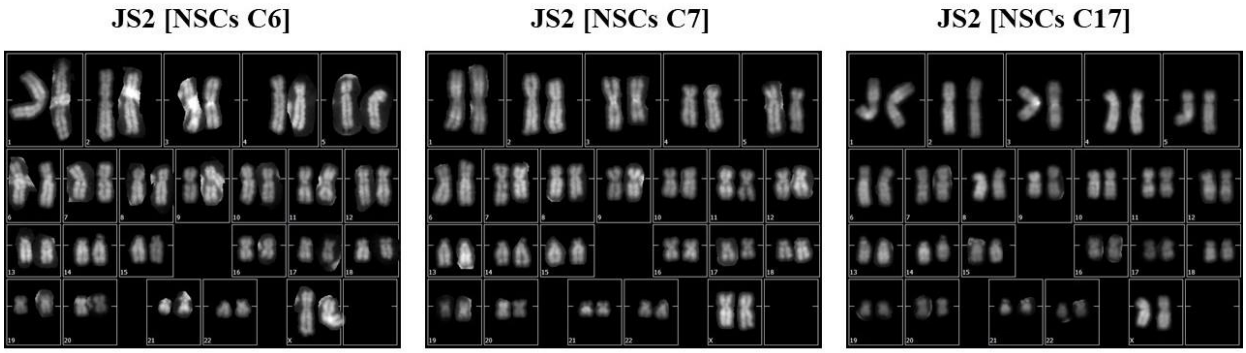

Figure 4-24. Q-banding chromosome analysis of JS-derived NSCs. Representative images of karyotype analysis of three NSC lines derived from JS2 NSCs show a normal female karyotype (46, XX). Bands resolution: 400-450.

4.11. Differentiation of JS-derived NSCs into neurons

iPSC-derived NSC lines of JS2 (C6), JS5 (C6), and BJ (C21) were differentiated into neurons following a standard protocol in GibcoTM Neurobiology Protocol Handbook (Thermo Fisher Scientific). The NSCs were seeded on poly-L-ornithine- and laminin-coated 6-well culture plates in complete StemPro NSC SFM medium. After 48 hr, the NSCs transformed into intermediate neural

progenitor cells (NPCs) characterized by their elongated and radially aligned morphology compared to NSCs which form clusters (Fig.4-25), and the medium was replaced by the neural differentiation medium for 15 days. The spent medium was changed every 3-4 days. The cells continued their differentiation into mature neurons which are characterized by dendritic branching and axonal projections compared to NPCs viewed under an inverted phase contrast microscope (Fig.4-26). At day 15, the cells were collected to extract RNA for molecular characterization of the neurons as they started to detach from the poly-L-ornithine- and laminin-coated culture plates.

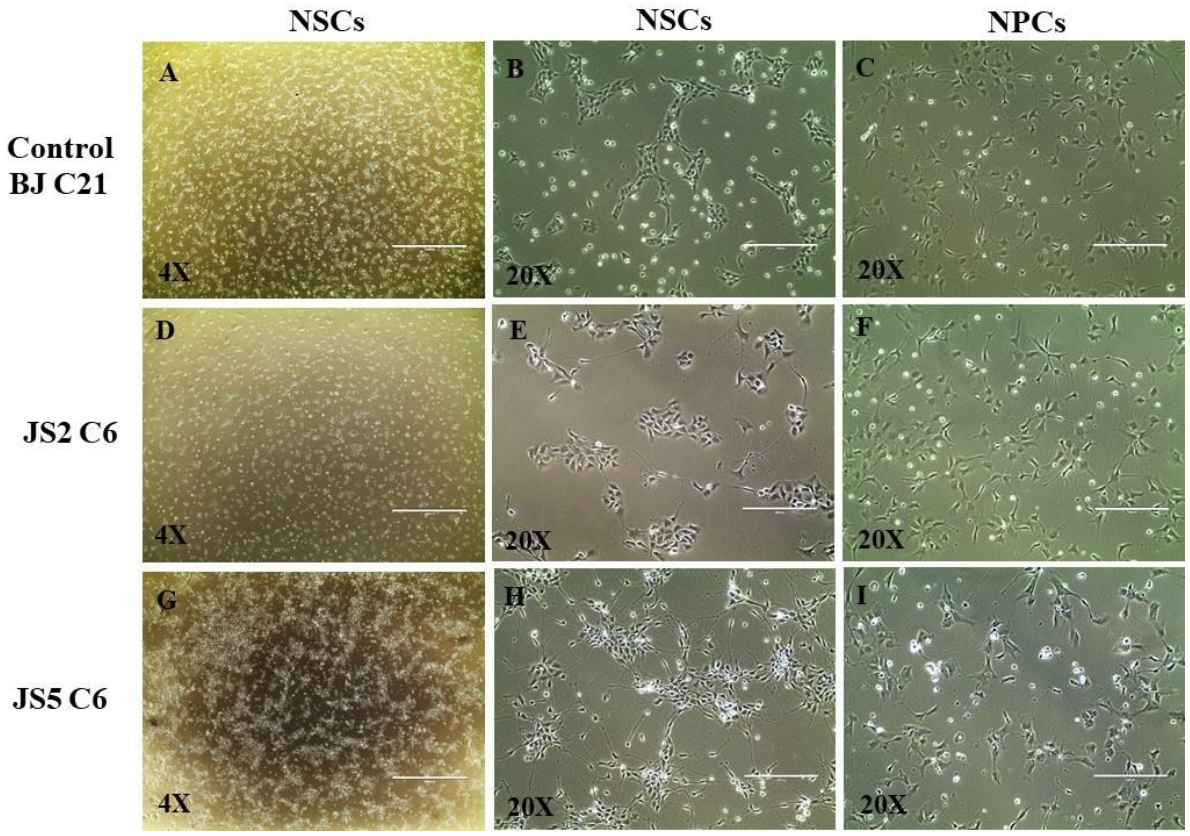

Figure 4-25. **NSCs and NPCs differentiated from JS- and BJ-derived iPSC lines.** Representative phase contrast images show morphological differences between NSCs and NPCs derived from iPSCs of BJ, JS2, and JS5 respectively. Scale bars correspond to 1000 µm and 200 µm in the images obtained using 4X and 20X microscope objectives respectively.

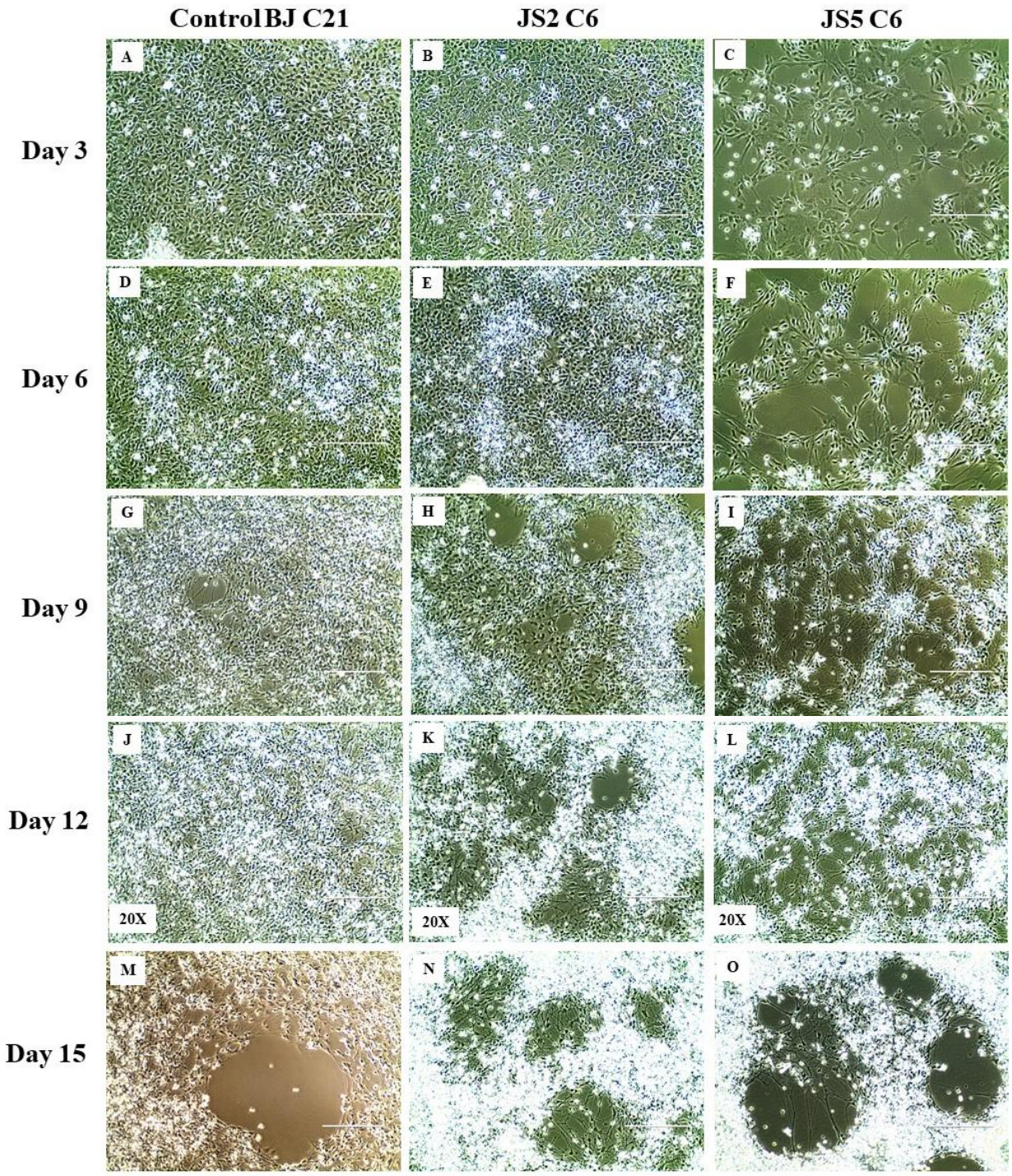

Figure 4-26. **JS- and BJ-derived neurons.** Representative phase contrast images show morphology of JS- and BJ-derived cells grown in the neural differentiation medium during differentiation of NSCs into neurons at day 3, 6, 9,12 and 15. The images were obtained using a 20X microscope objective. Scale bars correspond to 200 µm.

4.12. Characterization of JS-derived neuronal cell lines

4.12.1. Immunofluorescence assays for detection of neuronal markers

At day 15 in the neural differentiation medium, the cells differentiated from JS-derived NSC lines were stained to examine the expression of neural proteins during the differentiation of the NSCs into neurons. The cells were immunofluorescent-stained with MAP2 monoclonal (M13) and purified anti-tubulin β-3 (TUBB3) antibodies. Immature and mature neurons were identified by positive staining for TUBB3 and MAP2 respectively (Fig.4-27).

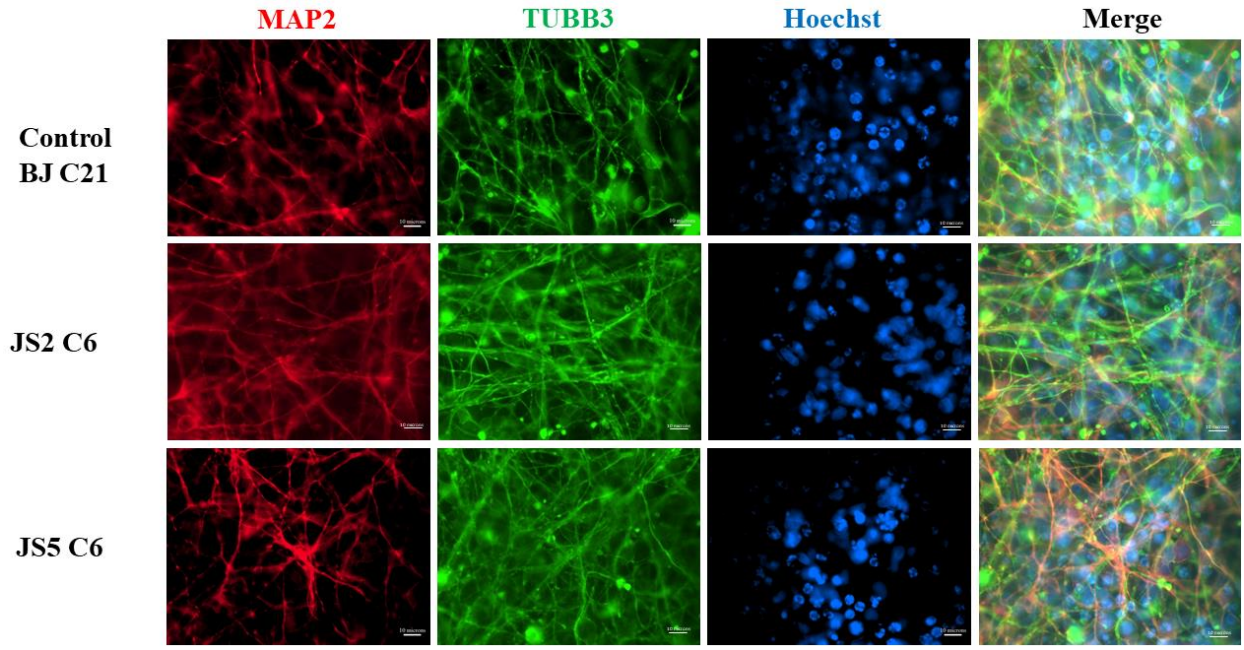

Figure 4-27. **Immunofluorescence analysis for detection of neuronal markers in the generated neuronal lines derived from JS2 and JS5 iPSCs.** Representative immunofluorescence images of the neurons show positively stained cells with anti-MAP2 (red) and anti-TUBB3 (green) antibodies. The nuclei are stained with Hoechst (blue). The images were obtained using a 60X microscope objective.

4.12.2.SYBR Green-based RT-qPCR gene expression analysis of neuronal markers

The neuronal differentiation performed was not directed towards any particular cell type but led to the growth of heterogeneous neuronal populations. Therefore, in order to assess which kind of neurons was predominant in the cellular culture obtained, a RT-qPCR on specific genes for the several typologies of neurons was carried out. Genes tested include glutamic acid decarboxylase (*GAD*) marker for GABAergic neurons, choline Acetyltransferase (*CHAT*) for cholinergic neuron, and tyrosine hydroxylase (*TH*) for dopaminergic neurons. In addition, to estimate the neuronal culture purity, expression of genes specific for glia cells (glial fibrillary acidic protein - *GFAP*) was also

evaluated. A similar gene expression patterns of the neuronal markers in all the cell lines was observed after 15 days of neural differentiation. Precisely, all samples exhibit an increased expression of *PAX6, DCX, MAP2, CHAT, GFAP*, and *TH* at day 15 confirming the neuronal phenotype acquired. This increase is not appreciable for *TUBB3*, and *GAD* because of their high expression also in the parental NSCs used as a calibrator in the relative quantification. Moreover, results in figure 4-28 show that the dopaminergic population was predominant in cell culture for all the samples, especially in the healthy donor BJ, and that a moderate contamination of glia cells expressing *GFAP* was present.

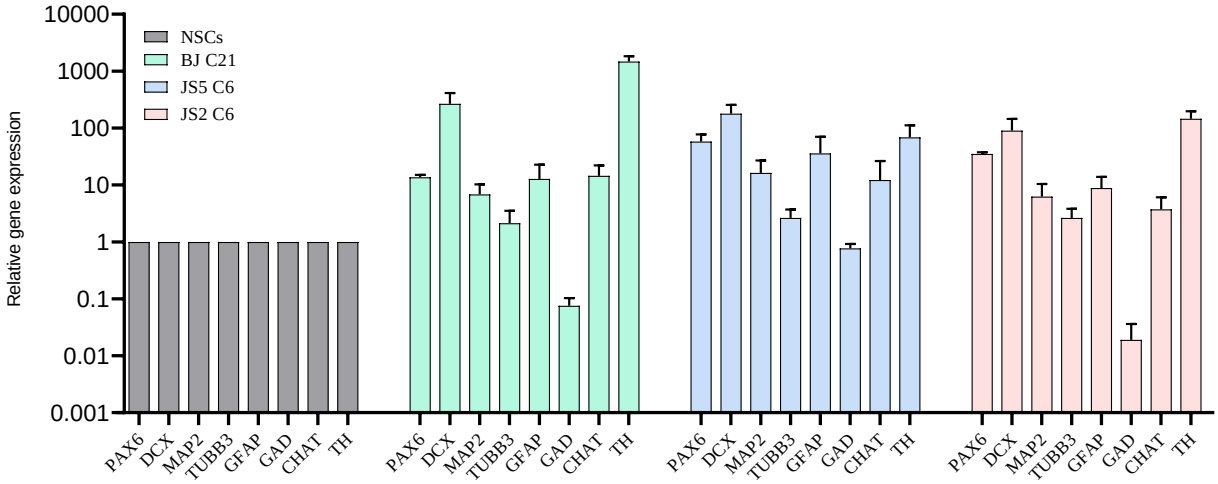

Figure 4-28. **Relative expression levels of neuronal markers in JS- and BJ-derived neuronal cell lines.** RT-qPCR analysis of relative gene expression of *PAX6, DCX, MAP2, TUBB3, GFAP, GAD, CHAT, and TH* in a JS- and BJ-derived neurons relative to the undifferentiated P0 NSCs derived from BJ. Each sample was analyzed in triplicate and the relative quantification (RQ) value was calculated from the mean Ct values of the triplicates.

4.13. Functional analysis of primary cilia in JS-derived cell lines

We explored the existence of primary cilia and characterized their phenotypes in BJ- and JS-derived fibroblasts, iPSCs, and NSCs. The cells were stained using a commercial primary antibody to target acetylated α-tubulin (AcTb), a commonly used primary cilia marker. Based on immunofluorescent staining for AcTb, the length of primary cilia and the number of ciliated cells were quantified.

4.13.1. Primary cilia in JS-derived fibroblasts

We performed immunofluorescent staining on fibroblasts of JS2 (P9), JS5(P7) and BJ (P22) to detect the expression of the AcTb. Fibroblasts of each cell line were cultured in DMEM media containing (10% FBS) and serum-starved DMEM media containing (0.5% FBS) for 24 hr. Fibroblasts of JS2 and JS5 grown in serum-starved DMEM media showed a significantly low percentage of ciliated cells (~4.5%) and (~11%) respectively, as compared to BJ-derived fibroblasts (~23.5%) (Fig.4-29B).

Likewise, the fibroblasts grown in complete DMEM media exhibited similar pattern of low percentage of ciliated fibroblasts in JS-derived fibroblasts (JS2, ~2.3% and JS5 ~2.4%) (Fig.4-29A). Unexpectedly, there was not a markedly difference in the length of primary cilia in all the ciliated fibroblasts cultured in both types of DMEM media between JS- and BJ-derived fibroblasts. The mean length of primary cilia was found to be (~4 µm) (Fig.4-30). The experiments were performed in triplicate for the fibroblasts grown in serum-starved and serum-enriched medium and the cells were counted from 30 randomly selected fields on a microscope slide.

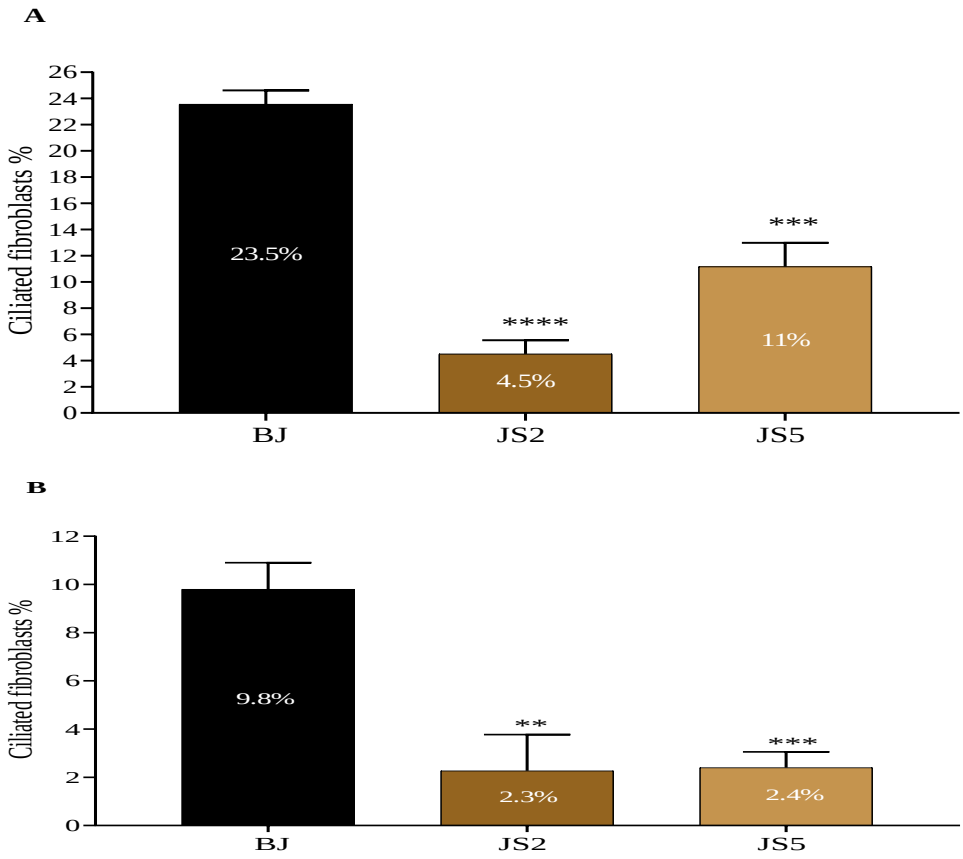

Figure 4-29. **Number of ciliated cells in JS- and BJ derived fibroblasts.** Percentage of ciliated fibroblasts grown in starved (A) and serum-enriched medium (B). Statistical significance was determined using an unpaired Student's t test (**$p < 0.002$, ***$p < 0.0006$, ****$p < 0.0001$).

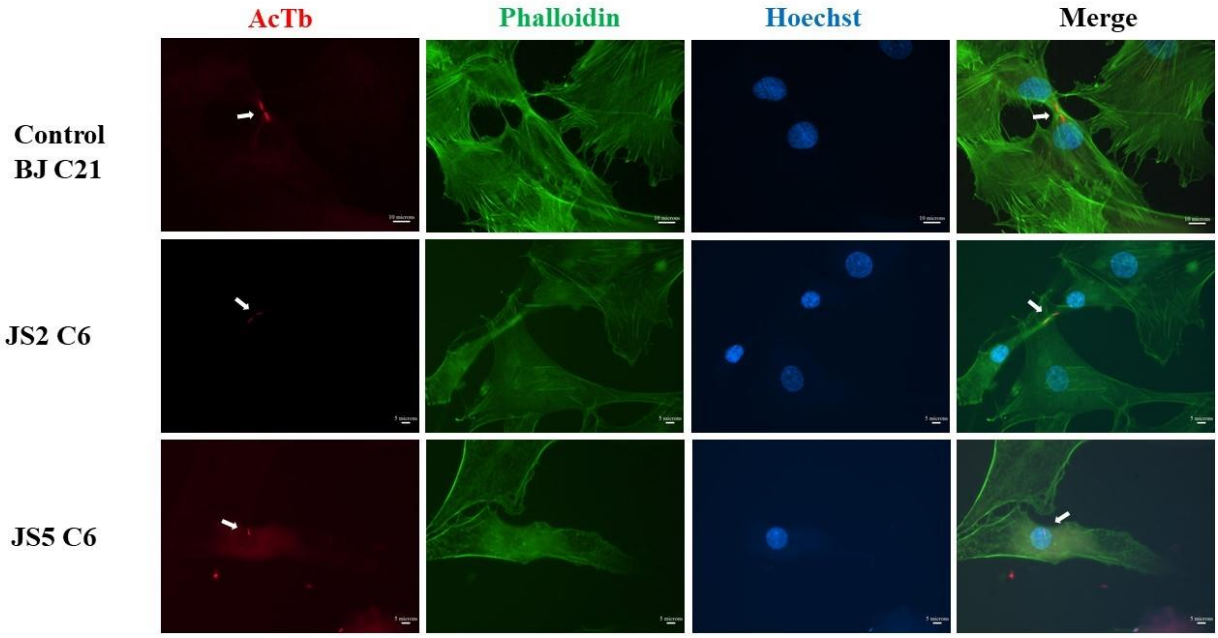

Figure 4-30. **Immunofluorescence analysis for detection of primary cilia in BJ- and JS-derived fibroblasts.** Representative immunofluorescence images of fibroblasts show positively stained primary cilia with anti-AcTb (red) antibody. The actin filaments in the cytoskeleton are stained with anti-phalloidin (green) antibody and the nuclei are stained with Hoechst (blue). The images were obtained using a 60X microscope objective. Scale bars correspond to 5 µm and 10 µm in JS- and BJ-derived fibroblasts images respectively.

4.13.2. Primary cilia in JS-derived iPSCs

The presence of primary cilia was examined in JS2-, JS5-, and BJ-derived iPSCs grown in complete NutriStem® hPSC XF Medium by immunofluorescence staining to visualize the AcTb-labelled primary cilia. As expected, the number of ciliated JS-derived iPSCs was significantly low compared to BJ-derived iPSCs (Fig.4-31). The percentage of ciliated iPSCs of BJ, JS2 and JS5 was ~7.9%, ~5.7%, and ~3.4% respectively. No significant variation in the length of primary cilia between JS- and BJ-derived iPSCs (~5-10 µm) (Fig.4-32). The experiments were performed in triplicate for each iPSC line and the cells were counted from 10 randomly selected fields on a microscope slide.

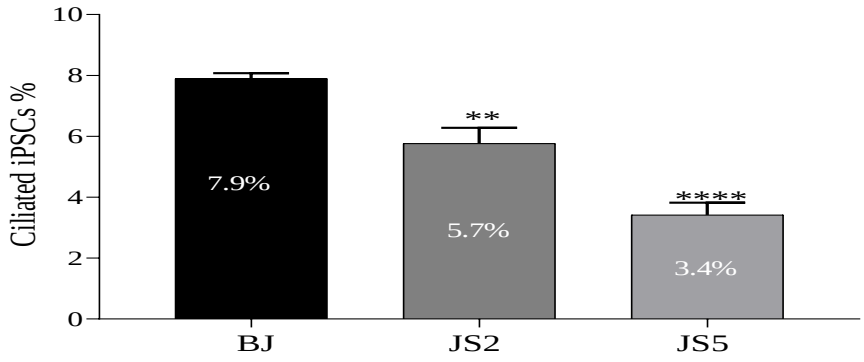

Figure 4-31. **Number of ciliated cells in JS- and BJ-derived iPSCs.** Statistical significance was determined using an unpaired Student's t test (**$p < 0.002$, ****$p < 0.0001$).

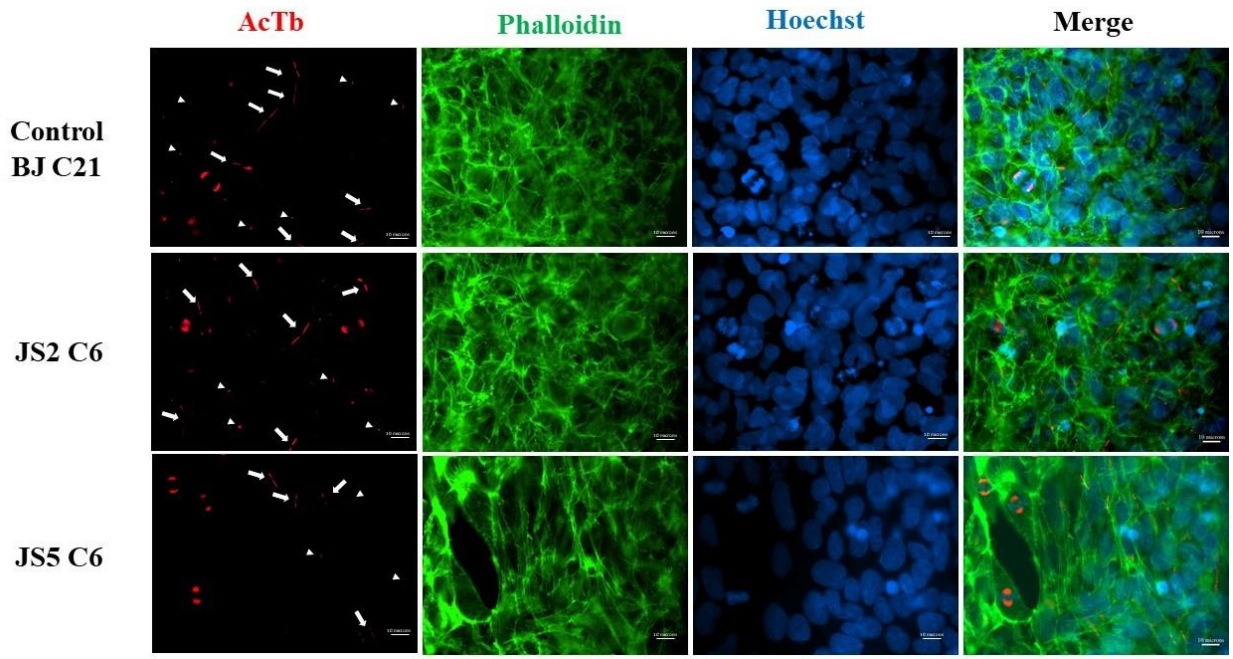

Figure 4-32. **Immunofluorescence analysis for detection of primary cilia in BJ- and JS-derived iPSCs.** Representative immunofluorescence images of iPSCs show positively stained primary cilia (indicated by arrows) with anti-AcTb (red) antibody. The actin filaments in the cytoskeleton are stained with anti-phalloidin (green) antibody and the nuclei are stained with Hoechst (blue). Arrowheads indicate extremely short primary cilia. The images were obtained using a 60X microscope objective. Scale bars correspond to 10 µm.

4.13.3.Primary cilia in JS-derived NSCs

AcTb-stained primary cilia were identified in NSCs of JS2 (P16), JS5 (P6) and BJ (P12) derived from iPSCs C6P26, C6P26, and C21P145 respectively. There was extreme variability in the number of ciliated NSCs between BJ-derived NSCs and JS-derived NSCs. The percentage of ciliated NSCs in BJ-derived NSCs was significantly higher (~7%) than of those in JS2- and JS5-derived NSCs ~2% and ~0.8% respectively (Fig.4-31). As observed in JS- and BJ-derived ciliated fibroblasts and iPSCs, measurement of the ciliary length in the NSCs showed no significant differences between the ciliated NSCs derived from JS2, JS5, and BJ (mean length was ~5µm) (Fig.4-32). The experiments were performed in triplicate for each NSC line grown in Neural Expansion Medium and the cells were counted from 10 randomly selected fields on a microscope slide.

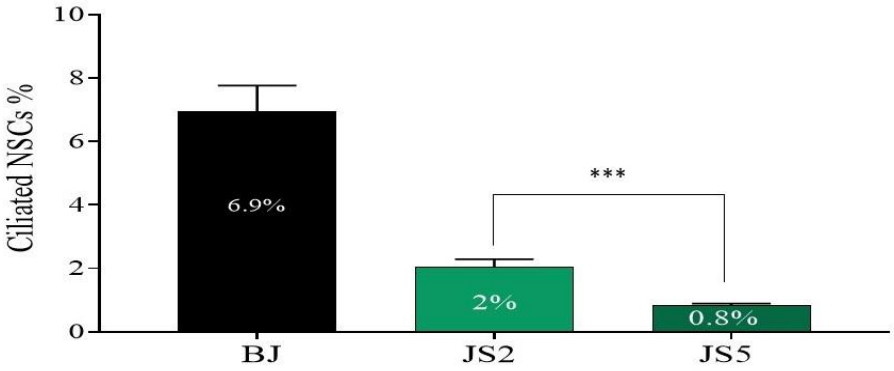

Figure 4-33. **Number of ciliated cells in JS- and BJ-derived iPSCs.** Statistical significance was determined using an unpaired Student's t test (***$p < 0.0006$).

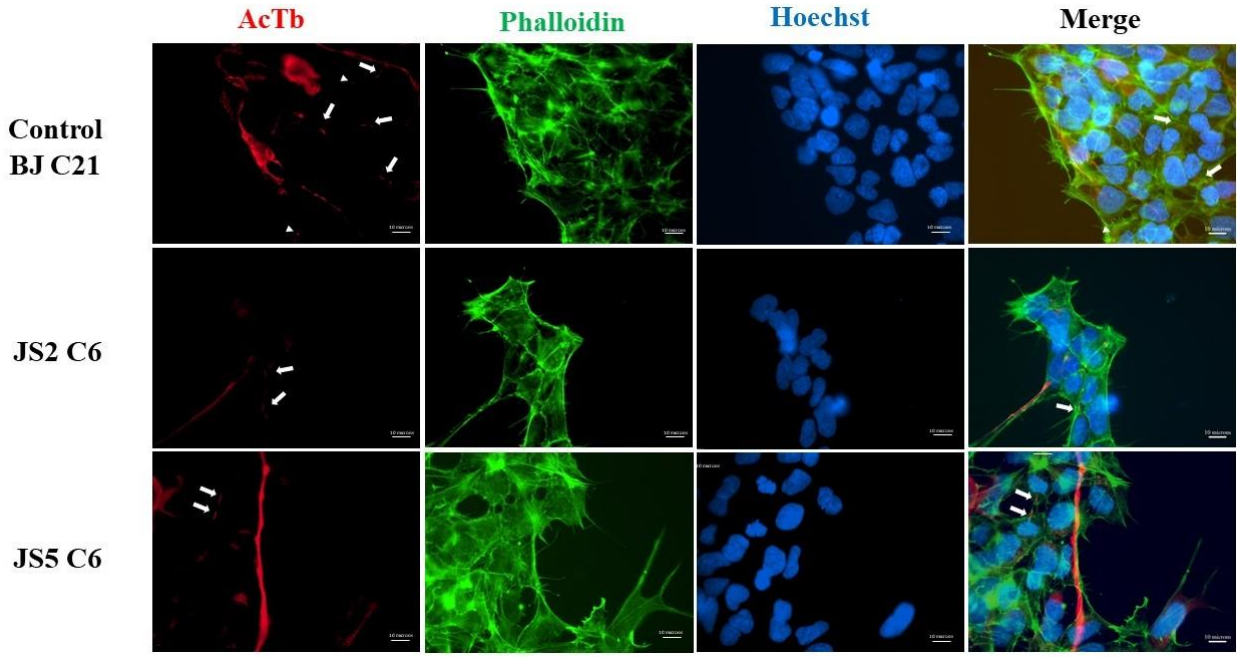

Figure 4-34. **Immunofluorescence analysis for detection of primary cilia in BJ- and JS-derived NSCs.** Representative immunofluorescence images of NSCs show positively stained primary cilia (indicated by arrows) with anti-AcTb (red) antibody. The actin filaments in the cytoskeleton are stained with anti-phalloidin (green) antibody and the nuclei are stained with Hoechst (blue). The images were obtained using a 60X microscope objective. Scale bars correspond to 10 µm.

4.14. Functional analysis of SHH signaling pathway in JS-derived cell lines

In this study, we carried out functional analysis of SHH signaling molecules Gli1, Gli2, Smo, and Ptch1 in JS- and BJ-derived fibroblast, iPSC, NSC, and neuronal lines. To determine whether the genetic defects in JS-derived cell lines affect the SHH signaling pathway, we used 2 µM of smoothened agonist (SAG) to induce the SHH signaling pathway in these cell types. The cells were SAG-stimulated for 24 hr in complete medium -except for the fibroblasts which were grown in a

serum-starved medium-before being collected for RNA extraction and further assessment of the expression patterns of SHH signaling molecules *Gli1, Gli2, Smo,* and *Ptch1* by RT-qPCR.

4.14.1.SHH signaling pathway in JS-derived fibroblasts

Quantitative RT-PCR analysis of SAG-stimulated fibroblasts derived from JS2, JS5, and BJ revealed a significant downregulation of *Gli1* in both JS-derived fibroblast lines as compared to the healthy control BJ. Considering the basal gene expression in non-stimulated fibroblasts, JS2- and JS5-derived fibroblasts showed a slight induction of *Gli1* and *Smo* after 24 hr SAG stimulation. No statistically significant differences were detected in gene expression of *Gli2* and *Ptch1* in SAG-stimulated fibroblasts of JS2, JS5 and BJ (Fig.4-35).

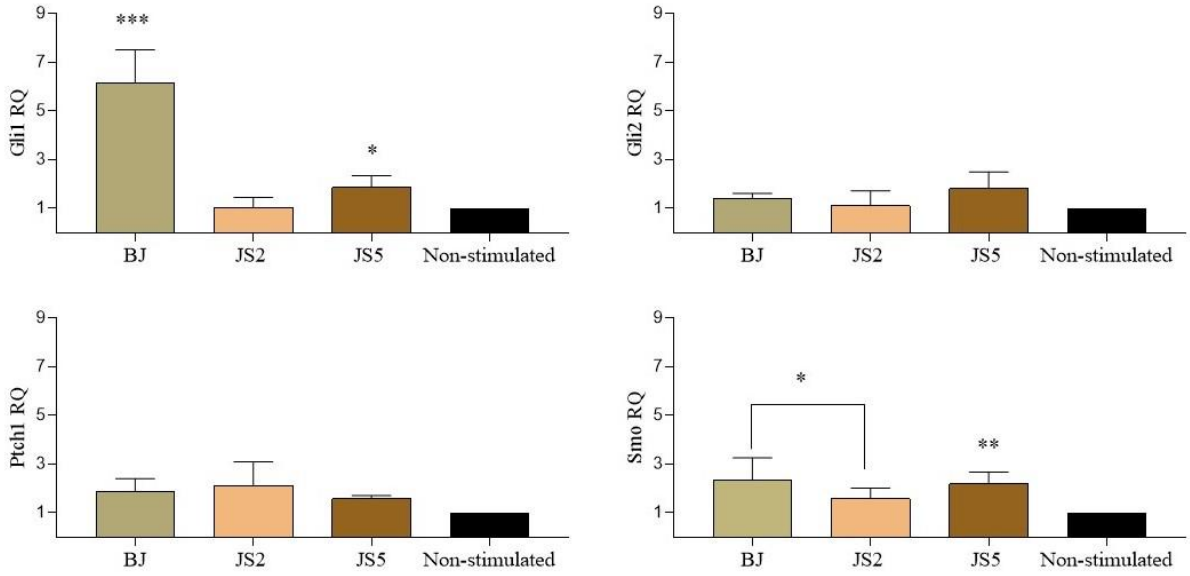

Figure 4-35. Relative expression levels of *Gli1, Gli2, Ptch1*, and *Smo* in SAG-stimulated fibroblasts of JS2, JS5, and BJ. RT-qPCR gene expression levels in the stimulated cells were calculated relative to non-stimulated fibroblasts of each cell line. Each sample was analyzed in triplicate and the relative quantification (RQ) value was calculated from the mean Ct values of the triplicates. Statistical significance was determined using an unpaired Student's t test (*$p < 0.03$, **$p < 0.002$, ***$p < 0.0003$).

4.14.2. SHH signaling pathway in JS-derived iPSCs

In SAG-stimulated iPSCs of JS2 and JS5, the expression levels of *Gli1*, *Gli2*, and *Smo* were relatively similar to those of SAG-stimulated control BJ and non-stimulated iPSCs. Interestingly, in SAG-stimulated iPSCs, *Ptch1*, a key activator of the SHH signaling pathway, showed a significantly high expression in BJ-derived iPSCs, while it exhibited no activation by SAG in JS2- and JS5-derived iPSCs (Fig.4-36).

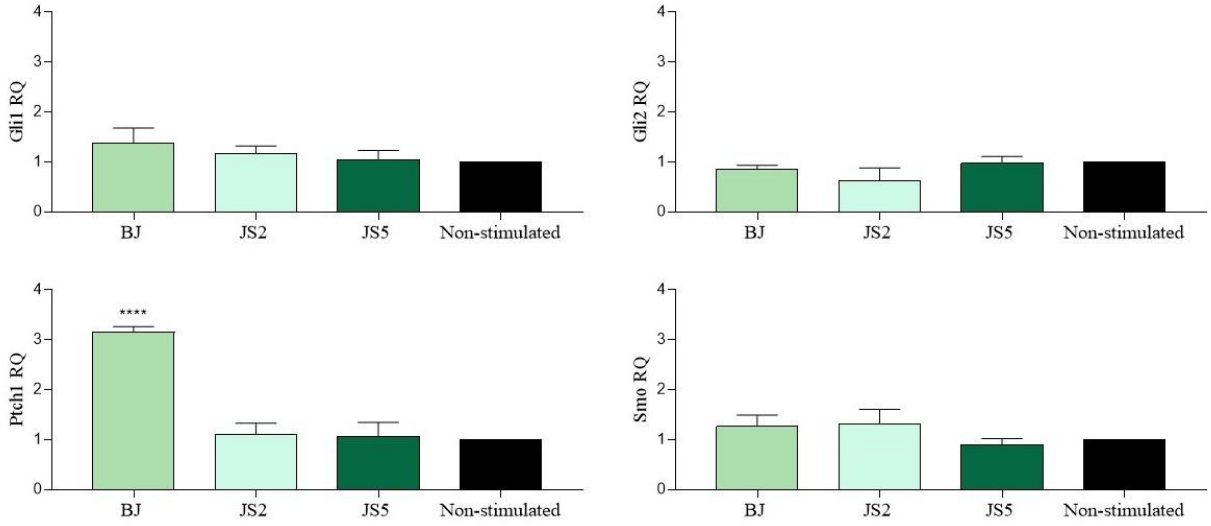

Figure 4-36. Relative expression levels of *Gli1, Gli2, Ptch1*, and *Smo* in SAG-stimulated iPSCs of JS2, JS5, and BJ. RT-qPCR gene expression levels in the stimulated cells were calculated relative to non-stimulated iPSCs of each cell line. Each sample was analyzed in triplicate and the relative quantification (RQ) value was calculated from the mean Ct values of the triplicates. Statistical significance was determined using an unpaired Student's t test (***$p <$ 0.0001).

4.14.3. SHH signaling pathway in JS-derived NSCs

Assessment of the effect of SAG stimulation on the expression levels of SHH signaling genes *Gli1*, *Gli2*, *Patch1*, and *Smo* in JS- and BJ-derived NSCs revealed that only *Gli1* and *Ptch1* were induced in this kind of cells. Moreover, the JS2- and JS5- derived NSCs showed a statistically significant reduction of *Gli1* and *Ptch1* gene expression as compared to BJ-derived NSCs (Fig.4-37).

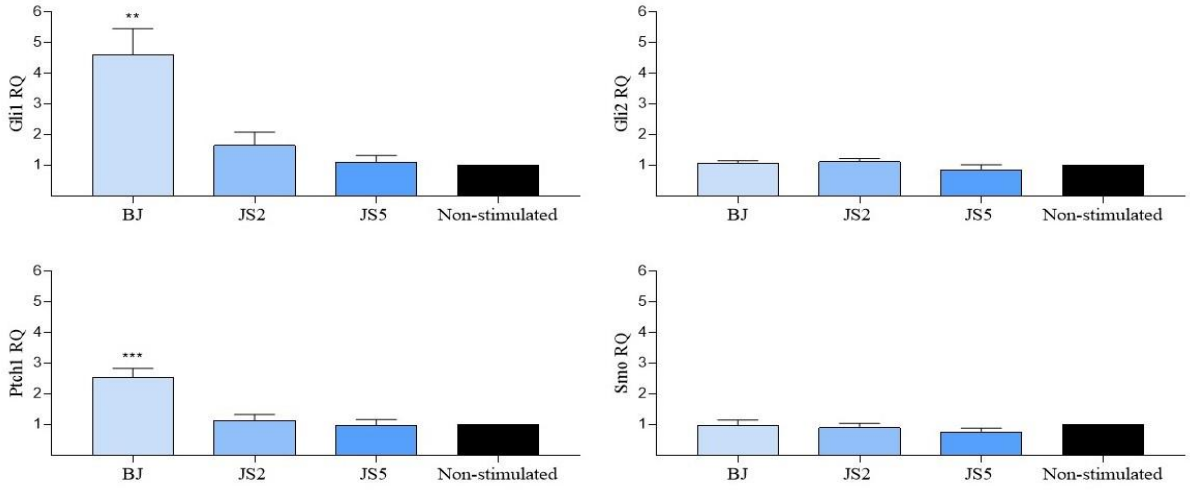

Figure 4-37. Relative expression levels of *Gli1, Gli2, Ptch1*, and *Smo* in SAG-stimulated NSCs of JS2, JS5, and BJ. RT-qPCR gene expression levels in the stimulated cells were calculated relative to non-stimulated NSCs of each cell line. Each sample was analyzed in triplicate and the relative quantification (RQ) value was calculated from the mean Ct values of the triplicates. Statistical significance was determined using an unpaired Student's t test (**$p <$ 0.001, ***$p <$ 0.0007).

4.14.4. SHH signaling pathway in JS-derived neurons

The expression patterns of *Gli1, Gli2, Ptch1*, and *Smo* in the SAG-stimulated neurons of JS2, JS5, and BJ were evaluated by RT-qPCR. No induction of *Gli2, Ptch1*, and *Smo* was detected in this cell type. Only *Gli1* showed increased expression after SAG stimulation, in particular a high expression was noted in BJ-derived neurons, while in JS-derived neurons, *Gli1* was significantly reduced. *Gli2* and *Ptch1* were significantly downregulated in JS5-derived neurons (Fig.4-38).

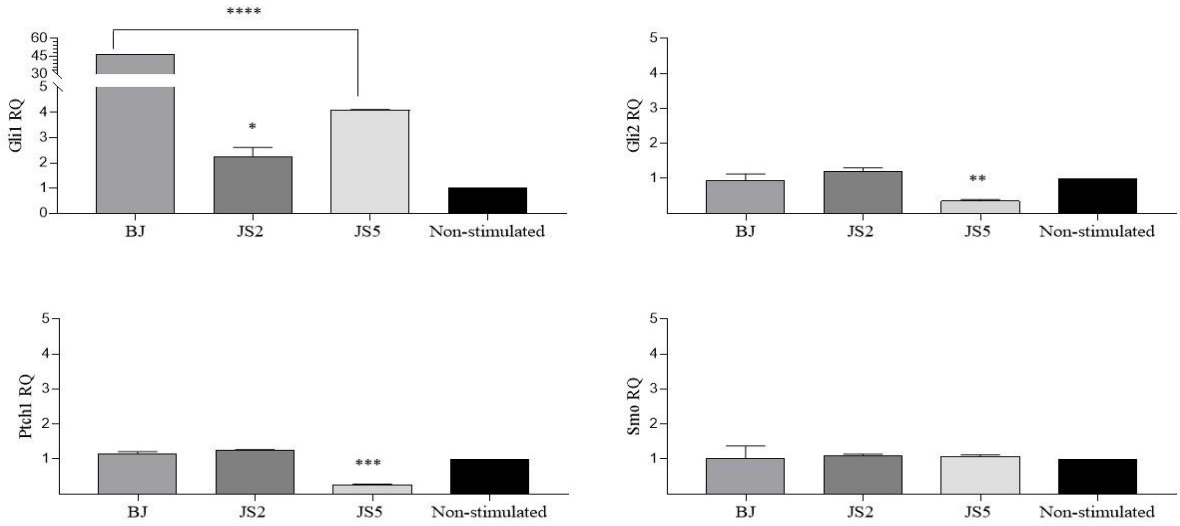

Figure 4-38. Relative expression levels of *Gli1, Gli2, Ptch1*, and *Smo* in SAG-stimulated neurons of JS2, JS5, and BJ. RT-qPCR gene expression levels in the stimulated cells were calculated relative to non-stimulated neurons of each cell line. Each sample was analyzed in triplicate and the relative quantification (RQ) value was calculated from the mean Ct values of the triplicates. Statistical significance was determined using an unpaired Student's t test (*$p < 0.03$, **$p < 0.002$, ***$p < 0.0002$, ****$p < 0.0001$).

DISCUSSION

5. DISCUSSION

5.1. Establishment of JS-derived iPSC lines

For decades, establishing human models for neurological diseases have been considered as a far-fetched dream since the challenge to obtain live neurons from the CNS or peripheral nervous system (PNS) of patients or healthy individuals. This obstacle has led scientists to utilize animal models (Chesselet & Carmichael, 2012) and neural cells isolated from human post-mortem tissues to study the neurological diseases (Chu et al., 2020; Anand et al., 1995). As a result of modeling neurological disorders by using primary neural cells, immortal cell lines, animal models, and analysis of human post-moretm-derived neural tissues, great advancements in understanding the mechanisms of several neurological disorders have been achieved in addition to their essential role in pre-clinical studies (Chesselet & Carmichael, 2012). However, there are certain limitations in using animal models for studying human neurological disorders (Cenci et al., 2002). Full recapitulation of disease phenotypes is hindered by species differences which may lead to high rates of failure during drug screening. In clinical translation of roughly 500 novel therapeutic agents that have shown promising results in rodent models of stroke, only one drug has been approved as a new therapy for stroke (Sena et al., 2010; Macleod et al., 2006). However, many of these unsuccessful preclinical trials could descend from incorrect study design and data analysis approaches used rather than from the animal models themselves (Scott et al., 2008; Macleod et al., 2008). It is also important to note that the disappointing outcomes in clinical trials may result from uncertainty of the relevance of these models to the human disease (Chesselet & Carmichael, 2012). The development of iPSC technology (Takahashi & Yamanaka, 2006) and the rapid advancements in genome editing approaches (Perez-Pinera et al., 2013; Ding et al., 2013; Jinek et al., 2012; Hockemeyer et al., 2011) have revolutionized the field of disease modeling and translational research particularly for neurological disorders. In the last decade, many human iPSC-derived models have been developed for several neurological disorders including ALS, familial and sporadic AD, and PD (di Domenico et al., 2019; Israel et al., 2012; Dimos et al., 2008). In this PhD study, we primarily aimed to establish human *in vitro* models of JS by generating disease-specific iPSCs and subsequently differentiating them into neural cell lines. JS is a rare neurological disorder characterized by hypotonia, psychomotor impairment, intellectual disability, and a hallmark finding on brain MRI known as the molar tooth sign (MTS). Other clinical features of JS include eye abnormalities such as retinal dystrophy, ocular colobomas, oculomotor apraxia (OMA) (Wang et al., 2018), liver and kidney disease (Strongin et al., 2018; Bachmann- Gagescu et al., 2015). The pathological basis of JS is still not well-understood. However, it is known to be associated with structural and/or functional defects of primary cilia. There are a heterogenous group

of disorders that overlap genetically and phenotypically with JS and are known as ciliopathies (Romani et al., 2013). These disorders are associated with ciliary dysfunction due to mutations in genes that encode ciliary proteins or their interacting proteins such as B9/tectonic-like complex. This protein network includes AHI1, B9D1, B9D2, CC2D2A, CEP290, TCTN1, TCTN2, TMEM67, TMEM231, and TMEM237. It blocks certain proteins from passing through the TZ and simultaneously allows specific proteins to diffuse into the ciliary compartment (Okazaki et al., 2020; Gonçalves & Pelletier, 2017). Due to unavailability of an approved therapy for JS and lack of a comprehensive understanding of the pathogenic mechanisms associated with this neurological disease, it has become necessary to incorporate iPSC-derived neuronal models of JS into the pre-clinical and translational research of JS. The core objective of this research was establishment of JS-derived iPSC lines by reprogramming of fibroblasts obtained from five patients with JS harbouring different mutations in *C5orf42, CC2D2A,* and *TMEM67,* and subsequent differentiation of the generated iPSCs into neuronal cell lines. To the best of our knowledge, to date only two reports on patient-derived iPSC models of JS have been described from an Italian research team showed establishment of two patient-specific iPSC models of JS with a homozygous missense mutation (p.H896R) and (c.2168G > A) in *AHI1* respectively (Altieri et al., 2019; Rosati., 2018). Two new reports are part of this Ph.D thesis (Ali et al., 2021; 2020).

In this study, we demonstrate the successful generation of high-quality iPSC lines from dermal fibroblasts obtained from five patients with JS (JS1-JS5) using the CytoTune™-iPS 2.0 Sendai Reprogramming Kit (Fusaki et al., 2009). Patient-derived fibroblasts carrying mutations in *CC2D2A* (JS1 and JS2), *TMEM67* (JS3 and JS4), and *C5orf42* (JS5), were transduced with four reprogramming factors *OCT3/4, SOX2, KLF4,* and *c-MYC*. Following 24 hr in culture, substantial number of dead fibroblasts were observed due to a high uptake of the viral vectors. All the transfected fibroblast lines showed gradual morphological changes that were clearly observed under an inverted phase contrast microscope. Approximately 3 weeks post-transduction, ESC-like colonies have emerged indicative of reprogrammed cells. To establish JS-derived iPSC lines, at least 15 TRA-1-60- positive iPSC clones from each fibroblast line were manually picked and expanded for >20 passages. In order to assess their capacity for self-renewal, pluripotency, and genetic integrity following long-term maintenance in culture, 3 clones from the generated iPSC lines were selected for further expansion and characterization. iPSCs from different passages of each clone were cryopreserved.

From a biosafety perspective, the genomic integrity of iPSCs during reprogramming and long-term culture is of great importance in translational medicine. The genomic and epigenomic defects may compromise the differentiation capacity of iPSCs and induce tumorgenesis in patients treated with iPSC-derived cell therapies (Zhang et al., 2012; Martins-Taylor et al., 2011; Taapken et al., 2011).

Moreover, they will not be used as reliable disease model. Therefore, it was essential to investigate the genomic stability of the generated iPSCs during reprogramming and long-term maintenance in culture. All the iPSC lines have shown no structural or numerical chromosomal aberration during their prolonged culture. These results suggest that the reprogramming of somatic cells does not instigate massive genomic instability. On the other hand, our STR analysis has revealed that JS-derived iPSCs retain parental fibroblasts genotype. Additionally, Sanger sequencing results have shown persistence of the parental cells mutations in *C5orf42, CC2D2A*, and *TMEM67*. For further characterization of the generated iPSC lines, the stemness capacity of the cells was evaluated with immunofluorescence staining and subsequently with RT-qPCR analysis. All the iPSCs stained positively with antibodies against TRA-1-60 and OCT4, while RT-qPCR analysis of the stemness-related markers *OCT4, SOX2, KLF4*, and *c-MYC* have shown significantly high expression of these markers in all the JS-derived iPSC lines except JS2 and JS4 as compared to the expression pattern in BJ-derived iPSCs which were previously validated as fully pluripotent stem cells (Park et al., 2008). To verify that the reprogrammed cells of JS2 and JS4 have the stemness capacity, we re-evaluated the expression pattern of stemness markers in these cells relative to their parental fibroblasts. The expression analysis has shown significantly high expression levels of the markers in reprogrammed cells when compared to their parental counterparts. We suggest that these variations in the expression profile of stemness markers in JS2- and JS4-derived iPSCs could be attributed to the genetic mutations in the parental cells. Finally, to assess the differentiation capability of the generated iPSC lines, we have successfully differentiated three JS-derived iPSC lines namely: JS2-, JS4-, and JS5-iPSCs, into ectodermal, mesodermal and endodermal cells using the StemMACS Trilineage Differentiation Kit (Miltenyi Biotec). This differentiation into the three germ layer lineages have been validated by TaqMan-based RT-qPCR assay which has shown expression of lineage-specific markers. These results demonstrate that the generated iPSCs are pluripotent. Taken together, our results have confirmed the establishment of JS-derived iPSC lines as an initial step towards developing neuronal models of JS.

5.2. Induction of NSCs from JS-derived iPSC lines and neural differentiation

As previously mentioned, animal models provide an indispensable tool for modeling neurological diseases. However, undeniable limitations such as species-specific differences and variations in pharmaco- and toxico-kinetics of substances make it difficult to recapitulate the biochemical and molecular hallmarks of human neurological diseases and to persistently translate the novel findings into new therapies for humans. These obstacles have been overcome by the development of iPSC technology and the ability to create patient-specific iPSCs that can be differentiated into almost all types of neural cells, including but not limited to NSCs, NPCs, neurons, oligodendrocytes, astrocytes,

and microglia (Li & Shi, 2018). To accomplish the second objective of this study, we have differentiated iPSC derived from JS2 (C6), JS5 (C6), and the healthy control BJ (C21) into neurons. The differentiation process of iPSCs into neurons passes through an intermediate phase when the iPSCs are induced to NSCs using complete PSC Neural Induction Medium for 7 days following by Neural Expansion Medium for further passaging. We have induced the iPSC lines into NSCs and analyzed the generated cells by immunofluorescence and qPCR assay. From the morphological point of view, all the NSC lines assume a neuronal-like phenotype as compared to the iPSCs morphology before the induction and positively stained for the NSC markers SOX1, SOX2 and NESTIN. This has been confirmed by qPCR assay exhibiting high expression levels of the same NSC markers and *PAX6*, and no expression of the pluripotency marker *OCT4* as compared to undifferentiated iPSCs. However, the expression of *SOX2* and *NESTIN* was relatively low as compared to *SOX1* and *PAX6* as they are also expressed in iPSCs. The neuroectodermal markers SOX1 and PAX6 are critical in regulating neurogenesis, proliferation and multipotency in the CNS (Venere et al., 2012; Mo & Zecevic, 2008; Pevny et al., 1998). Additionally, DNA sequencing and karyotype analysis of the generated NSCs have shown that they retained the same genetic mutations identified in the parental cells and normal karyotypes. These results confirmed the induction of JS-derived iPSC lines into NSC lines.

The generated NSC lines maintained in culture have been cryopreserved before being differentiated into neurons. Initially, the NSCs transformed into NPCs after 48 hr in complete StemPro NSC SFM medium. Replacement of the spent medium by the neural differentiation medium has facilitated the differentiation of the NPSs into a heterogeneous population including mature neurons. This was validated by observing distinct morphological features of neurons under the microscope and positive staining of the neuronal markers MAP2 and TUBB3. Differentiation of the NSCs into neurons has yielded heterogeneous neuronal populations. Therefore, it was important to determine the predominant type of neurons in the cell cultures obtained. The neuronal phenotype acquired was confirmed by qPCR assay which revealed increased expression of *PAX6, DCX, MAP2, CHAT, GFAP*, and *TH*. It is important to note that *TUBB3* and *GAD* have shown low expression levels in the generated neuronal cells because their expression was significantly high in the parental NSCs used as a calibrator in the relative quantification. Furthermore, our results revealed that dopaminergic neurons were predominant in all the cell lines, particularly in the healthy control BJ. All the cell lines have shown expression of *GFAP* indicative of a moderate contamination of glia cells. It is worth noting that differentiation of JS-derived iPSCs into specific neuronal cell types rather than heterogenous populations of neurons could be more useful to develop efficient models for JS. However well-characterized patient-specific *in vitro* neuronal cell culture systems, as reported here, remain necessary to uncover disease mechanisms and develop therapeutic strategies.

5.3.Functional analysis of primary cilia and SHH signaling pathway in JS-derived lines

As all JS-related genes encode ciliary proteins or their interacting proteins, it has become evident that primary cilia play a crucial role in the SHH signaling pathway and pathogenic mechanisms of JS and other genetic disorders known as ciliopathies (Valente et al., 2014). Genetic mutations in JS-related genes often result in defective ciliogenesis and/or dysfunction of the primary cilia, however, the mechanisms underlying this is poorly understood. The vast majority of research on the role of primary cilia in JS and other ciliopathies has been carried out on animal or *in vitro* models (Veleri et al., 2014; Srour et al., 2012; Gorden et al., 2008). Therefore, we have investigated the correlation between the genetic mutations in the *CC2D2A* and *C5orf42* corresponding to JS2 and JS5 and the number and length of primary cilia in different JS-derived cell types. The length of primary cilia and the number of ciliated cells were quantified based on immunofluorescent staining for the ciliary marker acetylated α-tubulin (AcTb)) using serum-starvation or complete medium as SHH is activated by starvation.

In JS- and BJ-derived fibroblasts grown in serum-starved medium for 24 hr, the number of ciliated fibroblasts was significantly low in JS2- and JS5-derived fibroblasts ~4.5% and ~11% respectively, as compared to ~23.5% in BJ-derived fibroblasts. Similarly, the fibroblasts grown in serum-enriched medium exhibited low number of ciliated cells in JS-derived fibroblasts as the number of ciliated fibroblasts was 4-fold higher in the fibroblast culture of the healthy control BJ than in the fibroblast culture of JS. These results are consistent with previous data reported on two JS patients with mutations in *C5orf42* and analyzed after 4 days of starvation. (Asadollahi etal., 2018). Unexpectedly, we found no difference in the length of primary cilia in all the ciliated fibroblasts grown in both types of media between JS- and BJ-derived fibroblasts. The mean length of primary cilia was found to be ~4 µm which was within the normal range 1-6 µm (Schneider et al., 2005). Notably, another study has reported, under the same culture conditions, a significantly higher number of ciliated cells in both serum-enriched and serum-starved fibroblasts cultures of a healthy donor ~23% and ~53% respectively than in our healthy control BJ ~9.8% and 23.5% respectively (Nathwani et al., 2014). However, the variation in the number of ciliated cells could be attributed to low number of total cells counted in aforementioned report 30/129 cells and 30/57 cells in serum-enriched and serum-starved medium respectively (Nathwani et al., 2014) as compared to our study 285/2894 cells in serum-enriched medium and 640/2670 cells in serum-starved medium. Interestingly, abnormally long dysmorphic cilia have been associated with compound heterozygous mutations in *CEP290* gene in three JS patients. However, ciliogenesis was decreased in the fibroblasts of the three patients (Shimada et al., 2017). These results suggest that genetic defects in *CC2D2A* and *C5orf42* contribute to the low number of ciliated cells in the JS-derived fibroblasts. In other words, ciliogenesis affected

in patients with JS. This finding was supported by data from the cc2d2a (-/-) mouse embryonic fibroblasts (MEFs) which showed complete lack of cilia (Veleri et al., 2014).

We have also examined the presence of primary cilia in JS2-, JS5-, and BJ-derived iPSCs grown only in complete NutriStem® hPSC XF complete Medium as iPSCs tend to die under serum-deprived conditions. In accordance with the results of our fibroblast lines, the number of ciliated JS-derived iPSCs was low with no significant differences in the ciliary length (~5-10 µm) as compared to the control iPSCs. In contrast, two previous studies have reported that the number of ciliated cells in H1 hESCs (Kiprilov et al., 2008) and hiPSCs (Nathwani et al., 2014) derived from healthy donors and grown in serum-enriched conditions was ~33% and ~19% respectively as compared to ~7.9% in our control BJ iPSCs. These differences in the number of ciliated cells are likely due to variations in the number of days in culture (H1 hESCs:5 days, hiPSCs: 2 days, and BJ iPSC: 5 days) or the total number of cells counted (H1 hESCs: 25/75 cells, hiPSCs: 30/159 cells, and BJ iPSC: 2123/23373 cells). However, prominent tiny red spots were observed in BJ- and JS2-derived iPSCs which we thought to be extremely short primary cilia that were in early ciliogenesis or normal intact cilia that have lost their axoneme by normal cilia disassembly mechanisms. It is important to note that ciliogenesis was decreased in our iPSCs compared to their parental fibroblasts and this was consistent with a previous study on hiPSCs (Nathwani et al., 2014). Our experiments on JS- and BJ-derived NSCs have revealed significant differences in the number of ciliated cells between the healthy control and JS-derived NSCs. While the number of ciliated cells in JS2- and JS5-derived NSCs was ~2% and ~0.8% respectively, it was as high as ~7% in BJ-derived NSCs. The ciliary length in NSCs showed no notable differences between the ciliated NSCs derived from JS patients and BJ (mean length was ~5µm) consistent with our previous observations in JS- and BJ-derived ciliated fibroblasts and iPSCs. These findings suggest that unlike the reduced percentage of ciliated cells, ciliary length is not an established biomarker for JS or at least for JS caused by mutations in *C5orf42* and *CC2D2A.*

Furthermore, we carried out functional analysis to evaluate the ability of smoothened agonist (SAG) to induce the SHH signaling pathway in JS- and BJ-derived fibroblasts, iPSCs, NSCs, and neurons. To assess the effect of SAG stimulation on SHH signaling molecules Gli1, Gli2, Smo, and Ptch1 in these cells, we performed qPCR assays. The cells were SAG-stimulated for 24 hr in a complete medium except for the fibroblasts which were grown in a serum-starved medium. SAG-stimulated fibroblasts derived from JS2, JS5, and BJ showed that *Gli1 was* significantly down-regulated in both JS-derived fibroblast lines as compared to the healthy control BJ. In general, JS-derived fibroblasts showed a slight induction of *Gli1* and *Smo* after 24 hr of SAG stimulation, while *Gli2* and *Ptch1* were not induced in SAG-stimulated fibroblasts of JS2, JS5, and BJ. These results are partially consistent

with results of a recent study showing similar pattern of *Gli1* expression in fibroblasts obtained from two JS patients with compound heterozygous mutations in *C5orf42* and healthy controls (Asadollahi etal., 2018). In contrast to our results the expression of *Ptch1* in fibroblasts of the patients showed lower expression as compared to the controls. This variation could be due to duration of starvation and treatment with SAG as these cells were treated with SAG for 48 hr following 48 hr serum starvation. These results suggest that *Gli1* expression in JS-derived fibroblasts is negatively affected by the genetic defects in *C5orf42* and *CC2D2A.* In SAG-stimulated iPSCs, we found that SAG significantly enhanced *Ptch1* expression only in the control, while it showed no effect on *Gli1, Gli2,* and *Smo* in both control and patient-derived iPSCs. In agreement with our results, two previous studies showed elevated *Ptch1* expression in SAG-induced H1 hESCs (Kiprilov et al., 2008) and hiPSCs (Nathwani et al., 2014) obtained from healthy donors. However, a significant induction of *Gli1* and *Gli2* in H1 hESCs and *Gli1, Gli2,* and *Smo* in hiPSCs was revealed. It is important to note that H1 hESCs and hiPSCs were stimulated with SAG in a serum-starved medium for 18-20 hr, while our iPSCs were treated with SAG for 24 hr in complete NutriStem® hPSC XF complete Medium because iPSCs tend to die under serum-deprived conditions. These observations support the notion that serum-deprived conditions promote SHH signaling cascade and that SHH pathway is strictly regulated by the timing and concentration of SAG exposure.

Taking into consideration the fact that JS is a neurological disorder and associated with dysregulation of SHH signaling pathway (Abdelhamed et al., 2013; Aguilar et al., 2012), we also evaluated the effect of SAG stimulation on the expression levels of *Gli1, Gli2, Patch1,* and *Smo* in JS- and BJ-derived NSCs and neurons. Upregulation of *Gli1* and *Ptch1* was observed in SAG-stimulated NSCs of the control BJ, while JS-derived NSCs showed no induction of these molecules. Interestingly, in SAG-stimulated neurons, *Gli1* showed a significant high expression in the control which was ~22-folds and ~11-folds higher than in JS2 and JS5 respectively. Unexpectedly, *Gli2* and *Ptch1* were significantly downregulated in JS5-derived neurons following their treatment with SAG. It is noteworthy that after SAG stimulation the expression of *Gli1* in BJ neurons was extremely higher (~10-folds) than in BJ NSCs. This was also noted to a lesser extent in JS-derived neurons and their corresponding NSCs. These results are supported by several previous findings in *in vitro* and *in vivo* models which showed high expression level of *Gli1* in NSCs in the subventricular zone (SVZ) of adult mouse brain (Ihrie et al., 2011) and primary culture of the cortical/hippocampal cells (Bragina et al., 2010). Collectively, we have assessed the expression of SHH signal-related genes in fibroblasts, iPSCs, NSCs, and neurons derived from two JS patients with heterozygous and homozygous mutations in *CC2D2A* and *C5orf42* respectively, and a healthy control BJ. Our results showed

significant differences in the expression levels of the signaling molecules in JS-derived cells as compared to the control and non-stimulated cells.

CONCLUSION & FUTURE PRESPECTIVES

6. CONCLUSIONS AND FUTURE PERSPECTIVES

The primary objective of this PhD thesis was to develop iPSC-based models of JS by reprogramming fibroblasts obtained from skin biopsies of five JS patients using a non-integrating reprogramming method. We have successfully generated and established JS-derived iPSC lines which were well-characterized for stemness and pluripotent features. Our second objective was to establish neuronal models of JS by differentiating the generated JS-derived iPSCs into NSCs and subsequently into neurons. We selected JS2-, JS5-, and BJ-derived iPSC lines and established their corresponding neuronal models. The intermediate JS-derived NSC lines were characterized and cryopreserved to be utilized -instead of iPSCs- in the future as a readily available source of patient-specific cells that can be differentiated into specific neural lineage cells. We generated heterogenous neural populations from each NSC-line with dopaminergic neurons as a predominant population in all the cell cultures. These patient-specific neural cells serve as an indispensable *in vitro* JS models that will enable us to uncover the molecular and cellular mechanisms underlying the pathogenesis of JS and to develop therapeutic interventions for treatment of JS.

The third objective of our study was to evaluate the effect of the genetic defects in JS-derived cells on the number and length of primary cilia in JS-derived fibroblasts, iPSCs, and NSCs. We confirmed the presence of primary cilia in all the cell types studied. As expected, we found a significantly decreased number of ciliated cells in all JS-derived cell cultures as compared to the healthy control and that could be attributed to defects in the ciliary genes *CC2D2A* and *C5orf42* in patient-derived cells. Strikingly, despite the variation in the number of ciliated cells between the patients and control, no notable differences were found in the ciliary length between them. We suggest that variation in ciliary length cannot be utilized as a biomarker for JS or at least for *C5orf42*- and *CC2D2A*-related JS.

Finally, the fourth objective of this study was to assess the expression patterns of the key molecules in SHH signaling pathway namely: *Gli1, Gli2, Smo,* and *Ptch1* in JS-derived fibroblasts, iPSCs, NSCs, and neurons. Our findings revealed alteration in the expression levels of these molecules in JS-derived cells as compared to the control and non-stimulated cells, especially for *Gli1* that was markedly reduced in all the cell types analyzed, confirming the correlation between defects in the ciliary genes and dysregulation of SHH signaling pathway found in animal model studies.

Future investigations are necessary for deciphering the role of primary cilia and JS-related genes in disease mechanisms and evaluating distinct therapeutic approaches. Our recommendations for further studies include, but not limited to, differentiation of JS-derived NSCs into Purkinje cells to assess the

functional defects in this type of neurons which are predominant in the cerebellum, development of cerebellar organoids from JS-derived NSCs for better understanding of development and progression of JS, development of JS-derived glia cells, the non-neuronal cells in the CNS and PNS that provide support and protection for neurons, due to the crucial role of neuronal-glial interactions in the CNS. Moreover, utilizing CRISPR/Cas9 genome-editing system to correct the genetic mutations in patient-specific iPSCs as an approach for development of gene therapy and an in-depth study of the role of primary cilia and SHH signaling pathway in the pathogenesis of JS could be of great importance for development of effective cellular and chemical therapeutics for treatment of JS.

BIBLIOGRAPHY

7. BIBLIOGRAPHY

Abdelhamed, Z. A., Wheway, G., Szymanska, K., Natarajan, S., Toomes, C., Inglehearn, C., & Johnson, C. A. (2013). Variable expressivity of ciliopathy neurological phenotypes that encompass Meckel–Gruber syndrome and Joubert syndrome is caused by complex de-regulated ciliogenesis, Shh and Wnt signalling defects. *Human molecular genetics*, *22*(7), 1358-1372.

Adams, M., Simms, R. J., Abdelhamed, Z., Dawe, H. R., Szymanska, K., Logan, C. V., ... & Blair, E. (2012). A meckelin–filamin A interaction mediates ciliogenesis. *Human molecular genetics*, *21*(6), 1272-1286.

Aguilar, A., Meunier, A., Strehl, L., Martinovic, J., Bonniere, M., Attie-Bitach, T., ... & Spassky, N. (2012). Analysis of human samples reveals impaired SHH-dependent cerebellar development in Joubert syndrome/Meckel syndrome. Proceedings of the National Academy of Sciences, 109(42), 16951-16956.

Akizu, N., Silhavy, J. L., Rosti, R. O., Scott, E., Fenstermaker, A. G., Schroth, J., ... & Kara, M. (2014). Mutations in CSPP1 lead to classical Joubert syndrome. *The American Journal of Human Genetics*, *94*(1), 80-86.

Aldahmesh, M. A., Li, Y., Alhashem, A., Anazi, S., Alkuraya, H., Hashem, M., ... & Al Hazzaa, S. A. (2014). IFT27, encoding a small GTPase component of IFT particles, is mutated in a consanguineous family with Bardet–Biedl syndrome. *Human molecular genetics*, *23*(12), 3307-3315.

Ali, E., Ferraro, R. M., Lanzi, G., Masneri, S., Piovani, G., Mazzoldi, E. L., ... & Giliani, S. C. (2020). Generation of induced pluripotent stem cell (iPSC) lines from a Joubert syndrome patient with compound heterozygous mutations in C5orf42 gene. Stem Cell Research, 49, 102007.

Alkanderi, S., Molinari, E., Shaheen, R., Elmaghloob, Y., Stephen, L. A., Sammut, V., ... & Rice, S. J. (2018). ARL3 mutations cause Joubert syndrome by disrupting ciliary protein composition. *The American Journal of Human Genetics*, *103*(4), 612-620.

Altieri, F., D'Anzi, A., Martello, F., Tardivo, S., Spasari, I., Ferrari, D., ... & Rosati, J. (2019). Production and characterization of human induced pluripotent stem cells (iPSC) CSSi007-A (4383) from Joubert Syndrome. *Stem cell research*, 38, 101480.

Alvarez Retuerto, A. I., Cantor, R. M., Gleeson, J. G., Ustaszewska, A., Schackwitz, W. S., Pennacchio, L. A., & Geschwind, D. H. (2008). Association of common variants in the Joubert syndrome gene (AHI1) with autism. *Human molecular genetics*, 17(24), 3887-3896.

Amin, N. D., & **Paşca**, S. P. (2018). Building models of brain disorders with three-dimensional organoids. *Neuron*, *100*(2), 389-405.

Anand, P., Parrett, A., Martin, J., Zeman, S., Foley, P., Swash, M., ... & Sinicropi, D. V. (1995). Regional changes of ciliary neurotrophic factor and nerve growth factor levels in post-mortem spinal cord and cerebral cortex from patients with motor disease. *Nature medicine*, 1(2), 168-172.

Andrews, P. W. (1984). Retinoic acid induces neuronal differentiation of a cloned human embryonal carcinoma cell line in vitro. *Developmental biology*, *103*(2), 285-293.

Archer, F. L., & **Wheatley**, D. N. (1971). Cilia in cell-cultured fibroblasts. II. Incidence in mitotic and post-mitotic BHK 21-C13 fibroblasts. *Journal of anatomy*, 109(Pt 2), 277.

Arellano, J. I., Guadiana, S. M., Breunig, J. J., Rakic, P., & Sarkisian, M. R. (2012). Development and distribution of neuronal cilia in mouse neocortex. *Journal of Comparative Neurology*, 520(4), 848-873.

Asadollahi, R., Strauss, J. E., Zenker, M., Beuing, O., Edvardson, S., Elpeleg, O., ... & Rauch, A. (2018). Clinical and experimental evidence suggest a link between KIF7 and C5orf42-related ciliopathies through Sonic Hedgehog signaling. *European journal of human genetics*, 26(2), 197-209.

Autologous transplantation of induced pluripotent stem cell-derived retinal pigment epithelium for geographic atrophy associated with age-related macular degeneration. (2020, April 9). *Clinical Trials.gov*. Available from: https://clinicaltrials.gov/ct2/show/NCT04339764?term=AMD&recrs=af&cond=Macular+Degeneration&cntry=US&phase=01&draw=2&rank=1.

Avasthi, P., & **Marshall**, W. F. (2013). Ciliary regulation: disassembly takes the spotlight. *Current Biology*, *23*(22), R1001-R1003.

Baala, L., Romano, S., Khaddour, R., Saunier, S., Smith, U. M., Audollent, S., ... & Munnich, A. (2007). The Meckel-Gruber syndrome gene, MKS3, is mutated in Joubert syndrome. *The American Journal of Human Genetics*, *80*(1), 186-194.

Bachmann-Gagescu, R., Dempsey, J. C., Bulgheroni, S., Chen, M. L., D'Arrigo, S., Glass, I. A., ... & Knutzen, D. (2020). Healthcare recommendations for Joubert syndrome. *American Journal of Medical Genetics Part A*, *182*(1), 229-249.

Bachmann-Gagescu, R., Dempsey, J. C., Phelps, I. G., O'Roak, B. J., Knutzen, D. M., Rue, T. C., ... & Boyle, E. A. (2015). Joubert syndrome: a model for untangling recessive disorders with extreme genetic heterogeneity. *Journal of medical genetics*, *52*(8), 514-522.

Bachmann-Gagescu, R., Dona, M., Hetterschijt, L., Tonnaer, E., Peters, T., de Vrieze, E., ... & Keunen, J. E. (2015). The ciliopathy protein CC2D2A associates with NINL and functions in RAB8-MICAL3-regulated vesicle trafficking. *PLoS genetics*, *11*(10).

Bagley, J. A., Reumann, D., Bian, S., Lévi-Strauss, J., & Knoblich, J. A. (2017). Fused cerebral organoids model interactions between brain regions. *Nature methods*, *14*(7), 743.

Baker, B. M., & **Chen**, C. S. (2012). Deconstructing the third dimension–how 3D culture microenvironments alter cellular cues. *Journal of cell science*, *125*(13), 3015-3024.

Ban, K., Wile, B., Kim, S., Park, H. J., Byun, J., Cho, K. W., ... & Bao, G. (2013). Purification of cardiomyocytes from differentiating pluripotent stem cells using molecular beacons that target cardiomyocyte-specific mRNA. *Circulation*, *128*(17), 1897-1909.

Bangs, F., & **Anderson**, K. V. (2017). Primary cilia and mammalian hedgehog signaling. *Cold Spring Harbor perspectives in biology*, *9*(5), a028175.

Banito, A., Rashid, S. T., Acosta, J. C., Li, S., Pereira, C. F., Geti, I., ... & Vallier, L. (2009). Senescence impairs successful reprogramming to pluripotent stem cells. Genes & development, 23(18), 2134-2139.

Bardy, C., Van Den Hurk, M., Eames, T., Marchand, C., Hernandez, R. V., Kellogg, M., ... & Bang, A. G. (2015). Neuronal medium that supports basic synaptic functions and activity of human neurons in vitro. *Proceedings of the National Academy of Sciences*, *112*(20), E2725-E2734.

Barker, A. R., Renzaglia, K. S., Fry, K., & Dawe, H. R. (2014). Bioinformatic analysis of ciliary transition zone proteins reveals insights into the evolution of ciliopathy networks. *BMC genomics*, *15*(1), 1-9.

Behal, R. H., Miller, M. S., Qin, H., Lucker, B. F., Jones, A., & Cole, D. G. (2012). Subunit interactions and organization of the Chlamydomonas reinhardtii intraflagellar transport complex A proteins. *Journal of Biological Chemistry*, *287*(15), 11689-11703.

Bernabé-Rubio, M., & **Alonso**, M. A. (2017). Routes and machinery of primary cilium biogenesis. *Cellular and Molecular Life Sciences*, *74*(22), 4077-4095.

Bershteyn, M., Nowakowski, T. J., Pollen, A. A., Di Lullo, E., Nene, A., Wynshaw-Boris, A., & Kriegstein, A. R. (2017). Human iPSC-derived cerebral organoids model cellular features of lissencephaly and reveal prolonged mitosis of outer radial glia. *Cell stem cell*, *20*(4), 435-449.

Bielas, S. L., Silhavy, J. L., Brancati, F., Kisseleva, M. V., Al-Gazali, L., Sztriha, L., ... & Kayserili, H. (2009). Mutations in INPP5E, encoding inositol polyphosphate-5-phosphatase E, link phosphatidyl inositol signaling to the ciliopathies. *Nature genetics*, *41*(9), 1032.

Bonnard, C., Shboul, M., Tonekaboni, S. H., Ng, A. Y. J., Tohari, S., Ghosh, K., ... & Stichelbout, M. (2018). Novel mutations in the ciliopathy-associated gene CPLANE1 (C5orf42) cause OFD syndrome type VI rather than Joubert syndrome. *European journal of medical genetics*, *61*(10), 585-595.

Bonnier, F., Keating, M. E., Wrobel, T. P., Majzner, K., Baranska, M., Garcia-Munoz, A., ... & Byrne, H. J. (2015). Cell viability assessment using the Alamar blue assay: a comparison of 2D and 3D cell culture models. *Toxicology in vitro*, *29*(1), 124-131.

Braddock, S. R., Henley, K. M., & Maria, B. L. (2007). The face of Joubert syndrome: a study of dysmorphology and anthropometry. *American Journal of Medical Genetics Part A*, *143*(24), 3235-3242.

Bragina, O., Sergejeva, S., Serg, M., Žarkovsky, T., Maloverjan, A., Kogerman, P., & Žarkovsky, A. (2010). Smoothened agonist augments proliferation and survival of neural cells. Neuroscience letters, 482(2), 81-85.

Brailov, I., Bancila, M., Brisorgueil, M. J., Miquel, M. C., Hamon, M., & Vergé, D. (2000). Localization of 5-HT6 receptors at the plasma membrane of neuronal cilia in the rat brain. *Brain research*, *872*(1-2), 271-275.

Brancati, F., Barrano, G., Silhavy, J. L., Marsh, S. E., Travaglini, L., Bielas, S. L., ... & Bertini, E. (2007). CEP290 mutations are frequently identified in the oculo-renal form of Joubert syndrome–related disorders. *The American Journal of Human Genetics*, *81*(1), 104-113.

Brancati, F., Camerota, L., Colao, E., Vega-Warner, V., Zhao, X., Zhang, R., ... & Novelli, G. (2018). Biallelic variants in the ciliary gene TMEM67 cause RHYNS syndrome. *European Journal of Human Genetics*, *26*(9), 1266-1271.

Brancati, F., Dallapiccola, B., & Valente, E. M. (2010). Joubert Syndrome and related disorders. *Orphanet journal of rare diseases*, *5*(1), 20.

Brancati, F., Iannicelli, M., Travaglini, L., Mazzotta, A., Bertini, E., Boltshauser, E., ... & Gentile, M. (2009). MKS3/TMEM67 mutations are a major cause of COACH Syndrome, a Joubert Syndrome related disorder with liver involvement. *Human mutation*, *30*(2), E432-E442.

Brancati, F., Travaglini, L., Zablocka, D., Boltshauser, E., Accorsi, P., Montagna, G., ... & Rigoli, L. (2008). RPGRIP1L mutations are mainly associated with the cerebello-renal phenotype of Joubert syndrome-related disorders. *Clinical genetics*, *74*(2), 164-170.

Branco, M. A., Dias, T. P., Cotovio, J. P., Rodrigues, C. A., Fernandes, T. G., Cabral, J. M., & Diogo, M. M. (2020). 3D Microwell Platform for Cardiomyocyte Differentiation of Human Pluripotent Stem Cells.

Brooks, B. P., Zein, W. M., Thompson, A. H., Mokhtarzadeh, M., Doherty, D. A., Parisi, M., ... & Mullikin, J. C. (2018). Joubert syndrome: Ophthalmological findings in correlation with genotype and hepatorenal disease in 99 patients prospectively evaluated at a single center. *Ophthalmology*, *125*(12), 1937-1952.

Burrows, C. K., Banovich, N. E., Pavlovic, B. J., Patterson, K., Gallego Romero, I., Pritchard, J. K., & Gilad, Y. (2016). Genetic variation, not cell type of origin, underlies the majority of identifiable regulatory differences in iPSCs. *PLoS genetics*, *12*(1), e1005793.

Byers, B., Cord, B., Nguyen, H. N., Schüle, B., Fenno, L., Lee, P. C., ... & Palmer, T. D. (2011). SNCA triplication Parkinson's patient's iPSC-derived DA neurons accumulate α-synuclein and are susceptible to oxidative stress. *PloS one*, *6*(11), e26159.

Camp, J. G., Badsha, F., Florio, M., Kanton, S., Gerber, T., Wilsch-Bräuninger, M., ... & Knoblich, J. A. (2015). Human cerebral organoids recapitulate gene expression programs of fetal neocortex development. *Proceedings of the National Academy of Sciences*, *112*(51), 15672-15677.

Cano, D. A., Murcia, N. S., Pazour, G. J., & Hebrok, M. (2004). Orpk mouse model of polycystic kidney disease reveals essential role of primary cilia in pancreatic tissue organization. *Development*, *131*(14), 3457-3467.

Cantagrel, V., Silhavy, J. L., Bielas, S. L., Swistun, D., Marsh, S. E., Bertrand, J. Y., ... & Traver, D. (2008). Mutations in the cilia gene ARL13B lead to the classical form of Joubert syndrome. *The American Journal of Human Genetics*, *83*(2), 170-179.

Caspary, T., Larkins, C. E., & Anderson, K. V. (2007). The graded response to Sonic Hedgehog depends on cilia architecture. *Developmental cell*, *12*(5), 767-778.

Castori, M., Valente, E. M., Donati, M. A., Salvi, S., Fazzi, E., Procopio, E., ... & Bertini, E. (2005). NPHP1 gene deletion is a rare cause of Joubert syndrome related disorders. *Journal of medical genetics*, *42*(2), e9-e9.
Cavallo, R. A., Cox, R. T., Moline, M. M., Roose, J., Polevoy, G. A., Clevers, H., ... & Bejsovec, A. (1998). Drosophila Tcf and Groucho interact to repress Wingless signalling activity. *Nature*, *395*(6702), 604-608.

Cenci, M. A., Whishaw, I. Q., & Schallert, T. (2002). Animal models of neurological deficits: how relevant is the rat?. Nature Reviews Neuroscience, 3(7), 574-579.

Chaudhari, U., Nemade, H., Sureshkumar, P., Vinken, M., Ates, G., Rogiers, V., ... & Sachinidis, A. (2018). Functional cardiotoxicity assessment of cosmetic compounds using human-induced pluripotent stem cell-derived cardiomyocytes. *Archives of toxicology*, *92*(1), 371-381.

Chen, S. D., Yang, J. L., Hwang, W. C., & Yang, D. I. (2018). Emerging Roles of Sonic Hedgehog in Adult Neurological Diseases: Neurogenesis and Beyond. *International journal of molecular sciences*, *19*(8), 2423.

Chen, Y., Li, S., Tong, C., Zhao, Y., Wang, B., Liu, Y., ... & Jiang, J. (2010). G protein-coupled receptor kinase 2 promotes high-level Hedgehog signaling by regulating the active state of Smo through kinase-dependent and kinase-independent mechanisms in Drosophila. *Genes & development*, *24*(18), 2054-2067.

Chesselet, M. F., & Carmichael, S. T. (2012). Animal models of neurological disorders. *Neurotherapeutics*, 9, 241–244.

Chih, B., Liu, P., Chinn, Y., Chalouni, C., Komuves, L. G., Hass, P. E., ... & Peterson, A. S. (2012). A ciliopathy complex at the transition zone protects the cilia as a privileged membrane domain. *Nature cell biology*, *14*(1), 61-72.

Choi, S. H., Kim, Y. H., Hebisch, M., Sliwinski, C., Lee, S., D'Avanzo, C., ... & Klee, J. B. (2014). A three-dimensional human neural cell culture model of Alzheimer's disease. *Nature*, *515*(7526), 274-278.

Christian, M., Cermak, T., Doyle, E. L., Schmidt, C., Zhang, F., Hummel, A., ... & Voytas, D. F. (2010). Targeting DNA double-strand breaks with TAL effector nucleases. *Genetics*, *186*(2), 757-761.

Chu, Y., Bartus, R. T., Manfredsson, F. P., Olanow, C. W., & Kordower, J. H. (2020). Long-term post-mortem studies following neurturin gene therapy in patients with advanced Parkinson's disease. *Brain*, *143*(3), 960-975.

Clevers, H. (2006). Wnt/β-catenin signaling in development and disease. *Cell*, *127*(3), 469-480.

Coene, K. L., Roepman, R., Doherty, D., Afroze, B., Kroes, H. Y., Letteboer, S. J., ... & Azhimi, M. (2009). OFD1 is mutated in X-linked Joubert syndrome and interacts with LCA5-encoded lebercilin. *The American Journal of Human Genetics*, *85*(4), 465-481.

Cole, D. G., & **Snell**, W. J. (2009). SnapShot: intraflagellar transport. *Cell*, *137*(4), 784-784.

Cooke, M. J., Stojkovic, M., & Przyborski, S. A. (2006). Growth of teratomas derived from human pluripotent stem cells is influenced by the graft site. *Stem Cells and Development*, *15*(2), 254-259.

Cooper, O., Seo, H., Andrabi, S., Guardia-Laguarta, C., Graziotto, J., Sundberg, M., ... & Hargus, G. (2012). Pharmacological rescue of mitochondrial deficits in iPSC-derived neural cells from patients with familial Parkinson's disease. *Science translational medicine*, *4*(141), 141ra90-141ra90.

Corbit, K. C., Aanstad, P., Singla, V., Norman, A. R., Stainier, D. Y., & Reiter, J. F. (2005). Vertebrate Smoothened functions at the primary cilium. *Nature*, *437*(7061), 1018-1021.

Correia, C., Koshkin, A., Duarte, P., Hu, D., Carido, M., Sebastião, M. J., ... & Alves, P. M. (2018). 3D aggregate culture improves metabolic maturation of human pluripotent stem cell derived cardiomyocytes. *Biotechnology and bioengineering*, *115*(3), 630-644.

Cyranoski, D. (2018). 'Reprogrammed'stem cells approved to mend human hearts for the first time. *Nature*, *557*(7706), 619-619.

D'Aiuto, L., Zhi, Y., Kumar Das, D., Wilcox, M. R., Johnson, J. W., McClain, L., ... & Viggiano, L. (2014). Large-scale generation of human iPSC-derived neural stem cells/early neural progenitor cells and their neuronal differentiation. *Organogenesis*, *10*(4), 365-377.

Dahl, H. A. (1963). Fine structure of cilia in rat cerebral cortex. *Zeitschrift für Zellforschung und mikroskopische Anatomie*, *60*(3), 369-386.

Dang, J., Tiwari, S. K., Lichinchi, G., Qin, Y., Patil, V. S., Eroshkin, A. M., & Rana, T. M. (2016). Zika virus depletes neural progenitors in human cerebral organoids through activation of the innate immune receptor TLR3. *Cell stem cell*, *19*(2), 258-265.

Davis, R. L., Weintraub, H., & Lassar, A. B. (1987). Expression of a single transfected cDNA converts fibroblasts to myoblasts. *Cell*, *51*(6), 987-1000.

de Leeuw, V. C., van Oostrom, C. T., Westerink, R. H., Piersma, A. H., Heusinkveld, H. J., & Hessel, E. V. (2020). An efficient neuron-astrocyte differentiation protocol from human embryonic stem cell-derived neural progenitors to assess chemical-induced developmental neurotoxicity. *Reproductive Toxicology*.

De Mori, R., Romani, M., D'Arrigo, S., Zaki, M. S., Lorefice, E., Tardivo, S., ... & Micalizzi, A. (2017). Hypomorphic recessive variants in SUFU impair the Sonic Hedgehog pathway and cause Joubert syndrome with cranio-facial and skeletal defects. *The American Journal of Human Genetics*, *101*(4), 552-563.

Deane, J. A., Cole, D. G., Seeley, E. S., Diener, D. R., & Rosenbaum, J. L. (2001). Localization of intraflagellar transport protein IFT52 identifies basal body transitional fibers as the docking site for IFT particles. *Current Biology*, *11*(20), 1586-1590.

Del Cerro, M. P., Snider, R. S., & Lou Oster, M. (1969). The Purkinje cell cilium. *The Anatomical Record*, *165*(2), 127-139.

Dempsey, J. C., Phelps, I. G., Bachmann-Gagescu, R., Glass, I. A., Tully, H. M., & Doherty, D. (2017). Mortality in Joubert syndrome. *American Journal of Medical Genetics Part A*, *173*(5), 1237-1242.

Deng, J., Shoemaker, R., Xie, B., Gore, A., LeProust, E. M., Antosiewicz-Bourget, J., ... & Zhang, K. (2009). Targeted bisulfite sequencing reveals changes in DNA methylation associated with nuclear reprogramming. *Nature biotechnology*, *27*(4), 353-360.

Deuse, T., Hu, X., Agbor-Enoh, S., Koch, M., Spitzer, M. H., Gravina, A., ... & Yang, Y. (2019). De novo mutations in mitochondrial DNA of iPSCs produce immunogenic neoepitopes in mice and humans. *Nature biotechnology*, *37*(10), 1137-1144.

di Domenico, A., Carola, G., Calatayud, C., Pons-Espinal, M., Muñoz, J. P., Richaud-Patin, Y., ... & Soriano, J. (2019). Patient-specific iPSC-derived astrocytes contribute to non-cell-autonomous neurodegeneration in Parkinson's disease. *Stem Cell Reports*, *12*(2), 213-229.

Dimos, J. T., Rodolfa, K. T., Niakan, K. K., Weisenthal, L. M., Mitsumoto, H., Chung, W., ... & Wichterle, H. (2008). Induced pluripotent stem cells generated from patients with ALS can be differentiated into motor neurons. *science*, *321*(5893), 1218-1221.

Ding, Q., Regan, S. N., Xia, Y., Oostrom, L. A., Cowan, C. A., & Musunuru, K. (2013). Enhanced efficiency of human pluripotent stem cell genome editing through replacing TALENs with CRISPRs. *Cell stem cell*, *12*(4), 393.

Dirik, M. A., Yiş, U., & Dirik, E. (2013). Molar tooth sign is not pathognomonic for Joubert syndrome. *Pediatric neurology*, *49*(6), 515-516.

Dixon-Salazar, T., Silhavy, J. L., Marsh, S. E., Louie, C. M., Scott, L. C., Gururaj, A., ... & Gleeson, J. G. (2004). Mutations in the AHI1 gene, encoding jouberin, cause Joubert syndrome with cortical polymicrogyria. *The American Journal of Human Genetics*, *75*(6), 979-987.

Djuric, U., Cheung, A. Y., Zhang, W., Mok, R. S., Lai, W., Piekna, A., ... & Salter, M. W. (2015). MECP2e1 isoform mutation affects the form and function of neurons derived from Rett syndrome patient iPS cells. Neurobiology of disease, 76, 37-45.

Doherty, D. (2009, September). Joubert syndrome: insights into brain development, cilium biology, and complex disease. In *Seminars in pediatric neurology* (Vol. 16, No. 3, pp. 143-154). WB Saunders.

Doherty, D., Parisi, M. A., Finn, L. S., Gunay-Aygun, M., Al-Mateen, M., Bates, D., ... & Gahl, W. A. (2010). Mutations in 3 genes (MKS3, CC2D2A and RPGRIP1L) cause COACH syndrome (Joubert syndrome with congenital hepatic fibrosis). *Journal of medical genetics*, *47*(1), 8-21.

Doi, A., Park, I. H., Wen, B., Murakami, P., Aryee, M. J., Irizarry, R., ... & Feinberg, A. P. (2009). Differential methylation of tissue-and cancer-specific CpG island shores distinguishes human induced pluripotent stem cells, embryonic stem cells and fibroblasts. *Nature genetics*, *41*(12), 1350-1353.

Dong, X., Xu, S. B., Chen, X., Tao, M., Tang, X. Y., Fang, K. H., ... & Liu, Y. (2020). Human cerebral organoids establish subcortical projections in the mouse brain after transplantation. *Molecular Psychiatry*, 1-13.

Doss, M. X., & **Sachinidis**, A. (2019). Current challenges of iPSC-based disease modeling and therapeutic implications. *Cells*, *8*(5), 403.

Duval, K., Grover, H., Han, L. H., Mou, Y., Pegoraro, A. F., Fredberg, J., & Chen, Z. (2017). Modeling physiological events in 2D vs. 3D cell culture. *Physiology*, *32*(4), 266-277.

Edvardson, S., Shaag, A., Zenvirt, S., Erlich, Y., Hannon, G. J., Shanske, A. L., ... & Elpeleg, O. (2010). Joubert syndrome 2 (JBTS2) in Ashkenazi Jews is associated with a *TMEM216* mutation. *The American Journal of Human Genetics*, *86*(1), 93-97.

Ebert, A. D., Yu, J., Rose, F. F., Mattis, V. B., Lorson, C. L., Thomson, J. A., & Svendsen, C. N. (2009). Induced pluripotent stem cells from a spinal muscular atrophy patient. *Nature*, *457*(7227), 277-280.

Eggenschwiler, J. T., Bulgakov, O. V., Qin, J., Li, T., & Anderson, K. V. (2006). Mouse Rab23 regulates hedgehog signaling from smoothened to Gli proteins. *Developmental biology*, *290*(1), 1-12.

Endicott, S. J., & **Brueckner**, M. (2018). NUP98 sets the size-exclusion diffusion limit through the ciliary base. *Current Biology*, *28*(10), 1643-1650.

Engel, B. D., Ishikawa, H., Wemmer, K. A., Geimer, S., Wakabayashi, K. I., Hirono, M., ... & Marshall, W. F. (2012). The role of retrograde intraflagellar transport in flagellar assembly, maintenance, and function. *Journal of Cell Biology*, *199*(1), 151-167.

Enokizono, M., Aida, N., Niwa, T., Osaka, H., Naruto, T., Kurosawa, K., ... & Matsumoto, N. (2017). Neuroimaging findings in Joubert syndrome with C5orf42 gene mutations: A milder form of molar tooth sign and vermian hypoplasia. *Journal of the neurological sciences*, *376*, 7-12.

Eschenhagen, T., & **Weinberger**, F. (2019). Heart Repair With Myocytes: Why Not Take Your Own?. *Circulation research*, *124*(6), 843-845.

Evans, M. J., & **Kaufman**, M. H. (1981). Establishment in culture of pluripotential cells from mouse embryos. *Nature*, *292*(5819), 154-156.

Fate Therapeutics announces FDA clearance of IND application for first-ever iPSC-derived CAR T-Cell therapy. (2020, July 9). *Fate Therapeutics*. Available from: https://ir.fatetherapeutics.com/news-releases/news-release-details/fate-therapeutics-announces-fda-clearance-ind-application-first.

Fennell, E. B., Gitten, J. C., Dede, D. E., & Maria, B. L. (1999). Cognition, behavior, and development in Joubert syndrome. *Journal of child neurology*, *14*(9), 592-596.

Ferland, R. J., Eyaid, W., Collura, R. V., Tully, L. D., Hill, R. S., Al-Nouri, D., ... & Shugart, Y. Y. (2004). Abnormal cerebellar development and axonal decussation due to mutations in AHI1 in Joubert syndrome. *Nature genetics*, *36*(9), 1008-1013.

Feyen, D. A., McKeithan, W. L., Bruyneel, A. A., Spiering, S., Hörmann, L., Ulmer, B., ... & Liao, Z. (2020). Metabolic Maturation Media Improve Physiological Function of Human iPSC-Derived Cardiomyocytes. *Cell reports*, *32*(3), 107925.

Field, M., Scheffer, I. E., Gill, D., Wilson, M., Christie, L., Shaw, M., ... & Friend, K. (**2012**). Expanding the molecular basis and phenotypic spectrum of X-linked Joubert syndrome associated with OFD1 mutations. *European Journal of Human Genetics*, *20*(7), 806-809.

Fleming, L. R., Doherty, D. A., Parisi, M. A., Glass, I. A., Bryant, J., Fischer, R., ... & Mullikin, J. C. (**2017**). Prospective evaluation of kidney disease in Joubert syndrome. *Clinical journal of the American Society of Nephrology*, *12*(12), 1962-1973.

Flores-Hernández, E., Velázquez, D. M., Castañeda-Patlán, M. C., Fuentes-García, G., Fonseca-Camarillo, G., Yamamoto-Furusho, J. K., ... & Robles-Flores, M. (2020). Canonical and non-canonical Wnt signaling are simultaneously activated by Wnts in colon cancer cells. *Cellular Signalling*, 109636.

Forsythe, E., & **Beales**, P. L. (**2015**). Bardet-Biedl Syndrome. *GeneReviews®*, *NCBI*. Available from: https://www.ncbi.nlm.nih.gov/books/NBK1363/?report=reader.

Fusaki, N., Ban, H., Nishiyama, A., Saeki, K., & Hasegawa, M. (**2009**). Efficient induction of transgene-free human pluripotent stem cells using a vector based on Sendai virus, an RNA virus that does not integrate into the host genome. *Proceedings of the Japan Academy, Series B*, *85*(8), 348-362.

Garcia-Gonzalo, F. R., Corbit, K. C., Sirerol-Piquer, M. S., Ramaswami, G., Otto, E. A., Noriega, T. R., ... & García-Verdugo, J. M. (2011). A transition zone complex regulates mammalian ciliogenesis and ciliary membrane composition. *Nature genetics*, *43*(8), 776-784.

Goetz, S. C., & **Anderson**, K. V. (**2010**). The primary cilium: a signalling centre during vertebrate development. *Nature Reviews Genetics*, *11*(5), 331-344.

Goetz, S. C., Ocbina, P. J., & Anderson, K. V. (**2009**). The primary cilium as a Hedgehog signal transduction machine. In *Methods in cell biology* (Vol. 94, pp. 199-222). Academic Press.

Gogendeau, D., Lemullois, M., Le Borgne, P., Castelli, M., Aubusson-Fleury, A., Arnaiz, O., ... & Tassin, A. M. (2020). MKS-NPHP module proteins control ciliary shedding at the transition zone. *PLoS biology*, *18*(3), e3000640.

Gonçalves, J., & **Pelletier**, L. (2017). The Ciliary Transition Zone: Finding the Pieces and Assembling the Gate. *Molecules and cells*, 40(4), 243–253.

Gore, A., Li, Z., Fung, H. L., Young, J. E., Agarwal, S., Antosiewicz-Bourget, J., ... & Zhang, K. (2011). Somatic coding mutations in human induced pluripotent stem cells. *Nature*, *471*(7336), 63-67.

Gorden, N. T., Arts, H. H., Parisi, M. A., Coene, K. L., Letteboer, S. J., van Beersum, S. E., ... & Alswaid, A. F. (2008). CC2D2A is mutated in Joubert syndrome and interacts with the ciliopathy-associated basal body protein CEP290. *The American Journal of Human Genetics*, *83*(5), 559-571.

Goversen, B., van der Heyden, M. A., van Veen, T. A., & de Boer, T. P. (2018). The immature electrophysiological phenotype of iPSC-CMs still hampers in vitro drug screening: Special focus on IK1. *Pharmacology & Therapeutics*, *183*, 127-136.

Grigor'eva, E. V., Malankhanova, T. B., Surumbayeva, A., Pavlova, S. V., Minina, J. M., Kizilova, E. A., ... & Malakhova, A. A. (2020). Generation of GABAergic striatal neurons by a novel iPSC differentiation protocol enabling scalability and cryopreservation of progenitor cells. *Cytotechnology*, *72*, 649-663.

Guenther, M. G., Frampton, G. M., Soldner, F., Hockemeyer, D., Mitalipova, M., Jaenisch, R., & Young, R. A. (2010). Chromatin structure and gene expression programs of human embryonic and induced pluripotent stem cells. *Cell stem cell*, *7*(2), 249-257.

Guha, P., Morgan, J. W., Mostoslavsky, G., Rodrigues, N. P., & Boyd, A. S. (2013). Lack of immune response to differentiated cells derived from syngeneic induced pluripotent stem cells. *Cell stem cell*, *12*(4), 407-412.

Guillotin, B., Souquet, A., Catros, S., Duocastella, M., Pippenger, B., Bellance, S., ... & Guillemot, F. (2010). Laser assisted bioprinting of engineered tissue with high cell density and microscale organization. *Biomaterials*, *31*(28), 7250-7256.

Gunay-Aygun, M., Parisi, M. A., Doherty, D., Tuchman, M., Tsilou, E., Kleiner, D. E., ... & Heller, T. (2009). MKS3-related ciliopathy with features of autosomal recessive polycystic kidney disease, nephronophthisis, and Joubert syndrome. *The Journal of pediatrics*, *155*(3), 386-392.

Gurdon, J. B. (1962). Adult frogs derived from the nuclei of single somatic cells. *Developmental biology*, *4*(2), 256-273.

Hackam, D. G., & **Redelmeier**, D. A. (2006). Translation of research evidence from animals to humans. *Jama*, *296*(14), 1727-1732.

Han, Y. L., Wang, S., Zhang, X., Li, Y., Huang, G., Qi, H., ... & Xu, F. (2014). Engineering physical microenvironment for stem cell based regenerative medicine. *Drug discovery today*, *19*(6), 763-773.

Händel, M., Schulz, S., Stanarius, A., Schreff, M., Erdtmann-Vourliotis, M., Schmidt, H., ... & Höllt, V. (1999). Selective targeting of somatostatin receptor 3 to neuronal cilia. *Neuroscience*, *89*(3), 909-926.

Haws, R., Brady, S., Davis, E., Fletty, K., Yuan, G., Gordon, G., ... & Yanovski, J. (2020). Effect of setmelanotide, a melanocortin-4 receptor agonist, on obesity in Bardet-Biedl syndrome. *Diabetes, Obesity and Metabolism*, *22*(11), 2133-2140.

Haycraft, C. J., Banizs, B., Aydin-Son, Y., Zhang, Q., Michaud, E. J., & Yoder, B. K. (2005). Gli2 and Gli3 localize to cilia and require the intraflagellar transport protein polaris for processing and function. *PLoS genetics*, *1*(4).

Hendriks, W. T., Warren, C. R., & Cowan, C. A. (2016). Genome editing in human pluripotent stem cells: approaches, pitfalls, and solutions. *Cell stem cell*, *18*(1), 53-65.

Heng, B. C., Richards, M., Shu, Y., & Gribbon, P. (2009). Induced pluripotent stem cells: a new tool for toxicology screening?. *Archives of toxicology*, *83*(7), 641-644.

Hildebrandt, F., Strahm, B., Nothwang, H. G., Gretz, N., Schnieders, B., Singh-Sawhney, I., ... & APN Study Group. (1997). Molecular genetic identification of families with juvenile nephronophthisis type 1: rate of progression to renal failure. *Kidney international*, *51*(1), 261-269.

Hilton, L. K., Gunawardane, K., Kim, J. W., Schwarz, M. C., & Quarmby, L. M. (2013). The kinases LF4 and CNK2 control ciliary length by feedback regulation of assembly and disassembly rates. *Current Biology*, *23*(22), 2208-2214.

Hockemeyer, D., Soldner, F., Beard, C., Gao, Q., Mitalipova, M., DeKelver, R. C., ... & Meng, X. (2009). Efficient targeting of expressed and silent genes in human ESCs and iPSCs using zinc-finger nucleases. *Nature biotechnology*, *27*(9), 851-857.

Hockemeyer, D., Wang, H., Kiani, S., Lai, C. S., Gao, Q., Cassady, J. P., ... & Zeitler, B. (2011). Genetic engineering of human pluripotent cells using TALE nucleases. *Nature biotechnology*, *29*(8), 731-734.

Hong, H., Takahashi, K., Ichisaka, T., Aoi, T., Kanagawa, O., Nakagawa, M., ... & Yamanaka, S. (2009). Suppression of induced pluripotent stem cell generation by the p53–p21 pathway. *Nature*, *460*(7259), 1132-1135.

Hou, P., Li, Y., Zhang, X., Liu, C., Guan, J., Li, H., ... & Deng, H. (2013). Pluripotent stem cells induced from mouse somatic cells by small-molecule compounds. *Science*, *341*(6146), 651-654.

Houdebine, L. M. (2007). Transgenic animal models in biomedical research. In *Target Discovery and Validation Reviews and Protocols* (pp. 163-202). Humana Press.

Hu, B. Y., Weick, J. P., Yu, J., Ma, L. X., Zhang, X. Q., Thomson, J. A., & Zhang, S. C. (2010). Neural differentiation of human induced pluripotent stem cells follows developmental principles but with variable potency. *Proceedings of the National Academy of Sciences*, *107*(9), 4335-4340.

Huang, L., Szymanska, K., Jensen, V. L., Janecke, A. R., Innes, A. M., Davis, E. E., ... & Greenberg, C. R. (2011). *TMEM237* is mutated in individuals with a Joubert syndrome related disorder and expands the role of the TMEM family at the ciliary transition zone. *The American Journal of Human Genetics*, *89*(6), 713-730.

Huang, P., & **Schier**, A. F. (2009). Dampened Hedgehog signaling but normal Wnt signaling in zebrafish without cilia. *Development*, *136*(18), 3089-3098.

Huangfu, D., Liu, A., Rakeman, A. S., Murcia, N. S., Niswander, L., & Anderson, K. V. (2003). Hedgehog signalling in the mouse requires intraflagellar transport proteins. *Nature*, *426*(6962), 83-87.

Huangfu, D., Maehr, R., Guo, W., Eijkelenboom, A., Snitow, M., Chen, A. E., & Melton, D. A. (2008). Induction of pluripotent stem cells by defined factors is greatly improved by small-molecule compounds. *Nature biotechnology*, *26*(7), 795-797.

Huangfu, D., & **Anderson**, K. V. (2005). Cilia and Hedgehog responsiveness in the mouse. *Proceedings of the National Academy of Sciences*, *102*(32), 11325-11330.

Huet, D., Blisnick, T., Perrot, S., & Bastin, P. (2014). The GTPase IFT27 is involved in both anterograde and retrograde intraflagellar transport. *Elife*, *3*, e02419.

Hussein, S. M., Batada, N. N., Vuoristo, S., Ching, R. W., Autio, R., Närvä, E., ... & Otonkoski, T. (2011). Copy number variation and selection during reprogramming to pluripotency. *Nature*, *471*(7336), 58-62.

Iannicelli, M., Brancati, F., Mougou-Zerelli, S., Mazzotta, A., Thomas, S., Elkhartoufi, N., ... & Boltshauser, E. (2010). Novel *TMEM67* mutations and genotype-phenotype correlates in meckelin-related ciliopathies. *Human mutation*, *31*(5), E1319-E1331.

Ihrie, R. A., Shah, J. K., Harwell, C. C., Levine, J. H., Guinto, C. D., Lezameta, M., ... & Alvarez-Buylla, A. (2011). Persistent sonic hedgehog signaling in adult brain determines neural stem cell positional identity. *Neuron*, 71(2), 250-262.

Ikeda, K., Nagata, S., Okitsu, T., & Takeuchi, S. (2017). Cell fiber-based three-dimensional culture system for highly efficient expansion of human induced pluripotent stem cells. *Scientific reports*, *7*(1), 1-10.
Israel, M. A., Yuan, S. H., Bardy, C., Reyna, S. M., Mu, Y., Herrera, C., ... & Carson, C. T. (2012). Probing sporadic and familial Alzheimer's disease using induced pluripotent stem cells. *Nature*, *482*(7384), 216-220.

Jaenisch, R., & **Young**, R. (2008). Stem cells, the molecular circuitry of pluripotency and nuclear reprogramming. *Cell*, *132*(4), 567-582.

Jia, F., Wilson, K. D., Sun, N., Gupta, D. M., Huang, M., Li, Z., ... & Wu, J. C. (2010). A nonviral minicircle vector for deriving human iPS cells. *Nature methods*, *7*(3), 197-199.

Jiang, J., & **Hui**, C. C. (2008). Hedgehog signaling in development and cancer. *Developmental cell*, *15*(6), 801-812.

Jin, H., & **Nachury**, M. V. (2009). The bbsome. *Current Biology*, *19*(12), R472-R473.

Jinek, M., Chylinski, K., Fonfara, I., Hauer, M., Doudna, J. A., & Charpentier, E. (2012). A programmable dual-RNA–guided DNA endonuclease in adaptive bacterial immunity. science, 337(6096), 816-821.

Joubert, M., Eisenring, J. J., & Andermann, F. (1968). Familial dysgenesis of the vermis: a syndrome of hyperventilation, abnormal eye movements and retardation. *Neurology*, 18(3), 302-303.

Juric-Sekhar, G., Adkins, J., Doherty, D., & Hevner, R. F. (2012). Joubert syndrome: brain and spinal cord malformations in genotyped cases and implications for neurodevelopmental functions of primary cilia. *Acta neuropathologica*, *123*(5), 695-709.

Karp, N., Grosse-Wortmann, L., & Bowdin, S. (2012). Severe aortic stenosis, bicuspid aortic valve and atrial septal defect in a child with Joubert Syndrome and Related Disorders (JSRD)–A case report and review of congenital heart defects reported in the human ciliopathies. *European journal of medical genetics*, *55*(11), 605-610.

Kasahara K., Miyoshi, K., Murakami, S., Miyazaki, I., & Asanuma, M. (2015). Visualization of astrocytic primary cilia in the mouse brain by immunofluorescent analysis using the cilia marker Arl13b. *Acta Med Okayama*, 68(6), 317–22.

Katoh, Y., & **Katoh**, M. (2006). Hedgehog signaling pathway and gastrointestinal stem cell signaling network. *International journal of molecular medicine*, *18*(6), 1019-1023.

Kim, C., Wong, J., Wen, J., Wang, S., Wang, C., Spiering, S., ... & Marine, J. E. (2013). Studying arrhythmogenic right ventricular dysplasia with patient-specific iPSCs. Nature, 494(7435), 105-110.

Kim, D., Kim, C. H., Moon, J. I., Chung, Y. G., Chang, M. Y., Han, B. S., ... & Kim, K. S. (2009). Generation of human induced pluripotent stem cells by direct delivery of reprogramming proteins. *Cell stem cell*, *4*(6), 472.

Kim, K., Doi, A., Wen, B., Ng, K., Zhao, R., Cahan, P., ... & Yabuuchi, A. (2010). Epigenetic memory in induced pluripotent stem cells. *Nature*, *467*(7313), 285-290.

Kimmelman, J., Heslop, H. E., Sugarman, J., Studer, L., Benvenisty, N., Caulfield, T., ... & Daley, G. Q. (2016). New ISSCR guidelines: clinical translation of stem cell research. *The Lancet*, *387*(10032), 1979-1981.

King, N. M., & **Perrin**, J. (2014). Ethical issues in stem cell research and therapy. *Stem Cell Research & Therapy*, *5*(4), 85.

King, S. M. (2016). Axonemal dynein arms. *Cold Spring Harbor Perspectives in Biology*, *8*(11), a028100.

Kiprilov, E. N., Awan, A., Desprat, R., Velho, M., Clement, C. A., Byskov, A. G., ... & Hirsch, R. E. (2008). Human embryonic stem cells in culture possess primary cilia with hedgehog signaling machinery. *The Journal of cell biology*, *180*(5), 897-904.

Kise, Y., Morinaka, A., Teglund, S., & Miki, H. (2009). Sufu recruits GSK3β for efficient processing of Gli3. *Biochemical and biophysical research communications*, *387*(3), 569-574.

Koch, P., Breuer, P., Peitz, M., Jungverdorben, J., Kesavan, J., Poppe, D., ... & Hoffmann, P. (2011). Excitation-induced ataxin-3 aggregation in neurons from patients with Machado–Joseph disease. *Nature*, *480*(7378), 543-546.

Koivumäki, J. T., Naumenko, N., Tuomainen, T., Takalo, J., Oksanen, M., Puttonen, K. A., ... & Tavi, P. (2018). Structural immaturity of human iPSC-derived cardiomyocytes: in silico investigation of effects on function and disease modeling. *Frontiers in physiology*, *9*, 80.

Komatsu, Y., Suzuki, T., Tsurusaki, Y., Miyake, N., Matsumoto, N., & Yan, K. (2016). TMEM67 mutations found in a case of Joubert syndrome with renal hypodysplasia. *CEN case reports*, *5*(2), 137-140.

Kozminski, K. G., Beech, P. L., & Rosenbaum, J. L. (1995). The Chlamydomonas kinesin-like protein FLA10 is involved in motility associated with the flagellar membrane. *The Journal of cell biology*, *131*(6), 1517-1527.

Kozminski, K. G., Johnson, K. A., Forscher, P., & Rosenbaum, J. L. (1993). A motility in the eukaryotic flagellum unrelated to flagellar beating. *Proceedings of the National Academy of Sciences*, *90*(12), 5519-5523.

Kuckhahn, A., Ramsperger-Gleixner, M., Distler, J., Spriewald, B., Ensminger, S., Weyand, M., & Heim, C. (2020). The Canonical Wnt Pathway in the Pathogenesis of Cardiac Allograft Vasculopathy. *The Journal of Heart and Lung Transplantation*, *39*(4), S90.

Kumaran, N., Pennesi, M. E., Yang, P., Trzupek, K. M., Schlechter, C., Moore, A. T., ... & Michaelides, M. (2018). Leber congenital amaurosis/early-onset severe retinal dystrophy overview. In *GeneReviews®[Internet]*. University of Washington, Seattle.

Kunitomi, A., Yuasa, S., Sugiyama, F., Saito, Y., Seki, T., Kusumoto, D., ... & Egashira, T. (2016). H1foo has a pivotal role in qualifying induced pluripotent stem cells. *Stem cell reports*, *6*(6), 825-833.

Kyttälä, A., Moraghebi, R., Valensisi, C., Kettunen, J., Andrus, C., Pasumarthy, K. K., ... & Van Handel, B. (2016). Genetic variability overrides the impact of parental cell type and determines iPSC differentiation potential. *Stem cell reports*, *6*(2), 200-212.

Lamba, D. A., McUsic, A., Hirata, R. K., Wang, P. R., Russell, D., & Reh, T. A. (2010). Generation, purification and transplantation of photoreceptors derived from human induced pluripotent stem cells. *PloS one*, *5*(1), e8763.

Lancaster, M. A., Louie, C. M., Silhavy, J. L., Sintasath, L., DeCambre, M., Nigam, S. K., ... & Gleeson, J. G. (2009). Impaired Wnt–β-catenin signaling disrupts adult renal homeostasis and leads to cystic kidney ciliopathy. *Nature medicine*, *15*(9), 1046-1054.

Lancaster, M. A., Renner, M., Martin, C. A., Wenzel, D., Bicknell, L. S., Hurles, M. E., ... & Knoblich, J. A. (2013). Cerebral organoids model human brain development and microcephaly. *Nature*, *501*(7467), 373-379.

Lancaster, M. A., Schroth, J., & Gleeson, J. G. (2011). Subcellular spatial regulation of canonical Wnt signalling at the primary cilium. *Nature cell biology*, *13*(6), 700-707.

Lapasset, L., Milhavet, O., Prieur, A., Besnard, E., Babled, A., Aït-Hamou, N., ... & Lehmann, S. (2011). Rejuvenating senescent and centenarian human cells by reprogramming through the pluripotent state. *Genes & development*, *25*(21), 2248-2253.

Larkins, C. E., Aviles, G. D. G., East, M. P., Kahn, R. A., & Caspary, T. (2011). Arl13b regulates ciliogenesis and the dynamic localization of Shh signaling proteins. *Molecular biology of the cell*, *22*(23), 4694-4703.

Laurent, L. C., Ulitsky, I., Slavin, I., Tran, H., Schork, A., Morey, R., ... & Ku, S. (2011). Dynamic changes in the copy number of pluripotency and cell proliferation genes in human ESCs and iPSCs during reprogramming and time in culture. *Cell stem cell*, *8*(1), 106-118.

Lee, J. E., & **Gleeson**, J. G. (2011). Cilia in the nervous system: linking cilia function and neurodevelopmental disorders. *Current opinion in neurology*, *24*(2), 98.

Lee, J. H., & **Gleeson**, J. G. (2010). The role of primary cilia in neuronal function. *Neurobiology of disease*, *38*(2), 167-172.

Lehman, A. M., Eydoux, P., Doherty, D., Glass, I. A., Chitayat, D., Chung, B. Y. H., ... & Trnka, P. (2010). Co-occurrence of Joubert syndrome and Jeune asphyxiating thoracic dystrophy. *American Journal of Medical Genetics Part A*, *152*(6), 1411-1419.

Lei, Y., & **Schaffer**, D. V. (2013). A fully defined and scalable 3D culture system for human pluripotent stem cell expansion and differentiation. *Proceedings of the National Academy of Sciences*, *110*(52), E5039-E5048.

Li, L., Chao, J., & Shi, Y. (2018). Modeling neurological diseases using iPSC-derived neural cells. *Cell and tissue research*, *371*(1), 143-151.

Li, X. J., Zhang, X., Johnson, M. A., Wang, Z. B., LaVaute, T., & Zhang, S. C. (2009). Coordination of sonic hedgehog and Wnt signaling determines ventral and dorsal telencephalic neuron types from human embryonic stem cells. *Development*, *136*(23), 4055-4063.

Liang, G., & **Zhang**, Y. (2013). Genetic and epigenetic variations in iPSCs: potential causes and implications for application. *Cell stem cell*, *13*(2), 149-159.

Lienkamp, S., Ganner, A., & Walz, G. (2012). Inversin, Wnt signaling and primary cilia. *Differentiation*, *83*(2), S49-S55.

Lin, F., Hiesberger, T., Cordes, K., Sinclair, A. M., Goldstein, L. S., Somlo, S., & Igarashi, P. (2003). Kidney-specific inactivation of the KIF3A subunit of kinesin-II inhibits renal ciliogenesis and produces polycystic kidney disease. *Proceedings of the National Academy of Sciences*, *100*(9), 5286-5291.

Liu, A., Wang, B., & Niswander, L. A. (2005). Mouse intraflagellar transport proteins regulate both the activator and repressor functions of Gli transcription factors. *Development*, *132*(13), 3103-3111.

Liu, G., David, B. T., Trawczynski, M., & Fessler, R. G. (2020). Advances in pluripotent stem cells: history, mechanisms, technologies, and applications. *Stem cell reviews and reports*, *16*(1), 3-32.

Livak, K. J., & **Schmittgen**, T. D. (2001). Analysis of relative gene expression data using real-time quantitative PCR and the 2− ΔΔCT method. *Methods*, 25(4), 402-408.

Logan, C. Y., & **Nusse**, R. (2004). The Wnt signaling pathway in development and disease. *Annu. Rev. Cell Dev. Biol.*, *20*, 781-810.

Lopez, E., Thauvin-Robinet, C., Reversade, B., El Khartoufi, N., Devisme, L., Holder, M., ... & Kaori, I. (2014). C5orf42 is the major gene responsible for OFD syndrome type VI. *Human genetics*, *133*(3), 367-377.

Lu, Q., Yu, M., Shen, C., Chen, X., Feng, T., Yao, Y., ... & Tu, W. (2014). Negligible immunogenicity of induced pluripotent stem cells derived from human skin fibroblasts. *PLoS One*, *9*(12), e114949.

Luciani, M., Gritti, A., & Meneghini, V. (2020). Human iPSC-Based Models for the Development of Therapeutics Targeting Neurodegenerative Lysosomal Storage Diseases. *Frontiers in Molecular Biosciences*, *7*, 224.

Macleod, M. R., Donnan, G. A., Horky, L. L., van der Worp, B. H., & Howells, D. W. (2006). 1,026 experimental treatments in acute stroke. Ann. Neurol., 59, 467-477.

Macleod, M. R., Van Der Worp, H. B., Sena, E. S., Howells, D. W., Dirnagl, U., & Donnan, G. A. (2008). Evidence for the efficacy of NXY-059 in experimental focal cerebral ischaemia is confounded by study quality. Stroke, 39(10), 2824-2829.

Maekawa, M., Yamaguchi, K., Nakamura, T., Shibukawa, R., Kodanaka, I., Ichisaka, T., ... & Yamanaka, S. (2011). Direct reprogramming of somatic cells is promoted by maternal transcription factor Glis1. *Nature*, *474*(7350), 225-229.

Mali, P., Chou, B. K., Yen, J., Ye, Z., Zou, J., Dowey, S., ... & Yusa, K. (2010). Butyrate greatly enhances derivation of human induced pluripotent stem cells by promoting epigenetic remodeling and the expression of pluripotency-associated genes. *Stem cells*, *28*(4), 713-720.

Malicdan, M. C. V., Vilboux, T., Stephen, J., Maglic, D., Mian, L., Konzman, D., ... & Zein, W. M. (2015). Mutations in human homologue of chicken talpid3 gene (KIAA0586) cause a hybrid ciliopathy with overlapping features of Jeune and Joubert syndromes. *Journal of medical genetics*, *52*(12), 830-839.

Malicki, J., Avanesov, A., Li, J., Yuan, S., & Sun, Z. (2011). Analysis of cilia structure and function in zebrafish. In *Methods in cell biology* (Vol. 101, pp. 39-74). Academic Press.

Mandai, M., Watanabe, A., Kurimoto, Y., Hirami, Y., Morinaga, C., Daimon, T., ... & Terada, M. (2017). Autologous induced stem-cell–derived retinal cells for macular degeneration. *New England Journal of Medicine*, *376*(11), 1038-1046.

Maria, B. L., Hoang, K. B., Tusa, R. J., Mancuso, A. A., Hamed, L. M., Quisling, R. G., ... & Yachnis, A. T. (1997). " Joubert syndrome" revisited: key ocular motor signs with magnetic resonance imaging correlation. *Journal of child neurology*, *12*(7), 423-430.

Maria, B. L., Boltshauser, E., Palmer, S. C., & Tran, T. X. (1999). Clinical features and revised diagnostic criteria in Joubert syndrome. *Journal of child neurology*, *14*(9), 583-590.

Marshall, W. F., Qin, H., Brenni, M. R., & Rosenbaum, J. L. (2005). Flagellar length control system: testing a simple model based on intraflagellar transport and turnover. *Molecular biology of the cell*, *16*(1), 270-278.

Martins-Taylor, K., Nisler, B. S., Taapken, S. M., Compton, T., Crandall, L., Montgomery, K. D., ... & Xu, R. H. (2011). Recurrent copy number variations in human induced pluripotent stem cells. Nature biotechnology, 29(6), 488-491.

Masui, S., Nakatake, Y., Toyooka, Y., Shimosato, D., Yagi, R., Takahashi, K., ... & Ko, M. S. (2007). Pluripotency governed by Sox2 via regulation of Oct3/4 expression in mouse embryonic stem cells. *Nature cell biology*, *9*(6), 625-635.

Mayshar, Y., Ben-David, U., Lavon, N., Biancotti, J. C., Yakir, B., Clark, A. T., ... & Benvenisty, N. (2010). Identification and classification of chromosomal aberrations in human induced pluripotent stem cells. *Cell stem cell*, *7*(4), 521-531.

Mendicino M, Fan Y, Griffin D, Gunter KC, Nichols K. Current state of US Food and Drug Administration regulation for cellular and gene therapy products: potential cures on the horizon. Cytotherapy. 2019; 21:699-724.

Menon, S., Shailendra, S., Renda, A., Longaker, M., & Quarto, N. (2016). An overview of direct somatic reprogramming: the ins and outs of iPSCs. *International journal of molecular sciences*, *17*(1), 141.

Mertens, J., Paquola, A. C., Ku, M., Hatch, E., Böhnke, L., Ladjevardi, S., ... & Gonçalves, J. T. (2015). Directly reprogrammed human neurons retain aging-associated transcriptomic signatures and reveal age-related nucleocytoplasmic defects. *Cell stem cell*, *17*(6), 705-718.

Mertens, J., Reid, D., Lau, S., Kim, Y., & Gage, F. H. (2018). Aging in a dish: iPSC-derived and directly induced neurons for studying brain aging and age-related neurodegenerative diseases. *Annual review of genetics*, *52*, 271-293.

Mirvis, M., Siemers, K. A., Nelson, W. J., & Stearns, T. P. (2019). Primary cilium loss in mammalian cells occurs predominantly by whole-cilium shedding. *PLoS biology*, *17*(7), e3000381.

Mo, Z., & **Zecevic**, N. (2008). Is Pax6 critical for neurogenesis in the human fetal brain?. *Cerebral Cortex*, 18(6), 1455-1465.

Morizane, A., Doi, D., Kikuchi, T., Okita, K., Hotta, A., Kawasaki, T., ... & Takahashi, J. (2013). Direct comparison of autologous and allogeneic transplantation of iPSC-derived neural cells in the brain of a nonhuman primate. *Stem cell reports*, *1*(4), 283-292**.**

Mougou-Zerelli, S., Thomas, S., Szenker, E., Audollent, S., Elkhartoufi, N., Babarit, C., ... & Gonzales, M. (2009). CC2D2A mutations in Meckel and Joubert syndromes indicate a genotype–phenotype correlation. *Human mutation*, *30*(11), 1574-1582.

Nachury, M. V., Loktev, A. V., Zhang, Q., Westlake, C. J., Peränen, J., Merdes, A., ... & Jackson, P. K. (2007). A core complex of BBS proteins cooperates with the GTPase Rab8 to promote ciliary membrane biogenesis. *Cell*, *129*(6), 1201-1213.

Nakagawa, M., Koyanagi, M., Tanabe, K., Takahashi, K., Ichisaka, T., Aoi, T., ... & Yamanaka, S. (2008). Generation of induced pluripotent stem cells without Myc from mouse and human fibroblasts. *Nature biotechnology*, *26*(1), 101-106.

Nathwani, B. B., Miller, C. H., Yang, T. L. T., Solimano, J. L., & Liao, J. C. (2014). Morphological differences of primary cilia between human induced pluripotent stem cells and their parental somatic cells. *Stem cells and development*, *23*(2), 115-123.

Nekrasov, E. D., Vigont, V. A., Klyushnikov, S. A., Lebedeva, O. S., Vassina, E. M., Bogomazova, A. N., ... & Bobrovsky, P. A. (2016). Manifestation of Huntington's disease pathology in human induced pluripotent stem cell-derived neurons. *Molecular neurodegeneration*, 11(1), 27.

Neufurth, M., Wang, X., Schröder, H. C., Feng, Q., Diehl-Seifert, B., Ziebart, T., ... & Müller, W. E. (2014). Engineering a morphogenetically active hydrogel for bioprinting of bioartificial tissue derived from human osteoblast-like SaOS-2 cells. *Biomaterials*, *35*(31), 8810-8819.

Newman, A. M., & **Cooper**, J. B. (2010). Lab-specific gene expression signatures in pluripotent stem cells. *Cell stem cell*, *7(*2), 258-262.

Nguyen, H. N., Byers, B., Cord, B., Shcheglovitov, A., Byrne, J., Gujar, P., ... & Palmer, T. D. (2011). LRRK2 mutant iPSC-derived DA neurons demonstrate increased susceptibility to oxidative stress. *Cell stem cell*, *8*(3), 267-280.

Niwa, H. (2007). How is pluripotency determined and maintained?. *Development*, *134*(4), 635-646.

Noor, A., Windpassinger, C., Patel, M., Stachowiak, B., Mikhailov, A., Azam, M., ... & Lutfullah, M. (2008). CC2D2A, encoding a coiled-coil and C2 domain protein, causes autosomal-recessive mental retardation with retinitis pigmentosa. *The American Journal of Human Genetics*, *82*(4), 1011-1018.

Nuovo, S., Bacigalupo, I., Ginevrino, M., Battini, R., Bertini, E., Borgatti, R., ... & Serpieri, V. (2020). Age and sex prevalence estimate of Joubert syndrome in Italy. *Neurology*, *94*(8), e797-e801.

Nusse, R., & **Clevers**, H. (2017). Wnt/β-catenin signaling, disease, and emerging therapeutic modalities. *Cell*, *169*(6), 985-999.

Nüsslein-Volhard, C., & **Wieschaus**, E. (1980). Mutations affecting segment number and polarity in Drosophila. *Nature*, *287*(5785), 795-801.

O'Callaghan, C., Sikand, K., & Rutman, A. (1999). Respiratory and brain ependymal ciliary function. *Pediatric research*, *46*(6), 704-704.

Ocbina, P. J. R., & **Anderson**, K. V. (2008). Intraflagellar transport, cilia, and mammalian Hedgehog signaling: analysis in mouse embryonic fibroblasts. *Developmental dynamics: an official publication of the American Association of Anatomists*, *237*(8), 2030-2038.

Ocbina, P. J. R., Tuson, M., & Anderson, K. V. (2009). Primary cilia are not required for normal canonical Wnt signaling in the mouse embryo. *PloS one*, *4*(8), e6839.

Ohnuki, M., & **Takahashi**, K. (2015). Present and future challenges of induced pluripotent stem cells. *Philosophical Transactions of the Royal Society B: Biological Sciences*, *370*(1680), 20140367.

Okazaki, M., Kobayashi, T., Chiba, S., Takei, R., Liang, L., Nakayama, K., & Katoh, Y. (2020). Formation of the B9-domain protein complex MKS1–B9D2–B9D1 is essential as a diffusion barrier for ciliary membrane proteins. *Molecular Biology of the Cell*, *31*(20), 2259-2268.

Okita, K., Ichisaka, T., & Yamanaka, S. (2007). Generation of germline-competent induced pluripotent stem cells. *Nature*, *448*(7151), 313-317.

Okita, K., Matsumura, Y., Sato, Y., Okada, A., Morizane, A., Okamoto, S., ... & Yamanaka, S. (2011). A more efficient method to generate integration-free human iPS cells. *Nature methods*, *8*(5), 409-412.

Ozonoff, S., Williams, B. J., Gale, S., & Miller, J. N. (1999). Autism and autistic behavior in Joubert syndrome. *Journal of child neurology*, *14*(10), 636-641.

Parisi, M. A. (2009). Clinical and molecular features of Joubert syndrome and related disorders. In *American Journal of Medical Genetics Part C: Seminars in Medical Genetics*, 151(4), 326-340.

Parisi, M. A. (2019). The molecular genetics of Joubert syndrome and related ciliopathies: The challenges of genetic and phenotypic heterogeneity. *Translational science of rare diseases*, *4*(1-2), 25-49.

Parisi, M. A., Bennett, C. L., Eckert, M. L., Dobyns, W. B., Gleeson, J. G., Shaw, D. W., ... & Glass, I. A. (2004). The NPHP1 gene deletion associated with juvenile nephronophthisis is present in a subset of individuals with Joubert syndrome. *The American Journal of Human Genetics*, *75*(1), 82-91.

Parisi, M. A., Doherty, D., Chance, P. F., & Glass, I. A. (2007). Joubert syndrome (and related disorders) (OMIM 213300). *European Journal of Human Genetics*, *15*(5), 511-521.

Parisi, M. A., Doherty, D., Eckert, M. L., Shaw, D. W., Ozyurek, H., Aysun, S., ... & Bakhsh, E. (2006). AHI1 mutations cause both retinal dystrophy and renal cystic disease in Joubert syndrome. *Journal of medical genetics*, *43*(4), 334-339.

Parisi, M & **Glass**, I. (July 9, 2003). Joubert Syndrome. *GeneReviews™, NCBI*. Available from: https://www.ncbi.nlm.nih.gov/books/NBK1325/.

Park, I. H., Zhao, R., West, J. A., Yabuuchi, A., Huo, H., Ince, T. A., ... & Daley, G. Q. (2008). Reprogramming of human somatic cells to pluripotency with defined factors. *Nature*, *451*(7175), 141-146.

Park, T. J., Mitchell, B. J., Abitua, P. B., Kintner, C., & Wallingford, J. B. (2008). Dishevelled controls apical docking and planar polarization of basal bodies in ciliated epithelial cells. *Nature genetics*, *40*(7), 871-879.

Pearson, B. L., Simon, J. M., McCoy, E. S., Salazar, G., Fragola, G., & Zylka, M. J. (2016). Identification of chemicals that mimic transcriptional changes associated with autism, brain aging and neurodegeneration. *Nature communications*, *7*(1), 1-12.

Pedersen, L. B., & **Akhmanova**, A. (2014). Kif7 keeps cilia tips in shape. *Nature cell biology*, *16*(7), 623-62.

Perel, P., Roberts, I., Sena, E., Wheble, P., Briscoe, C., Sandercock, P., ... & Khan, K. S. (2007). Comparison of treatment effects between animal experiments and clinical trials: systematic review. *Bmj*, *334*(7586), 197.

Perez-Pinera, P., Kocak, D. D., Vockley, C. M., Adler, A. F., Kabadi, A. M., Polstein, L. R., ... & Guilak, F. (2013). RNA-guided gene activation by CRISPR-Cas9–based transcription factors. *Nature methods*, 10(10), 973-976.

Pevny, L. H., Sockanathan, S., Placzek, M., & Lovell-Badge, R. (1998). A role for SOX1 in neural determination. *Development*, *125*(10), 1967-1978.

Phelps, I. G., Dempsey, J. C., Grout, M. E., Isabella, C. R., Tully, H. M., Doherty, D., & Bachmann-Gagescu, R. (2018). Interpreting the clinical significance of combined variants in multiple recessive disease genes: systematic investigation of Joubert syndrome yields little support for oligogenicity. *Genetics in medicine*, *20*(2), 223-233.

Pigino, G., Geimer, S., Lanzavecchia, S., Paccagnini, E., Cantele, F., Diener, D. R., ... & Lupetti, P. (2009). Electron-tomographic analysis of intraflagellar transport particle trains in situ. *Journal of Cell Biology*, *187*(1), 135-148.

Plotnikova, O. V., Nikonova, A. S., Loskutov, Y. V., Kozyulina, P. Y., Pugacheva, E. N., & Golemis, E. A. (2012). Calmodulin activation of Aurora-A kinase (AURKA) is required during ciliary disassembly and in mitosis. *Molecular biology of the cell*, *23*(14), 2658-2670.

Polo, J. M., Liu, S., Figueroa, M. E., Kulalert, W., Eminli, S., Tan, K. Y., ... & Natesan, S. (2010). Cell type of origin influences the molecular and functional properties of mouse induced pluripotent stem cells. *Nature biotechnology*, *28*(8), 848-855.

Poretti, A., Alber, F. D., Brancati, F., Dallapiccola, B., Valente, E. M., & Boltshauser, E. (2009). Normal cognitive functions in Joubert syndrome. *Neuropediatrics*, *40*(06), 287-290.

Poretti, A., Boltshauser, E., & Valente, E. M. (2014). The molar tooth sign is pathognomonic for Joubert syndrome! *Pediatric neurology*, *50*(6), e15-e16.

Poretti, A., Huisman, T. A. G. M., Scheer, I., & Boltshauser, E. (2011). Joubert syndrome and related disorders: spectrum of neuroimaging findings in 75 patients. *American journal of neuroradiology*, *32*(8), 1459-1463.

Poretti, A., Snow, J., Summers, A. C., Tekes, A., Huisman, T. A., Aygun, N., ... & NISC Comparative Sequencing Program. (2017). Joubert syndrome: neuroimaging findings in 110 patients in correlation with cognitive function and genetic cause. *Journal of medical genetics*, *54*(8), 521-529.

Poretti, A., Vitiello, G., Hennekam, R. C., Arrigoni, F., Bertini, E., Borgatti, R., ... & Huisman, T. A. (2012). Delineation and diagnostic criteria of Oral-Facial-Digital Syndrome type VI. *Orphanet journal of rare diseases*, *7*(1), 1-14.

Porter, K. R. (1955). The submicroscopic morphology of protoplasm. *Harvey Lectures*, *51*, 175.

Pugacheva, E. N., Jablonski, S. A., Hartman, T. R., Henske, E. P., & Golemis, E. A. (2007). HEF1-dependent Aurora A activation induces disassembly of the primary cilium. *Cell*, *129*(7), 1351-1363.

Putoux, A., Thomas, S., Coene, K. L., Davis, E. E., Alanay, Y., Ogur, G., ... & Bennett, C. L. (2011). KIF7 mutations cause fetal hydrolethalus and acrocallosal syndromes. *Nature genetics*, *43*(6), 601-606.

Qian, X., Nguyen, H. N., Song, M. M., Hadiono, C., Ogden, S. C., Hammack, C., ... & Yoon, K. J. (2016). Brain-region-specific organoids using mini-bioreactors for modeling ZIKV exposure. *Cell*, *165*(5), 1238-1254.

Qin, J., Lin, Y., Norman, R. X., Ko, H. W., & Eggenschwiler, J. T. (2011). Intraflagellar transport protein 122 antagonizes Sonic Hedgehog signaling and controls ciliary localization of pathway components. *Proceedings of the National Academy of Sciences*, *108*(4), 1456-1461.

Qiu, L., LeBel, R. P., Storm, D. R., & Chen, X. (2016). Type 3 adenylyl cyclase: a key enzyme mediating the cAMP signaling in neuronal cilia. *International journal of physiology, pathophysiology and pharmacology*, *8*(3), 95.

Rais, Y., Zviran, A., Geula, S., Gafni, O., Chomsky, E., Viukov, S., ... & Maza, I. (2013). Deterministic direct reprogramming of somatic cells to pluripotency. *Nature*, *502*(7469), 65-70.

Rakovic, A., Shurkewitsch, K., Seibler, P., Grünewald, A., Zanon, A., Hagenah, J., ... & Klein, C. (2013). Phosphatase and Tensin Homolog (PTEN)-induced Putative Kinase 1 (PINK1)-dependent Ubiquitination of Endogenous Parkin

Attenuates Mitophagy STUDY IN HUMAN PRIMARY FIBROBLASTS AND INDUCED PLURIPOTENT STEM CELL-DERIVED NEURONS. *Journal of Biological Chemistry*, *288*(4), 2223-2237.

Rao, M. S., & **Malik**, N. (2012). Assessing iPSC reprogramming methods for their suitability in translational medicine. *Journal of cellular biochemistry*, *113*(10), 3061-3068.

Reinhardt, P., Schmid, B., Burbulla, L. F., Schöndorf, D. C., Wagner, L., Glatza, M., ... & Wu, G. (2013). Genetic correction of a LRRK2 mutation in human iPSCs links parkinsonian neurodegeneration to ERK-dependent changes in gene expression. *Cell stem cell*, *12*(3), 354-367.

Rho, J. Y., Yu, K., Han, J. S., Chae, J. I., Koo, D. B., Yoon, H. S., ... & Han, Y. M. (2006). Transcriptional profiling of the developmentally important signalling pathways in human embryonic stem cells. *Human Reproduction*, *21*(2), 405-412.

Riggs, J. W., Barrilleaux, B. L., Varlakhanova, N., Bush, K.M., Chan, V., & Knoepfler, P. S. (2013). Induced pluripotency and oncogenic transformation are related processes. *Stem cells and development*, *22*(1), 37-50.

Rohatgi, R., Milenkovic, L., Corcoran, R. B., & Scott, M. P. (2009). Hedgehog signal transduction by Smoothened: pharmacologic evidence for a 2-step activation process. *Proceedings of the National Academy of Sciences*, *106*(9), 3196-3201.

Rohwedel, J., Sehlmeyer, U., Shan, J., Meister, A., & Wobus, A. M. (1996). Primordial germ cell-derived mouse embryonic germ (eg) cellsin vitroresemble undifferentiated stem cells with respect to differentiation capacity and cell cycle distribution. *Cell biology international*, *20*(8), 579-587.

Rojas, S. V., Kensah, G., Rotaermel, A., Baraki, H., Kutschka, I., Zweigerdt, R., ... & Martens, A. (2017). Transplantation of purified iPSC-derived cardiomyocytes in myocardial infarction. *PLoS One*, *12*(5), e0173222.

Romani, M., Micalizzi, A., & Valente, E. M. (2013). Joubert syndrome: congenital cerebellar ataxia with the molar tooth. *The Lancet Neurology*, *12*(9), 894-905.

Romani, M., Micalizzi, A., Kraoua, I., Dotti, M. T., Cavallin, M., Sztriha, L., ... & Hanene, B. (2014). Mutations in B9D1 and MKS1 cause mild Joubert syndrome: expanding the genetic overlap with the lethal ciliopathy Meckel syndrome. *Orphanet journal of rare diseases*, *9*(1), 72.

Ronquillo, C. C., Bernstein, P. S., & Baehr, W. (2012). Senior–Løken syndrome: A syndromic form of retinal dystrophy associated with nephronophthisis. *Vision research*, *75*, 88-97.

Rosati, J., Altieri, F., Tardivo, S., Turco, E. M., Goldoni, M., Spasari, I., ... & Vescovi, A. L. (2018). Production and characterization of human induced pluripotent stem cells (iPSCs) from Joubert Syndrome: CSSi001-A (2850). *Stem cell research*, 27, 74-77.

Rosenbaum, J. L., & **Witman**, G. B. (2002). Intraflagellar transport. *Nature reviews Molecular cell biology*, *3*(11), 813-825.

Rubin, L. L., & **de Sauvage**, F. J. (2006). Targeting the Hedgehog pathway in cancer. *Nature reviews Drug discovery*, *5*(12), 1026-1033.

Ryan, K. E., & **Chiang**, C. (2012). Hedgehog secretion and signal transduction in vertebrates. *Journal of Biological Chemistry*, *287*(22), 17905-17913.

Ryan, S. D., Dolatabadi, N., Chan, S. F., Zhang, X., Akhtar, M. W., Parker, J., ... & Lee, B. (2013). Isogenic human iPSC Parkinson's model shows nitrosative stress-induced dysfunction in MEF2-PGC1α transcription. *Cell*, *155*(6), 1351-1364.

Salaris, F., Colosi, C., Brighi, C., Soloperto, A., Turris, V., Benedetti, M. C., Ghirga, S., Rosito, M., Di Angelantonio, S., & Rosa, A. (2019). 3D Bioprinted Human Cortical Neural Constructs Derived from Induced Pluripotent Stem Cells. *Journal of clinical medicine*, *8*(10), 1595.

Salinas, P. C. (2012). Wnt signaling in the vertebrate central nervous system: from axon guidance to synaptic function. *Cold Spring Harbor perspectives in biology*, *4*(2), a008003.

Samata, B., Doi, D., Nishimura, K., Kikuchi, T., Watanabe, A., Sakamoto, Y., ... & Takahashi, J. (2016). Purification of functional human ES and iPSC-derived midbrain dopaminergic progenitors using LRTM1. *Nature communications*, *7*(1), 1-11.

Sang, L., Miller, J. J., Corbit, K. C., Giles, R. H., Brauer, M. J., Otto, E. A., ... & Huntzicker, E. G. (2011). Mapping the NPHP-JBTS-MKS protein network reveals ciliopathy disease genes and pathways. *Cell*, *145*(4), 513-528.

Sardo, V. L., Ferguson, W., Erikson, G. A., Topol, E. J., Baldwin, K. K., & Torkamani, A. (2017). Influence of donor age on induced pluripotent stem cells. *Nature biotechnology*, *35*(1), 69-74.

Satir, P. (2005). Tour of organelles through the electron microscope: A reprinting of Keith R. Porter's classic Harvey Lecture with a new introduction. *The Anatomical Record Part A: Discoveries in Molecular, Cellular, and Evolutionary Biology: An Official Publication of the American Association of Anatomists*, *287*(2), 1184-1204.

Satir, P., & **Christensen**, S. T. (2007). Overview of structure and function of mammalian cilia. *Annu. Rev. Physiol.*, *69*, 377-400.

Satran, D., Pierpont, M. E. M., & Dobyns, W. B. (1999). Cerebello–oculo–renal syndromes including Arima, Senior-Löken and COACH syndromes: More than just variants of Joubert syndrome. *American journal of medical genetics*, *86*(5), 459-469.

Sayer, J. A., Otto, E. A., O'Toole, J. F., Nurnberg, G., Kennedy, M. A., Becker, C., ... & Utsch, B. (**2006**). The centrosomal protein nephrocystin-6 is mutated in Joubert syndrome and activates transcription factor ATF4. *Nature genetics*, *38*(6), 674-681.

Schneider, L., Clement, C. A., Teilmann, S. C., Pazour, G. J., Hoffmann, E. K., Satir, P., & Christensen, S. T. (2005). PDGFRαα signaling is regulated through the primary cilium in fibroblasts. *Current Biology*, *15*(20), 1861-1866.

Schneuwly, S., Klemenz, R., & Gehring, W. J. (1987). Redesigning the body plan of Drosophila by ectopic expression of the homoeotic gene Antennapedia. *Nature*, *325*(6107), 816-818.

Scholey, J. M. (**2008**). Intraflagellar transport motors in cilia: moving along the cell's antenna. *The Journal of cell biology*, *180*(1), 23-29.

Schuster, B., Junkin, M., Kashaf, S. S., Romero-Calvo, I., Kirby, K., Matthews, J., ... & Tay, S. (2020). Automated microfluidic platform for dynamic and combinatorial drug screening of tumor organoids. *Nature Communications*, *11*(1), 1-12.

Scott, J. A., Schumann, C. M., Goodlin-Jones, B. L., & Amaral, D. G. (**2009**). A comprehensive volumetric analysis of the cerebellum in children and adolescents with autism spectrum disorder. *Autism Research*, *2*(5), 246-257.

Scott, S., Kranz, J. E., Cole, J., Lincecum, J. M., Thompson, K., Kelly, N., ... & Heywood, J. A. (2008). Design, power, and interpretation of studies in the standard murine model of ALS. Amyotrophic Lateral Sclerosis, 9(1), 4-15.

Sena, E. S., Van Der Worp, H. B., Bath, P. M., Howells, D. W., & Macleod, M. R. (2010). Publication bias in reports of animal stroke studies leads to major overstatement of efficacy. *PLoS Biol*, *8*(3), e1000344.

Shaheen, R., Faqeih, E., Alshammari, M. J., Swaid, A., Al-Gazali, L., Mardawi, E., ... & Farra, C. (**2013**). Genomic analysis of Meckel–Gruber syndrome in Arabs reveals marked genetic heterogeneity and novel candidate genes. *European Journal of Human Genetics*, *21*(7), 762-768.

Shaheen, R., Jiang, N., Alzahrani, F., Ewida, N., Al-Sheddi, T., Alobeid, E., ... & Abdulwahab, F. (**2019**). Bi-allelic Mutations in FAM149B1 Cause Abnormal Primary Cilium and a Range of Ciliopathy Phenotypes in Humans. *The American Journal of Human Genetics*, *104*(4), 731-737.

Shaheen, R., Szymanska, K., Basu, B., Patel, N., Ewida, N., Faqeih, E., ... & Alazami, A. M. (2016). Characterizing the morbid genome of ciliopathies. *Genome biology*, *17*(1), 242.

Shi, Y., Inoue, H., Wu, J. C., & Yamanaka, S. (2017). Induced pluripotent stem cell technology: a decade of progress. *Nature reviews. Drug discovery*, *16*(2), 115–130.

Shimada, H., Lu, Q., Insinna-Kettenhofen, C., Nagashima, K., English, M. A., Semler, E. M., ... & Swaroop, A. (2017). In vitro modeling using ciliopathy-patient-derived cells reveals distinct cilia dysfunctions caused by CEP290 mutations. Cell reports, 20(2), 384-396.

Shinde, V., Sureshkumar, P., Sotiriadou, I., Hescheler, J., & Sachinidis, A. (2016). Human embryonic and induced pluripotent stem cell-based toxicity testing models: future applications in new drug discovery. *Current medicinal chemistry*, *23*(30), 3495-3509.

Simons, M., Gloy, J., Ganner, A., Bullerkotte, A., Bashkurov, M., Krönig, C., ... & Mlodzik, M. (2005). Inversin, the gene product mutated in nephronophthisis type II, functions as a molecular switch between Wnt signaling pathways. *Nature genetics*, *37*(5), 537-543.

Singla, V., & **Reiter**, J. F. (**2006**). The primary cilium as the cell's antenna: signaling at a sensory organelle. *science*, *313*(5787), 629-633.

Sjöstrand, F. S. (**1953**). The ultrastructure of the inner segments of the retinal rods of the guinea pig eye as revealed by electron microscopy. *Journal of cellular and comparative physiology*, *42*(1), 45-70.

Skardal, A., Shupe, T., & Atala, A. (2016). Organoid-on-a-chip and body-on-a-chip systems for drug screening and disease modeling. *Drug discovery today*, *21*(9), 1399-1411.

Slaats, G. G., Isabella, C. R., Kroes, H. Y., Dempsey, J. C., Gremmels, H., Monroe, G. R., ... & Knutzen, D. M. (2016). MKS1 regulates ciliary INPP5E levels in Joubert syndrome. *Journal of medical genetics*, *53*(1), 62-72.

Smith, K. N., Singh, A. M., & Dalton, S. (2010). Myc represses primitive endoderm differentiation in pluripotent stem cells. *Cell stem cell*, *7*(3), 343-354.

Smith, U. M., Consugar, M., Tee, L. J., McKee, B. M., Maina, E. N., Whelan, S., ... & Aligianis, I. A. (2006). The transmembrane protein meckelin (MKS3) is mutated in Meckel-Gruber syndrome and the wpk rat. *Nature genetics*, *38*(2), 191-196.

Soldner, F., Hockemeyer, D., Beard, C., Gao, Q., Bell, G. W., Cook, E. G., ... & Isacson, O. (2009). Parkinson's disease patient-derived induced pluripotent stem cells free of viral reprogramming factors. *Cell*, *136*(5), 964-977.

Song, B., Cha, Y., Ko, S., Jeon, J., Lee, N., Seo, H., ... & Luna, M. J. (2020). Human autologous iPSC–derived dopaminergic progenitors restore motor function in Parkinson's disease models. *The Journal of Clinical Investigation*, *130*(2), 904-920.

Song, Z., Zhang, X., Jia, S., Yelick, P. C., & Zhao, C. (2016). Zebrafish as a model for human ciliopathies. *Journal of Genetics and Genomics*, *43*(3), 107-120.

Sorokin, S. (1962). Centrioles and the formation of rudimentary cilia by fibroblasts and smooth muscle cells. *The Journal of cell biology*, *15*(2), 363-377.

Srivastava, S., Molinari, E., Raman, S., & Sayer, J. A. (2018). Many genes—one disease? Genetics of Nephronophthisis (NPHP) and NPHP-associated disorders. *Frontiers in pediatrics*, *5*, 287.

Srour, M., Hamdan, F. F., McKnight, D., Davis, E., Mandel, H., Schwartzentruber, J., ... & Ospina, L. H. (2015). Joubert syndrome in French Canadians and identification of mutations in CEP104. *The American Journal of Human Genetics*, *97*(5), 744-753.

Srour, M., Hamdan, F. F., Schwartzentruber, J. A., Patry, L., Ospina, L. H., Shevell, M. I., ... & Massicotte, C. (2012). Mutations in TMEM231 cause Joubert syndrome in French Canadians. *Journal of medical genetics*, *49*(10), 636-641.

Srour, M., Schwartzentruber, J., Hamdan, F. F., Ospina, L. H., Patry, L., Labuda, D., ... & Samuels, M. E. (2012). Mutations in C5ORF42 cause Joubert syndrome in the French Canadian population. *The American Journal of Human Genetics*, *90*(4), 693-700.

Stadtfeld, M., Nagaya, M., Utikal, J., Weir, G., & Hochedlinger, K. (2008). Induced pluripotent stem cells generated without viral integration. *Science*, *322*(5903), 945-949.

Steinlin, M., Schmid, M., Landau, K., & Boltshauser, E. (1997). Follow-up in children with Joubert syndrome. *Neuropediatrics*, *28*(04), 204-211.

Stephen, J., Vilboux, T., Mian, L., Kuptanon, C., Sinclair, C. M., Yildirimli, D., ... & Mullikin, J. C. (2017). Mutations in KIAA0753 cause Joubert syndrome associated with growth hormone deficiency. *Human genetics*, *136*(4), 399-408.

Sterpka, A., & **Chen**, X. (2018). Neuronal and astrocytic primary cilia in the mature brain. *Pharmacological research*, *137*, 114-121.

Sterpka, A., Yang, J., Strobel, M., Zhou, Y., Pauplis, C., & Chen, X. (**2020**). Diverged morphology changes of astrocytic and neuronal primary cilia under reactive insults. *Molecular Brain*, *13*(1), 1-16.

Strongin, A., Heller, T., Doherty, D., Glass, I. A., Parisi, M. A., Bryant, J., ... & Vemulapalli, M. (2018). Characteristics of liver disease in 100 individuals with Joubert syndrome prospectively evaluated at a single center. *Journal of pediatric gastroenterology and nutrition*, *66*(3), 428.

Studer, L., Vera, E., & Cornacchia, D. (2015). Programming and reprogramming cellular age in the era of induced pluripotency. *Cell stem cell*, *16*(6), 591-600.

Summers, A. C., Snow, J., Wiggs, E., Liu, A. G., Toro, C., Poretti, A., ... & Doherty, D. (2017). Neuropsychological phenotypes of 76 individuals with Joubert syndrome evaluated at a single center. *American Journal of Medical Genetics Part A*, *173*(7), 1796-1812.

Sundberg, M., Bogetofte, H., Lawson, T., Jansson, J., Smith, G., Astradsson, A., ... & Hallett, P. (2013). Improved cell therapy protocols for Parkinson's disease based on differentiation efficiency and safety of hESC-, hiPSC-, and non-human primate iPSC-derived dopaminergic neurons. *Stem cells*, *31*(8), 1548-1562.

Taapken, S. M., Nisler, B. S., Newton, M. A., Sampsell-Barron, T. L., Leonhard, K. A., McIntire, E. M., & Montgomery, K. D. (2011). Karyotypic abnormalities in human induced pluripotent stem cells and embryonic stem cells. Nature biotechnology, 29(4), 313-314.

Tada, M., Takahama, Y., Abe, K., Nakatsuji, N., & Tada, T. (2001). Nuclear reprogramming of somatic cells by in vitro hybridization with ES cells. *Current Biology*, *11*(19), 1553-1558.

Takahashi, K., & **Yamanaka**, S. (2006). Induction of pluripotent stem cells from mouse embryonic and adult fibroblast cultures by defined factors. *cell*, *126*(4), 663-676.

Takahashi, K., Tanabe, K., Ohnuki, M., Narita, M., Ichisaka, T., Tomoda, K., & Yamanaka, S. (2007). Induction of pluripotent stem cells from adult human fibroblasts by defined factors. *cell*, *131*(5), 861-872.

Takahashi, T. N., Farmer, J. E., Deidrick, K. K., Hsu, B. S., Miles, J. H., & Maria, B. L. (2005). Joubert syndrome is not a cause of classical autism. *American Journal of Medical Genetics Part A*, *132*(4), 347-351.

Tallila, J., Jakkula, E., Peltonen, L., Salonen, R., & Kestilä, M. (2008). Identification of CC2D2A as a Meckel syndrome gene adds an important piece to the ciliopathy puzzle. *The American Journal of Human Genetics*, *82*(6), 1361-1367.

Tang, C., & **Drukker**, M. (2011, November). Potential barriers to therapeutics utilizing pluripotent cell derivatives: intrinsic immunogenicity of in vitro maintained and matured populations. In *Seminars in immunopathology* (Vol. 33, No. 6, p. 563). Springer-Verlag.

Taschner, M., Bhogaraju, S., & Lorentzen, E. (2012). Architecture and function of IFT complex proteins in ciliogenesis. *Differentiation*, *83*(2), S12-S22.

The Nobel Prize in Chemistry 2020. (2020, October 7). *The Noble Prize.* Available from: https://www.nobelprize.org/prizes/chemistry/2020/press-release/.

The Nobel Prize in Physiology or Medicine 2012. (2012, October 28). *The Noble Prize.* Available from: https://www.nobelprize.org/prizes/medicine/2012/press-release/.

Theunissen, J. W., & **de Sauvage**, F. J. (2009). Paracrine Hedgehog signaling in cancer. *Cancer research*, *69*(15), 6007-6010.

Thomson, J. A., Itskovitz-Eldor, J., Shapiro, S. S., Waknitz, M. A., Swiergiel, J. J., Marshall, V. S., & Jones, J. M. (1998). Embryonic stem cell lines derived from human blastocysts. *science*, *282*(5391), 1145-1147.

Tran, P. V., Haycraft, C. J., Besschetnova, T. Y., Turbe-Doan, A., Stottmann, R. W., Herron, B. J., ... & Yoder, B. K. (2008). THM1 negatively modulates mouse sonic hedgehog signal transduction and affects retrograde intraflagellar transport in cilia. *Nature genetics*, *40*(4), 403-410.

Tuz, K., Bachmann-Gagescu, R., O'Day, D. R., Hua, K., Isabella, C. R., Phelps, I. G., ... & Alswaid, A. (2014). Mutations in CSPP1 cause primary cilia abnormalities and Joubert syndrome with or without Jeune asphyxiating thoracic dystrophy. *The American Journal of Human Genetics*, *94*(1), 62-72.

Valente, E. M., Brancati, F., & Dallapiccola, B. (2008). Genotypes and phenotypes of Joubert syndrome and related disorders. *European journal of medical genetics*, *51*(1), 1-23.

Valente, E. M., Brancati, F., Silhavy, J. L., Castori, M., Marsh, S. E., Barrano, G., ... & Abdel-Salam, G. M. (**2006**). AHI1 gene mutations cause specific forms of Joubert syndrome–related disorders. *Annals of neurology*, *59*(3), 527-534.

Valente, E. M., Logan, C. V., Mougou-Zerelli, S., Lee, J. H., Silhavy, J. L., Brancati, F., ... & Adams, M. (2010). Mutations in TMEM216 perturb ciliogenesis and cause Joubert, Meckel and related syndromes. *Nature genetics*, *42*(7), 619-625.

Valente, E. M., Rosti, R. O., Gibbs, E., & Gleeson, J. G. (**2014**). Primary cilia in neurodevelopmental disorders. *Nature Reviews Neurology*, *10*(1), 27-36.

Valente, E. M., Silhavy, J. L., Brancati, F., Barrano, G., Krishnaswami, S. R., Castori, M., ... & Fazzi, E. (2006). Mutations in CEP290, which encodes a centrosomal protein, cause pleiotropic forms of Joubert syndrome. *Nature genetics*, *38*(6), 623-625.

Varlakhanova, N. V., Cotterman, R. F., deVries, W. N., Morgan, J., Donahue, L. R., Murray, S., ... & Knoepfler, P. S. (2010). Myc maintains embryonic stem cell pluripotency and self-renewal. *Differentiation*, *80*(1), 9-19.

Veleri, S., Manjunath, S. H., Fariss, R. N., May-Simera, H., Brooks, M., Foskett, T. A., ... & Rachel, R. A. (2014). Ciliopathy-associated gene Cc2d2a promotes assembly of subdistal appendages on the mother centriole during cilia biogenesis. *Nature communications*, *5*(1), 1-12.

Venere, M., Han, Y. G., Bell, R., Song, J. S., Alvarez-Buylla, A., & Blelloch, R. (2012). Sox1 marks an activated neural stem/progenitor cell in the hippocampus. Development, 139(21), 3938-3949.

Vera, E., & **Studer**, L. (2015). When rejuvenation is a problem: challenges of modeling late-onset neurodegenerative disease. *Development*, *142*(18), 3085-3089.

Verheyen, E. M., & **Gottardi**, C. J. (2010). Regulation of Wnt/beta-catenin signaling by protein kinases. *Developmental dynamics: an official publication of the American Association of Anatomists*, *239*(1), 34–44.

Verloes, A., Lambotte, C., Neri, G., & Reynolds, J. F. (1989). Further delineation of a syndrome of cerebellar vermis hypo/aplasia, oligophrenia, congenital ataxia, coloboma, and hepatic fibrosis. *American journal of medical genetics*, *32*(2), 227-232.

Vilboux, T., Doherty, D. A., Glass, I. A., Parisi, M. A., Phelps, I. G., Cullinane, A. R., ... & Oden, N. L. (2017). Molecular genetic findings and clinical correlations in 100 patients with Joubert syndrome and related disorders prospectively evaluated at a single center. *Genetics in Medicine*, *19*(8), 875-882.

Vilboux, T., Malicdan, M. C. V., Roney, J. C., Cullinane, A. R., Stephen, J., Yildirimli, D., ... & NISC Comparative Sequencing Program. (**2017**). CELSR2, encoding a planar cell polarity protein, is a putative gene in Joubert syndrome with cortical heterotopia, microophthalmia, and growth hormone deficiency. *American journal of medical genetics Part A*, *173*(3), 661-666.

Wang, S. F., Kowal, T. J., Ning, K., Koo, E. B., Wu, A. Y., Mahajan, V. B., & Sun, Y. (2018). Review of ocular manifestations of Joubert syndrome. *Genes*, *9*(12), 605.

Warren, L., Manos, P. D., Ahfeldt, T., Loh, Y. H., Li, H., Lau, F., ... & Rossi, D. J. (2010). Highly efficient reprogramming to pluripotency and directed differentiation of human cells with synthetic modified mRNA. *Cell stem cell*, *7*(5), 618-630.

Wei, Q., Zhang, Y., Li, Y., Zhang, Q., Ling, K., & Hu, J. (2012). The BBSome controls IFT assembly and turnaround in cilia. *Nature cell biology*, *14*(9), 950-957.

Wemmer, K. A., & Marshall, W. F. (**2007**). Flagellar length control in Chlamydomonas—a paradigm for organelle size regulation. *International review of cytology*, *260*, 175-212.

Wernig, M., Meissner, A., Cassady, J. P., & Jaenisch, R. (2008). c-Myc is dispensable for direct reprogramming of mouse fibroblasts. *Cell stem cell*, *2*(1), 10-12.

Wheatley, D. N., Wang, A. M., & Strugnell, G. E. (**1996**). Expression of primary cilia in mammalian cells. *Cell biology international*, *20*(1), 73-81.

Wheway, G., Abdelhamed, Z., Natarajan, S., Toomes, C., Inglehearn, C., & Johnson, C. A. (2013). Aberrant Wnt signalling and cellular over-proliferation in a novel mouse model of Meckel–Gruber syndrome. *Developmental biology*, *377*(1), 55-66.
Wheway, G., Nazlamova, L., & Hancock, J. T. (2018). Signaling through the primary cilium. *Frontiers in cell and developmental biology*, *6*, 8.

Wilmut, I., Schnieke, A. E., McWhir, J., Kind, A. J., & Campbell, K. H. (1997). Viable offspring derived from fetal and adult mammalian cells. *Nature*, *385*(6619), 810-813.

Woltjen, K., Michael, I. P., Mohseni, P., Desai, R., Mileikovsky, M., Hämäläinen, R., ... & Nagy, A. (2009). piggyBac transposition reprograms fibroblasts to induced pluripotent stem cells. *Nature*, *458*(7239), 766-770.

Xu, M., Lee, E. M., Wen, Z., Cheng, Y., Huang, W. K., Qian, X., ... & Jacob, F. (2016). Identification of small-molecule inhibitors of Zika virus infection and induced neural cell death via a drug repurposing screen. *Nature medicine*, *22*(10), 1101-1107.

Yamanaka, S. (2012). Induced pluripotent stem cells: past, present, and future. *Cell stem cell*, *10*(6), 678-684.

Yoshida, Y., & **Yamanaka**, S. (2017). Induced pluripotent stem cells 10 years later: for cardiac applications. *Circulation research*, *120*(12), 1958-1968.

Yoshida, Y., Takahashi, K., Okita, K., Ichisaka, T., & Yamanaka, S. (2009). Hypoxia enhances the generation of induced pluripotent stem cells. *Cell stem cell*, *5*(3), 237-241.

Yu, C. H. E. N. G., Meiling, H. A. O., Jing, X. U. E., & Jiemin, Q. I. (2020). BMAL1 influences proliferation of gastric cancer MGC-803 cells through SHH signaling pathway. *China Oncology*, *30*(9), 661-666.

Yu, J., Vodyanik, M. A., Smuga-Otto, K., Antosiewicz-Bourget, J., Frane, J. L., Tian, S., ... & Slukvin, I. I. (2007). Induced pluripotent stem cell lines derived from human somatic cells. *science*, *318*(5858), 1917-1920.

Zeng, H., Jia, J., & Liu, A. (2010). Coordinated translocation of mammalian Gli proteins and suppressor of fused to the primary cilium. *PLoS One*, *5*(12), e15900.

Zhang, G., Shang, B., Yang, P., Cao, Z., Pan, Y., & Zhou, Q. (2012). Induced pluripotent stem cell consensus genes: implication for the risk of tumorigenesis and cancers in induced pluripotent stem cell therapy. *Stem cells and development*, *21*(6), 955-964.

Zhang, Q., Seo, S., Bugge, K., Stone, E. M., & Sheffield, V. C. (2012). BBS proteins interact genetically with the IFT pathway to influence SHH-related phenotypes. *Human molecular genetics*, *21*(9), 1945-1953.

Zhang, S., & **Cui**, W. (2014). Sox2, a key factor in the regulation of pluripotency and neural differentiation. *World journal of stem cells*, 6(3), 305.

Zhang, Z., Zhang, Y., Gao, F., Han, S., Cheah, K. S., Tse, H. F., & Lian, Q. (2017). CRISPR/Cas9 genome-editing system in human stem cells: current status and future prospects. *Molecular Therapy-Nucleic Acids*, *9*, 230-241.

Zhao, T., Zhang, Z. N., Rong, Z., & Xu, Y. (2011). Immunogenicity of induced pluripotent stem cells. *Nature*, *474*(7350), 212-215.

Zou, J., Maeder, M. L., Mali, P., Pruett-Miller, S. M., Thibodeau-Beganny, S., Chou, B. K., ... & Porteus, M. H. (2009). Gene targeting of a disease-related gene in human induced pluripotent stem and embryonic stem cells. *Cell stem cell*, 5(1), 97-110.

Zwaka, T. P., & **Thomson**, J. A. (2009). Homologous recombination in human embryonic stem cells. In Essentials of Stem Cell Biology (pp. 417-422). Academic Press.